RESOLVING THE LIVER SINUSOIDAL ENDOTHELIAL PHENOTYPE IN HEALTH AND DISEASE

by

PANTELITSA PAPAKYRIACOU

A thesis submitted to the University of Birmingham for the degree of

DOCTOR OF PHILOSOPHY

The Institute of Immunology and Immunotherapy

College of Medical and Dental Sciences

University of Birmingham

April 2023

ACKNOWLEDGEMENTS

I would like to extend my sincere thanks and to everyone who supported me throughout the completion of this PhD, both within the lab as well as during the construction of this thesis. I thank everyone in Centre for Liver and Gastrointestinal Research, particularly Gary Reynolds, Janine Fear, Subin Modit and Norma Gregory for all the technical support they provided. I would like to express my thanks and gratitude to my supervisor Dr. Patricia F. Lalor for all her support and guidance as well as to Dr. Daniel J. Nieves for introducing me to the world of biophysics and all the training and support he provided. I also need to thank Laura Harford and Alex Wilkinson, for always being there through the most difficult lab days. Thank you to Emma Shepherd and Daniel Patten for all the support and advice. It has been a pleasure to meet and work with all the participants of the DeLiver consortium, that my PhD project was a part of, which encouraged knowledge transfer, the development of new research ideas as well as valued friendships. I thank Alessandra Dellaquila and Ana Rita Faria in particular, for the fun time we had planning crazy experiments during their secondments in our lab. To my parents, thank you for always believing in me. Lastly and most importantly, this PhD could not have been completed without the support of my partner, Marius Adrian Neata.

ABSTRACT

The burden of liver disease is continuously increasing globally, and this emphasises the need for the development of therapeutics. In order for this to be achieved, potential cellular and molecular targets need to be identified. Liver sinusoidal endothelial cells (LSECs) play a key role in maintaining liver homeostasis and their dysfunction drives liver disease pathophysiology and this role needs to be further elucidated.

In order to identify phenotypic differences in LSECs in health and disease, a combination of analytical techniques such as immunohistochemistry and qPCR was applied on human tissue specimens. To confirm whether these changes are recapitulated *in vitro*, I isolated LSECs from human healthy and cirrhotic tissue specimens for the establishment of culture model of human LSECs. Validation of functional and phenotypic characteristics of LSECs *in vitro* was carried out using immunocytochemistry and qPCR. Furthermore, the development and optimisation of a super-resolution imaging protocol for the visualisation of LSEC fenestrations was performed.

Altered expression and downregulation of scavenger receptors in LSECs was identified in diseased human tissue specimens compared to healthy specimens and this confirmed capillarisation of sinusoidal endothelial cells in liver disease. Expression of scavenger receptors and key regulatory molecules was maintained in LSECs *in vitro*. The phenotypic changes in LSECs identified in liver tissue specimens were partially recapitulated in LSECs *in vitro*. The application of pharmaceutical molecules for the enhancement of nitric oxide (NO) signalling in LSECs revealed an altered genotype in healthy and cirrhotic LSECs. Finally, fenestrations were visualised on the LSEC membrane using the developed super-resolution imaging protocol and improvement in LSEC porosity following the application of sildenafil citrate.

Hence these findings emphasise the relevance of appropriate culture models and imaging approaches to study phenotypic changes in LSECs in relation to disease and highlight the therapeutic potential of sildenafil citrate in improving LSECs porosity.

Table of Contents

List of Figures

List of Tables

List of abbreviations

AFM, atomic force microscopy
AIH, autoimmune hepatitis
ALD, alcoholic liver disease
APP, acute-phase proteins
αSMA, α-smooth muscle actin
BCKAs, branched-chain keto acids
BSA, bovine serum albumin
CD32B, FcγRIIb
cDNA, complementary deoxyribonucleic acid
cGMP, cyclic guanosine monophosphate
CK19, cytokeratin-19
CLEC4M, C-type Lectin domain family 4 member M
CLGR, Centre for Liver and Gastrointestinal research
CMDR, CellMask Deep Red plasma membrane dye
CRP, C-reactive protein
CYP450, Cytochrome P450
DAMPs, damage-associated molecular patterns
DAPI, 4', 6'-Diamidino-2-Phenylindole
Dll4, Delta-like ligand 4
DMSO, dimethyl sulfoxide
dSTORM, direct stochastic optical reconstruction microscopy
ECM, extracellular matrix
EM, electron microscopy
eNOS, endothelial nitric oxide synthase
FACR, fenestrae associated cytoskeletal rings
FATP, fatty acid transport protein
FFC, fenestrae-forming centres
FFPE, formalin-fixed paraffin embedded
FITC-BSA, Albumin-fluorescein isothiocyanate conjugate
GATA4, GATA binding protein 4
GLUT2, glucose transporter 2
H&E, Haematoxylin and Eosin
HA, hyaluronan
HGF, hepatocyte growth factor
HOCs, hepatic oval cells
HSCs, hepatic stellate cells
ICAM1, intercellular adhesion molecule 1
IHVR, intrahepatic vascular resistance

IL-1β, interleukin-1β
IL-6, interleukin-6
IMC, isotype matched control
iNOS, inducible nitric oxide synthase
KC, Kupffer cells
LPS, lipopolysaccharide
LSECs, liver sinusoidal endothelial cells
LYVE-1, lymphatic vessel endothelial hyaluronan receptor
MEA, mercaptoethylamine
MHC, major histocompatibility complex
mRNA, messenger ribonucleic acid
NASH, non-alcoholic steatohepatitis
NF-κB, nuclear factor-κB
NK, Natural Killer cells
NKT, Natural Killer T cells
NO, nitric oxide
PALM, photo-activated localisation microscopy
PAMPs, pathogen-associated molecular patterns
PBC, primary biliary cirrhosis
PBS, phosphate buffered saline
PBS-T, phosphate buffered saline with supplemented with 0.1% Tween®20
PD-L1, programmed death ligand 1
PD1, programmed cell death protein 1
PDE, phosphodiesterase
PECAM1/CD31, platelet/endothelial adhesion molecule 1
PFA, paraformaldehyde
PSC, primary sclerosing cholangitis
PSF, point spread function
RNA, ribonucleic acid
ROS, reactive oxygen species
RTC, rat tail collagen
SAP, serum amyloid p component
SEM, scanning electron microscopy
SIM, structured illumination microscopy
SMLM, Single Molecule Localisation Microscopy
STAT3, transcription factor 3
STED, stimulated emission depletion
TEM, transmission electron microscopy
TNF-α, tumour necrosis factor-α
VAP1, vascular adhesion protein 1
VCAM1, vascular cell adhesion molecule 1

VEGF, vascular endothelial growth factor
VLDLs, very low-density lipoproteins
vWF, von Willebrand factor

1 General introduction

1.1 Liver anatomy and function

1.1.1 The importance of studying liver disease

The burden of liver disease is continuously increasing globally, with liver cancer ranked within the top three causes of cancer mortality in 46 different countries (1). Epidemiological data has illustrated that liver cirrhosis is a major cause of death and morbidity worldwide and was associated with 2.4% of deaths globally in 2019 (2). Liver disease aetiologies include alcoholic liver disease (ALD) and non-alcoholic steatohepatitis (NASH) which is commonly referred to as an epidemic due to its exponential increase in prevalence. Both aetiologies are leading causes of progression to liver cirrhosis and cancer thereby contributing significantly to the overall burden of liver disease (3,4). Even though a liver transplant is the only curative option, it is an unattainable goal for thousands of cases of liver disease worldwide due to the limitation of organ shortage (5). Living donor organ transplantation is an alternative option however this is also severely impacted by the high occurrence of NASH and obesity (6). The scientific advancement of machine perfusion of livers with the goal to rehabilitate the organs to meet transplant criteria has shown great potential (7). The development of extracorporeal hepatic systems through the decellularisation of cirrhotic livers to create a scaffold which can be repopulated by hepatic progenitor cells is another promising, alternative approach to liver transplantation (8,9).

Deciphering the pathophysiological cellular and molecular mechanisms in a liver disease-specific setting which eventually lead to fibrosis and cirrhosis is required for the development of therapeutic interventions tailored to target specific pathological pathways. Liver sinusoidal

endothelial cells (LSECs) are a key player in liver homeostasis as well as in the pathophysiological initiation and progression of cirrhosis. There is however a knowledge gap into the phenotypic and genotypic changes that LSECs undergo during chronic liver disease and how they contribute to disease progression, and this will be the focus of this thesis. Therefore, the following sections in this introduction will cover general liver biology, LSECs specific endothelial biology, changes in disease as well as current strategies for assessing EC phenotype and function.

1.1.2 Liver anatomy and physiology

The liver is the human body's largest internal organ, crucial to the maintenance of systemic and metabolic homeostasis. In adults, the liver lies under the diaphragm and is situated in the upper right quadrant of the abdomen (10). The liver is separated into lobes, the right, left, caudate and quadrate. The caudate lobe is situated between the right and left lobes in an anterior and superior position, while the quadrate lobe is found on the inferior surface of the right lobe (11). The Glisson's capsule is a thin layer of collagenous connective tissue, enclosing the liver as well as encapsulating the portal vein, hepatic artery and bile ducts comprising the portal triad (12). It is composed of type I collagen fibres, scattered type III fibres and contains fibroblasts (13).

A dual blood supply reaches the liver at the porta hepatis, whereby oxygenated blood arrives though the hepatic artery while the portal vein delivers poorly oxygenated blood flowing from the pancreas, intestines, and spleen, to be filtered within the liver. The two blood sources meet at the portal tracts surrounding each liver lobule which comprises the metabolic unit of the liver. Each portal tract (also referred to as portal triad) is composed of three elements,

namely the hepatic artery, hepatic vein, and bile duct as shown in Figure 1.1. The blood is then filtered within the hepatic sinusoidal capillaries by a highly specialised type of endothelial cells called, liver sinusoidal endothelial cells before it eventually drains from branches of the hepatic venous network as well as through the central vein within each liver lobule (14–16) as shown in Figure 1.2. Further details on the anatomy and function of LSECs as well as their role in pathophysiology of liver disease will follow in subsequent sections of this introduction.

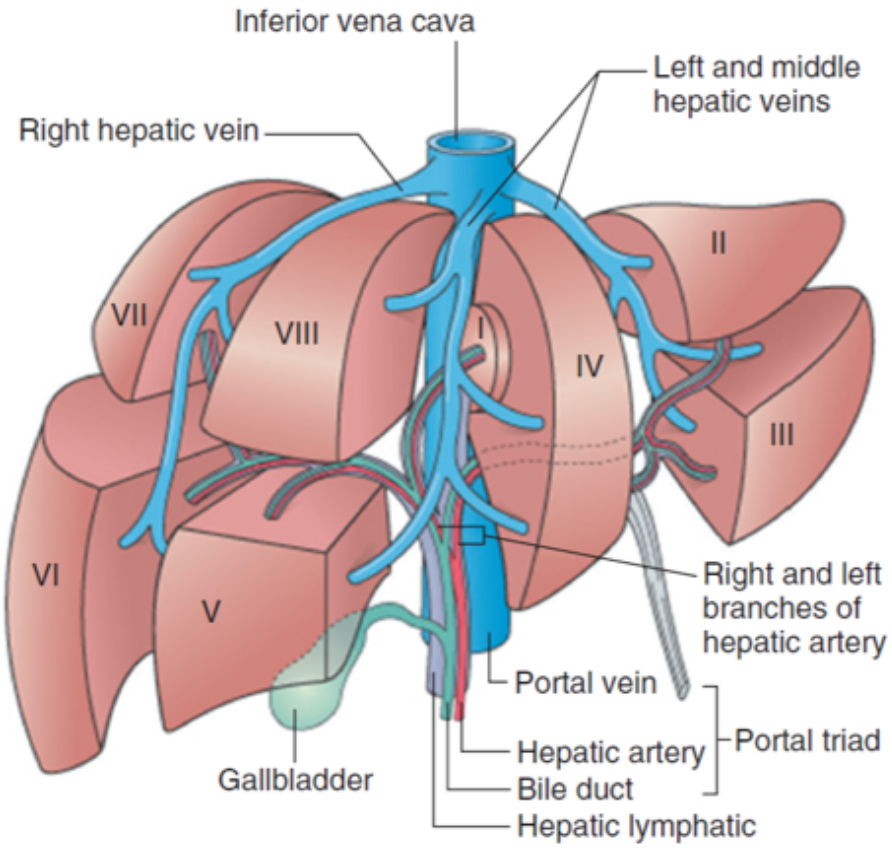

Figure 1.1: Anatomical segmentation of the liver

Segmentation of the liver based on the main divisions of the portal vein and hepatic artery. The left lobe is composed of segments II to IV and the right lobe is formed by segments V to VIII. The hepatic artery (red vessels), portal vein (blue vessels) as bile ducts (green vessels), extend into each segment of the liver where they meet at the portal triads surrounding each liver lobule (492).

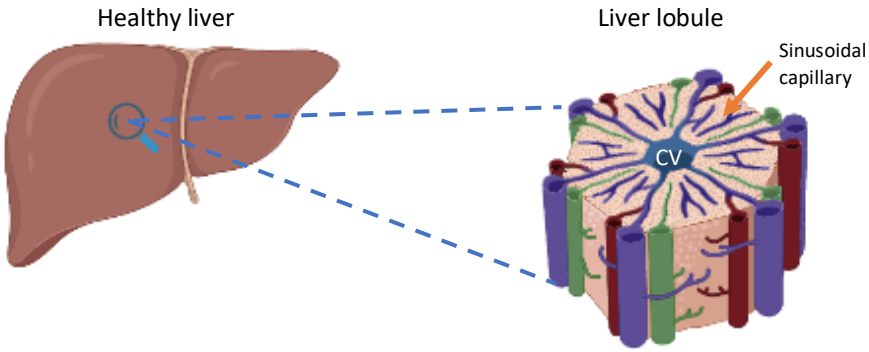

Figure 1.2: Structural organisation of the liver lobule
The liver is composed of liver lobules, termed as the structural unit of the liver (right). Each liver lobule is arranged in a hexagonal shape, with portal triads located at the vertices; composed of the hepatic artery (red), portal vein (purple) and bile duct (green) with blood filtered through sinusoidal capillaries before getting drained through the central vein. CV: central vein. Created with BioRender.com

1.1.3 Anatomy of the hepatic structural and functional unit

The terms *lobule* and *acinus* are used interchangeably to describe the microarchitecture of liver's functional unit. The first description of the 'liver lobule' was documented by Kiernan in 1833 (17) whereby the microarchitecture is defined as a hexagonal structure with the central vein in the middle and portal tracts in the surrounding apexes. The anatomic unit of the liver is represented by the lobule, while the functional unit is the hepatic acinus. The hepatic acinar model recognises a smaller triangular unit in a concept proposed by Rappaport (18–20) whereby the central vein is located at the periphery instead of the centre as in the anatomic model. The acinar zones 1, 2 and 3 correspond to the distance from arterial blood supply (21) as illustrated in Figure 1.3.

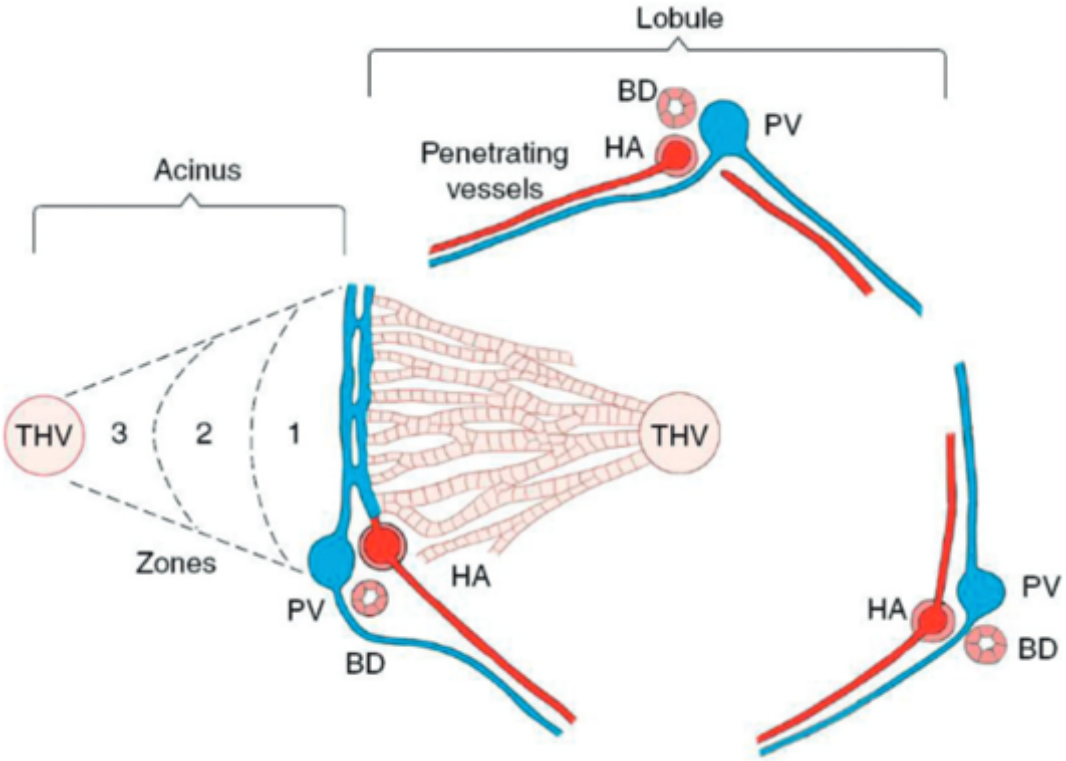

Figure 1.3: The structure of the hepatic acinus and hepatic lobule

The functional unit is represented by the acinar model is shown on the left and the anatomic unit formed by the liver lobule is portrayed on the right (493). **PV**: portal vein, **HA**: hepatic artery, **BD**: bile duct, **THV**: terminal hepatic vein.

1.1.4 Zonation of the liver lobule

The distribution of blood into the liver means that regions within the lobule have different microenvironments or zones. Zone 1 includes the periportal region closest to the portal tracts where blood enters each liver lobule through the portal hepatic vein and artery. It is therefore rich in oxygenated blood and nutrients sourced from vascular inflow. The mid-parenchymal region constitutes zone 2, and zone 3 is closest to the central vein and is exposed to blood which has the lowest oxygen content. The lobular gradient generated, results in differences in metabolic activity of the cells in each area (11). Blood flow slows down significantly within the sinusoids, creating the conditions required for efficient filtration and uptake of nutrients and

waste macromolecules from circulating blood (22). There have been recent advances in unravelling the metabolic zonation patterns in hepatocytes. It has been illustrated that 55% of the hepatic proteome presents with zonation, whereby oxidative phosphorylation, complement as well as coagulation cascades and gluconeogenesis exhibited periportal zonation. Furthermore, lipid metabolism, bile acid biosynthesis and cytochrome P450 xenobiotic metabolism displayed pericentral zonation (23). Interestingly, gene expression profiles for enzymes expressed by hepatocytes revealed that *Cyp8b1* which encodes for a protein localised in the endoplasmic reticulum membrane involved in bile acid metabolism (member of the P450 enzyme superfamily), was highest in zones 2 and 3 of the liver lobule. Additional genes within the P450 superfamily of enzymes, *Cyp7a1* and *Hsd3b7,* which encode for enzymes involved in the catalysis of cholesterol into bile acids, were abundantly expressed pericentrally. The expression of the gene encoding bile acid-CoA: amino acid N-acyltransferase, *Baat,* was absent in hepatocytes located in the pericentral zone (24).

It is not only hepatocytes which show spatial separation of gene expression. Spatial mapping of gene expression in mouse liver using a paired-cell RNA sequencing (paired hepatocyte and LSECs) has been implemented in order to infer LSECs location using the expression of hepatocyte landmark genes. This approach has revealed spatial heterogeneity in LSECs whereby the zonation pattern of genes of ligands such as *Wnt2*, *Wnt9b* and *Rspo3* were found to be enriched in pericentral cells (25). Moreover, Delta-like ligand 4 (*Dll4*) previously found to be enriched in arterial endothelial cells (26), exhibited periportal zonation in LSECs along with *Efnb2* and *Cldn5*.

1.1.5 Liver embryonic development

In mice, the foregut endoderm gives rise to the liver and expression of albumin is initially observed at E8.5 within the newly formed hepatic endoderm. Fibroblast growth factor signalling from the developing heart to the gut tube (27,28) as well as bone morphogenic protein signals from the septum transversum mesenchyme result in hepatoblast differentiation. Consequently, this leads to the formation of the liver bud at E10.5 (29–31). During embryonic development, the human liver acquires its vascular architecture by 17-25 weeks of gestation however the vessels composing the hepatic vasculature have variable embryonic origins. As such, portal vessels originate from vitelline veins while the sinusoidal network forms from capillary vessels of the septum transversum. By week 20 of gestation, the highly specialised hepatic sinusoidal endothelium acquires its fenestrated phenotype, a process led by the transcription factor GATA binding protein 4 (GATA4) (32,33).

1.2 The liver as a multi-functional metabolic engine

1.2.1 Carbohydrate metabolism

The liver is the lead engine of metabolic processes in the human body, and careful maintenance of these process is vital for sustaining homeostatic balance. Hepatocytes are responsible for carrying out the detoxification, major metabolic function, protein synthesis and storage within the liver. As the human body requires energy to function and maintain homeostasis, blood glucose levels are balanced between feeding and fasting states. Glucose homeostasis in the liver is influenced by hormones secreted by the pancreas such as glucagon

and insulin (34,35). After a meal, surplus glucose present in the bloodstream following digestion, leads to glycogenesis. Glucose reaches the liver via the portal vein and is absorbed by hepatocytes through the glucose transporter 2 (GLUT2) (36). The increase in glucose levels activates glucokinase, which is the first enzyme involved in the conversion of glucose to glycogen, a form of carbohydrate that can be stored in the liver. Alternatively, glycogenolysis takes place to mediate the release of glucose from hepatocytes into the bloodstream during a fasting state (37,38). In order to meet the glucose requirements (125g/day in a 70 kg human) when glycogen stores have been depleted, the liver performs gluconeogenesis and uses substrates such as glucogenic amino acids (e.g., glutamine and alanine), lactate and pyruvate (39,40).

1.2.2 Protein synthesis and storage

The human body's source of energy does not rely on glucose alone. The liver is the main site of synthesis of multiple amino acids which serve as an energy source such as glutamate, aspartate and glycine which also form the building units for the synthesis of integral proteins such as albumin and also serve as a substrate for glutathione synthesis which is one of the most abundant antioxidants in cells (39,41). Under normal conditions in a healthy individual, the liver will produce approximately 20 g of albumin daily (42). Amino acids sourced in the liver, originate from dietary intake of protein which reaches the liver through the portal vein and is thereafter metabolised by hepatocytes, or via amino acid catabolism (43). This process excludes branched chain amino acids whereby hepatocytes accumulate branched-chain keto acids (BCKAs) which are produced in muscle tissues. Branched chain α-keto-acid

dehydrogenase expressed by hepatocytes then irreversibly mediates the oxidative decarboxylation of BCKAs (44–46).

1.2.3 Lipid metabolism

The liver can both synthesise as well as oxidise fatty acids which along with glycerol comprise the main reserve of energy in mammals (47). The liver plays a crucial role in intestinal lipid absorption as bile acids secreted by hepatocytes mediate the emulsification of lipid droplets after a meal, making them available for lipase hydrolysation. More than 95% of dietary fat absorbed by the small intestine, either reaches the liver through the hepatic portal vein (48) or is converted by enterocytes into chylomicrons which constitute the largest group of lipoproteins found in circulation. Chylomicrons are then released into the lymphatic vessels, to be transported to the liver and adipose tissues (49). In addition, the liver contributes to the plasma fatty acid content by synthesising triacylglycerol which is packaged as very low-density lipoproteins (VLDLs) and secreted into blood circulation (43). Fatty acids bound to albumin in blood circulation, reach hepatocytes either by passively diffusing across their membrane or via fatty acid transport proteins (FATP) expressed by hepatocytes such as FATP2 and FATP5, or caveolin-1 (50,51). Hepatocyte mitochondria are responsible for carrying out β-oxidation, a process mediating fatty acid degradation. *De novo* lipogenesis on the other hand, leads to the synthesis of fatty acids within the cytosol of hepatocytes using excess dietary amino acids and carbohydrates, a process mediated by the acetyl co-enzyme A (43).

1.2.4 Xenobiotic metabolism

The liver also carries out detoxification in the body which is a crucial defence mechanism. Drug metabolising enzymes are the primary drivers of xenobiotic metabolism within the liver,

starting with Phase I enzymes such as cytochrome P450 (CYP450) (52). Drug metabolism mediates a series of chemical reactions that result in in the conversion of chemicals that the body is challenged with, into water-soluble metabolites which can be more easily eliminated from the body through urine. The reactions that take place in the process of chemical and toxin degradation can be divided into Phase I and Phase II, with specific metabolising enzymes involved in each one (53). The majority of drug metabolising enzymes required, are expressed by hepatocytes and these include CYP450, aldehyde dehydrogenase, monoamine oxidases and alcohol dehydrogenase, although alcohol dehydrogenase 1 as well as CYP2E1 have been reported to be expressed by LSECs thereby suggesting that sinusoidal endothelium is also involved in metabolising alcohol (54).

1.2.5 Blood clearance

The filtration capacity of the liver is mainly dominated by LSECs which mediate blood clearance of and filtration through their multitudinous fenestrae as well as endocytic capabilities. LSECs and Kupffer cells (KC) both contribute to viral clearance. It has been demonstrated that LSECs are involved in the removal of polyomavirus from circulation where mouse LSECs were observed to efficiently endocytose blood borne BK- as well as JC-VLPs which were found to colocalise with the mannose receptor as assessed by immunofluorescent labelling and subsequent confocal imaging (55). Similarly, examination of *in vivo* viral uptake by LSECs and KC in mice, revealed that 90% of adenovirus clearance was mediated by LSECs while the contribution of KC to adenovirus uptake was only 10% (56). Additionally, the clearance of HIV-like particles in mice followed a similar pattern whereby 90% of uptake was localised to LSECs, with KC accounted for only 10% of uptake. The hepatic sinusoids exhibit an impressive clearance capacity of 100 million HIV-like particles per minute (57). The dynamic sieving

properties of LSECs fenestrations have been demonstrated by reports such as the forced sieving of 400 nm sized liposomes through LSECs fenestrae in experiments carried out in rat LSECs (58). As fenestrations facilitate bidirectional exchange of substrates, they are also permissive of the passage of albumin as well as albumin-bound substrates and experiments have demonstrated that that albumin distribution is influenced by alterations in fenestrae (59).

It has been demonstrated by Fraser et al. that LSECs participate in lipoprotein metabolism as fenestrations mediate the filtration of chylomicron remnants, circulating lipoproteins with atherogenic properties (60), thereby allowing their uptake by hepatocytes. It has been suggested that the function of LSECs in chylomicron filtration and clearance, plays a crucial part in the prevention and development of atherosclerosis (61,62). LSECs have also been shown to expedite the uptake of oxidised LDL via the endocytic receptor stabilin-1 (63). The scavenging functions and fenestrations of LSECs will be discussed further in section 1.5 of this introduction.

1.2.6 The role of the liver in immune surveillance

The liver's capacity to detect and clear pathogens is a dynamic combination of its anatomy and resident cell types. As the liver has a dual blood supply, it can detect pathogens of both gut and systemic origin. Bacteria-derived molecules such as lipopolysaccharide (LPS) are abundantly present in portal blood. In case of injury to the gut epithelium, intact pathogens can translocate from the gut into portal blood thereby lead directly to the liver (64).

Hepatocytes play critical role in activation of innate immunity, as their protein synthesis function contributes to fighting pathogens. Proteins secreted by hepatocytes have been found

to be elevated following bacterial infection. Inflammatory signals received by hepatocytes lead to the rapid production of innate immunity proteins such as C-reactive protein (CRP) and serum amyloid p component (SAP), termed as acute-phase proteins (APP) (65). The mechanism employed by APP to eliminate bacteria directly or stimulate the immune pathway for pathogen clearance is evolutionary conserved. APP production is regulated by inflammatory cytokines such as interleukin-6 (IL-6), interleukin-1β (IL-1β) and tumour necrosis factor-α (TNF-α) which activate transcription factor 3 (STAT3) which mediates signal transduction as well as nuclear factor-κB (NF-κB) activation. Consequently, hepatocytes act as effector cells in the delivery of APPs in response to stimulating cytokines such as IL-6 and IL-1β thereby coordinating the immune response (66).

The liver also contains the largest macrophage population (Kupffer cells), the highest densities of Natural Killer (NK) cells and natural Killer T (NKT) cells as well as the largest network of reticuloendothelial cells in the body (67). LSECs contribute to hepatic immune function by clearing small immune complexes from blood thereby preventing their pathologic accumulation. This is specifically facilitated by the receptor FcγRIIb (CD32B) expressed by LSECs (68). Within the sinusoidal network, the rate of blood flow slows down and blood pressure is reduced 50-fold in comparison to arterial blood. This optimisation of blood flow enables the screening and capture of pathogens from blood passing through sinusoidal capillaries (69).

The liver's critical role in regulating response to pathogens has been demonstrated in mouse models where animals depleted of KC, were treated with *Listeria monocytogenes*. The depleted animals exhibited 100% mortality (70) thereby confirming the key role of pathogen

clearance by KC. NKT cells are act as pathogen patrol as they actively search for pathogens within the hepatic vasculature by crawling along the sinusoidal walls regardless of the direction of blood flow. When activated, they no longer crawl but rather adhere to the sinusoidal wall (71,72). Once activated they can produce regulatory cytokines and chemokines to orchestrate and appropriate response to the invading pathogen. The patrolling function of NKT cells has been visualised within the liver using intra-vital microscopy in live mice expressing green fluorescent protein (GFP) (73).

1.3 Chronic liver disease and hepatic fibrosis

A critical point in liver injury progression, as a result of aetiologies such as ALD, primary biliary cirrhosis (74) or autoimmune hepatitis, is the progression to significant liver inflammation as a result of the leukocyte recruitment to the liver. The balance between clearance and persistence of immune cell subsets within the liver, is a key determining factor in whether the injury will resolve, persist, or progress to liver failure or chronic hepatitis and cirrhosis (75). Abnormal or persistent activation of LSEC throughout chronic liver injury also triggers fibrogenesis as the cells are no longer able to maintain HSC quiescence or angiocrine factor release which regulate the equilibrium between regeneration and fibrosis (76). Therefore, LSEC dysfunction precedes hepatic fibrosis which eventually progresses to cirrhosis. These processes are accompanied by fundamental changes in hepatic tissue architecture such as the development of bridging fibrosis and regenerative nodules of hepatocytes throughout the liver as well as gradual deterioration of liver functions (77).

Fibrosis is a dynamic process involving crosstalk between parenchymal and non-parenchymal cells within the liver, characterized by the accumulation of extracellular matrix in the space of Disse and the formation of a sub-endothelial basement membrane (78). Although myofibroblasts no longer inhabit the liver after embryonic development when they are replaced by portal fibroblasts, liver injury leads to their re-emergence though the activation of stromal cell populations such as portal fibroblasts or hepatic stellate cells (HSCs) (79). Consequently, myofibroblasts are primarily involved in tissue repair and remodelling occurring throughout chronic liver injury and are particularly found within scar tissue in cirrhotic livers. They highly express α-smooth muscle actin which enables them to apply traction forces and produce extracellular matrix (ECM) components and matrix metalloproteinases (80). This gradually progresses to the capillarisation of sinusoids which is the progressive defenestration of LSEC and phenotypic switch to a phenotype akin to continuous vascular endothelia. The process of capillarisation also involves the loss of GATA4 signalling, and upregulation of platelet and endothelial adhesion molecule 1 (CD31) expression (64,81).

Morphologically, LSECs of diseased livers are characterised by cytoplasmic swelling while the cell body protrudes into the sinusoidal lumen. There is an increase in rough endoplasmic reticulum in cytoplasmic processes that are closely associated with basement membrane-like material, and reticulin fibres in the space of Disse (82,83). One of the most frequent aetiologies of chronic liver disease is alcoholic liver disease in which LSEC defenestration has been well-documented. In a baboon alcohol model, alcohol feeding from 4 to 24 months led to a decrease in fenestration frequency and an increase in their mean diameter compared to controls (84). Alcohol induced fenestration of the hepatic sinusoids has been implicated in the development of hyperlipoproteinemia as a consequence of the reduced chylomicron

clearance of the liver sieve (85,86). Moreover, fibrotic changes in mid-lobular zone of the lobule have been reported as perivenous and perisinusoidal fibrosis. TEM combined with SEM imaging of liver needle biopsies from normal livers has shown smaller fenestration diameter but higher frequency in zone 3 in comparison to zone 1. In contrast to this, in cases of ALD with or without fibrosis, fenestration frequency and porosity was significantly lower compared to non-alcoholic liver cases (87,88). Proteomic investigations have revealed differential expression of proteins in a rat model of ALD. Alcohol dehydrogenase was downregulated after 1 month of daily 5% ethanol administration in the rats' diet while aldehyde dehydrogenase was upregulated at 3 months which has been linked to a hepatic protection mechanism against ethanol toxicity. An additional development in the pathophysiology of ALD as well as NASH is fat infiltration which was found to be increased in ethanol-fed rats compared to controls (89).

A key regulator of the LSEC fenestrated phenotype is the constant release of NO as a result of shear stress from sinusoidal blood flow and the release of vascular endothelial growth factor (VEGF) by hepatocytes. NO signalling involves the endothelial isoform of the enzyme nitric oxide synthase (eNOS) which is impaired in chronic liver disease, and this leads to vasoconstriction followed by an increase in intrahepatic vascular resistance (90,91). Upregulation of the inducible isoform of nitric oxide synthase (iNOS) in LSEC has been associated with their capillarisation (92,93). iNOS expression can also be induced by LPS and cytokines and is associated with LSEC dysfunction (94).

1.4 Hepatic cell types

Cell type organisation and function within the liver is in line with the principle of 'function follows form'. LSEC constitute the first line of defence within the liver, forming part of the reticuloendothelial system which is a concept introduced by Aschoff in 1924. This concept also includes macrophages and cells residing in the sinusoids of lymph nodes, spleen, bone marrow, adrenal and pituitary glands (95). Originally, LSECs and KCs were considered to be the same hepatic cell population, until LSECs were distinguished as a separate cell type from KCs and were recognised as a specialised type of endothelial cell with high endocytic capacity (96). Strategically lining the sinusoidal capillary wall, LSEC act as a permeable barrier between circulating blood and the main liver parenchyma (Figure 1.4) while the absence of a basement membrane in LSEC allows for the bidirectional flow of particles and macromolecules (97). The following sections will summarise the main hepatic cell types and a separate section focusing on LSEC phenotype and function is presented in section 1.5.

The main cell types residing within the liver include parenchymal cells which are hepatocytes and non-parenchymal cell populations formed of LSEC, cholangiocytes, epithelial cells, KCs and hepatic stellate cells (HSCs) (Figure 1.4) as well as additional endothelial populations and liver specific innate and adaptive immune cell populations. Endothelial cell transcription within the liver is regulated by the GATA family of transcription factors and the types of endothelial cells within the liver include portal and central vein endothelium as well as lymphatic endothelium. The heterogeneity exhibited by endothelial cell phenotypes is directly linked to the heterogeneity in function. Vascular endothelium lines the hepatic artery and portal vein and these endothelial cells form a continuous monolayer in contrast to the

discontinuous endothelium lining the sinusoidal capillaries (98). Vascular endothelium is surrounded by layers of smooth muscle cells as well as basal lamina, a morphological characteristic which emphasises the difference between vascular and sinusoidal endothelium within the liver (99). Endothelium lining portal tract and central vein vessels can be labelled using CD31 and the transmembrane glycoprotein CD34 which are classic endothelial markers (100). Lymphatic vessels within the liver lobule are localised to portal tract areas and lack proximal smooth muscle cells and pericytes. They are characterised by lymphatic vessel endothelial hyaluronan receptor (LYVE-1), Prox1 and podoplanin expression while functionally they contribute to the immune cell trafficking (101). Lymphatic endothelium dysfunction was shown to be involved in the development of a fatty liver in mice (102).

1.4.1 Hepatocytes

The perisinusoidal space called space of Disse, is located between LSEC and hepatocytes (Figure 1.4) which compose the liver parenchyma, representing 60% of the total hepatic cell population and approximately 80% of the total hepatic volume. Hepatocytes are polarised epithelial cells with a polyhedral shape and a diameter of approximately 20 µm to 30 µm, arranged into anastomosing plates. Parenchymal organisation has been well demonstrated by scanning electron microscopy (103). The plasma membrane regions of hepatocytes vary according to the function they associate with. The basal surface of the hepatocyte plasma membrane is orientated towards the sinusoidal capillary, with microvilli spreading into the space of Disse thereby maximising the surface area available for substance exchange between blood plasma and hepatocytes. The lateral plasma membrane is the interface between adjoining hepatocyte cells. The basal and lateral domains are considered a combined

functional unit and therefore referred to as the basolateral plasma membrane which serves as a point for endocytosis and protein secretion.

Hepatocytes exhibit phenotypic and functional heterogeneity across the liver lobule whereby periportal hepatocytes within zone 1 are primarily involved in gluconeogenesis and β-oxidation (104). The periportal region of the liver parenchyma is the first to be exposed to toxins and microbes originating from the gut as well as interacting with blood rich in oxygen and nutrients (105). Single-cell RNA sequencing data from human liver samples has shown enrichment of genes in relation to lipid and cholesterol synthesis such as *SCD*, *HMGSC1* and *ACSS2* which match genes enriched in periportal hepatocytes in mice (106). On the contrary, pericentral hepatocytes have access to lower concentrations of oxygen and nutrients and are therefore characterised by metabolic functions such as enhanced glycolysis, lipogenesis, and detoxification (105). The resulting gradient in nutrients and oxygenation within the liver lobule is reflected by the corresponding gene expression within each region, with periportal cells expressing high levels of genes involved in innate inflammatory responses such as *PGLYP2* which mediates an anti-inflammatory response against bacteria, for the digestion of the peptidoglycan wall (104,107).

Transport of bile acids is another important function that hepatocytes perform with bile acids extracted at a high rate from circulating plasma (108). Bile canaliculi form a network of channels passing directly through adjoining hepatocytes, comprising the apical area of the hepatocyte plasma membrane. The apical membrane also has microvilli extensions that increase the surface area available for secretion and is separated from the basolateral domains by a layer of tight junctions. Bile is secreted by hepatocytes into canalicular space

and is drained towards the portal tracts within the bile canalicular network, in order to be collected by the biliary system (109).

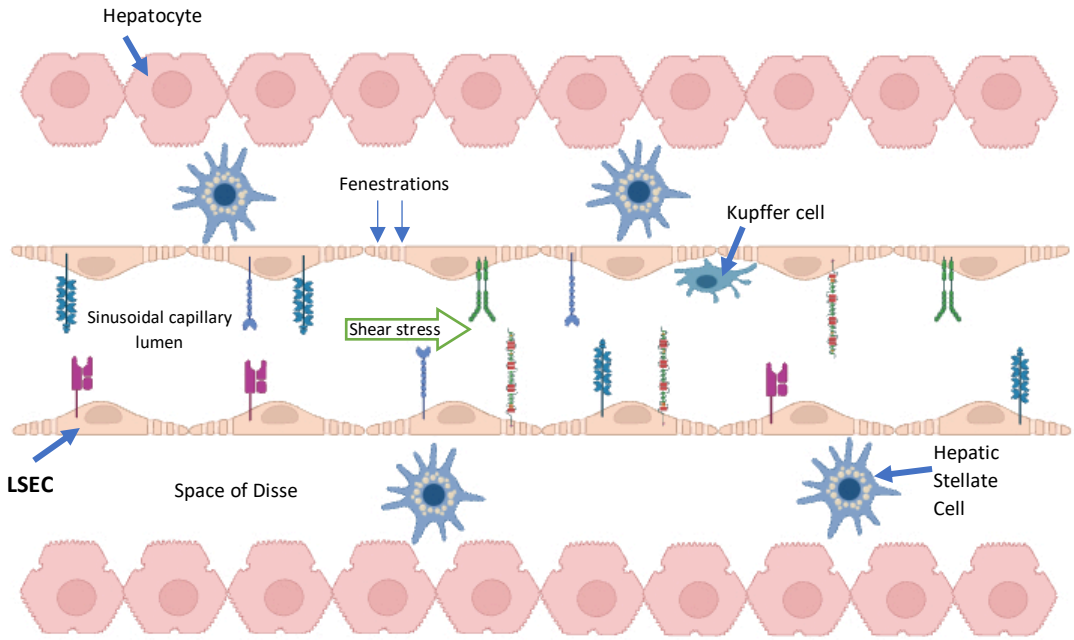

Figure 1.4: Structural organisation of the main hepatic cell types.

LSEC line sinusoidal capillaries within the liver lobule, forming a barrier between the space of Disse and hepatocytes. Hepatic stellate cells reside within the space of Disse while Kupffer cells localise to the sinusoidal lumen. The LSEC perform dynamic filtration of the blood through fenestrations (gaps in the membrane), as well as scavenging and antigen presentation through the expression of multiple receptors. Created with BioRender.com

1.4.2 Cholangiocytes

Cholangiocytes or biliary epithelial cells (BEC) are dynamic epithelial cells that contribute 3% to 5% of the hepatic cell population and form the lining of the ductal network of the biliary tree which consists of the canals of Hering, bile ductules as well as the intrahepatic and extrahepatic bile duct system. Heterogeneity is common in cholangiocytes throughout the biliary tree, and this is also observed on a structural level as their diameter increases in a basal-to-apical direction which results in increased diameter of the biliary lumen (110). Generally, their size differs and is directly impacted by the size of the ducts they line. Cuboidal cholangiocytes are found in small bile ducts while they shift to a columnar morphology within larger bile ducts (111). Cholangiocytes are primarily involved in the absorption and secretion of water and electrolytes thereby altering bile composition while it is transported through bile ducts (112–114). The ductal epithelium is responsible for the production of 40% of bile in humans. Bile secretion is mediated by sodium and bicarbonate transport from cholangiocytes towards the duct lumen along with the controlled passage of water arriving through the intercellular tight junctions (115) while secretion is dependent on hormonal regulation by secretin and somatostatin (116). The bile absorptive function of cholangiocytes is mediated by the expression of transport proteins on their apical and basolateral plasma membranes. The absorption of a proportion of secreted bile which is then recirculated back to hepatocytes is termed as the cholehepatic shunt. Passive diffusion of unconjugated bile acids (secreted by hepatocytes into bile) into cholangiocytes, takes place via their apical plasma membrane (117,118). Unconjugated bile acids are then transported back to hepatocytes through the peribiliary vascular plexus. This is followed by re-secretion into bile canaliculi and this stimulates the secretion of bicarbonate ions ($HCO3^-$) (119). On the contrary, transport of

conjugated bile acids depends on specific transporters such as Na^+-dependent bile acid transporter (ASBT/SLC10A2) which is expressed on the apical plasma membrane of cholangiocytes (120). Additionally, cholangiocytes are also involved in the absorption and transport of glucose from bile.

1.4.3 Hepatic oval cells

The liver is known for its capacity to regenerate, and in specific circumstances of liver damage where hepatocyte proliferation has been impaired, this is achieved through the activity of hepatic oval cells (HOCs) which arise from the canal of Hering in the portal areas of the liver lobule (121). They were first detected in the rat liver and are characterised by a high nuclear to cytoplasm ratio and have an ovoid nucleus (122). HOCs are derived from biliary epithelial cells and just as fetal hepatoblasts, oval cells have bipotential properties which allow them to differentiate into hepatocytes or cholangiocytes as necessary. Adult hepatocytes are estimated to have an average life span between 200 and 300 days under homeostatic conditions (123). Hepatocyte proliferation in response to liver damage is normally mediated by hepatocytes that are proliferatively quiescent, which then enter the proliferative cycle (124). In contrast to this, proliferation of HOCs and their differentiation into hepatocytes is initiated by specific kinds of liver damage, such as chronic liver damage by chemicals such as galactosamine and DL-ethionine, as demonstrated in rat models (122). This is a case of progenitor-dependent liver regeneration and therefore the oval progenitor cells can be regarded as a 'facultative liver stem cell' (125). Oval cells express both ductal epithelium markers such as cytokeratin-19 (CK19) and hepatocyte markers such as albumin. An additional

characteristic that oval cells have in common with fetal hepatoblasts is a high level of α-fetoprotein expression (122).

1.4.4 Hepatic stellate cells

Hepatic stellate cells or Ito cells, originally described by Boll and Kupffer in the 1870s, are mesenchymal cells found within the perisinusoidal space of Disse (Figure 1.4) and account for 5-8% of the hepatic cell population. They have an astral phenotype with dendritic-like extensions which wrap around the sinusoids and intersect parenchymal hepatocytes, which places them in an ideal position for the regulation of hepatic blood flow (126,127). HSCs express smooth muscle proteins such as α-smooth muscle actin (αSMA) and desmin and are primarily involved in vitamin A storage which can be seen as cytoplasmic lipid droplets within the cell cytoplasm, a characteristic that is lost in condition of stress or liver injury. Under normal conditions, HSCs are involved in maintaining ECM turn-over within the liver by synthesising and secreting ECM molecules, metalloproteinases for matrix degradation as well as cytokines and growth factors (128). Liver injury occurring during chronic liver disease, activates HSCs leading to a phenotypic shift and trans-differentiation from a quiescent to a fibrinogenic state. They then acquire a myofibroblast phenotype and significantly contribute to the excess production of collagen which gradually disrupts the liver's normal architecture, leading to the development of liver fibrosis, scarring and ultimately cirrhosis (129). Therefore, their phenotypic differentiation during chronic liver disease also contributes to the capillarisation of the sinusoids. The phenotypic differentiation of activated HSCs to myofibroblasts is mediated by proinflammatory cytokines released by infiltrating immune cells as well as an increase in reactive oxygen species (ROS). ECM and protease secretion as

well as migration of HSC upon activation are energy demanding processes and this is reflected by the augmented glucose transport capacity as well as glycolytic activity of primary activated HSC *in vitro* (130). Single cell transcriptomic studies have revealed a link between spatial zonation and function of HSCs throughout liver fibrosis, whereby HSCs localised within the central vein area of the liver lobule appear to be leading pathogenic collagen production during fibrosis as a result of liver injury initiated in that specific area. Moreover, single cell RNA sequencing has revealed three distinct mesenchymal sub-populations in the fibrotic mouse liver. The portal niche identified, consists of $CD34^+$, $PDGFR\beta^+$ cells, localised next to $PanCK^+$ biliary epithelial cells. $Reelin^+$ and $PDGFR\beta^+$ mesenchymal cells were located within the perisinusoidal space, while $PDGFR\beta^+$ and Calponin 1^+ were found within the walls of both the hepatic artery and portal vein (131).

1.4.5 Immune cell populations

An additional liver-specific cell type residing within the sinusoidal lumen, are KC (Figure 4), constituting the liver's resident macrophage population and one of the liver's innate immune cell populations. They contribute to hepatic clearance and scavenging by expressing markers such as the mannose receptor, a characteristic they have in common with LSEC (132). Even though there is evidence from bone marrow and liver transplant studies that suggests KC are derived from circulating monocytes (133), they do have the capacity to proliferate which is a property allowing the Kupffer cell population to expand during liver injury (134,135). Additionally, from a developmental point of view, KC appear in the mouse liver before the appearance of circulating monocytes and there is evidence supporting that they could originate from macrophages within the yolk sac (136,137). Functionally, KC focus on

phagocytosis and rapidly clear apoptotic hepatocytes as well as removing and degrading soluble matter from portal blood. Emerging evidence is increasingly supporting the fact that the immune microenvironment within the liver is a major player in maintaining homeostasis as well as driving disease-specific pathophysiological processes. Single cell transcriptomics have deconvolved the existence of two distinct populations of intrahepatic macrophages within all normal liver specimens analysed. Both populations were $CD68^{+}$, however one of the populations exhibited enriched expression of *LYZ*, *CSTA*, *CD74*, which indicated that this subpopulation represented inflammatory macrophages. The second $CD68^{+}$ macrophage population identified, was characterised by enriched expression of genes related to the tolerogenic function of macrophages such as VSIG4 whose tolerogenic properties have also been confirmed in mice (106,138).

The liver immune microenvironment is shaped by resident innate immune cells including KCs, invariant NKT (iNKT) cells, natural killer (NK) cells, mucosal-associated invariant T (MAIT) cells, $\gamma\delta$ T cells, dendritic cells as well as innate lymphoid cells (139–143). The tolerogenic environment existing within the liver under homeostatic conditions, primes resident innate immune cells which are also involved in the clearance of pathogen-associated molecular patterns (PAMPs) and damage-associated molecular patterns (DAMPs) they frequently encounter (144–147). KCs contribute to the maintenance of hepatic homeostasis through the clearance of senescent and dead cells, phagocytosis as well as by participating in the tissue repair process (64,148). The production of immunosuppressive metabolites such as IL-10 and prostaglandin is mediated by KCs in mice as well as the expression of V-set and Ig domain-containing 4 (VSIG4) which is involved in the inception of immune tolerance in T and NKT cells. The liver microenvironment is enriched in IL-10 which is involved in the up-regulation of

programmed death ligand 1 (PD-L1) expression on KCs. PD-L1 is then indirectly stimulate the development of Tregs by promoting T cell inhibition (149–152).

Adaptive immune cells within the liver include T cells such as regulatory T cells (Tregs), cytotoxic T lymphocytes and Type 1, 2, 17 and 22 helper T cells as well as B cells and plasma cells (153–155). Tregs are major players in maintaining hepatic tolerance through the expression of immunoregulatory markers such as cytotoxic T lymphocyte-associated protein 4 (CTLA-4) and lymphocyte-activation gene 3 (LAG-3). They are responsible for IL-10 secretion which harbours anti-inflammatory properties, and this is vital for the conservation of immune tolerance within the liver as well as preventing immunopathogenesis (156,157). In mice, immune tolerance is mediated by the cooperation of hepatic immune cell populations such as Tregs and KCs in order to reinforce a local suppressive environment, thereby preventing the progression of a cytotoxic T lymphocyte response (158).

1.5 The liver sinusoidal endothelial cell and its role in health and disease

1.5.1 Phenotypic, structural, and functional characteristics of LSEC

As the hepatic cell type of interest in this thesis is LSEC and how their phenotype and function is altered in disease, section 1.5 will focus on the current knowledge on LSEC phenotype and function. The distinction between LSEC and KC was brought forward by Eddie Wisse who submitted evidence supporting the presence of an endothelial cell population inhabiting the hepatic sinusoids as opposed to KC only (96). LSEC form a unique endothelial population within the liver and line the capillaries carrying blood through the hepatic sinusoidal network (Figure 1.4). Consequently, they are strategically positioned, and this is in accordance with their structure as well as the wide range of functions they perform in maintaining hepatic homeostasis. To begin with, they lack a basal lamina and are arranged in a thin cytoplasmic layer which is approximately 50 nm to 80 nm thick. Their plasma membrane is decorated with dynamic, transmembrane nanopores called fenestrations or fenestrae (Figure 1.4) that lack diaphragms and carry out a critical filtration function (159). The fenestrated membrane of LSEC allows for direct access to the liver parenchyma through the space of Disse thereby creating bidirectional route for the exchange of substrates; hence why the fenestrated LSEC membrane is often referred to as a molecular sieve. Pharmaceutical molecules, lipoproteins, and macromolecules flow through fenestrae to reach hepatocytes and waste output flows through fenestrae back into the bloodstream (160).

1.5.2 eNOS-mediated regulation of LSEC function

The endothelial isoform of the nitric oxide synthase (eNOS) is constitutively expressed by LSEC, and its activation is mediated by stimuli such as VEGF and shear stress. eNOS is responsible for the constant release of small amounts of nitric oxide (NO) which is vital for preservation of vascular tone and hepatic blood flow as well as HSC quiescence (161,162). NO was originally named as the 'endothelial-derived relaxation factor' by Robert Furchgott and regardless of the fact that it is a highly reactive and diffusible signalling molecule, it mediates post-translational modification of target proteins via S-nitrosylation (163). NO synthesis is the result of the conversion of the amino acid L-arginine and oxygen (O_2) to NO and L-citrulline (164). cGMP is the primary mediator of NO signalling, and its downstream targets include cGMP-dependent protein kinases (PKGs), phosphodiesterases (PDEs) and cGMP-gated cation channels.

The localisation of eNOS within LSEC influences protein targeting for S-nitrosylation and it usually localises to intracellular membrane domains which include the cytoplasmic side of the Golgi apparatus as well as plasma membrane caveolae (165). Experiments comparing the localisation of mutant and wild type eNOS have demonstrated that eNOS compartmentalisation at the Golgi apparatus affects cell functions such as protein trafficking by decreasing the transport velocity of proteins from the endoplasmic reticulum to the Golgi and from the Golgi to reach the plasma membrane (166). The fact that eNOS localises to the Golgi apparatus is associated with regulation of Golgi function through S-nitrosylation of proteins such as extracellular matrix metalloproteinase inducer (EMM-PRIN) and Golgi phosphoprotein 3 (GOLPH3) in endothelial cells (167,168).

1.5.3 It's all about fenestrae

Fenestrae were first identified as a structural feature on LSEC by Yamagishi in 1959 using transmission electron microscopy (TEM) in ultrathin sections and described further by Eddie Wisse in 1970 (169,170). Fenestrations are also found on the membrane of glomerular endothelial cells in the kidney (171). In LSEC, these nanopores occupy 2-20% the plasma membrane's surface area as described from scanning electron micrographs (172) and they are organised in clusters called sieve plates situated between cytoplasmic arms. Fenestrae cover the flattest regions found in the periphery of the LSEC membrane as well as having perinuclear localisation (173,174). The reported size range of fenestrations is typically between 50 nm and 300 nm and these values are species dependent (175–177).

The frequency and diameter of LSEC fenestrae vary across the liver lobule. When looking at fenestrations from periportal to pericentral cells, there is a slight decrease in diameter with measurements of 110.7±0.25 nm to 104.8±0.22 nm respectively (measurements taken after critical point drying for SEM) (178). In addition, fenestrae frequency was increased across the liver lobule, thereby leading to an increase in porosity. Fenestrae measurements carried out from transition electron microscopy (TEM) images on the other hand, indicate diameter values of 174.6 ± 1.0 and 147.2 ± 0.9 nm for periportal and pericentral LSEC respectively (179). These measurements clearly illustrate the differences between different sample preparation approach for specific imaging techniques.

1.5.4 Maintenance of fenestrae

Vascular endothelial growth factor (VEGF) is a major player in the maintenance of LSEC fenestrae by acting as a vascular permeability factor (180). It is released by hepatocytes and cholangiocytes as part of paracrine signalling and maintains LSEC porosity through the release of NO (181). LSEC also express the VEGF receptors VEGF receptor 1 (VEGFR1, *FLT1*) and VEGF receptor 2 (VEGFR2, *KDR*) which participate in the VEGF signalling cascade. VEGFR2 mediates signalling associated with LSEC proliferation and survival while VEGR1 has been linked to pathological angiogenesis (182). Maintenance of the liver sieve is a closely regulated process, with NO constantly produced in small amounts by eNOS which maintains the dynamic filtration capacity of the liver sieve.

1.5.5 Decoding the regulation of fenestrae

Recent advances in the study of fenestral dynamics have contributed to the puzzle of how these nanopores are maintained and regulated. Such studies have suggested four different hypotheses to explain the process. Firstly, the idea that fenestration frequency is regulated by actin (de)polymerisation was introduced by Braet et al. in 1995 where fenestrae-associated cytoskeleton rings (FACR) were shown to border individual fenestrae (183) as well as sieve plates and individual fenestrae within them (184). The treatment of rat LSEC with actin depolymerising drugs such as latrunculin, illustrated the relationship between fenestrae and the cytoskeleton since alterations in LSEC cytoskeleton were detected as well as an increase in the number of fenestrae (185). Secondly, the hypothesis that calcium ions regulate fenestrae diameter has also been proposed. The concept is supported by the role of calcium, calmodulin and actomyosin in the contraction of fenestrations whereby calcium-calmodulin

signalling modulates myosin light chain phosphorylation. The close association of calmodulin and actin microfilaments with the LSEC plasma membrane, indicates that the occurrence of calcium ions, calmodulin and actin microfilaments could be contributing to the contraction and dilatation of fenestrae (186). A mechanism for the contraction and dilatation of fenestrae were brought forward by Van der Smissen et al. and Oda et al. in 1986 and suggested that regulation of fenestrae diameter was influenced by a calcium-calmodulin-actomyosin system surrounding the nanopores (187,188). It is well known that fenestrae and fenestrae-forming centres (FFC) predominantly occur in the flat areas of the LSEC plasma membrane across the cell periphery. The sieve-raft hypothesis for the regulation of fenestrations indicates that the flat areas of the plasma membrane where fenestrations occur are situated between lipids rafts (189). These have been characterised as dynamic membrane micro-domain clusters enriched with cholesterol and sphingolipids, susceptible to morphological changes in response to intra- or extracellular stimuli (190). The existence of lipid rafts is a controversial concept itself, as it based on the idea that living membranes are not laterally homogeneous, however solid evidence towards how lipid rafts contribute to the regulation of signalling at the plasma membrane has yet to emerge (191). The final hypothesis concerning the regulation of fenestrae involves the scaffolding protein spectrin in the closed and open states of fenestrae (192). Spectrin mediates the connection of the plasma membrane to the actin cytoskeleton and is therefore integral in maintaining membrane integrity and transmembrane protein arrangement (193,194). Super-resolution fluorescence microscopy has significantly contributed to the establishment of the structural association between the actin cytoskeleton and fenestrae within sieve plates (184,195,196). It has been demonstrated that actin encircles fenestrations (184,192), and super-resolution images have indicated the uniform distribution

of actin and spectrin within the LSEC plasma membrane and specifically within sieve plates. It has also been deduced that a complete fenestrae-associated cytoskeletal ring (FACR) is required to mediate the transition to an open pore state thereby controlling fenestrae formation and the rapid switching between an open and closed state, termed 'blinking'. Moreover, it has been hypothesised that the 'blinking' of fenestrae is mediated by the fine tuning of actin depolymerisation and cytoskeleton degradation with the involvement of spectrin oxidation (192).

The remodelling of the LSEC cytoskeleton influencing fenestrae frequency is also of particular importance when isolating LSEC since cultured cells undergo a shift from an *in vivo* to an *in vitro* state. Imaging of live LSEC using Atomic Force Microscopy (AFM), has demonstrated the opening, and closing of individual fenestrations as well as sieve plates during LSEC attachment to the substrate provided *in vitro* (197). Even though fenestrae dynamics were shown to gradually slow down, within 20-minute window, fenestrae still maintained the capacity to migrate and alter their diameter up to 200% (198).

The inducibility of fenestrae on the LSEC membrane was first demonstrated by Steffan et al. in 1986 (199) by treating mouse LSEC with cytochalasin B which is a microfilament-inhibiting agent. Cytochalasin B induced an increase in fenestration number confirming the relationship between fenestrae and the cytoskeleton. This change proved to be reversible upon removal of cytochalasin B after a three-hour treatment. In contrast to this, colchicine which has a microtubule-disrupting effect did not impact the number of fenestrae and these findings emphasise the importance of the actin-cytoskeleton in fenestrae formation (200). As fenestrae are dynamic structures, their diameter can be altered leading to an overall change

in porosity of LSEC. Substances such as alcohol, dietary nutrients as well as pharmacological agents such as sildenafil citrate can rapidly mediate changes in fenestrations. An example of this is the enlargement of fenestrae to a range of 0.5-3 μm in diameter following acetaminophen treatment in mice assessed by TEM and SEM (201).

Sildenafil citrate indirectly increases the bioavailability of NO to LSEC which is a key regulatory molecule in liver homeostasis and disease, thereby promoting fenestrae formation (re-fenestration) and altering LSEC porosity. Sildenafil citrate has previously been used in mouse LSECs and was found to increase LSEC porosity (202). The mechanism of action involves the inhibition of phosphodiesterase type 5 (PDE-5) thereby inhibiting the breakdown of cGMP. The increased presence of cGMP in vasculature, and sinusoidal capillaries within the liver, leads to vasodilation (203).

1.5.6 LSEC as scavengers within the hepatic microcirculation

LSEC owe their very efficient blood clearance and endocytic properties to the fenestrations decorating their plasma membrane and also to the impressive array of receptors and adhesion molecules they express. LSEC are highly involved in the fine tuning of hepatic homeostasis by having a critical role in blood clearance by efficiently removing nanoparticles and waste macromolecules via receptor mediated endocytosis (204). As a result of the constant release of matrix macromolecule fragments such as collagens and connective tissue polysaccharides, e.g. hyaluronan, a large proportion of these molecules escapes lymph node clearance to and enter the general circulation. Here they reach the hepatic microcirculation where they are rapidly endocytosed and degraded by LSEC. The main receptors expressed by LSECs are

reviewed in the following section and their expression patterns in human LSEC *in vitro* will be presented in chapters 3 and 4.

The mannose receptor (CD206) is a type I transmembrane receptor within the C-type lectin receptor family. It plays a major role in blood clearance as it is a multi-ligand receptor. This is illustrated by its binding affinity for several different ligands through three different ligand binding domains it expresses. Within the liver, it is abundantly expressed by LSEC, and also by subgroups of macrophages such as KC but to a lesser extent (205). The C-type (C-type lectin) domain, which is calcium dependent, is responsible for carbohydrate binding, is present in eight copies and binds mannose and N-acetylglucosamine (206,207). A second domain, formed by a single fibronectin type II repeat, specifically recognises alpha chains present in collagen types I – IV and therefore effectively clears collagen waste molecules as well as the fibrinolytic tissue plasminogen activator (208,209). The third domain which is rich in cysteine and is characterised by a high affinity for sulphated N-acetyl-galactosamine residues (GalNAc-4-SO_4). As a result of this cysteine rich domain of the mannose receptor, hormone level control is carried out through the recognition and clearing of hormones such as lutropin and thyrotropin (210). A genetic fingerprint for human LSEC composed of 30 genes was established using GFP+ LSEC from *Tie2*-GFP mice. Only genes corresponding to human orthologs were included in the final fingerprint and microarray quantification revealed the mannose receptor (*Mrc1*) was within the top three abundant LSEC markers (211).

The scavenging activity of LSEC also contributes to hepatic immune function through the high expression of FcγRIIb (CD32B) which is the only inhibitory Fc receptor expressed by LSEC. It plays a key role in immune and inflammatory mechanisms by clearing small soluble immune

complexes (212). Functional evidence supporting the expression of Fc receptors on LSEC and not only KC, was presented by Muro et al. in mouse, rat, and human liver where small immune complexes were evenly distributed across the sinusoidal wall and binding was observed both on the luminal and abluminal compartments of LSEC with higher occurrence on the luminal side. It is also noteworthy that most of the immune complex binding was observed in LSEC compared to KC and was absent in portal veins and arteries as well as central veins (213,214). In mice, 90% of FcγRIIb expression can be assigned to LSEC, while lack of this receptor leads to the development of systemic lupus erythematosus (215). FcγRIIb is therefore an essential receptor for the efficient elimination of immune complexes which would otherwise be deposited on tissues and trigger an inflammatory response. Following the binding of immune complexes to FcγRIIb, they are internalised via clathrin-coated pits (212). This endocytic pathway distinguishes LSEC from other endothelial cells as in general, endothelial cells follow caveolae-mediated endocytosis. Despite the fact that LSEC express Caveolin-1, endocytosis via caveolae has not been reported (216). As a result of mRNA splicing, there are two splice variants of FcγRIIb receptor, namely FcγRIIb1 and FcγRIIb2 (217). The difference between them lies in the cytoplasmic tail of FcγRIIb2 which includes a domain required for the accumulation in coated pits. In FcγRIIb1 however, this domain is interrupted by a 47 amino acid insertion and therefore, endocytosis and internalisation via coated pits can only be mediated through FcγRIIb2 (218). As well as clearance of small soluble immune complexes, FcγRIIb ligands include fibrinogen-like protein 2 (FGL2) (219) and measles virus nucleocapsid protein (220). The distribution of FcγRIIb along the liver lobule varies between rodents and humans, with even distribution throughout the entire liver lobule in rat and mouse liver (56,132). In contrast to this, expression of FcγRIIb in human liver is absent in periportal areas

(100). In liver cirrhosis and hepatocellular carcinoma however, expression of FcγRIIb is downregulated (221,222).

Stabilin 1 (STAB1, FEEL-1, CLEVER-1) is a homeostatic endocytic receptor expressed on sinusoidal endothelium as well as macrophages although its expression in KCs has not been reported (223,224). It is involved in receptor mediated endocytosis and recycling and shuttles between the endosomal compartment and trans-Golgi network. Its role in the endocytosis of different forms of LDL such as oxidised LDL and acetylated (ac)LDL has been demonstrated using CHO and HeLa cells which were transiently transfected with stabilin-1 (225,226). Trafficking of stabilin-1/acLDL has been shown to be dependent on PI3K activity throughout the lysosomal-targeted endocytic pathway which confirmed that stabilin-1 mediated trafficking of acLDL utilises the classical endocytic pathway (227,228). The homeostatic function of stabilin-1 is illustrated by its ability to internalise and clear the glycoprotein SPARC, a well-known regulator of tissue remodelling and wound healing which has been implicated in the inhibition of VEGF interaction with the endothelial surface (229–231). SPARC expression is increased during chronic liver injury and its accumulation has been implicated in fibrogenesis in NASH (232).

Stabilin-2 is regarded as the main endocytic receptor for hyaluronan (233) and although it is structurally similar to stabilin-1 it is exclusively expressed on LSEC (234,235). Its involvement in hyaluronan uptake has been further illustrated in cultured LSEC using an anti-stabilin-2 antibody which inhibited hyaluronan accumulation in LSEC at a level > 98% (236). Additional ligands for endocytosis by stabilin-2 include formaldehyde-treated BSA, acLDL and glycosaminoglycan (237). The distribution of stabilin-2 expression was reported to be up to

50% on the plasma membrane and was also found to be more abundant than stabilin-1 on the cell surface (238). In terms of the involvement of stabilin-2 in pathogenic processes, reduction of stabilin-2 expression has been found to contribute to protection against atherosclerosis (239) while high expression levels have been associated with a poor prognosis in non-small cell lung cancer (240).

LYVE-1 is a member of the link protein superfamily, and its expression is a characteristic LSEC have in common with lymphatic endothelium where it functions as a hyaluronan receptor. LYVE-1 expression has been reported in healthy sinusoidal endothelium while downregulation of expression was observed in cirrhotic livers as well as cases of hepatocellular carcinoma (241). Characterisation of LYVE-1 expression using immunohistochemistry in chronically inflamed livers of varying aetiologies such as Hepatitis C, ALD, NASH and PBC has revealed reduced LYVE-1 expression while LSEC in livers marked by complete septal cirrhosis lacked LYVE-1 expression altogether (242). In addition, hepatic metastasis of WT31 melanoma cells in a LYVE-1 knock out mouse model was significantly reduced, thereby suggesting a regulatory role of LYVE-1 in hepatic metastasis (243).

LSECs also express C-type lectin domain family 4 member M (CLEC4M) endocytic receptor, which mediates the uptake of von Willebrand factor (VWF) and the blood coagulation factor VIII (FVIII) which circulate in blood plasma in dynamic equilibrium (244). The internalisation of VWF in CLEC4M expressing HEK 293 cells has been reported whereby it is transported to early endosomes (245). Further characterisation of the endocytic pathway mediating VWF uptake has revealed the involvement of clathrin-coated pits (246). CLE4M is also involved in the uptake of bacterial and viral pathogens (247).

1.5.7 The role of LSEC in leukocyte trafficking within the liver

LSEC mediate 70-80% of leukocyte adhesion during liver inflammation. Activation of the leukocyte adhesion cascade (248) involves a sequence of steps beginning with initial tethering and rolling of leukocytes to the luminal side of the blood vessel or capillary and enter a state of arrest which allows for strong adhesion. The adhesion of leukocytes is mediated by integrins activated by chemokines released within the tissue, which bind immunoglobulins expressed on the endothelial luminal surface. This is followed by transmigration into the tissue through the endothelial barrier to reach the site of inflammation. Transmigration is achieved through a series of changes to the cytoskeleton of both the endothelium and leukocytes as well as receptor-ligand interactions which allow leukocytes to migrate with no disruption to the vascular barrier (249,250). Although in general, tethering of leukocytes to the endothelial barrier involves selectins and E -selectin in particular is an adhesion molecule previously described to be upregulated in LSECs during disease (251), leukocyte tethering within the liver can be independent of selectins and rolling activity is generally not observed. Physical trapping of leukocytes instead of molecular adhesion within the sinusoids has also been proposed. This could be attributed to the fact that anatomically the sinusoidal capillaries are narrow, characterised by low shear stress and depending on the zonal location they are not wider than a flowing leukocyte (252).

In liver disease, LSEC express high levels of the conventional adhesion molecules involved in leukocyte attachment to the endothelium such as intercellular adhesion molecule 1 (ICAM1) and vascular cell adhesion molecule 1 (VCAM1) (253,254). The involvement of both ICAM1 and VCAM1 in lymphocyte recruitment has been demonstrated both *in vitro* and *in vivo*

assays. Lymphocytes bind to VCAM1 via $\alpha 4\beta 1$ integrin binding and this facilitates their capture from circulating blood as well as stabilisation (75,255). ICAM1 mediates strong adhesion by binding to integrin $\alpha L\beta 2$ (252). It has been demonstrated that mucosal vascular addressin cell adhesion molecule 1 (MADCAM1) which mediates lymphocyte trafficking to the gut through mucosal vessels, is upregulated in some chronic liver diseases. In these cases, it facilitates the recruitment of activated T cells expressing high levels of $\alpha 4\beta 7$ integrin within the gut. This strengthens the association of IBD with inflammatory liver disease such as primary sclerosing cholangitis (256,257). Molecules contributing to unconventional adhesion and migratory routes of lymphocytes within the hepatic sinusoids include vascular adhesion protein 1 (VAP1), an amine oxidase which was initially described to be involved in lymphocyte adhesion to post-capillary endothelial venules within lymph nodes (258). LSEC express VAP1 at high levels in chronic liver disease. The first study to report data from human LSEC on the activity of VAP1, demonstrated that VAP1 promotes lymphocyte adhesion and transmigration across LSEC under physiological shear stress. Blocking of VAP-1 resulted in decreased lymphocyte adhesion to LSEC stimulated by tumour necrosis factor α (TNF-α) by 50%, under conditions of flow, while the number of adherent lymphocytes that transmigrated across LSEC activated with LPS was significantly reduced (259). Several studies have confirmed that the enzyme activity of VAP1 can indirectly upregulate leukocyte recruitment by inducing the over-expression of adhesion molecules on LSEC (260–263). Additionally, Stabilin-1 and Stabilin-2, members of the scavenger receptor family, have also been implicated in leukocyte trafficking to the liver. Stabilin-1 expression is increased in chronic liver disease as well as hepatocellular carcinoma thereby mediating lymphocyte transmigration under conditions of shear stress. It

has also been suggested that Stabilin-1 might boost the recruitment of regulatory T cells (264). Stabilin-2 also plays a role in lymphocyte adhesion to LSECs by binding αMβ2 integrin (265).

Both paracellular and a transcellular routes of leukocyte transmigration across the hepatic sinusoids have been described. In the paracellular route, adherence to LSEC is followed by crawling along the endothelial surface prior to transmigration through endothelial junctions (266,267). Visualisation of migrating lymphocytes across LSEC under conditions of flow using confocal microscopy, has illustrated that 50% of cells followed the transcellular route of migration, thereby traveling directly through the endothelial cell body in contrast to the paracellular route (264). The transcellular migration route included the creation of ICAM1-rich channels which enabled lymphocyte migration (268). Intracellular crawling of lymphocytes within LSECs has also been described, whereby lymphocytes migrate to adjacent LSECs through cell junctions (269).

1.5.8 LSEC as antigen presenting cells

LSECs utilise scavenger receptors, the mannose receptor in particular to contribute to the regulation of adaptive immunity within the liver. LSECs ability for antigen-presentation to $CD8^+$ T cells has been demonstrated whereby the mannose receptor mediated the endocytosis, processing, and transfer of antigen to major histocompatibility complex (MHC) class I (270,271). Antigen uptake via the LSEC mannose receptor contributes to $CD8^+$ T cell tolerance, as well as tumour antigen tolerance (272,273). Moreover, antigen presentation including orally derived antigens, and expression of programmed cell death 1 ligand 1 (PDL1) by LSEC, mediates a tolerogenic response in naïve $CD8^+$ T cells. This is achieved by the activation of the receptor programmed cell death protein 1 (PD1) on naïve T cells (274–276).

T cell activation mediated by LSEC is adaptable and drives rapid effector T cell responses, depending on antigen load and the presence of local inflammatory factors. This has been illustrated *in vitro*, where mouse LSEC received antigens at variable concentrations for the purpose of cross presentation to $CD8^+$ T cells. Higher concentrations of antigen presented by LSEC lead to differentiation of T cells from a tolerogenic to an effector state resulting from enhanced T cell receptor signalling which overpowered PD-1 driven tolerogenic responses (277). MHC class II molecules are also expressed by LSEC which allow antigen presentation to $CD4^+$ T cells(278). The fact that LSEC express co-stimulatory molecules leads to regulatory T cell development instead of mediating the differentiation of naïve $CD4^+$ T cells to T helper cells (279,280). In mice it has been demonstrated that the tolerance inducing properties of LSEC regulate autoimmunity whereby an interaction between LSEC and circulating inflammatory $CD4^+$ T cells was shown to successfully suppress inflammatory cytokine release (281).

1.6 Imaging approaches for visualisation of fenestrae

1.6.1 Electron microscopy

Microscopy has always guided biological knowledge and discovery. Many of the receptors and features described in the preceding sections have been identified using traditional microscopy approaches. However, the size of the average LSEC fenestration means that specialised microscopy approaches are required for the visualisation of fenestrations. Electron microscopy (EM) specifically, initially used for the exploration of matter within the fields of material and soil sciences, has contributed immensely to the study of liver biology with the first description of fenestrations recorded by Yamagishi in 1959 using TEM. Eddie Wisse's work

with electron microscopy has also contributed enormously to the characterisation of LSEC fenestrae.

Electron microscopy utilises a focused beam of electrons to image a sample as opposed to photons used in light microscopy. Scanning electron microscopy (SEM) offers the advantage of providing a greater field depth to; therefore, a larger surface area of a sample can be imaged in a single field of view at nanometre resolution. The scanning electron microscope offers a view of the surface of a sample whereas for transmission electron microscopy (TEM), samples are sectioned thereby looking through a sample to visualise internal features. When the electron beam comes in contact with matter such as a biological sample, the interaction gives rise to high energy backscattered electrons, secondary electrons, and X-rays which are then collected by appropriate detectors. The advantage of EM is that electrons have a shorter wavelength than photons and this results in superior resolution (282). As with all imaging approaches, EM comes with limitations or compromises with regards to sample preparation.

1.6.2 The principle of fluorescence

Fluorescence microscopy has been an invaluable tool in studying cell physiology such as identifying and characterising transmembrane receptor expression or quantifying fluorescently labelled vesicles endocytosed by cells. The fundamental principle of fluorescence is based on light energy absorption in the form of a photon. This is followed by the emission of part of absorbed light energy in a matter of nanoseconds. This process results in some energy loss whereby the photon emitted has less energy than the photon absorbed. Based on the fact that light with a short wavelength (i.e 405 nm) has higher energy compared to longer light wavelengths (i.e 647 nm), emitted light from a fluorophore will usually have a

longer wavelength compared to the wavelength of the absorbed light at the point of excitation. This difference between excitation and emission wavelengths is termed as the Stokes shift (283). Laser scanning confocal microscopy is an essential imaging tool for the characterisation of expression of the repertoire of phenotypic markers contributing to LSEC identity (269). The use of fluorescent labels allows for the visualisation of the distribution of phenotypic markers such as scavenger receptors across the cell surface or tissue sample. Additionally, colocalization of different markers can be identified. The acquired image originates only from the focal plane with optical removal of noise emerging from sample thickness. The approach of optical sectioning employed by confocal microscopy is also suitable for imaging liver tissue sections. In confocal imaging, the chosen field of view in a specimen is focused on by the objective lens and scanning is carried out across it so that illumination and light detection are derived strictly from that specimen region. The pinhole can be adjusted to eliminate out of focus light and is recommended to image at 1AU, while a PMT detector situated behind it collects the light. Specialised computer software synchronised with the microscope build an image of the specimen, from the PMT detector output (284,285). A limitation of confocal microscopy is that it is a diffraction limited technique and therefore cannot resolve structural features below 300 nm such as fenestrations.

1.6.3 Seeing beyond the diffraction limit using super-resolution microscopy

The development of super-resolution fluorescence microscopy has reformed biological research in the last couple of decades by overcoming the resolution limit posed by the diffraction of light. Conventional microscopy is restricted to a resolution limit of $\sim\lambda/(2\,NA)$ (λ

is the wavelength and NA is the numerical aperture of the microscope system) referred to as the Abbe diffraction limit (286). Structured illumination microscopy (SIM) (287), stimulated emission microscopy (STED) (288), photo-activated localisation microscopy (PALM) (289,290), stochastic optical reconstruction microscopy (STORM) and *direct* stochastic optical reconstruction microscopy (*d*STORM). Super-resolution approaches such as STED overcome the diffraction limit by optically controlling the point spread function (PSF) which in the acquired image, is a blurred representation of how a single point looks like in the actual specimen (291). In a diffraction limited image for instance two PSFs closer than 300 nm apart would be seen as one blurred point within the image. STORM, *d*STORM and PALM, are super-resolution optical microscopy techniques also referred to as single molecule localisation microscopy techniques. STORM was developed in 2006 (292) and is known for its capability to achieve sub-diffraction resolution through single molecule localisation. This is achieved by the use of photo-switchable fluorescent probes which are sequentially switched “on” and “off” shifting between the excited state and dark state respectively, in each image frame. The continuous photo-switching throughout image frame acquisition allows for only a subset of fluorophores to be switched on in a given frame. A localisation algorithm is then used to determine the centres of all single fluorescent emitters within each frame at nanometre precision. Image resolution can be improved by 10 times, as long as sufficient localised fluorophores have been acquired from a large enough set of image frames (between 5000 – 40000 frames). Although the computational reconstruction and analysis of (*d*)STORM images can be a tedious process, this imaging approach offers a resolution down to approximately 20 nm using standard organic dyes (292–294). Even though the dye or fluorophore of choice is sample and imaging target dependent, localisation accuracy can be impacted by the number

of photons emitted as there can be single or multiple emitters within each acquired frame. *d*STORM can be carried out on a sample labelled with a standard organic fluorescent dye such as Alexa Fluor 647 (293) while STORM required an activator-reporter dye pair such as Alexa Fluor 405 - Alexa Fluor 647 (295).

*d*STORM has been successfully used for the imaging of fenestrations in rat LSEC so far (296). It is therefore within the scope of this thesis the explore the suitability of *d*STORM as an optical super-resolution imaging tool for imaging fenestrations in human LSEC *in vitro*. In order for *d*STORM to be successful, the synergy of the following factors is vital; 1) appropriate labelling (as well as density) of the imaging target, 2) achievement of sparse distribution of single fluorescent emitters within the field of view being acquired, through stochastic photo-activation of fluorophores during acquisition and finally, 3) accurate localisation of all single fluorescent emitters acquired in each image frame by choosing the correct reconstruction and image post-processing parameters. However, the fine tuning of the above parameters in order to achieve the most accurate imaging results possible presents a challenge in the field of biology (297). For the imaging of fenestrations in rat LSEC, the fluorescent probe used was CellMask™ Deep red plasma membrane stain (Thermo Fisher, C10046), which has also been used been used for the imaging of human LSEC as will be illustrated in Chapter 6. This is an indirect approach for the imaging of these nanopores which will be identified in each image as gaps in the membrane whereby there is an absence of signal as the result of the lack of labelling in those regions. Cell Mask™ Orange plasma membrane stain has also been used for imaging fenestrae in human LSEC using SIM however LSEC were isolated from liver tissue derived from patients undergoing hepatic resection for liver metastasis from colorectal cancer (298). CellMask™ Deep red is a suitable dye for *d*STORM as it is a far-red dye, and its

photo-switchable properties can be manipulated by using a chemical buffer which is added to the sample immediately prior to acquisition (296).

1.7 Scope of this work

The increasing burden and prevalence of liver disease and liver cirrhosis worldwide emphasise the need to understand the pathophysiological events leading the initiation and progression of fibrosis during chronic liver disease. As LSEC play a crucial role in maintaining hepatic homeostasis (299), it is crucial to study and compare the phenotype of LSEC in health and disease in order to uncover key phenotypic changes and molecular interactions contributing to their role in disease. Although major research progress has been made in the study of liver biology and disease in animal models (300) and *in vitro* (301), specific phenotypic changes of human LSEC in healthy and diseased conditions require further exploration.

The following aims will be explored in the data presented in this thesis:

- The identification of differences in expression of LSEC specific as well as classical endothelial markers at both protein and mRNA level in healthy donor and cirrhotic liver tissue
- The isolation of primary human LSEC from healthy donor and cirrhotic liver tissue specimens
- The confirmation of LSEC identity in vitro via scavenger receptor expression and endocytic capacity
- Analyse the effect of passaging on the development of an LSEC capillarised phenotype *in vitro.*

- Treatment of LSEC with NO-signaling enhancing agents to analyse the potential restoration of LSEC differentiated phenotype.
- Develop a dSTORM imaging protocol tailored to visualising fenestrations in human LSEC.
- Assess the effect of sildenafil citrate on LSEC fenestrations using the optimised dSTORM protocol.

2 Materials and methods

2.1 Use of human tissue samples

All tissue used in this study was collected at the Liver and Hepatobiliary Unit, Queen Elizabeth Hospital, Birmingham, with prior written informed patient consent and local research ethics committee approval 06/Q2708/61 (Immune Regulation) and 18-WA-0214 (Liver Inflammation)). Donor material was surplus to requirement for transplantation, whilst diseased tissue was collected from explanted livers upon transplantation for cirrhotic liver diseases (e.g. primary biliary cholangitis (PBC), alcoholic liver disease (ALD), primary sclerosing cholangitis (PSC), non-alcoholic steatohepatitis (NASH) and autoimmune hepatitis (AIH)). Samples from human tissue explants were fixed in formalin prior to paraffin embedding as well as gradually frozen in a foil boat over liquid nitrogen and stored in -80°C.

2.1.1 Antibodies used for immunohistochemistry and immunocytochemistry

A variety of immunohistochemical approaches were used to study LSEC in tissue and in culture. Thus, for clarity the reagents used have been combined into the tables to follow.

Company ref#	**Description**	**Species/Clone**	**Working concentration**	**Antigen retrieval Buffer**	**Secondary antibody reagent**
Abcam ab77093	Anti-CD32B	Goat polyclonal	3.8 µg/ml	pH 6	ImmPRESS HRP anti-goat polymer detection kit (MP-7405, Vector Labs)
Abcam ab45143	Anti-CD32B	Rabbit monoclonal/ EP888Y	0.995 µg/ml	pH 9	ImmPRESS HRP anti-rabbit polymer detection kit (MP-7401, Vector Labs)
Abcam 187377	Anti-CD31	Mouse monoclonal/ [C31.3] IgG1	2 µg/ml	pH 9	ImmPRESS HRP anti-mouse polymer detection kit (MP-7452, Vector Labs)
Abcam ab33682	Anti-LYVE1	Rabbit polyclonal	5 µg/ml	pH 9	ImmPRESS HRP anti-rabbit polymer detection kit (MP-7401, Vector Labs)
DAKO M0616	Anti-Von Willebrand Factor	Mouse monoclonal/ F8/86	0.252 mg/ml	pH 9	ImmPRESS HRP anti-mouse polymer detection kit (MP-7452, Vector Labs)
Sigma-Aldrich HPA042661	Anti-CLEC4M	Rabbit polyclonal	1 µg/ml	pH 9	ImmPRESS HRP anti-rabbit polymer detection kit (MP-7401, Vector Labs)
Invitrogen PA5-55447	Anti-Stabilin-2	Rabbit polyclonal	0.2 µg/ml	pH 9	ImmPRESS HRP anti-rabbit polymer detection kit (MP-7401, Vector Labs)
Abcam ab64693	Anti-Mannose	Rabbit polyclonal	2.5 µg/ml	pH 6	ImmPRESS HRP anti-rabbit polymer detection kit (MP-7401, Vector Labs)

Abcam ab192869	Anti-Caveolin-1	Rabbit monoclonal/ EPR15554	3 µg/ml	pH 9	ImmPRESS HRP anti-rabbit polymer detection kit (MP-7401, Vector Labs)
Abcam ab34710	Anti-Collagen I	Rabbit polyclonal	5 µg/ml	pH 9	ImmPRESS HRP anti-rabbit polymer detection kit (MP-7401, Vector Labs)
Thermo Fisher cat#02-6202	Goat IgG isotype control	Goat	3.8 µg/ml	Primary antibody dependent	ImmPRESS HRP anti-goat polymer detection kit (MP-7405, Vector Labs)
DAKO X0931	Mouse IgG1 isotype control	Mouse	0.252 mg/ml and 2 µg/ml	Primary antibody dependent	ImmPRESS HRP anti-mouse polymer detection kit (MP-7452, Vector Labs)
Abcam ab34417	Rabbit polyclonal isotype control	Rabbit	0.995-5 µg/ml	Primary antibody dependent	ImmPRESS HRP anti-rabbit polymer detection kit (MP-7401, Vector Labs)

Table 2.1: Antibodies use for immunohistochemistry

Company ref#	**Description**	**Species/Clone**	**Working concentration**	**Secondary antibody reagent**
Abcam ab33682	Anti-LYVE1	Rabbit polyclonal	5 µg/ml	Goat anti-rabbit IgG Alexa Fluor plus 594 (A32740, Thermo Fisher)
Abcam ab151497	Anti-CD32B	Rabbit polyclonal	2 µg/ml	Goat anti-rabbit IgG Alexa Fluor plus 594 (A32740, Thermo Fisher)
Abcam ab187377	Anti-CD31	Mouse monoclonal/ [C31.3] IgG1	2 µg/ml	Goat anti-mouse IgG1 Alexa 488 (A21121, Thermo Fisher)

Table 2.2: Antibodies used for immunocytochemistry and immunofluorescence

2.1.2 Studies using human tissue samples

2.1.2.1 Histology

2.1.2.1.1 Haematoxylin and Eosin (H&E)

General morphology and level of steatosis of human tissue sections were assessed by conducting haematoxylin and eosin (H&E) staining. Formalin fixed paraffin embedded (FFPE) tissue sections cut at 4µm thickness were stained using in house protocol consisting of sequential baths of reagents in the order and duration indicated in Table 2.3. Sections were mounted with a 24x40 mm #1.5 glass coverslip (0102192, Paul Marienfeld) in DPX mounting medium (SEA-1304-00A, Cell Path) at the end of the staining procedure and left to air-dry overnight. Each section was scanned using Zeiss Axioscan Z1 slide scanner (Zeiss) with a 20x objective. Representative fields of view were taken using Zen Blue software (Zeiss).

Reagent	Duration
Xylene	2 min (3x)
Alcohol	2 min (3x)
Water	2 min (2x)
Harris Haematoxylin	4 min
Water	2 min
Acid alcohol	30 secs
Water	2 min
Scott's tab water substitute	30 secs
Water	2 min
Eosin	1 min
Water	2 min
Alcohol	2 min (4x)
Xylene	2 min (3x)

Table 2.3: Protocol for H&E staining

2.1.2.2 Van Gieson staining

The degree of fibrosis and collagen deposition in human tissue sections was assessed using Van Gieson (VG) staining. Formalin fixed paraffin embedded (FFPE) tissue sections cut at 4µm thickness were stained using an in-house protocol consisting of sequential baths of reagents in the order and duration indicated in Table 2.4. Sections were mounted with a 24x40 mm #1.5 glass coverslip in DPX mounting medium at the end of the staining procedure and left to air-dry overnight. Each section was scanned using Zeiss Axioscan Z1 slide scanner (Zeiss) with a 20x objective. Representative fields of view were taken using Zen Blue software (Zeiss).

Reagent	Duration
Xylene	2 min (3x)
Alcohol	2 min (2x)
Water	5 min
Celestine Blue	5 min
Water	2 min
Water	2 min
Harris Haematoxylin	4 min
Water	2 min
Acid Alcohol	30 secs
Water	2 min
Scott's tab water substitute	30 secs
Water	2 min
Van Gieson	3 min
Alcohol	3 min (2x)
Xylene	2 min (3x)

Table 2.4: Protocol for van Gieson staining

2.1.3 Immunohistochemical analysis of liver sinusoidal endothelial cell markers in normal and cirrhotic liver tissue

Characterisation of the expression of LSEC markers in human liver tissue was carried out using immunohistochemistry on formalin-fixed paraffin-embedded (FFPE) sections cut from normal and cirrhotic liver samples at 4 µm thickness. Sections were dewaxed in sequential baths of xylene and alcohol and rehydrated using water as outlined in Table 2.5. Depending on the primary antibody being used, the sections were then immersed in citrate based (H-3300, Vector Labs) or Tris-based (H-3301, Vector Labs) antigen retrieval buffer to expose antigens masked by cross linking as a result of formalin fixation. The antigen retrieval solution was prepared by adding 10 ml of antigen retrieval buffer to 1L of distilled water and preheating in the microwave for 10 minutes. Heat-induced antigen retrieval (HIAR) on the dewaxed and rehydrated tissue sections was then carried out in the microwave for 30 min. Following HIAR, sections were cooled by running cold tab water directly into the antigen retrieval solution. Tissue sections were then washed in phosphate buffered saline (PBS) supplemented with 0.1% Tween®20 (PBS-T) (Sigma, P1379) for 5 minutes with constant agitation provided by a magnetic stirrer.

Using a hydrophobic pen (Vector Labs), a frame was drawn around each section before proceeding with blocking steps. The sections were carefully positioned in a humidified chamber which was placed on a rocker during long incubation steps. Endogenous peroxidase activity was blocked using BLOXALL (SP-6000, Vector Labs) solution for 20 minutes followed by a 5-minute wash step in PBS-T with constant agitation. Protein binding activity was blocked for 30 minutes using 2x casein (SP-5020, Vector labs) prepared in distilled water. The primary antibodies were prepared at the appropriate working concentration (Table 2.1) using PBS-T

and incubated for 1 hour at room temperature or at 4°C overnight. This was followed by a 5-minute wash step with PBS-T and then 2-3 drops of the ImmPRESS HRP polymer detection kit of the appropriate species was applied on each section for 30 minutes. This was followed by washing the sections twice in PBS-T and the immunoreaction was visualised by incubating with ImmPACT DAB Substrate, Peroxidase (HRP) (SK-4105, Vector Labs) for 5 minutes. Following this, sections were washed with water and nuclei were counterstained with filtered Mayer's Haematoxylin. Finally, sections were washed with water, dehydrated, and cleared in sequential baths of alcohol and xylene as indicated in Table 2.5 and mounted in DPX mounting medium. Sections were left to dry overnight, and all staining was initially assessed under a bright field microscope, followed by scanning using Zeiss Axioscan Z1 slide scanner with a 20x objective. Five representative fields of view per case were taken using Zen Blue software (Zeiss) including isotype matched controls. Fiji software (302) was used for quantification of the staining as follows. Each field of view obtained using Zen Blue software was imported into Fiji and thresholded to select for stained the stained area. The area was then quantified using measure function in Fiji. The average area per biological replicate was then used for statistical analysis.

Reagent	Duration
Xylene	3 min (3x)
Alcohol	3 min (3x)
Water	3 min (2x)

Table 2.5: Liver tissue dewaxing and rehydration steps for immunohistochemistry

2.1.4 Immunofluorescent labelling of liver sinusoidal endothelial cell markers in human liver tissue

The co-expression of liver sinusoidal endothelial cell markers in human liver tissue was characterised using dual immunofluorescent labelling and this was carried out by following the protocol described above (section 2.1.3) with the following modifications. Blocking of endogenous peroxidase activity was not necessary. Protein binding activity was blocked for 30 minutes using 2x casein (SP-5020, Vector labs) and 10% goat serum (31872, Thermo Fisher) prepared in distilled water. Primary antibody incubation and washing of tissue sections was carried out as described above. Secondary fluorescent antibodies (Table 2.2) were prepared in PBS at 4 μg/ml and 250-350 μl were applied to each tissue section depending on the size. The secondary reagent was incubated at room temperature for 30 minutes on a rocker. This was followed by washing the sections twice in PBS-T for 5 minutes. Nuclear counterstaining was carried out using 4', 6'-Diamidino-2-Phenylindole (DAPI) (D1306, Thermo Fisher) which was applied at 300 nM for 5 minutes. Tissue sections were then washed in distilled water for 5 minutes and mounted in fluorescence mounting medium (S3023, Agilent). Mounted sections were allowed to dry overnight while protected from light. Immunofluorescent labelling was visualised, and representative images were captured using LSM 880 confocal microscope (Zeiss). The captured Images were then processed using Zen Blue 3.1 software (Zeiss).

2.1.5 Isolation of Liver Sinusoidal Endothelial Cells (LSEC) from human liver tissue

The Centre for Liver and Gastrointestinal Research (CLGR) has a standard method for the isolation of LSEC (303) which was carried out as follows; a slice of liver tissue (between 40g and 50g) was mechanically chopped very finely using a scalpel and any obvious vascular areas were removed. The tissue was then incubated in 5 ml of Collagenase type I A (0.01g/ml; from Clostridium Histolyticum, C9891, Sigma Aldrich) in 20 ml sterile PBS at 37°C with continuous agitation for 20 to 30 minutes. Incubation periods were adjusted according to the texture of the liver tissue as cirrhotic specimens required a slight increase in incubation time with collagenase. The liver tissue digest was then filtered through a fine mesh while being washed through with sterile PBS at room temperature. This was then aliquoted into 8 universal tubes (approximately 20 ml per tube; 128AFS, Thermo Fisher) and centrifuged at 870 x *g* for 5 minutes (acceleration set at 9 and deceleration set at 9 for all downstream centrifugation steps unless otherwise specified, using the centrifuge Rotanta 460, Hettich®). The supernatant was discarded carefully in order to avoid loss of the pellet as it was quite loose at this step. The pellet was resuspended in 1.5 ml of PBS and two pellets were combined into one universal tube and the volume made up to 25 ml in each tube with PBS. The sample was then centrifuged at 870 x *g* for 5 minutes and these steps were repeated until all pellets wee combined into one universal tube and the volume was made up to 25 ml with PBS. This was layered in 3 ml aliquots over a Percoll gradient to separate parenchymal and non-parenchymal cell fractions. Percoll gradient stock solutions were prepared as follows; stock Percoll was prepared using 99ml Percoll (17089101, Sigma Aldrich) and 11ml 10x PBS. 33ml of the stock was added to 67ml of 1x PBS to prepare the 33% Percoll. 77ml of stock Percoll was added to 23ml of 1x PBS for the preparation of 77% Percoll. The gradient was prepared in each of 8

Falcon tubes (15 ml) with 3ml of 33% (top layer) and 3 ml 77% (bottom layer) Percoll. The Percoll gradients were centrifuged at 870 x *g* for 25 minutes with acceleration set at 9 and deceleration set at 2. Following Percoll gradient centrifugation, the top layer was aspirated and discarded, and the non-parenchymal cell layer was collected, located between the parenchymal and red cell fractions, as illustrated in Figure 2.1. Two layers were combined in one universal tube and after all non-parenchymal cell layers were collected, the 4 universal tubes were centrifuged at 870 x *g* for 5 minutes, the supernatant was discarded, and the pellet was resuspended in PBS. Two pellets were combined into one universal tube and the volume was made up to 25 ml. The two universal tubes were centrifuged as previously, the supernatants were discarded, and the two pellets were combined into one 15 ml Falcon tube which was centrifuged at 870 x *g* for 5 minutes and the supernatant was discarded. The pellet was then resuspended in 500 µl PBS. The next and final part of the protocol was the immunomagnetic selection of specific cell populations. Firstly, the negative selection of BEC was carried out using anti-EP-CAM mouse anti-human antibody (61004, Progen) at 2.5 µg/ml. Here a 50 µl working aliquot of anti-EP-CAM antibody was added to 500 µl of cell suspension and incubated for 30 minutes at 37°C with intermittent agitation in a 15 ml Falcon tube. At the end of incubation, PBS was added in order to make the volume up to 14 ml and the sample was centrifuged at 870 x *g* for 5 minutes. The pellet was resuspended in 500 µl ice cold PBS and 10 µl of goat anti-mouse magnetic beads (11033, Thermo Fisher) was added to the cell suspension. The Falcon tube was placed on ice and incubated for 30 minutes with constant agitation on a rocker at 4°C. This was followed by adding 5 ml ice cold PBS and mixing well before adding the tube to the cell separation magnet (DynaMag^{TM}, 12301D, Thermo Fisher) for 2 minutes. Magnetic-bead bound cells (EP-CAM positive) adhered to the sides of the tube

and the supernatant was collected and placed in a new 15 ml Falcon tube. This step was repeated twice more. The new Falcon tube containing the collected supernatant (EP-CAM negative cells) was placed in the magnet for 2 minutes to remove any residual beads. The supernatant was collected, placed in a new Falcon tube, and centrifuged at 870 x *g* for 5 minutes. After this, the supernatant was discarded, and the pellet was resuspended in 500 µl ice cold PBS. At this point LSEC were positively selected using 10µl of CD31 coated magnetic beads (11155D, Thermo Fisher) added to 500 µl of cell suspension or the anti-CD32b antibody (ab151497) at 2 µg/ml followed by 10 µl of Dynabeads™ M-280 sheep anti-rabbit IgG coated magnetic beads (11203D, Thermo Fisher). The Falcon tube was placed on ice and incubated for 30 minutes at 4°C with constant agitation provided by a rocker. This was followed by adding 5 ml ice cold PBS and mixing well before adding the tube to the magnet for 2 minutes. Magnetic bead bound cells (CD31/CD32B positive) were attached to the sides of the tube and supernatant was collected and discarded. This step was repeated twice more. The CD31 positive cells remaining in the Falcon tube were then resuspended in 5 ml of pre-warmed complete LSEC media, placed in a 25 cm^2 flask pre - coated with rat tail collagen (RTC) and incubated at 37°C. Details of these media are supplied below.

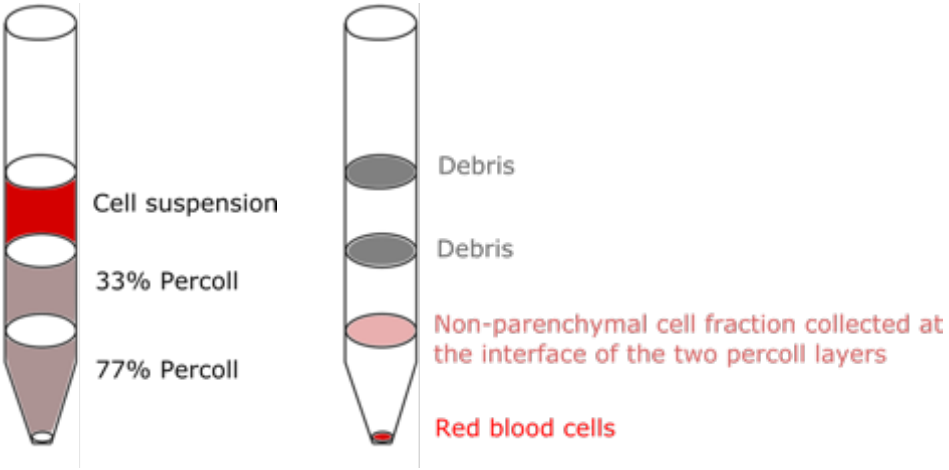

Figure 2.1: Schematic representation of Percoll gradients for separation of parenchymal and non-parenchymal liver cell populations

The images show the appearance of the gradient before and after centrifugation (left to right).

2.1.6 Isolation of RNA from human liver tissue

In order for downstream quantitation of mRNA expression levels of liver sinusoidal endothelial markers and regulatory molecules to be carried out, RNA was extracted from cryopreserved donor and explanted liver tissue specimens (section 2.1) as follows. Liver tissue specimens were kept on dry ice and 25 mg of each specimen was excised and weighed. The primary tissue material was then added to 2 ml reinforced tubes prefilled with 1.4 mm ceramic beads (1177770, Camlab) containing 600 µl RLT buffer (10 µl of β-mercaptoethanol was added per 1ml of buffer). All tubes were kept on ice. This was followed by tissue disruption and homogenisation by using the Omni Bead Ruptor 12 Bead Mill Homogeniser (Camlab) at speed level 4 for two cycles of 20 seconds. This was repeated twice, and samples were kept on ice in

between repeats. After tissue lysis and homogenisation, RNA was extracted using the Rneasy® Mini kit from QIAGEN as described in section 2.2.2.3.

2.2 Studying the phenotype of human liver sinusoidal endothelium *in vitro*

2.2.1 Culture and expansion of primary Liver Sinusoidal Endothelial Cells (LSECs)

Freshly isolated LSECs were resuspended in complete medium consisting of Human Endothelial serum free medium (11111044, Thermo Fisher) supplemented with penicillin and streptomycin solution (100 units/ml; 151 40-122, Thermo Fisher) human serum (10%, CS100-500, TCS Biosciences), 10ng/ml of each of Vascular Endothelial Growth Factor (VEGF; 100-20, Peprotech) and Hepatocyte Growth Factor (HGF; 100-39, Peprotech). LSEC were grown as a monolayer in a 25cm^2 tissue culture flask coated with RTC type I at 25 µg/ml (C3867, Sigma Aldrich) in sterile distilled water and incubated at 37°C with ambient O_2 and 5% CO_2. TryplE (12605010, Thermo Fisher) was used for harvesting and expansion of LSEC as follows; existing growth media was aspirated from the flask and discarded. Sterile PBS was used for washing the LSEC monolayer to remove all traces of human serum. TrypLE express enzyme (3ml; 12605028, Thermo Fisher) was added to a 25cm^2 flask and incubated for no longer than 3 minutes. Following light tapping of the flask and assessment under the light microscope to check for complete detachment of the cell monolayer, 5ml of PBS were added to the flask in order to dilute the TrypLE. All contents of the flask were immediately aspirated, transferred to a 15 ml Falcon tube, and centrifuged at 870 x *g* for 5 minutes. The supernatant was discarded and the LSEC pellet was resuspended in 10 ml of complete medium. The cell suspension was seeded in a 75cm^2 flask (pre-coated with RTC) and cultured until fully

confluent before being harvested as described above for further experiments. Cells were typically used between passage 2 (early) and 5 (late) for experimentation.

2.2.2 Phenotypic and functional analysis of primary human Liver Sinusoidal Endothelial Cells

2.2.2.1 Immunocytochemistry on cultured LSEC

Expression of markers indicating a differentiated sinusoidal endothelial phenotype was assessed by immunocytochemistry on LSEC at early and late-stage passages. Primary and secondary antibodies used are outlined in Table 2.2. LSEC were harvested as described above (2.2.1), seeded at 70 000 cells per channel in a 6-channel μ-slide (#80606, Ibidi) and incubated overnight at 37°C. Growth media was aspirated and LSEC were washed twice with PBS and then fixed with 4% paraformaldehyde (PFA) in PBS for 10 minutes at 37°C. After the PFA was aspirated, LSEC were washed by flushing 1 ml PBS though each channel. LSEC were permeabilised with 0.1% Triton™ X-100 (X100, Sigma Aldrich) in PBS for 5 minutes. This was followed by blocking of unspecific staining with 1% BSA and 10% goat serum in PBS for 30 minutes. Primary antibodies were prepared at the desired working concentration (Table 2.2) in PBS-T and incubated within the channel containing LSEC for 1 hour at room temperature or overnight at 4°C on a rocker. Isotype matched control (IMC) antibody was prepared at the same concentration as the primary antibody, in PBST. 100 μl of primary antibody solution or isotype matched control was added to each channel of the ibidi μ-slide. The primary antibody solution and IMC were aspirated and LSEC were washed 3 times by pipetting PBS-T through each channel. All secondary fluorescent antibodies were prepared at 4 μg/ml in PBS, 100 μl was added to each channel and incubated for 30 minutes at room temperature on a rocker.

The secondary antibody solution was then aspirated and LSEC were washed by pipetting 1 ml PBS-T through each channel. Cell nuclei were counterstained using DAPI (D1306, Thermo Fisher) which was applied at 300 nM for 5 minutes. DAPI was then aspirated and LSEC were washed by pipetting 1 ml PBS through each channel. Samples were stored and imaged in PBS on the LSM 880 Confocal Microscope with Airyscan (Zeiss) using a 40x water immersion objective and five fields of view were acquired per channel.

2.2.2.2 Tracking the effect of in vitro capillarisation on the endocytic capacity of LSEC

Albumin labelled with fluorescein isothiocyanate conjugate (FITC-BSA) (A9771, Sigma Aldrich) was used as a ligand in an uptake assay in order to assess the endocytic capacity of LSEC *in vitro*. LSEC were seeded at 70 000 cells per channel in an RTC coated 6-channel µ-slide with a #1.5 polymer coverslip (80606, Ibidi) and incubated overnight at 37°C. LSEC were then serum starved for two hours in Human Endothelial serum free medium and the FITC-BSA ligand was prepared in Human Endothelial serum free medium and was protected from light. The ligand was applied at 20 µg/ml for 30 minutes. The ligand solution was aspirated and LSEC were washed by flushing 1 ml of sterile PBS through each channel to remove any traces of FITC-BSA ligand and media. The PBS was aspirated and LSEC were fixed with 4% PFA for 10 minutes at 37°C. The PFA was aspirated and LSEC were washed by flushing 1 ml of sterile PBS through each channel. Cell nuclei were then permeabilised with 0.1% Triton™ X-100 (X100, Sigma Aldrich) in PBS for 5 minutes and stained with DAPI (as above) and Alexa Fluor 633 Phallloidin (A22284, Thermo Fisher) at 165 nM in PBS for 15 minutes at room temperature. LSEC were imaged using the LSM 880 Confocal microscope (Zeiss) using a 40x water immersion objective.

All images acquired were processed for quantitation of vesicles in each field of view as follows; each image was split into separate channels (i.e green for the FITC-BSA vesicles and blue for cell nuclei). First, the green channel was thresholded in order to segment the FITC-BSA vesicles. The thresholding was adjusted in order to exclude as much background as possible without compromising the number of vesicles detected and was then applied to the image. Using the analyse particles function in Fiji software the number of vesicles per field of view was determined. The same approach was applied for the quantitation of cell nuclei in the blue channel. The number of vesicles quantified in each field of view was normalised to the number of cell nuclei to obtain the value presented as vesicles/cell.

2.2.2.3 RNA extraction

Total ribonucleic acid (RNA) was extracted from treated LSEC and passaged LSEC in normal culture conditions using the RNeasy® Micro kit and Rneasy® Mini kit from QIAGEN, respectively, as per manufacturer's instructions. LSEC treated in 6-well plates were harvested from each well by washing with 1x PBS prior to adding 350 µl of buffer RLT. This was followed by scraping the cells from each well using a cell scraper. The cells were then aspirated, placed in a cryovial and vortexed followed by snap freezing in liquid nitrogen and storage at -80°C until RNA extraction. Both low and high passage cells were used to prepare RNA. Passaged LSEC were harvested from a 75 cm^2 flask as described above (section 2.2.1) and 600 µl of buffer RLT was added to the pellet and resuspended for pellet disruption, lysed further by resuspending the sample using a 19-gauge needle and 1ml syringe at least 8 times. The lysed

LSEC were homogenised by vortexing, snap frozen in liquid nitrogen and stored at -80°C until RNA extraction.

The following reagents were prepared as below before extracting RNA using the RNeasy® Micro kit:

- Buffer RLT: addition of 10 µl of β-mercaptoethanol per 1ml of buffer
- Buffer RPE: addition of 44 ml ethanol to 11ml concentrate
- 70% ethanol: dilution of 100% ethanol in RNase-free water
- 80% ethanol: dilution of 100% ethanol in RNase-free water
- DNase I stock solution: lyophilised DNase I (1500 Kunitz units) dissolved in 550 µl of RNase-free water and mixed gently by inverting the vial. Stock DNase I solution was then aliquoted into single use aliquots and stored at -20°C for future experiments.

The RNA extraction procedure was carried out as follows; for treated cell pellets, lysates were thawed on ice and vortexed. Proper lysis of cells was ensured by resuspending the sample using a 19-gauge needle and 1ml syringe at least 8 times. Then, 1 volume of 70% ethanol was added to the lysate and mixed well by pipetting. The sample was then transferred to a MinElute spin column placed in a 2 ml collection tube and centrifuged at 8000 x *g* for 15 seconds. The flow-through was discarded and 350 µl of Buffer RW1 was added to the column which was then centrifuged at 8000 x *g* for 15 seconds to wash the spin column membrane. The DNase I incubation mix was prepared by adding 10 µl DNase I stock to 70 µl Buffer RDD and mixed by inverting the tube. 80 µl of the DNase I incubation mix was added to each spin column, directly to the membrane, and incubated for 15 minutes at room temperature. Then, 350 µl of Buffer RW1 was added to the spin column which was centrifuged at 8000 x *g* for 15

seconds to wash the spin column membrane. The flow-through was discarded and the spin column was placed in a new 2 ml collection tube. 500 µl of Buffer RPE was added to the spin column which was centrifuged at 8000 x *g* for 15 seconds to wash the spin column membrane. Flow-through was discarded and 500 µl of 80% ethanol was added to the spin column which was centrifuged at 8000 x *g* for 2 minutes to wash the spin column membrane. Flow-through and collection tube were discarded. Each spin column was then placed in a new collection tube and centrifuged at full speed (16.3 x *g*) for 5 min. The flow through along with the collection tube were discarded and each spin column was placed in a new 1.5 ml collection tube. 14 µl of RNase-free water was added directly to the centre of each spin column membrane and samples were centrifuged for 1 min at full speed to elute the RNA.

For the RNA extraction from passaged LSEC samples, the RNeasy® Mini kit was used and the following reagents were prepared as below before extracting RNA:

- Buffer RLT: addition of 10 µl of β-mercaptoethanol per 1ml of buffer
- Buffer RPE: addition of 44 ml ethanol to 11ml concentrate
- 70% ethanol: dilution of 100% ethanol in RNase-free water
- DNase I stock solution: lyophilised DNase I (1500 Kunitz units??) dissolved in 550 µl of RNase-free water and mixed gently by inverting the vial. Stock DNase I solution was then aliquoted into single use aliquots and stored at -20°C for future experiments.

The RNA extraction procedure was carried out as follows; cell pellet lysates were thawed on ice and vortexed. 1 volume of 70% ethanol was added to the lysate and mixed well by pipetting. Up to 700 µl of the sample was then transferred to an RNeasy spin column placed in a 2 ml collection tube and centrifuged for 15 seconds at 8000 x *g*. Flow through was

discarded and any remaining lysate was transferred to the spin column and centrifuged for 15 seconds at 8000 x *g*. The resulting flow through was discarded and 700 µl Buffer RW1 was added to the spin column. This was centrifuged for 15 seconds at 8000 x *g* to wash the membrane and the flow through was discarded. Next, 500 µl Buffer RPE was added to the spin column which was centrifuged for 15 seconds at 8000 x *g* and flow through was discarded. 500 µl Buffer RPE was added to the spin column once more and centrifuged for 2 minutes at 8000 x *g* to dry the spin column membrane. The collection tube and flow through were discarded and the RNeasy spin column was placed in a new 2 ml collection tube and centrifuged at full speed for 1 minute. Finally, in order to elute the RNA, the spin column was placed in a new 1.5 ml collection tube and 30 µl RNAse-free water was directly added to the spin column membrane. This was centrifuged for 1 minute at 8000 x *g*.

Purity and concentration of extracted RNA were recorded using a NanoPhotometer (Implen, 7122 V2.1.0). The values for the ratios 260/280nm and 260/230nm were used to evaluate the purity of RNA where a value of 2 indicated a relatively pure RNA yield.

2.2.2.4 cDNA synthesis

RNA was reverse transcribed into single stranded complementary deoxyribonucleic acid (cDNA) for use in real-time PCR using the High-Capacity cDNA Reverse Transcription kit (#4368814, Applied Biosystems). Each sample was prepared using the same total RNA concentration in a final reaction volume of 20 µl. The reaction mixture consisted of 2 µg RNA, 2 µl 10x RT Buffer, 0.8 µl of dNTP mix, 2 µl Random Primers, 1 µl MultiScribe Reverse Transcriptase, 1 µl RNase inhibitor along with variable volumes of RNase-free water. Each

sample was gently mixed and centrifuged for 30 seconds before being placed in the thermal cycler. For the reverse transcription reaction, the samples were incubated at 25°C for 10 minutes, followed by 120 minutes at 37°C and 5 minutes at 85°C. The samples were then ready for immediate real-time PCR analysis or were stored at -20°C until further use.

2.2.2.5 Real-time PCR using Taqman primers

Analysis of gene expression by real-time PCR was carried out in triplicate for each sample in a final reaction volume of 10 µl. The reaction mixture was made up of 0.5 µl cDNA, 5 µl Applied Biosystems™ Taqman™ Universal Master Mix II NO UNG (4440040, Thermo Fisher), 0.5 µl of taqman primer and 4 µl water. The list of primer-probe sets of Taqman Gene Expression Assays (Thermo Fisher, USA) used is displayed in Table 2.6. The PCR plate was centrifuged briefly before being loaded onto the Roche LightCycler® 480 Real-time PCR system. Cycling conditions were as follows: 95°C for 15 seconds, 60°C for 1 minute and 72°C for 1 second.

Light Cycler® 480 software was used for data analysis by advanced relative quantification and gene expression levels were normalised to *SRSF4* housekeeping gene. The threshold cycle (C_T) value for each well was calculated on the real-time cycler software using the second derivative max setting. Gene expression data were then normalised to *SRSF4* messenger ribonucleic acid (mRNA) and relative transcript levels were calculated with the comparative Ct method ($2^{-\Delta\Delta CT}$) (304) For gene expression changes in LSEC treated with VEGF and sildenafil citrate, mRNA expression was expressed as fold change to control. GraphPad Prism 9.0 (GraphPad, US) was used for displaying the results.

Assay ID	Gene Symbol	Gene name
Hs01634996_s1	*FCGR2B*	Fc fragment of IgG receptor IIb
Hs01065279_m1	*PECAM1*	Platelet and endothelial cell adhesion molecule 1
Hs00272659_m1	*LYVE-1*	Lymphatic vessel endothelial hyaluronan receptor 1
Hs03805885_g1	*CLEC4M*	C-type lectin domain family 4 member M
Hs01000844_m1	*STAB2*	Stabilin-2 receptor
Hs00267207_m1	*MRC1*	Mannose receptor
Hs00354519_m1	*CD36*	CD36 molecule
Hs01574659_m1	*NOS3*	Endothelial nitric oxide synthase
Hs01052961_m1	*FLT1*	Fms related tyrosine kinase 1 (VEGFR1)
Hs00911700_m1	*KDR*	Kinase insert domain receptor (VEGFR2)
Hs00971716_m1	*CAV1*	Caveolin-1
Hs00171403_m1	*GATA4*	GATA binding protein 4
Hs00164004_m1	*COL1A1*	Collagen type I alpha 1
Hs00900675_m1	*SRSF4*	Serine and arginine rich spicing factor 4

Table 2.6: TaqMan primers used for real-time PCR

2.3 Investigating the regulators of LSEC phenotype *in vitro*

2.3.1 Gene expression changes in response to treatment

With the aim of elucidating the modifications in homeostatic signalling pathways as a result of *in vitro* capillarisation of LSEC in culture, treatment with growth factors and other pharmacological agents (Table 2.7) was carried out. These were compared to cells treated with media containing vehicle control. Post treatment assays included gene expression analysis (section 2.2.2.5) and super-resolution imaging (section 2.4). LSECs were harvested as described above (2.2.1) and seeded at 250 000 – 300 000 cells per well in complete medium in an RTC coated 6-well plate and incubated overnight or until a confluent monolayer was reached, at 37°C. This was followed by aspiration of complete media and washing with PBS. Human endothelial serum free media was added to each well and cells were serum starved overnight at 37°C. Treatment agents (Table 2.7) were prepared in Human Endothelial serum free medium. Serum free media was aspirated and LSEC were treated with varying concentrations of the appropriate agent for 4 hours a 37°C. At the end of the incubation period, the supernatants were collected in cryovials and snap-frozen in liquid nitrogen. The LSEC monolayer was washed with PBS which was aspirated and discarded. Next, 350 µl of RLT lysis buffer was added to each well followed by scraping using a cell scraper. A 19-gauge needle and syringe were used to further lyse the cells while still in the well. The lysate was collected into a cryovial, vortexed and snap frozen in liquid nitrogen. All supernatants and cell lysates were stored at -80°C until further analysis.

Substance	Company (ref)	Stock reconstitution	Concentrations applied
Recombinant Human $VEGF_{165}$	Peprotech (100-20)	100 µg/ml in 0.1% BSA in PBS	50, 100, 200, 300, 400 ng/ml
Sildenafil citrate	Sigma Aldrich (PZ0003)	5mg/ml in DMSO	2.5, 5, 10, 20, 25 µg/ml

Table 2.7: Agents used for LSEC treatments

2.4 Super-resolving the hepatic sinusoidal nanopores

One of my experimental aims was to develop methodology that could be used for super-resolution imaging of normal and cirrhotic human LSEC. This has been performed extensively on rodent LSEC but methodology for human cells has only been described for SIM imaging (298). The gold standard for confirming LSEC identity is the presence of fenestrations on the plasma membrane. In order to image fenestrations, an imaging approach which can overcome the limitations of light diffraction was required. Consequently, super-resolution imaging protocol for dSTORM was implemented in order to achieve this. The final protocols implemented are described below.

2.4.1 Preparation of glass bottom µ-slides

LSEC were imaged in a 6-channel µ-slide VI 0.5 with glass bottom #1.5H (#80607, Ibidi). Channels were washed with 1 M potassium hydroxide (P5958, Sigma) for 10 minutes at room temperature followed by washing through the channels with 1 ml sterile PBS. This was followed by RTC coating at 250 µg/ml overnight at 37°C. RTC was aspirated, and channels were washed with PBS and air dried under sterile conditions. These were then used immediately as described in the following section.

2.4.2 Liver sinusoidal endothelial cell preparation and treatments

LSEC isolated from normal and cirrhotic human liver tissue (typically passage 3-5) were seeded at 30 000 cells per channel (100 μl of cell suspension in each channel) in complete media and incubated overnight at 37°C. This was followed by serum-starvation for two hours as described above. To explore the re-fenestration capacity of LSEC *in vitro*, sildenafil citrate was used to treat the cells at 10 μg/ml. Treatments were prepared in Human Endothelial serum free medium (11111044, Thermo Fisher) and cells were incubated with sildenafil or vehicle control for up to 4 hours at 37°C. Treatments were then aspirated and cells were washed by flushing 1ml PBS though each channel. Next, the PBS was aspirated, and cells were fixed with freshly prepared 4% PFA in PBS for 10 minutes at 37°C. The fixative was aspirated, and the cells were washed by pipetting 1ml PBS though each channel. The PBS was then aspirated, and the cells were stored in 100 μl PBS at 4°C until staining and imaging. Completely untreated LSEC were cultured until they had spread well throughout the channel before fixing with freshly prepared 4% PFA as described above.

2.4.3 Immunofluorescent labelling of the LSEC plasma membrane and actin fibres

LSEC were stained with Cell Mask Deep Red plasma membrane stain (CMDR) (C10046, Thermo Fisher) prepared at 5 μg/ml in PBS and incubated for 10 minutes at room temperature. CMDR solution was then aspirated, and cells were washed by pipetting 1 ml of PBS-T through each channel which was immediately aspirated, and this was step was repeated using PBS to remove any traces of PBS-T. For two-colour dSTORM, following CMDR staining, Atto 488 Phalloidin (49409, Sigma Aldrich) was applied to the appropriate channel of LSEC at 0.1 μM in

PBS for 20 minutes for the staining of actin. This was then aspirated and the LSEC monolayer was washed by pipetting 1 ml of PBS through the μ-channel. Throughout image acquisition, a degree of sample drift is expected to take place and to enable correction for this, gold nanorod fiducials (25 x75 nm) (Nanopartz™) were used for CMDR imaging. These served as a reference point throughout the sample as they do not blink or bleach throughout imaging. LSEC were incubated with fiducials prepared at 2.5 μg/ml in PBS for 10 minutes. For two-colour dSTORM, TetraSpeck™ microscheres (0.1 μm) (T7279, Thermo Fisher) were applied as fiducial markers and were incubated in the appropriate channel for 10 minutes in PBS at a density of approximately 9 x 10^8 particles/ml. These are pre-stained with four different fluorescent dyes and display good separation in their emission/excitation peaks (505/515 nm (green), 660/680 nm (dark red)) and therefore could be used for both CMDR and phalloidin channels. The fiducial markers were then aspirated, and the imaging buffer was added to each channel immediately prior to imaging.

2.4.4 Imaging system specifications

Direct Stochastic Optical Reconstruction Microscopy (dSTORM), which is a variation of single molecule localisation microscopy, was carried out using the Nanoimager(305) by Oxford Nanoimaging (ONI). A standard oil immersion 100x objective was used, with a numerical aperture of 1.4. Images were acquired within a field of view of 50 μm x 80 μm per channel.

2.4.5 dSTORM imaging

Image acquisition was performed using NimOS software. CMDR and Atto 488 Phalloidin were acquired sequentially. CMDR fluorescent dye was excited with a 640 nm laser at 100% laser power. For the same field of view, acquisition of Alexa Fluor 488 Phalloidin was carried out using a 488 nm laser at 35-40% laser power. The 405 nm laser was used periodically to enhance photo switching of phalloidin fluorophores. Imaging was carried out in highly inclined optical sheet (HILO) illumination mode with an illumination angle of 53-53.5°. Images were collected with an integration time of 30 milliseconds for 20 000 frames. Five fields of view were acquired per condition.

Stochastic photo switching of CMDR and phalloidin fluorophores was achieved using an oxygen scavenging buffer, composed of the reagents described in Table 2.8. This works best when oxygen is excluded from the sample, therefore each channel was filled with buffer up to the very top of the inlet and outlet (about 160 µl).

Reagent	Company (ref)	Stock prepared in	Concentration in final buffer
Glucose oxidase from *Aspergillus niger*	G7141 – Sigma Aldrich	8 mg/ml in 10mM Tris with 50 mM NaCl	0.8 mg/ml
Cysteamine Hydrochloride	M6500 – Sigma Aldrich	2 M in 10mM Tris with 50 mM NaCl	150 mM
Catalase from bovine liver aqueous suspension	C30 – Sigma Aldrich	Ready to use in aqueous form	40 µg/ml
D-(+)-Glucose	G8270 – Sigma Aldrich	20% w/v in 10mM Tris with 50 mM NaCl	18%

Table 2.8: dSTORM imaging buffer components

2.4.6 Image reconstruction

Raw dSTORM data were imported into Fiji software and reconstructed using the ThunderSTORM (306) plugin with the selection of the following inbuilt parameters. Camera set up: pixel size: 117 nm, photoelectrons per A/D count: 0.47, base level [A/D] counts]: 100 and no EM gain. A Gaussian filter was applied for image filtering with a sigma pixel value of 1.6. approximate localisation of molecules was carried out using the local maximum method with a peak intensity threshold of 1000 (for CMDR) and 600 (for Atto 488 Phalloidin). Sub-pixel localisation of molecules was carried out using the integrated gaussian approach with a fitting radius of 3 pixels. Localisations were fitted using the maximum likelihood method. Images were rendered for visualisation of localisations using a 10 nm pixel size and lateral uncertainty of 20.

2.5 Image analysis

2.5.1 Membrane fenestration ground truth data simulations

Data were simulated using custom written code within R. 100 nm diameter circles were seeded, with their centres spaced 250 nm in x and 180 nm in y from each other, in the equivalent of an 8x8 µm region of interest. The difference between the 100 nm circles and the 8x8 µm region of interest was taken and used as the area in which to simulate high density single molecule localisation microscopy (SMLM) data, equivalent to that observed for membrane staining. The area within the 100 nm circles was used for simulating data equivalent to background labelling form the glass coverslip. Within these regions the x,y – coordinates of points were randomly generated and retained. For membrane staining the number of simulated points/μm^2 was stepped from 8,000 to 14,000 in 2,000-point increments, whereas the background simulated points/μm^2 was maintained at 3,000. Once the simulation had completed each simulated point were then shifted by randomly generated vector according to a localization precision value randomly selected from the measured localization precisions of experimental data. The simulated points were then exported into .csv format for further analysis.

2.5.2 Thresholding and analysis of simulated SMLM images

Simulated SMLM data were imported into the ThunderSTORM plugin within Fiji software and each point was convolved with a Gaussian kernel with a width corresponding to its localization

precision. The pixel intensities in the region of the images corresponding to the simulated membrane data were measured and retained for further analysis, this was measured for every simulated point density image. The convolved images were then saved for thresholding analysis. Each image was thresholded by a range of pixel intensity values from 0.3 to 0.7 in 0.05 increments, with the resulting binary images saved for each threshold and the area of each feature detected calculated. The average deviation of the measured areas compared to the ground truth area of the 100 nm diameter circles (i.e., 0.0078 μm^2) was calculated for each threshold within each simulated data set. The average deviation vs. the threshold value was fitted with a linear fit to determine where the average deviation reach zero, i.e., where the fit intersected with the threshold axis. This was repeated for each simulation point density, and the threshold value was plotted as a function of image pixel intensity (measured previously). These data were then fitted with a linear fit to determine the function of threshold vs pixel intensity (resulting in the function: threshold = 0.3129*pixel intensity + 0.1535), to allow choosing of the most appropriate thresholding value for real data.

2.5.3 Processing and analysis of real membrane fenestration SMLM data

The first step of image analysis for reconstructed dSTORM images of untreated and sildenafil citrate treated healthy donor and cirrhotic LSEC was the thresholding of each image. The thresholding value for each image was calculated according to the approach described above based on the point density. After thresholding, fenestrated areas of the plasma membrane in each image were selected and saved as separate fields of view which were analysed in Fiji to obtain measurements for the area (μm^2) of each fenestration in each field of view. This was

carried out using a batch macro for automation of the process (outlined below). In order to exclude single pixels, only fenestrations with area above 0.01 μm^2 in each field of view were selected. The measured fenestration area was then used to calculate the diameter of each fenestration (assuming circularity).

2.5.4 Automated detection of fenestrations and fenestration area measurement

For each field of view extracted from each dSTORM image, fenestrations were detected and fenestration area was measured using the following macro written in Fiji software:

```
dir1 = getDirectory("Choose Source Directory ");
format = "TIFF";
dir2 = getDirectory("Choose Destination Directory ");
list = getFileList(dir1);
setBatchMode(true);
for (i=0; i<list.length; i++) {
   showProgress(i+1, list.length);
   open(dir1+list[i]);
        run("Fill Holes");
        run("Erode");
        run("Dilate");
        run("Dilate");
        run("Create Selection");
        run("ROI Manager...");
        roiManager("Add");
        roiManager("Split");
        roiManager("Show All");
        roiManager("Measure");
        roiManager("Show All with labels");
```

```
saveAs("Tiff", dir2+list[i]);
selectWindow("Results");
        saveAs("results", dir2+list[i]+"_results.csv");
        indexes = roiManager("count");
        roiManager("select",Array.getSequence(indexes));
        roiManager("delete");
        close("Results");
        close("*_rois.tif");
        close("Roi Manager");
        }
```

All protocols for dSTORM image acquisition and image analysis were developed with support and guidance of Dr. Daniel J Nieves.

2.6 Statistical analysis

Statistical analysis was performed using GraphPad Prism 9.0 (GraphPad, US). Unpaired t-test, or Mann-Whitney test were applied based on normality according to the Shapiro-Wilk test. Ordinary one-way analysis of variance (ANOVA) was performed for the comparison of multiple groups The outcome of the statistical test was considered significant when *p*-values were below 0.05 and were shown in figures as follows: * $p < 0.05$, ** $p < 0.01$ and *** $p < 0.001$. Figure legends include details concerning the number of specimens for each experiment and data was expressed as mean ± standard error unless specified otherwise.

3 Characterisation of the expression of endothelial markers in normal and cirrhotic liver tissue

3.1 Introduction

The crucial role of LSEC in maintaining homeostasis is reflected by the myriad of markers that they express. LSEC exhibit heterogeneity in endothelial marker expression patterns across the liver lobule, from periportal endothelium in zone 1 to pericentral endothelium in zone 3 which has been demonstrated both by immunofluorescence as well as RNA sequencing (100,106). During the progression of chronic liver disease as well as aging (307), marked changes in tissue architecture and physiology take place within the liver lobule such as the deposition of collagen fibres in the space of Disse. This process, termed as capillarisation or age-related pseudo-capillarisation is accompanied by LSEC dysfunction, altered expression of scavenger receptors and glycoproteins as well as a dramatic decrease in both size and frequency of fenestrations (299,307). The ability of LSEC to maintain HSC in a quiescent state is compromised which contributes to the process of fibrogenesis and liver cirrhosis (162).

The classical endothelial marker CD31, is a membrane glycoprotein and its expression has been reported at low levels liver sinusoidal endothelium in comparison to HUVEC (308). The receptor CD32B or FcγRIIb is another biomarker expressed by LSEC which contributes to the clearance of soluble IgG complexes by endocytosis and has been described as the only Fcγ receptor expressed in LSEC (68). In addition, LYVE-1 is a transmembrane hyaluronic acid receptor, originally reported to only be expressed by lymphatic vessels, which is also expressed on LSEC (241). In contrast to these proteins, Von Willebrand Factor is a marker whose expression has been documented in LSEC in the context of liver injury and is associated

with platelet adhesion (309). Markers such as CD32B and LYVE-1 have been used to distinguish LSEC from vascular endothelium and altered expression of CD31, CD32B, LYVE-1 and vWF has been reported (242,310,311). Despite this however, data describing human disease specific expression levels of these markers in comparison to healthy control liver specimens is still lacking.

Therefore, prior to the establishment of an *in vitro* model for the study of LSEC phenotype and function, knowledge of the architecture of the primary tissue specimens available to us for LSEC isolation was required, as well as characterisation of the expression patterns of endothelial markers in healthy donor and cirrhotic, otherwise referred to as diseased liver tissue specimens. Healthy donor liver specimens originated from organs deemed unsuitable for transplantation which then become available for research purposes. Cirrhotic liver tissue specimens originate from explanted organs with aetiologies such as ALD or PBC.

This aim of this chapter is to characterise the architectural differences between healthy donor and cirrhotic liver tissue specimens and identify LSEC within the liver lobule based on expression patterns of the markers mentioned above. Additionally, quantification of the expression will be presented as well as variable expression patterns in a disease setting such as ALD. The method of isolation of LSEC from human liver tissue is presented as well as the maintenance of phenotypic and functional characteristics of LSEC *in vitro*.

I began with histological staining using H&E and Van Gieson stains, to assess how liver tissue architecture changes in ALD compared to healthy donor liver tissue. This was followed by the immunohistochemical analysis of endothelial markers in healthy donor and ALD liver tissue. LSEC were isolated from healthy donor and ALD liver tissue specimens and expanded in culture

followed by *in vitro* assessment of their endocytic capacity and expression of endothelial markers.

3.2 Histological analysis of human liver tissue

Histology enables the study of cells and tissue morphology under a light microscope by the use of chemical dyes that are retained within the cells and tissue after washing(312). An essential combination of stains used in histopathology to assess tissue architecture is haematoxylin and eosin (313).

Haematoxylin is a positively charged, basic dye that stains basophilic cellular components such as the nucleus in shades of violet and blue colour when exposed to an alkaline environment. Eosin is an acidic dye which stains the cell cytoplasm as well as extracellular matrix in varying shades of pink depending on the affinity of the tissue for the dye (314) (315). Elastin van Gieson staining can also be used to highlight pathologic changes in elastic fibres within connective tissue and provides differential staining of collagen(316).

First, van Gieson staining was performed in order to define the morphological characteristics and microarchitecture of healthy donor and ALD tissue samples followed by H&E staining. Representative images of van Gieson and H&E staining in healthy donor and ALD liver tissue specimens are shown in Figure 3.1 and Figure 3.2 respectively. Healthy donor liver tissue illustrated in panels A and C, revealed normal tissue architecture with distinct liver lobules showcasing a well branched network of sinusoidal capillaries connecting portal and central venules, surrounded by parenchymal hepatocytes. Liver tissue morphology in the chronically diseased ALD specimen collected upon explant for the complications of cirrhosis was significantly altered. Extracellular matrix fibres are evident as illustrated in Figure 3.1 and

Figure 3.2 panels B and D. Normal lobular architecture is disrupted and the tissue is organised into nodules separated by bridging fibrosis. This is illustrated more clearly in the van Gieson staining of cirrhotic liver tissue in Figure 3.1 (B) and (D), where fibrous connective tissue throughout the sample is evident in varying shades of magenta. Representative images of portal areas in healthy donor and ALD liver tissue are presented in Figure 3.2 (E) and (F). The portal area in healthy donor liver tissue (E) is composed of the portal vein (V), the hepatic artery (blue arrow) and bile duct (green arrow), with sinusoidal capillaries radiating outwards towards the central vein of the liver lobule. The accumulation of fat termed as steatosis, seen as white droplets (red arrows) surrounding the portal area is also evident. In contrast, the portal area architecture in ALD liver tissue (F) exhibits significant remodelling as it is surrounded by fibrous tissue which distorts the normal arrangement of the portal tract as observed in healthy donor liver tissue. Thus, while LSEC in a healthy liver are in close proximity with underlying hepatocytes, LSEC in cirrhosis exist within an environment with increased inflammatory mediators, hepatocellular death, and fibrosis.

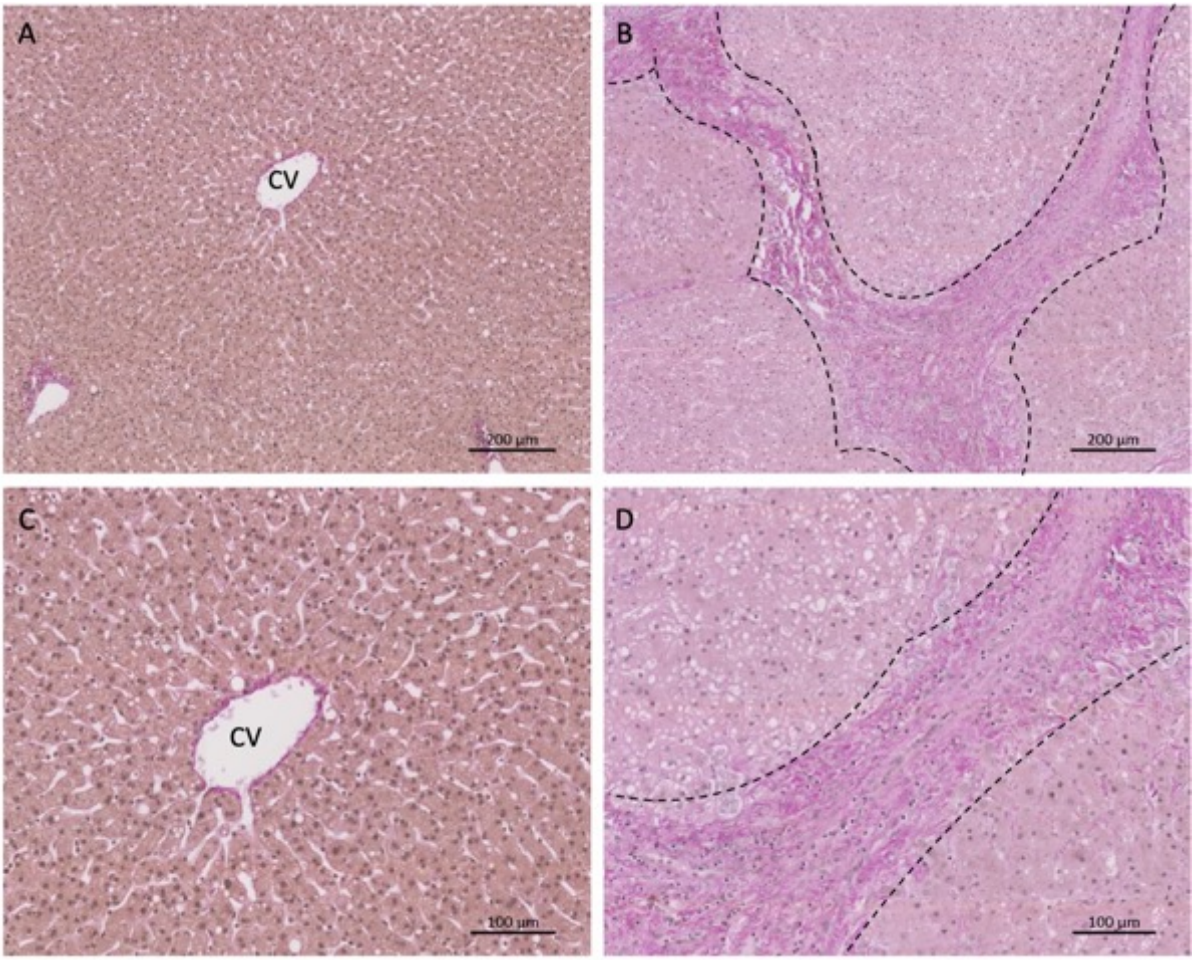

Figure 3.1: Van Gieson staining in healthy donor and ALD liver tissue sections

FFPE liver tissue was sectioned at 4 µm and Van Gieson staining was carried out. Representative images are shown from *n* = 3 healthy donor (A&C) and ALD (B & D) liver tissue specimens. H&E stained tissue specimens were imaged using Axio Scan Z1 Slide Scanner (Zeiss) using a 20x objective and processed in Zen 3.1 (Blue edition, Zeiss) software. CV: Central Vein. Areas within black dotted lines represent fibrous tissue. Scale bar: 200 µm (top row), 100 µm (bottom row).

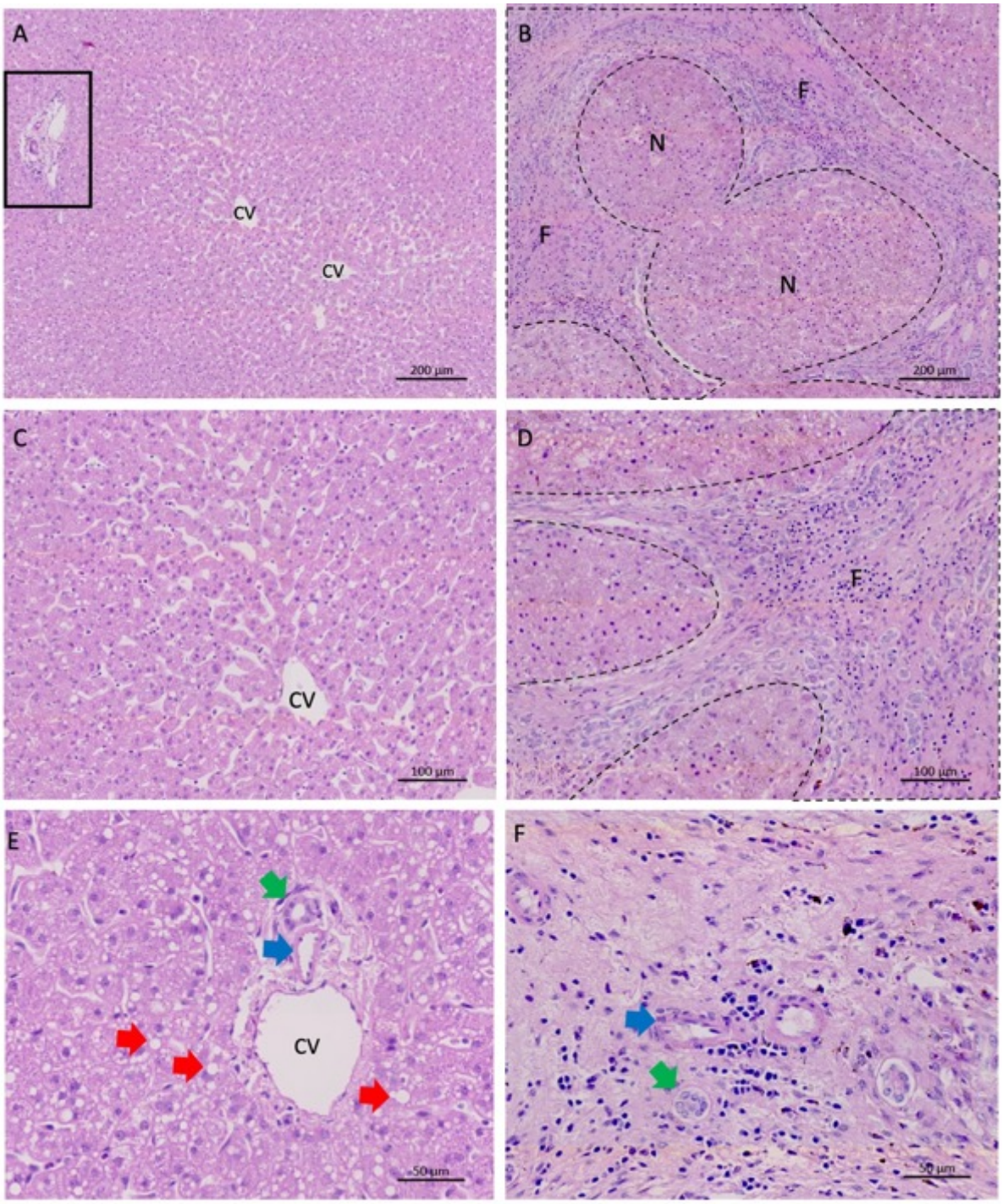

Figure 3.2: H&E staining in healthy donor and ALD liver tissue sections

FFPE liver tissue was sectioned at 4 µm and H&E staining was carried out. Representative images are shown from *n* = 3 healthy donor (A&C) and ALD (B & D) liver tissue specimens with representative fields of view illustrating portal areas in healthy donor (E) and ALD (F) liver tissue. H&E stained tissue specimens were imaged using Axio Scan Z1 Slide Scanner (Zeiss) using a 20x objective and processed in Zen 3.1 (Blue edition, Zeiss) software. CV: Central Vein. Area within black box indicates a portal triad located in zone 3 of the liver lobule. Areas within black dotted lines represent fibrous tissue. **N**: Liver nodule. **F**: Fibrous scarring. Green arrows indicate bile ducts within portal tracts, blue arrows show hepatic arteries, red arrows point to fat accumulation. Scale bar: 200 µm (top row), 100 µm (middle row), 50 µm (bottom row).

3.3 Immunohistochemical analysis of endothelial markers in human liver tissue

Next, immunochemical staining was performed, with a combination of primary antibodies, in order to characterise the expression of endothelial markers in liver tissue. The endothelial markers explored here are the following; CD31 (PECAM-1), CD32B (FcγRIIb), LYVE-1 and von Willebrand Factor (vWF). Representative images of CD31 stained healthy donor and cirrhotic liver tissue specimens are shown Figure 3.3. Panel A illustrates that in healthy donor liver, CD31 expression appears homogeneous throughout the liver lobule. The marker localises to sinusoidal endothelial cells within sinusoidal capillaries but is also present on vascular and arterial endothelial cells in the portal area. The intensity of expression appears similar across all these vessels. In addition to CD31 positive LSEC, KC residing within the sinusoids also express CD31 (black arrow, Figure 3.3 (C)). CD31 expression is maintained on LSEC in cirrhosis however the distribution pattern is altered. The representative example of cirrhotic ALD liver tissue shown in Figure 3.3 (B) and (D), illustrates that there is an accumulation of endothelial cells staining positive for CD31 at the periphery of the lobules but a corresponding loss of staining in central areas. Vascular endothelial cells remain positive. Morphometric analysis was used to calculate the percentage of stained area in each of *n*=5 random fields of from *n*=5 cases of healthy donor and ALD liver specimens. Although statistical analysis revealed no significant difference in CD31 expression between healthy donor and ALD liver tissue (Figure 3.3 (F)), staining quantification illustrates comparable CD31 expression between groups with the exception of one healthy donor isolate.

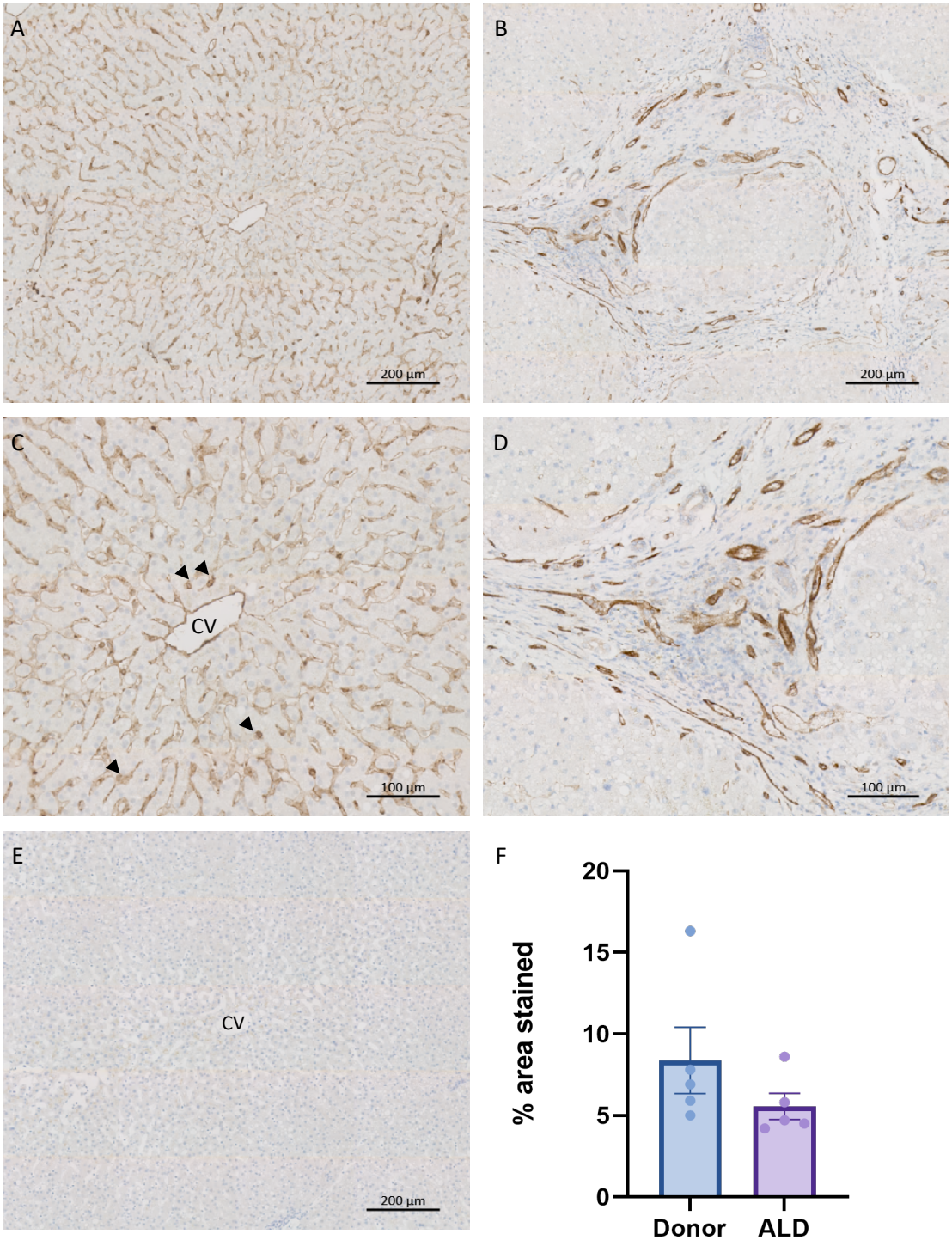

Figure 3.3: CD31 expression in healthy donor and chronic liver disease specimens

FFPE liver tissue was sectioned (4µm) and stained with anti-CD31 antibody (ab187377) at 2 ug/ml. Representative images of CD31 stained liver sections from a healthy donor (A & C) and alcoholic liver disease (ALD) (B & D) are shown. Mouse IgG (DAKO, X0931) was used as a negative control at 2 µg/ml and panel E shows a representative image of background staining. **F:** Microscopic quantification of percentage area stained, quantified from 5 random fields of view per section in *n*=5 cases per condition. Images were acquired using Axio Scan.Z1 slide scanner (Zeiss) using a 20x objective and quantified using ImageJ software. Data are expressed as mean +/- SEM percentage area (bars) and symbols indicate mean values per individual patient in the group. Mann Whitney test confirmed no significant difference in protein expression between groups.

Representative images of protein expression of the Fcγ receptor CD32B in healthy donor and cirrhotic liver tissue are shown Figure 3.4. CD32B expression exhibits uniform distribution throughout the liver lobule, with the marker localising in sinusoidal endothelium of normal liver tissue as illustrated in panels A and C. The staining intensity appears uniform throughout the liver lobule. In ALD tissue however, although CD32B expression is maintained, staining appears less intense and exhibits an irregular pattern. Figure 3.4 (B) and (D) shows maintained expression of CD32B within fibrous tissue areas as well as liver nodules. Following the same approach for staining quantification as described above, CD32B expression was found significantly reduced in chronically inflamed ALD specimens compared to healthy donor as shown in panel G.

LYVE-1 expression in LSEC exhibits similar staining pattern to CD32B in normal liver tissue, as illustrated by Figure 3.5 (A) and (C) which shows uniform distribution and intense staining throughout the liver lobule zones 1 to 3. In contrast to this, LYVE-1 expression is dramatically reduced in ALD tissue which shows minimal and sporadic staining in the hepatic sinusoids within liver nodules and fibrotic areas as indicated by Figure 3.5 (B) and (D). The dramatic decrease in LYVE-1 positive LSEC in ALD liver tissue specimens was confirmed by staining quantification, whereby expression was found significantly reduced in cirrhotic (ALD) tissue compared to healthy donor (Figure 3.5 (F)).

Expression of vWF in normal liver tissue LSEC was extremely low with distribution appearing in vascular endothelium and mainly absent from sinusoidal endothelium as shown in Figure 3.6 (A) and (C). It exhibits a significant increase in expression and intensity in ALD liver tissue sown in Figure 3.6 (B) and (D) whereby it is present on sinusoidal endothelium throughout as

well as on the periphery of the lobules. Expression on vascular endothelium is also maintained in cirrhotic tissue. Staining quantification for vWF revealed a significant increase in expression in ALD liver tissue compared to healthy donor liver specimens as illustrated by Figure 3.6 (F).

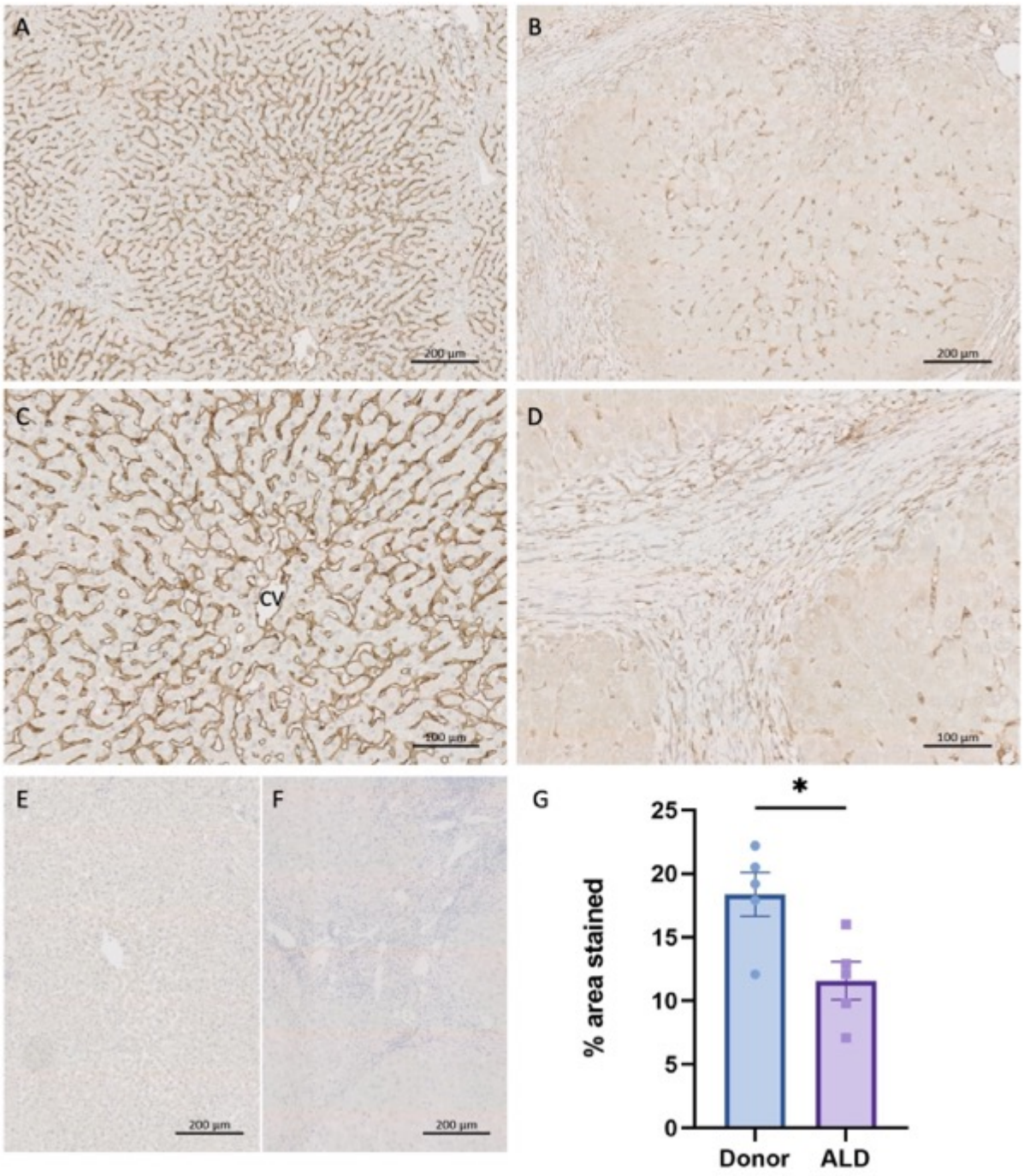

Figure 3.4: CD32B expression in healthy donor and cirrhotic liver disease specimens

FFPE liver tissue was sectioned (4µm) and stained with anti-CD32B antibody (ab77093) at 3.8 ug/ml (healthy donor) and anti-CD32B antibody (ab45143) at 0.995 µg/ml. Representative images of CD32B stained liver sections from a healthy donor (A & C) and alcoholic liver disease (ALD) (B & D) are shown. Goat (Thermo Fisher, #02-6202) and rabbit IgG (ab34417) were used as negative controls at 3.8 µg/ml and 0.995 µg/ml respectively and panels E and F show representative images of background staining. **G:** Microscopic quantification of percentage area stained, quantified from 5 random fields of view per section in *n*=5 cases per condition. Images were acquired using Axio Scan.Z1 slide scanner (Zeiss) using a 20x objective and quantified using ImageJ software. Data are expressed as mean +/- SEM percentage area (bars) and symbols indicate mean values per individual patient in the group. Mann Whitney test. P-value* < 0.05.

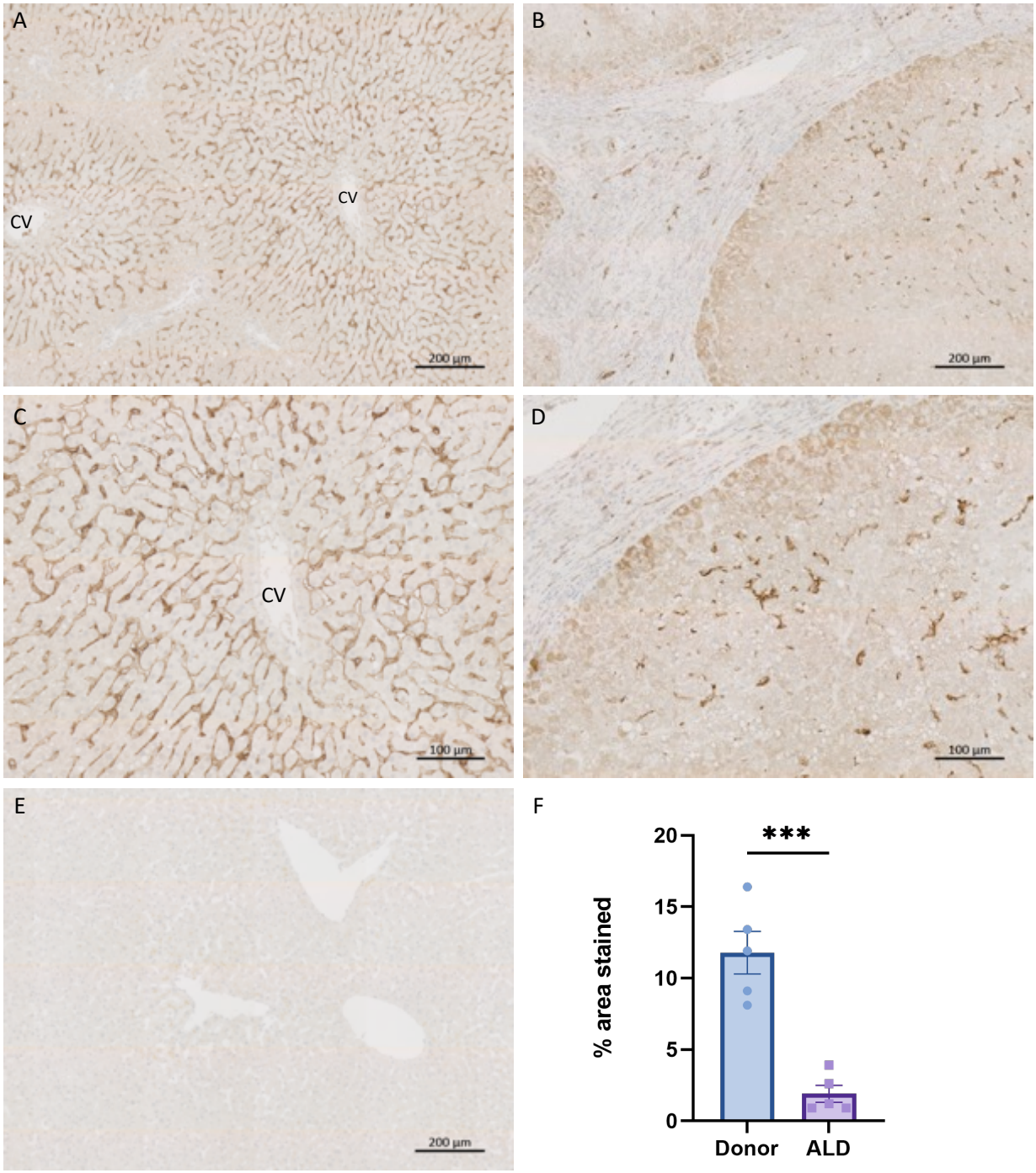

Figure 3.5: LYVE-1 expression in healthy donor and chronic liver disease specimens

FFPE liver tissue was sectioned (4µm) and stained with anti-LYVE-1 antibody (ab33682) at 5 ug/ml. Representative images of LYVE-1 stained liver sections from a healthy donor (A & C) and alcoholic liver disease (ALD) (B & D) are shown. Mouse IgG (DAKO, X0931) was used as a negative control at 5 µg/ml and panel E shows a representative image of background staining. **F:** Microscopic quantification of percentage area stained, quantified from 5 random fields of view per section in *n*=5 cases per condition. Images were acquired using Axio Scan.Z1 slide scanner (Zeiss) using a 20x objective and quantified using ImageJ software. Data are expressed as mean +/- SEM percentage area (bars) and symbols indicate mean values per individual patient in the group. Mann Whitney test. P-value *** < 0.001.

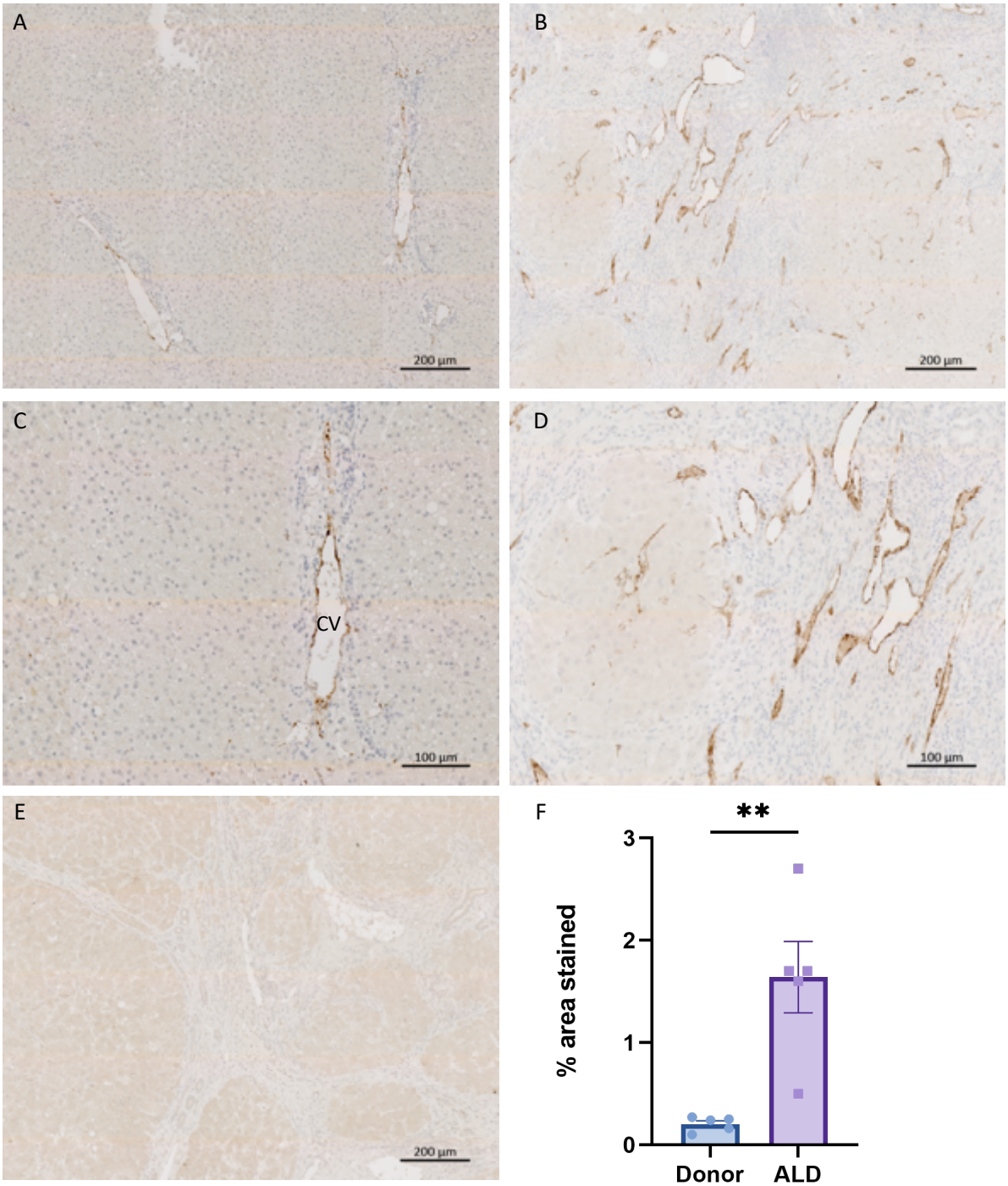

Figure 3.6: von Willebrand factor expression in healthy donor and chronic liver disease specimens

FFPE liver tissue was sectioned (4µm) and stained with anti-von Willebrand Factor antibody (DAKO, M0616) at 0.252 mg/ml. Representative images of anti-von Willebrand Factor stained liver sections from a healthy donor (A & C) and alcoholic liver disease (ALD) (B & D) are shown. Mouse IgG (DAKO, X0931) was used as a negative control at 0.252 mg/ml and panel E shows a representative image of background staining. **F:** Microscopic quantification of percentage area stained, quantified from 5 random fields of view per section in *n*=5 cases per condition. Images were acquired using Axio Scan.Z1 slide scanner (Zeiss) using a 20x objective and quantified using ImageJ software. Data are expressed as mean +/- SEM percentage area (bars) and symbols indicate mean values per individual patient in the group. Mann Whitney test. P-value ** < 0.01.

The co-expression of LSEC specific markers CD32B and LYVE-1 was assessed by dual immunofluorescence staining. A representative image of healthy donor liver tissue stained with CD32B and LYVE-1 is shown in Figure 3.7 (A) whereby CD32B expression is indicated in green and LYVE-1 positive staining in red. CD32B and LYVE-1 exhibit expression throughout the liver lobule, with LYVE-1 also expressed on KC within sinusoids (white arrows). The distribution pattern of both markers however is disrupted by the presence of steatosis within the sample, indicated by the regions enclosed within the white circles in panel A. The intensity profile shown in Figure 3.7 (B) illustrates CD32B and LYVE1 co-expression in a representative region marked by the white line in panel A which covers a pericentral to mid-lobular region. There is variability in intensities in CD32B (green) and LYVE-1 (red) staining within that region. The peaks pointed out by the regions marked in white rectangular outlines illustrate regions of colocalization between the two markers. Figure 3.7 (C) shows the region outlined in panel A at a higher magnification where labelling of the sinusoids with CD32B and LYVE-1 in the pericentral region of the lobule is visualised. The region is also marked by fat accumulation as indicated by the orange arrows.

Further to this, co-expression of LYVE-1 and CD32B was also assessed is cirrhotic liver tissue as shown in Figure 3.8. expression of the two markers is clearly diminished. This specific sample is from a PSC liver and expression is extremely low, to a level comparable to the negative control shown in Figure 3.8 (B). A magnified region from panel A is illustrated in Figure 3.8 (C) which emphasises the lack of expression of these two markers within the fibrotic area shown with the exception of weak CD32B positive staining in some regions (white arrows).

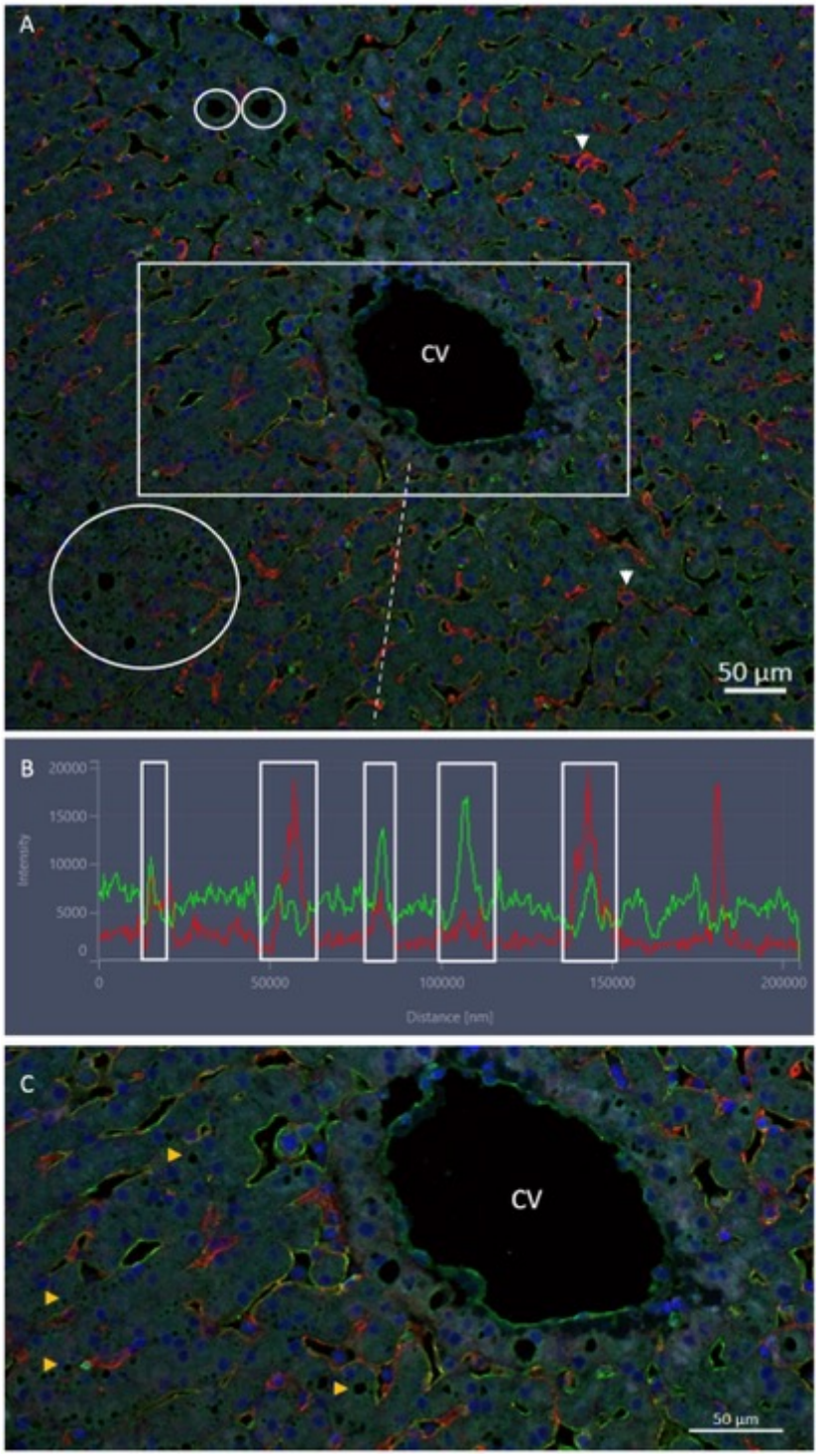

Figure 3.7: Co-expression of CD32B and LYVE1 in healthy donor liver specimens

(A) Representative image of FFPE liver tissue sectioned (4µm) and co-stained with anti-CD32B (ab77093) and anti-LYVE-1 (ab33682) antibodies followed by donkey anti-goat Alexa Fluor 488 (green) and donkey anti-rabbit Alexa Fluor 647 (red) secondary antibodies respectively. DAPI staining was carried out for nuclear counterstaining shown in blue. Images were acquired using LSM880 Confocal microscope (Zeiss) using a 10x objective. (B): Intensity profile generated in Zen 3.1 (Blue, Zeiss) software along the length of the dotted white line indicated in panel A. The peaks enclosed within the white boxes indicate regions of co-localisation. (C) Specified area indicated within the white box in panel A at a higher magnification; scale bar 50 µm. White circles and orange arrows indicate regions of steatosis. White arrows point to LYVE-1 positive Kupffer cells within sinusoidal capillaries.

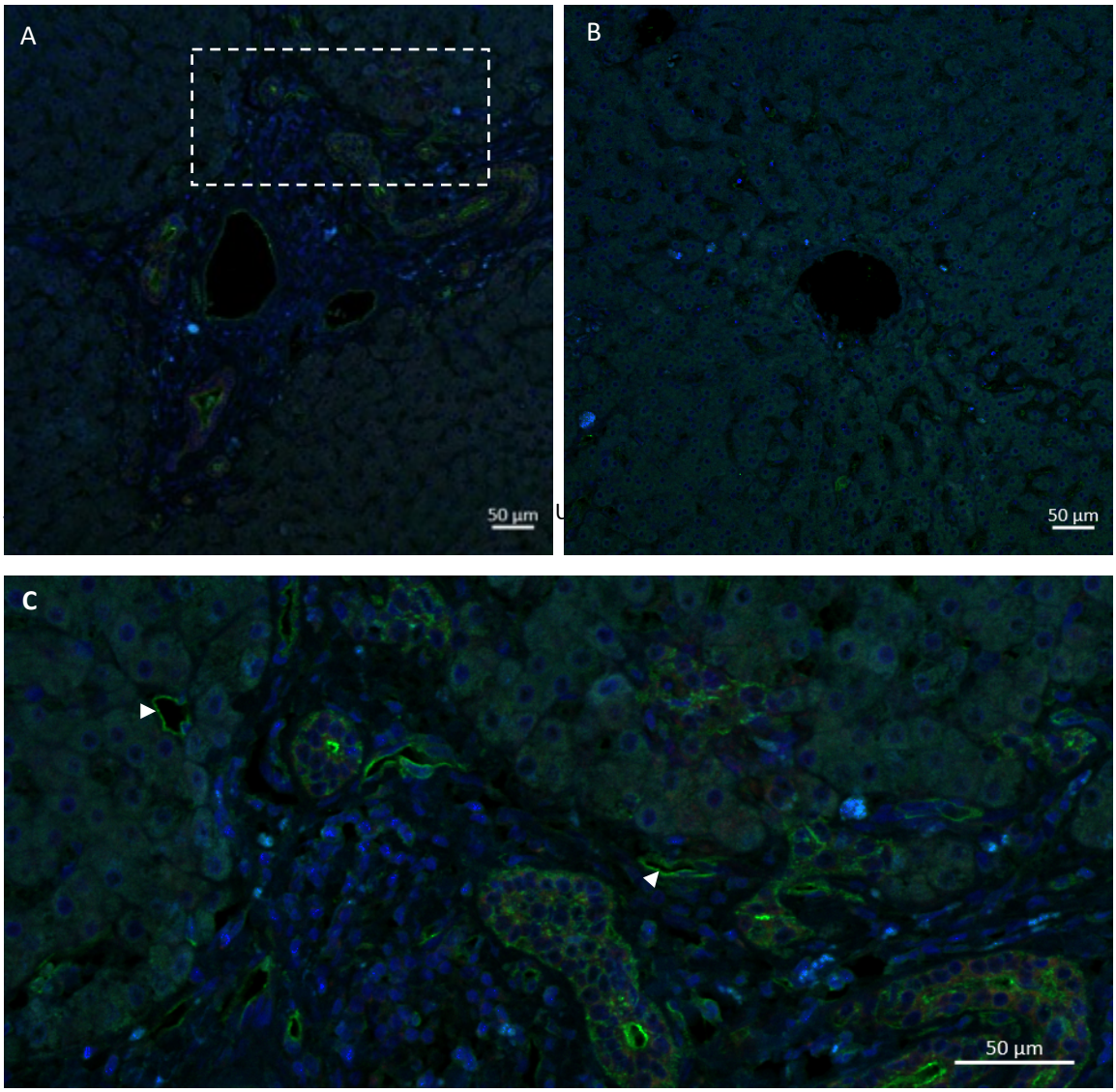

Figure 3.8: The expression of CD32B and LYVE-1 in cirrhotic liver specimens is severely diminished.

(A) Representative image of FFPE liver tissue sectioned (4µm) and co-stained with anti-CD32B (ab77093) and anti-LYVE-1 antibodies followed by donkey anti-goat Alexa Fluor 488 (green) and donkey anti-rabbit Alexa Fluor 647 (red) secondary antibodies respectively. DAPI staining was carried out for nuclear counterstaining shown in blue. Images were acquired using LSM880 Confocal microscope (Zeiss) using a 10x objective. (B) Representative image of goat and rabbit IgG negative control. (C) Magnified view of region specified in white rectangle in panel A. White arrows indicate CD32B positive staining.

The initial histological analysis confirmed that LSEC are still in evidence in cirrhotic tissue however they exhibit a de-differentiated phenotype as expected. In order to study these cells *in vitro* the next step was to isolate LSEC from healthy and diseased liver tissue samples. This was achieved by the implementation of the CLGR's standard LSEC isolation procedure (303) outlined in section 2.1.5 in Chapter 2 materials and methods, on human tissue sourced from normal donor and explanted liver tissue specimens. The basic protocol is outlined in Figure 3.9. A slice of liver tissue (40-50 g) was used as the starting material and was mechanically digested in preparation for further enzymatic digestion of the tissue carried out in the next step. As noted in Figure 3.1 and Figure 3.2, the amount of connective fibres within tissue varies between samples. Consequently, the incubation time of the enzymatic digestion was adjusted depending on tissue stiffness determined during mechanical digestion as well as liver tissue appearance. After a series of wash steps, the resulting tissue digest composed of all liver cell populations was aliquoted onto Percoll gradients, to facilitate the separation of parenchymal and non-parenchymal cell populations. LSEC, localised to the non-parenchymal cell fraction indicated by a white arrow in Figure 3.9 (D) which was collected from all Percoll gradients. As good expression of CD31 on LSEC even in cirrhosis was confirmed (Figure 3.3), CD31 was used as a positive selection marker. After approximately 7-10 days in culture, LSEC exhibit a cobblestone morphology. This methodology enabled successful isolation of LSEC from liver tissue of varying aetiologies including healthy donor and ALD specimens (a representative image of LSEC in culture is shown in Figure 3.9 panel F).

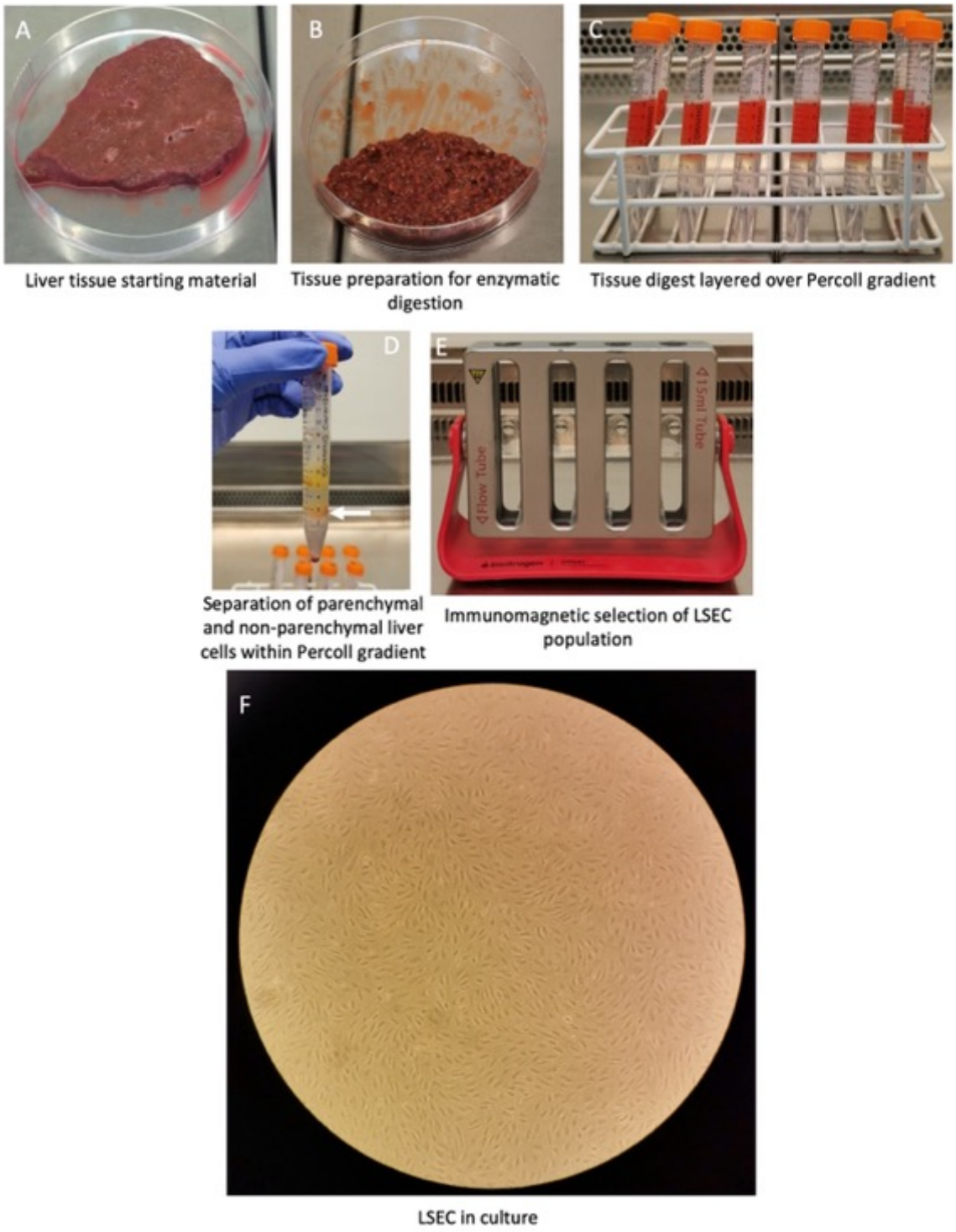

Figure 3.9: Schematic representation of the LSEC isolation procedure from human liver tissue.

(A) Representative image of liver tissue starting material followed by mechanically digested liver tissue (B) prepared for enzymatic digestion. Next, the liver digest is washed and aliquoted onto Percoll gradients for separation of parenchymal and non-parenchymal cell fractions (C). The non-parenchymal cell fraction is collected (white arrow in panel D) and subjected to immunomagnetic selection (E) using CD31 coated magnetic beads for the positive selection of LSEC (F).

3.4.1 Immunocytochemical analysis of LSEC markers *in vitro*

Following isolation and culture of LSEC, assessment of expression of the scavenger receptor LYVE-1 was carried out at the protein level by performing immunocytochemistry on fixed LSEC. Representative images of LYVE-1 expression are shown in Figure 3.10 in healthy donor (A) and cirrhotic (B) LSEC. These particular isolates of LSEC shown, were stained at passage 3 and 5 for healthy donor and cirrhotic (ALD) LSEC respectively. LYVE-1 exhibits a granular distribution throughout the cell cytoplasm of normal LSEC and cirrhotic LSEC with more intense foci present in the perinuclear region as well as in the cytoplasm. Expression of LYVE-1 confirms maintenance of scavenger receptor expression *in vitro* in CD31 isolated LSEC, which is a key phenotypic characteristic. Further scavenger receptor expression including LYVE-1 at the mRNA level in passaged LSEC has also been carried out and is presented in Chapter 4.

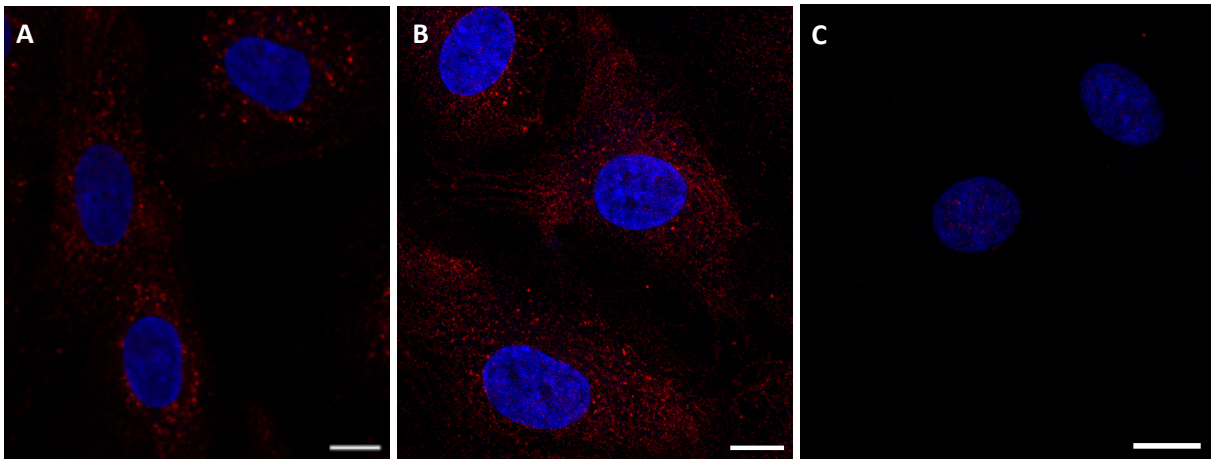

Figure 3.10: Expression of LYVE-1 in healthy donor and cirrhotic LSEC *in vitro*.

Representative images of LYVE-1 protein expression in healthy donor (A) and cirrhotic (B) LSEC *in vitro.* LSEC were stained with anti-LYVE-1 primary antibody (ab33682) and followed by goat anti-rabbit IgG Alexa Fluor 594 secondary antibody. Nuclear counterstain is shown in blue. Rabbit IgG was used as a negative control and panel C shows a representative image of background staining. Images are representative of *n*=2 of healthy donor and cirrhotic biological replicates. Image acquisition was carried out using LSM 880 Confocal microscope and processed in Fiji software. Contrast has been adjusted for illustration of labelling distribution. Scale bar: 10 µm.

3.4.2 Confirmation of LSEC phenotype by assessment of scavenging function

Confirmation of the LSEC phenotype *in vitro* was carried by immunocytochemistry as described above which provided evidence that LSEC isolated and passaged from donor and cirrhotic livers maintain detectable expression of key markers which are considered essential for LSEC function. As LSEC are considered masters of endocytosis, assessment of LSEC endocytic capacity *in vitro* was evaluated next. The general principle is, LSEC should be able to endocytose an appropriate ligand rapidly even in low concentrations(317). Consequently, formaldehyde treated albumin fused with FITC fluorescent protein (FITC-BSA) was used as a ligand of endocytosis and incubated with LSEC isolated from healthy donor and cirrhotic liver tissue.

Representative images of endocytosed FITC-BSA ligand in an uptake assay performed in diseased LSEC is shown in Figure 3.11 (A) and the ligand free control is shown in panel B. Endocytosed FTC-BSA can be seen as green, fluorescent vesicles distributed in the cell cytoplasm. LSECs at high passage were able to rapidly internalise labelled albumin. This was localised in the cytoplasm around the nucleus, as well as in proximity to the peripheral actin fibres stained with phalloidin as shown in representative images in Figure 3.11 (A). FITC-BSA vesicle size and intensity varies between cells as well as within individual cells.

Quantification of vesicles from *n*=5 fields of view from each of *n*=3 isolates of healthy donor and cirrhotic LSEC was carried out in Fiji software and the number of vesicles was normalised to the number of cells in each field of view. The average vesicle uptake of healthy donor and cirrhotic LSEC isolates is shown in Figure 3.12 (A) and (B) respectively, where each symbol represents a separate isolate of LSEC. The quantified vesicles are a measure of the ability of

the cells to internalise albumin. Both healthy donor and cirrhotic LSEC exhibit variability in endocytic function between biological isolates. Differences between FITC-BSA incubated LSEC and ligand free control were not statistically significant. Overall, isolated LSEC maintain the ability to endocytose *in vitro*, even after 3-5 passages, which is an essential functional characteristic of the LSEC phenotype.

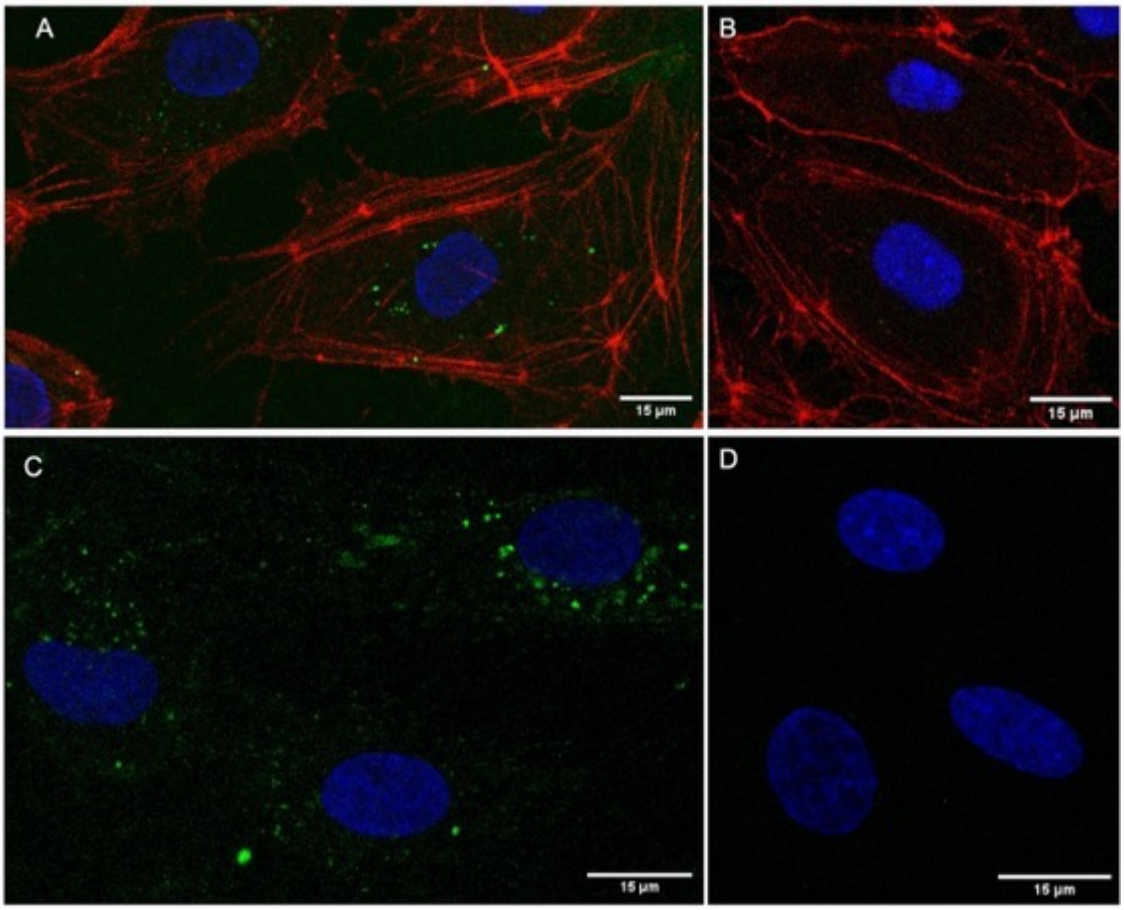

Figure 3.11: Uptake of FITC labelled albumin in human diseased LSEC.

(A) Representative image of the uptake of FITC-BSA ligand at 20 µg/ml in LSEC isolated from ALD liver tissue at 30 minutes. Endocytosed vesicles appear as green, fluorescent vesicles in the cytoplasm. (B) Representative image of ligand free uptake assay control. (C) Representative image of FITC-BSA uptake in healthy donor LSEC and ligand free control (D). F-actin fibres stained with Alexa Fluor™ 633 Phalloidin shown in red. Images are representative of *n*=5 fields of view per condition; all images were captured on LSM 880 confocal microscope (Zeiss) using a 40x objective.

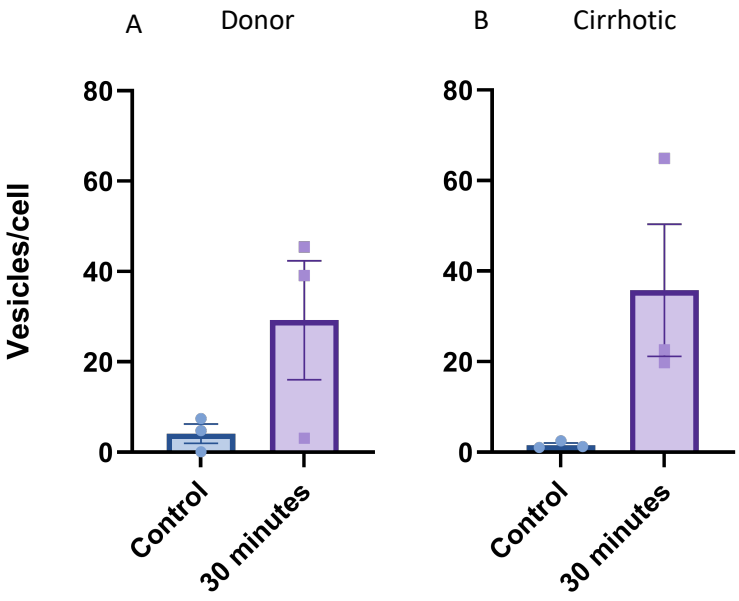

Figure 3.12: Uptake of FITC labelled albumin in healthy donor and cirrhotic LSEC.

Quantification of the uptake of FITC-BSA ligand in LSEC isolated from healthy donor (A) and ALD (B) liver tissue specimens at 30 minutes compared to ligand free control. Images were captured using LSM 880 confocal microscope, endocytosed vesicles were quantified using Fiji software and normalised to the number of cells per field of view. Data are expressed as mean +/- SEM (bars) and are representative of *n*=5 fields of view from each of *n*=3 healthy donor and cirrhotic liver specimens. Unpaired t-test revealed no significant difference between groups.

3.5 Discussion

3.5.1 Analysis of liver tissue specimens

The microscopic morphological differences illustrated between healthy donor and ALD liver tissue confirm liver tissue architecture remodelling throughout the course of chronic liver disease. Haematoxylin and Eosin stains have been the standard approach for histologic examination of human tissues for over a century (315). Tissue remodelling, more evident in the representative images of Van Gieson staining comparing normal donor and ALD live tissue in Figure 3.1, as a result of progressive fibrous collagen synthesis and deposition, is characteristic of hepatic fibrosis (318). Identification of these structural differences provides a better understanding of liver tissue remodelling during chronic liver disease as it is a crucial factor implicated in the process of capillarisation of LSECs (319). The protein expression of collagen within fibrotic areas has also been assessed and is presented in the next chapter.

LSEC within the hepatic microenvironment under homeostatic conditions perform filtration and endocytosis at a high capacity and this is achieved by the combination of the multiple scavenger and adhesion molecules they express, as well as the fenestrations that perforate the LSEC membrane. Characteristic expression in healthy LSEC includes the Fc receptor CD32B and scavenger receptor LYVE-1 while vWF exhibits very low levels in homeostatic conditions. In chronically inflamed livers however, expression of vWF is increased while CD32B expression is diminished (68,241,242,309,320,321). The classical endothelium marker CD31 is also expressed on LSECs and its expression is altered between homeostatic and chronically inflamed livers (322).

The analysis of classical and sinusoid specific endothelial markers in healthy donor and ALD liver tissue reflects the marked phenotypic capillarisation of LSEC in chronic liver disease. CD31 is a membrane glycoprotein and a classic endothelial marker expressed in endothelial cell intercellular junctions which has been reported to also be expressed in capillarised liver sinusoidal endothelium (97,323). Moreover, CD31 has been implicated in the process of trans-endothelial migration of leukocytes and this constitutes CD31 as an important molecule in the maintenance of hepatic homeostasis. In the data presented in this chapter, CD31 expression is abundant in healthy donor sinusoidal endothelium as well as in ALD cirrhotic specimens. It is noteworthy, that KC are also CD31 positive and as illustrated by the black arrows in Figure 3.3 (C), they are very frequently present in sinusoidal capillaries. Nevertheless, CD31 expression has been reported in human liver specimens irrespective of the presence of inflammation or cirrhosis, a report which is line with the CD31 expression data presented in this chapter (242). There have also been additional reports for the expression of CD31 in normal human liver specimens. The consistent expression of CD31 in LSEC beginning from peri-portal zone 1 of the liver lobule to the peri-central region (zone 3) (324). In relation to the absence of a detectable difference in CD31 expression between healthy donor and ALD liver tissue specimens, similar results have been reported in a rat model of acute liver damage recapitulated by carbon tetrachloride administration where no marked increase in CD31 expression was detected. CD31 positive expression assessed by immunohistochemistry was detected in rat and human healthy hepatic sinusoids as well as within the central vein lining (322). In general, CD31 expression in LSEC has long been matter of debate with contradictory results presented from different research groups. Reports from human liver specimens include low expression in normal liver tissue and increased expression in chronic liver disease

while others have reported expression in both normal and diseased liver tissue (97). In the data presented in this chapter, although no significant difference has been detected statistically between normal and diseased samples, the quantified immunoreaction exhibits a slightly decreasing trend in CD31 expression in ALD samples compared to normal. It is important to consider that, KC present in the sinusoids which are CD31 positive as shown in figure 3.3 (F), also contribute to the overall quantified expression of CD31 in normal donor tissue samples. Overall, LSEC along the portal-central axis of the liver lobule express CD31 in normal donor tissue whereas both sinusoidal and scar associated endothelium is CD31 positive in ALD samples. Vascular endothelium is CD31 positive in both cases.

The receptor CD32B or FcγRIIb is an LSEC specific biomarker contributing to the clearance of soluble IgG complexes by endocytosis and has been described to be the only Fcγ receptor expressed in LSEC (212). Expression of CD32B (SE-1 antigen in rat) has also been positively correlated with the presence of fenestrations in rat LSEC (325). The staining distribution patterns of CD32B shown in Figure 3.4 show uniform distribution in zones 1-3 of the liver lobule. CD32B distribution been represented by Strauss et al. (100) where expression was found to be low in LSEC located in zone 1 with increasing expression in LSEC within zone 2 and 3 of the liver lobule. In chronically inflamed liver tissue, ALD in particular as presented here, CD32B expression in significantly reduced and exhibits scattered expression in sinusoids within hepatic nodules. Single cell transcriptomics data presented by Su et al. (326) also confirm downregulation of CD32B in mouse cirrhotic livers. The importance of CD32B expression in LSEC, along with its homeostatic role within the liver has been demonstrated in the context of NASH. A negative correlation between serum collagen type IV and hyaluronan with CD32B expression. Increased type IV collagen and hyaluronan has been reported in NASH

and this suggests a decline in CD32B function. This supports the gradual LSEC dysfunction that takes place in chronic liver disease (327).

LYVE-1 is a transmembrane scavenger receptor, originally thought to only be expressed by lymphatic vessels however has also been reported to be expressed by LSEC (310). This is illustrated by the LYVE-1 expression data shown in Figure 3.5 (A) and (C) where LYVE-1 is abundantly expressed in zones 1-3 of the liver lobule. LYVE-1 expression has been reported in specific subsets of LSEC within the liver lobule in liver tissue specimens obtained from patients undergoing hepatic resection. Peri-portal LSEC localised in zone 1 of the liver lobule were found to express low levels of LYVE-1, with increasing expression exhibited in mid-lobular (zone 2), and peri-central (zone 3) LSECs (100). In contrast to this, and in line with previous reports stating a decrease in LYVE-1 expression in diseased liver specimens including ALD (242), Figure 3.5 (F) illustrates a significant reduction in LYVE-1 expression in LSEC in ALD liver tissue specimens. This illustrates that the process of capilarisation of LSEC within chronically diseased livers contributes to altered expression levels of LYVE-1. Co-expression of CD32B and LYVE-1 in zones 2 and 3 of the liver lobule, illustrated in Figure 3.7 has also been shown in by Strauss et al. (100).

Expression of Von Willebrand Factor has been documented in LSEC in the context of liver injury (64) and is associated with platelet adhesion (309). Conflicting conclusions on the expression of von Willebrand Factor across human, rat and mouse specimens have been reported. It is stored in cytoplasmic vesicles called Weibel Palade bodies and its absence has been shown in rat LSEC (328). Although evidence denying nor confirming the presence of Weibel Palade bodies in LSEC has not been illustrated, the expression of von Willebrand Factor

has been documented in human LSEC(329). It is mostly expressed in vascular endothelium(330) which explains its absence in heathy donor liver sinusoidal endothelium as well as its significant upregulation in diseased liver as shown in Figure 3.6 (B), (D) and (F). This is line with hepatic sinusoidal endothelium capillarisation during chronic liver disease and the fact that it exhibits a more vascular endothelial phenotype.

Single cell RNA sequencing of LSEC isolated from normal and diseased human livers has revealed several endothelial sub-populations residing throughout the liver lobule. The most abundant LSEC population, revealed enriched expression in F8 (Factor VIII), CD31 with low expression of CD32B, LYVE-1 and Stabilin-2 and these were proposed to be peri-portal LSEC. The second most abundant LSEC population however, exhibited enriched expression of CD32B, LYVE-1, Stabilin-2 as well as low expression of von Willebrand factor and was suggested to originate from the peri-central zone of the liver lobule (106). In general, biological variability between healthy donor as well diseased liver specimens regardless of aetiology, massively impacts marker expression results. In the CLGR, healthy donor livers originally destined for liver transplantation are regarded as 'normal' livers as there is no diagnosed pathological condition associated with them. However, patient age should be taken into consideration as LSEC do undergo age-related pseudocapilarisation (331,332) which could potentially impact marker expression.

3.5.2 Experiments on the phenotypic and functional profile of LSEC *in vitro*

LSEC isolation protocols vary between research groups and more importantly vary depending on the species the LSEC are isolated from. While LSEC isolated from rat liver tissue using CD31 have been reported to lack fenestrations, visualisation of fenestrations in CD31 isolated human LSEC from healthy donor and cirrhotic livers indicates the contrary (data presented in chapter 6). In rat, SE-1 (CD32B in human) has been successfully used to isolate a 98% pure LSEC yield in an immunoselection based method (333) while rat LSEC isolated using CD31 have been reported to have less fenestrae compared to LSEC isolated via elutriation (334). Onoe et al. (335) positively selected for mouse LSEC using CD105 marker in combination with MACS. This marker, however, is also expressed in hepatic stellate cells and myofibroblasts. The use of CD31 as a selection marker in the CLGR's LSEC isolation protocol (336), results in a human hepatic endothelial cell population that phenotypically and functionally matches LSEC characteristics as illustrated by immunocytochemistry and uptake assays. The abundance of LSEC as an endothelial population within the liver ensures that it is the primary endothelial population isolated from liver specimens. Despite the fact that healthy donor livers had no diagnosed pathological condition, the vast majority of them are steatotic and this massively impacts the resulting yield of isolated LSEC, some of which are eventually unusable as they do not proliferate efficiently *in vitro* in order to reach the cell numbers required to reliably perform experiments. CD31 is also expressed by KC which inevitably contaminate LSEC preparations. However, in absence of their proliferation, LSEC proliferate and expand, eventually leading to the detachment of KC from the flask which can be removed by washing the LSEC monolayer with PBS during media changes or prior to harvesting.

In response to this, I have tried preliminary testing of CD32B antibody (ab151497) in the standard LSEC isolation protocol. Figure 3.13 illustrates CD32B and CD31 expression on CD32B isolated LSEC from a diseased liver specimen (PBC) at passage 1. Granular staining of CD32B can be noted in the perinuclear area as well as throughout the cytoplasm. CD32B distribution is closely associated with CD31 positive regions within the cytoplasm as well as cytoplasmic extensions connecting neighbouring LSEC. Thus, in principle CD32B could represent a good and more selective strategy for isolating LSEC.

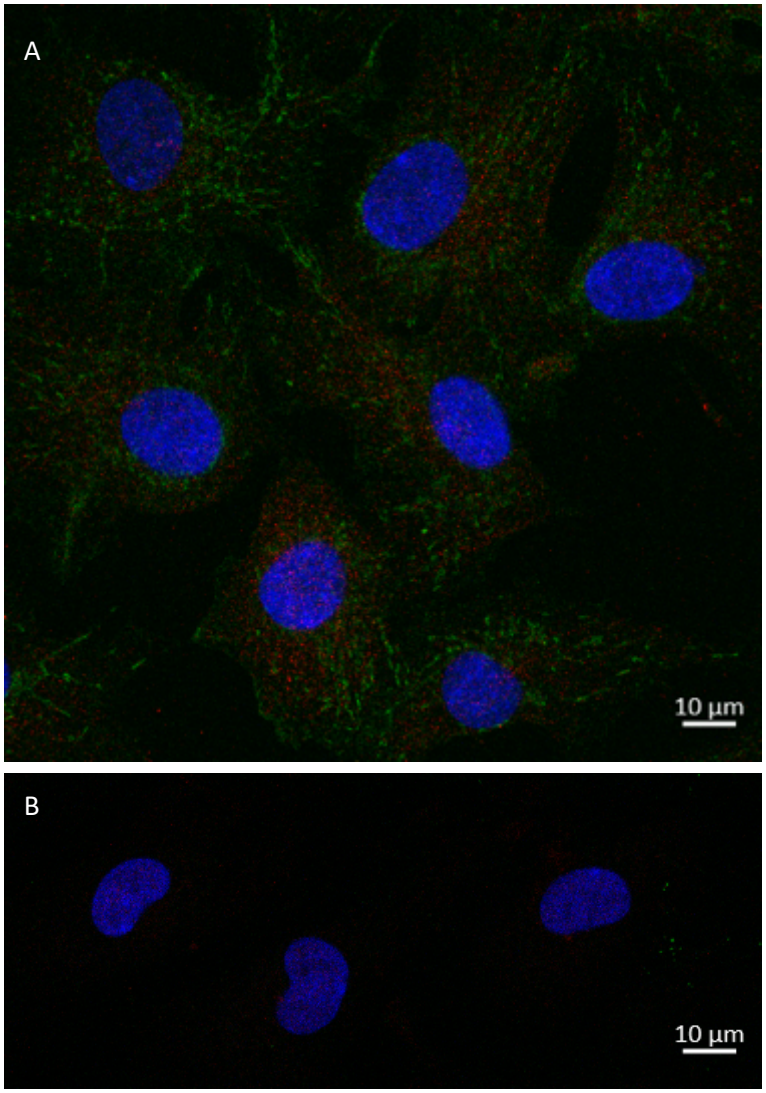

Figure 3.13: CD31 and CD32B expression in CD32B isolated LSEC

(A) Representative image of CD32B isolated LSEC stained with anti-CD32B (ab151497) and anti-CD31 (ab187377) primary antibodies followed by goat anti-rabbit IgG Alexa Fluor 594 and goat anti-mouse IgG1 Alexa Fluor 488 secondary antibodies respectively. (B) Representative image of rabbit and mouse IgG negative controls. Images were captured using LSM880 confocal microscope (Zeiss) with a 40x objective and processed in Zen Blue software (Zeiss).

Following successful isolation and expansion of human LSEC from healthy donor and cirrhotic liver tissue, maintenance of their phenotype *in vitro* was confirmed using immunocytochemistry. The expression of LYVE-1 in LSEC *in vitro* confirmed the maintenance of a sinusoidal phenotype of CD31 isolated healthy donor and cirrhotic LSEC. Moreover, successful uptake of FITC-BSA ligand by cultured and passaged LSEC affirms their scavenging function (337) *in vitro* which is a crucial functional characteristic(338).

In conclusion, the data presented in this chapter illustrates differences in liver architecture between healthy and diseased liver specimens as well as the differences in distribution and expression of the markers CD31, CD32B, LYVE-1 between healthy and diseased liver specimens. Human LSEC can be successfully isolated from heathy donor and disease liver using CD31 as a selection marker. LSEC maintain phenotypic and functional characteristics *in vitro* as shown by the expression of LYVE-1 and the uptake of FITC-BSA ligand. Consequently, they can be used *in vitro* to further elucidate key differences between normal and chronic liver disease derived LSEC.

4 LSEC capillarisation is recapitulated *in vitro*

4.1 Introduction

In this chapter, the effects of culture on the phenotype and genotype of LSECs will be considered. Thus, to begin with, this chapter will revisit some notable characteristics of LSECs as key players in the maintenance of hepatic homeostasis. Their specialised phenotype consists of the expression of scavenging and pattern recognition receptors such as the mannose receptor (339) and are involved in leukocyte recruitment (248) as well as regulation of hepatic blood flow.

Stabilin-2 is an endocytic receptor expressed in the hepatic sinusoids, venous sinuses of the spleen and medullary sinuses of lymph nodes and is specific for clearance of hyaluronan (HA) and chondroitin sulphate from blood in the liver (340). Stabilin-2 mediates the endocytosis of HA and chondroitin sulphate through the clathrin-coated pit pathway (341,342). This endocytic pathway is also employed by the mannose receptor.

LSEC participate in clearing denatured collagen from blood circulation via the scavenging activity of the mannose receptor (CD206) which is also expressed in Kupffer cells within sinusoidal capillaries in the liver (209,343). An additional function of LSEC is clearance of viral particles, a process which involves the expression of CLEC4M. CLEC4M is a C-type lectin receptor which engages in pathogen recognition and binding to sinusoidal endothelium (247,344).

A key characteristic of LSEC is the fact that their plasma membrane is perforated with transmembrane pores called fenestrations organised in groups forming sieves plates.

Throughout chronic liver disease and aging the LSEC phenotype undergoes important morphological and gene expression changes through the process of capillarisation (345). LSEC capillarisation occurs gradually, is characterised by perisinusoidal deposition of collagen and is linked to LSEC dysfunction. The capillarisation process includes progressive decline in porosity or defenestration of the LSEC membrane and this is associated with decreased ability of LSEC to filter chylomicrons and waste macromolecules from blood(346). Defenestration has been described to be particularly high in zone 3 of the liver lobule in alcoholic liver disease specimens which in fact precedes fibrosis (347,348). Additionally, as capillarisation leads to a phenotypic shift of LSEC to a more vascular phenotype, marked changes in scavenger receptor expression also take place in a disease setting (349).

Autophagy is a mechanism that's been linked to liver injury where its dysregulation can lead to oxidative stress as well as contribute to pathogenic lipid accumulation (350). Caveolin-1 (*CAV1*) is a structural protein and subcellular organelle localised to the plasma membrane, involved in LDL transcytosis in endothelial cells and has been proposed as a regulator of autophagy (351). Further highlighting it role as a homeostatic signalling molecule, Caveolin-1 also interacts with the endothelial isoform of nitric oxide synthase while acting as an endogenous inhibitor for the enzyme (352,353) thereby regulating its activity. eNOS is a key enzyme involved in the regulation of LSEC phenotype by fine-tuning the release of NO, a crucial molecule for the maintenance of fenestrations in LSEC (354,355). The expression of Caveolin-1 will therefore also be assessed in this chapter.

It is suggested that LSEC begin to capillarise soon after they are placed in monoculture which typically involves altered or loss of expression of LSEC-specific markers and defenestration of

the plasma membrane (356–358) and therefore it is vital to assess gene expression changes in LSEC in order to evaluate the degree to which the effects of capillarisation observed in chronic liver disease, are recapitulated *in vitro* and the mechanisms linked to these changes.

This chapter aims to describe capillarisation and pseudo-capillarisation of human LSEC, how this process impacts LSEC phenotype and the implications of this in chronic liver disease. For the data presented in this chapter, standard immunohistochemistry protocols and quantitative PCR were used to analyse and compare the expression of Stabilin-2, the mannose receptor, CLEC4M, Caveolin-1 and Collagen I in healthy donor and cirrhotic human liver tissue specimens. The extent of capillarisation *in vitro* was analysed by quantitative PCR in cultured LSECs of early (2-3) and late (4-5) passage as well as freshly isolated LSECs to assess the expression of LSEC-specific and endothelial markers.

4.2 Results

4.2.1 Immunohistochemical analysis of healthy donor and cirrhotic liver tissue specimens

Immunohistochemical analysis to characterise the nature of endothelial populations in the human liver in health and disease was performed. It was of particular interest to report the differences in scavenger and structural protein markers that are characteristic of LSEC in normal and cirrhotic tissue specimens.

Figure 4.1 illustrates the expression of Stabilin-2 in representative healthy donor and ALD cirrhotic human liver tissue sections. The image shows that Stabilin-2 expression is concentrated on discrete cells within the sinusoids observed intermittently throughout the entire liver lobule (Figure 4.1 A-D) in both healthy donor and cirrhotic livers. In addition to occasional Stabilin-2 positive sinusoidal border staining in keeping with LSEC, cells with the appearance of Kupffer cells were also periodically labelled throughout the liver lobule (panel B black arrow). Isotype control staining was negative (Figure 4.1 E). Quantification of staining in multiple fields of view in 5 individual cases per condition (Figure 4.1 F) shows that although a relatively small percentage of the tissue is stained, there was a tendency for increased expression in cirrhotic tissue.

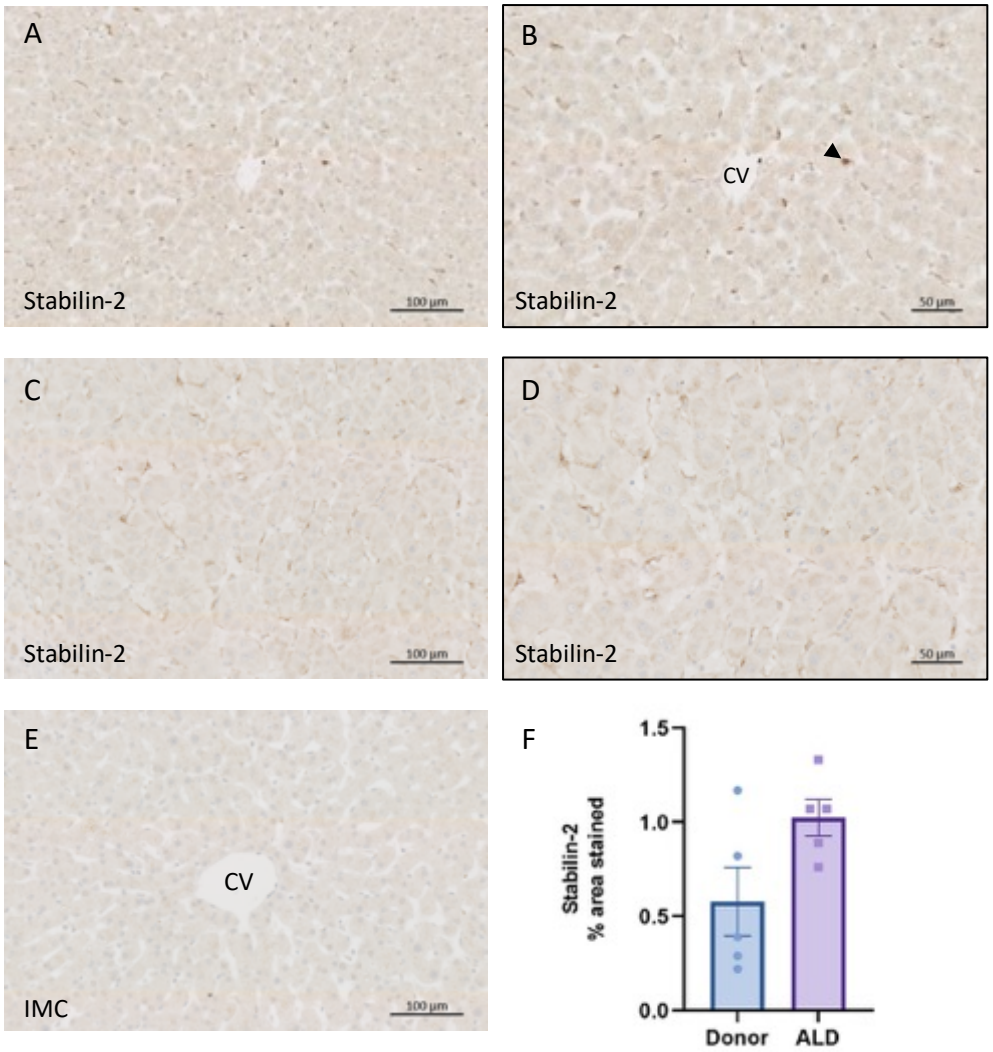

Figure 4.1: Stabilin-2 expression in healthy donor and chronic liver disease specimens

FFPE liver tissue was sectioned (4µm) and stained with anti-stabilin-2 receptor antibody (PA5-55447) at 0.2 ug/ml. Representative images of stabilin-2 stained liver sections from a healthy donor (A & B) and alcoholic liver disease (ALD) (C & d) are shown. Rabbit IgG (ab34417) was used as a negative control at 0.2 µg/ml and panel E shows a representative image of background staining. Scale bar: 100 µm and 50 µm, **F:** Microscopic quantification of percentage area stained, quantified from 5 random fields of view per section in *n*=5 cases per condition. Images were acquired using Axio Scan.Z1 slide scanner (Zeiss) and quantified using ImageJ software. Data are expressed as mean +/- SEM percentage area (bars) and symbols indicate mean values per individual patient in the group. Unpaired t-test confirmed no significant difference in protein expression between groups.

Figure 4.2 shows representative images of mannose receptor expression in healthy donor and ALD liver tissue sections. In contrast to the Stabilin-2 staining, this antigen was expressed in a pattern more characteristic of sinusoidal endothelial cells, with discrete localisation along the walls of the sinusoids. In healthy donor tissue, it was abundantly expressed across the entire liver lobule and localised to both LSEC and Kupffer cells within sinusoidal capillaries. The intensity of expression appears similar across sinusoidal capillaries of the liver lobule. The percentage of tissue staining positively for mannose receptor was much higher than that observed for Stabilin-2. However again there was no significant difference in the area stained when quantitative assessment in healthy donor and ALD liver tissue was performed (Figure 4.2H). In ALD tissue on the other hand, there was dispersed positive expression of mannose receptor on LSEC within nodules and it also localised to vessels within fibrotic septa.

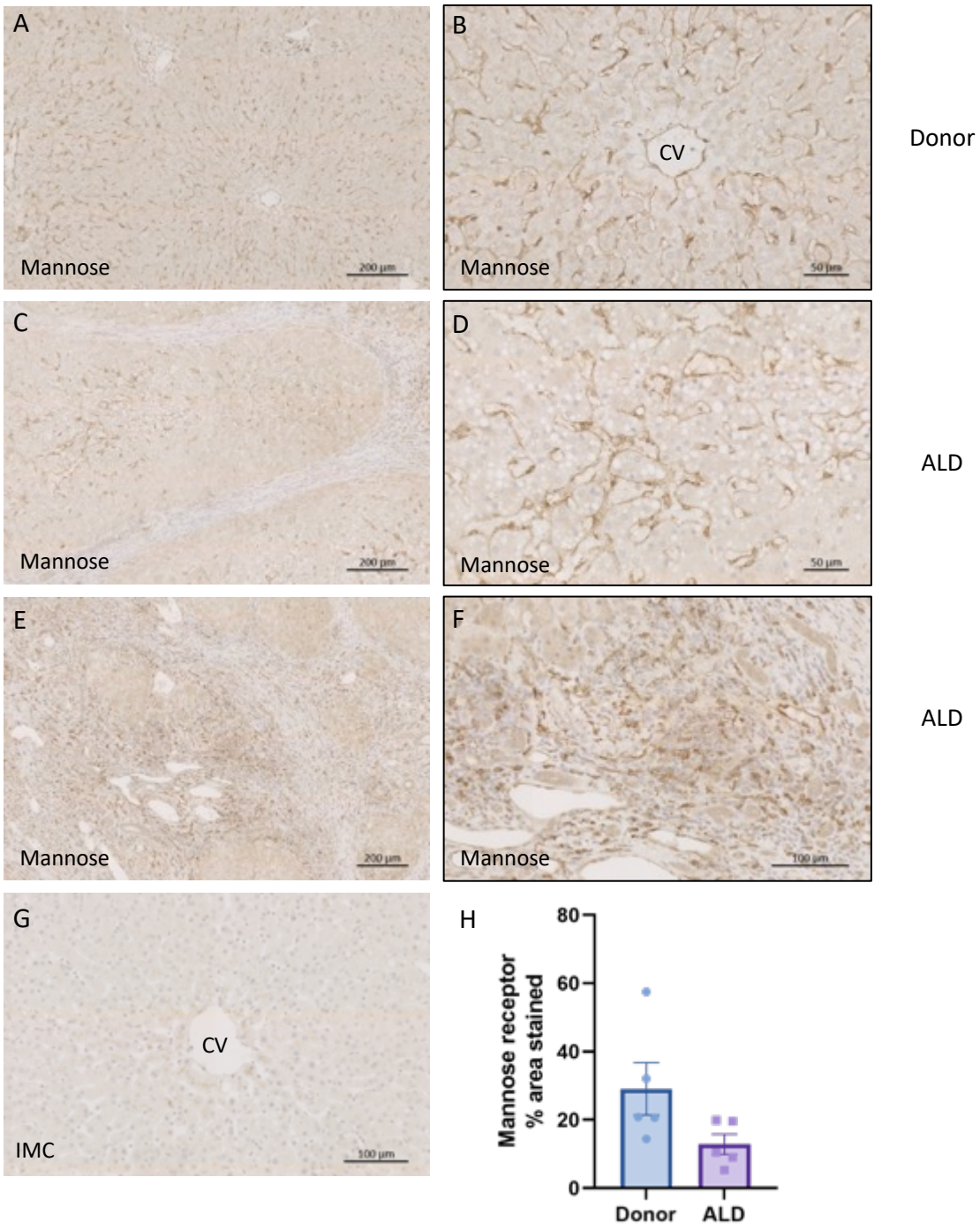

***Figur*e 4.2: Mannose receptor expression in healthy donor and cirrhotic liver tissue specimens**

FFPE liver tissue was sectioned (4µm) and stained with anti-mannose receptor antibody (ab64693) at 2 ug/ml. Representative images of mannose receptor stained liver sections from donor (A & B) and alcoholic liver disease (ALD) (C & D) are shown. Panels E and F show representative images of mannose expression in fibrotic septa of ALD specimens. Rabbit IgG (ab34417) was used as a negative control at 2 µg/ml and panel G shows a representative image of background staining. Scale bar: 100 µm and 50 µm, **H:** Microscopic quantification of percentage area stained, quantified from 5 random fields of view per section in *n*=5 cases per condition. Images were acquired using Axio Scan.Z1 slide scanner (Zeiss) and quantified using ImageJ software. Data are expressed as mean +/- SEM percentage area (bars) and symbols indicate mean values per individual patient in the group. Unpaired t-test confirmed no significant difference in protein expression between groups.

Next, assessment of CLEC4M expression was carried out and this receptor had a distinct expression pattern compared to the two previous proteins (Figure 4.3). In both healthy donor (panels A and B) and chronic liver disease liver tissue specimens (panels C and D), expression was again localised to cells on the sinusoidal walls but varied across the lobule. In healthy donor tissue specimens, CLEC4M expression was most intense in cells within sinusoidal capillaries in zone 2 with faint intermittent labelling in zone 3. Positive expression was absent in portal areas. This pattern was also seen in cirrhotic tissue but CLEC4M expression intensity was diminished in ALD tissue. Staining quantitation from multiple fields of view from a set of different cases of healthy donor and cirrhotic liver specimens revealed a significant reduction in CLEC4M positively stained cells in cirrhotic liver specimens (Figure 4.3F).

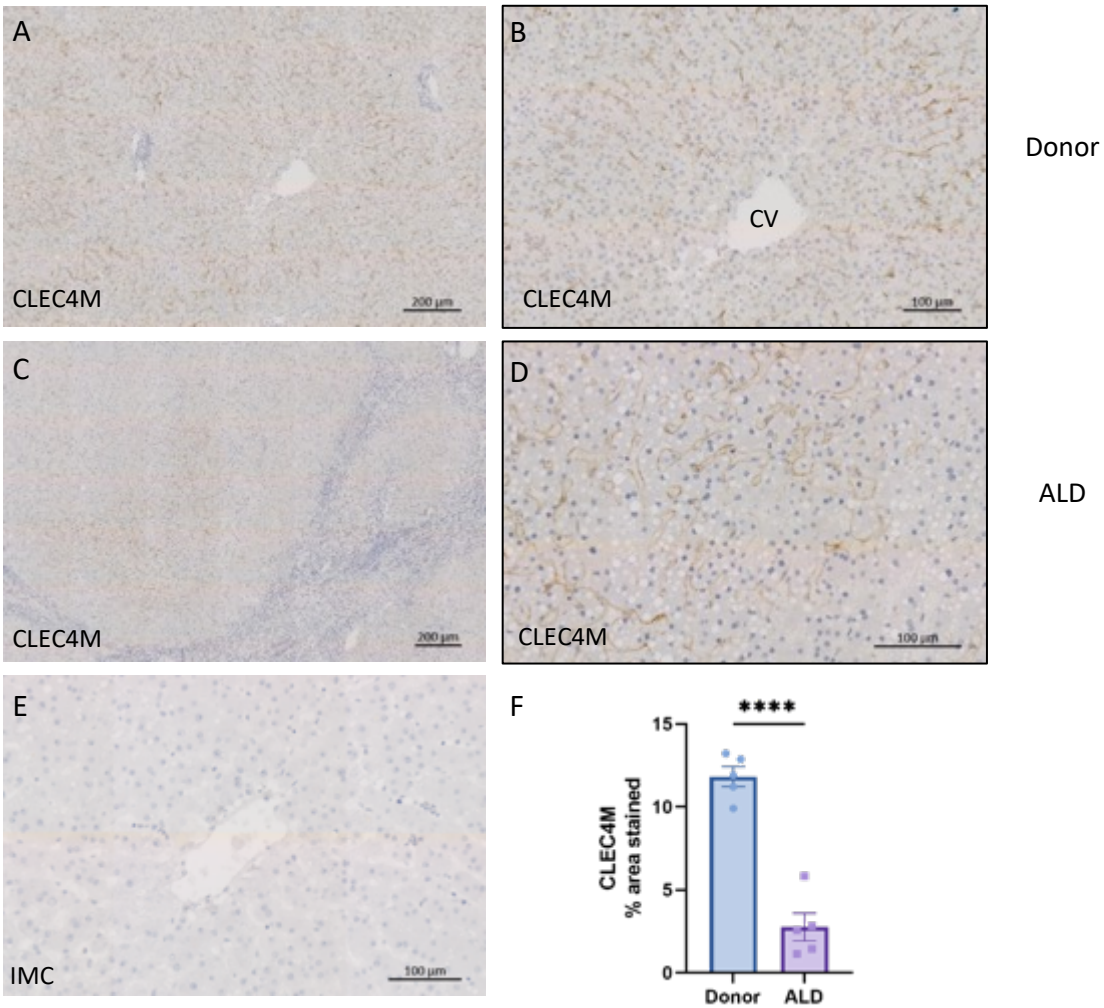

Figure 4.3: CLEC4M expression is significantly reduced in chronic liver disease specimens compared to healthy donor

FFPE liver tissue was sectioned (4µm) and stained with anti-CLEC4M antibody (HPA042661) at 1 ug/ml. Representative images of CLEC4M stained liver sections from healthy donor (A & B) and alcoholic liver disease (ALD) (C & D) are shown. Rabbit IgG (ab34417) was used as a negative control at 1 µg/ml and panel E shows a representative image of background staining. **F:** Microscopic quantification of percentage area stained, quantified from 5 random fields of view per section in *n*=5 cases per condition. Images were acquired using Axio Scan.Z1 slide scanner (Zeiss) and quantified using ImageJ software. Data are expressed as mean +/- SEM percentage area (bars) and symbols indicate mean values per individual patient in the group. Unpaired t-test confirmed a significant difference between groups with ****p-value <0.0001.

Figures 4.4 and 4.5 show representative images of Caveolin-1 expression in healthy donor and ALD liver tissue sections respectively. In healthy donor tissue, Caveolin-1 is abundantly expressed throughout the entire liver lobule and localises to both LSEC and Kupffer cells within sinusoidal capillaries as well as vascular and arterial vessels in portal areas as shown in Figure 4.4 B. The intensity of expression appears similar across sinusoidal capillaries and portal vessels. Caveolin-1 expression was also localised to endothelial cells in ALD specimens but there appeared to be less intense staining when compared to healthy donor as illustrated by Figure 4.5 panel A. Vessels within fibrotic septae in cirrhotic specimens were also positive. As seen previously with other proteins such as the mannose receptor however, altered expression was not statistically significant when staining quantitation was carried out from multiple donors (Figure 4.5 F).

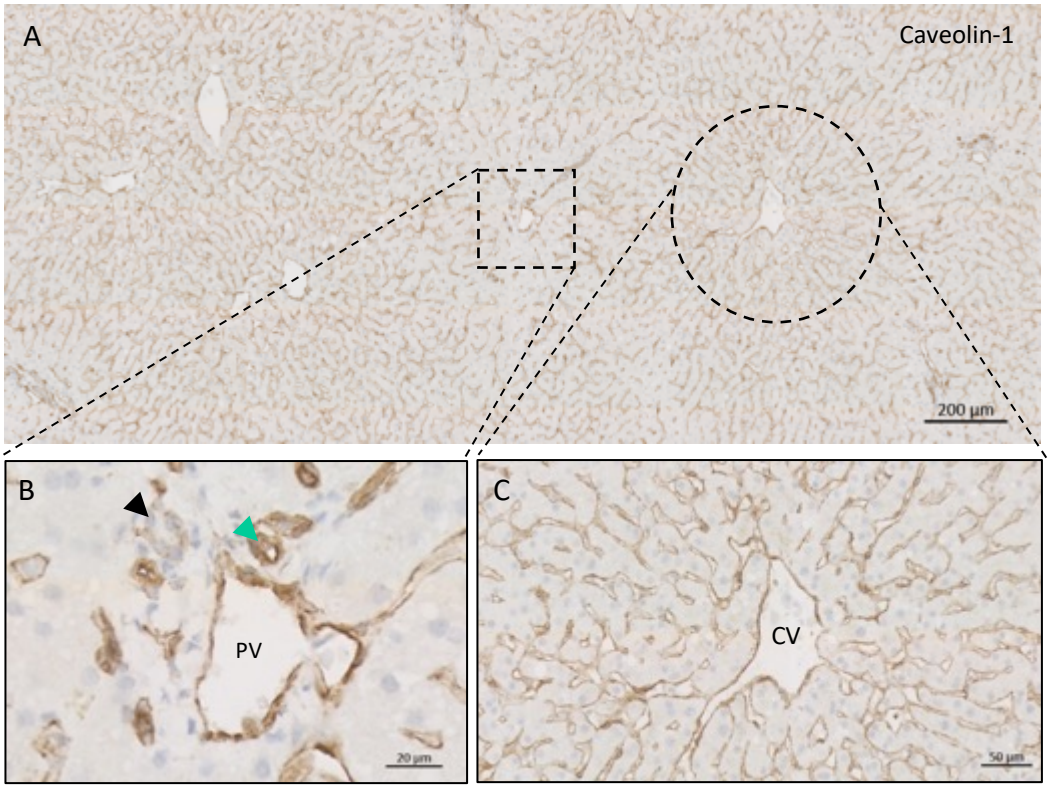

Figure 4.4: Caveolin-1 expression in healthy donor liver specimens

FFPE liver tissue was sectioned (4µm) and stained with anti-Caveolin-1 antibody (ab192869) at 3 ug/ml. Representative images of Caveolin-1 stained liver sections from healthy donor liver specimens are shown. Scale bar: 200 µm and 50 µm. **B:** Caveolin-1 expression in portal tract area; black arrow: bile duct; green arrow: portal artery; PV: portal vein **C:** CV: central vein.

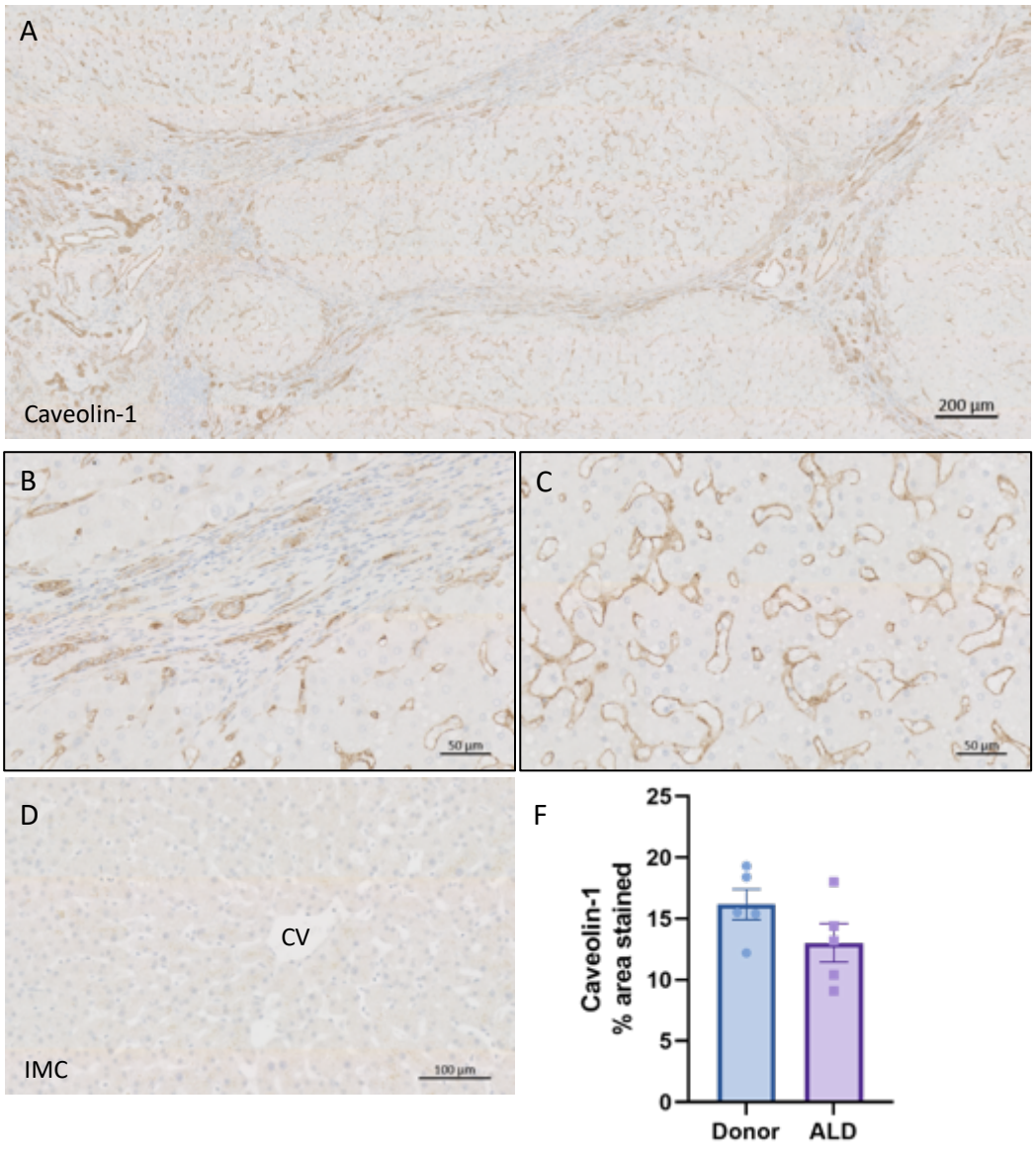

Figure 4.5: Caveolin-1 expression in chronic liver disease specimens

FFPE liver tissue was sectioned (4µm) and stained with anti-Caveolin-1 antibody (ab192869) at 3 ug/ml. Representative images of Caveolin-1 stained liver sections from alcoholic liver disease (ALD) liver tissue specimens are shown (A-C). Scale bar: 200 µm, 50 µm and 100 µm. Rabbit IgG (ab34417) was used as a negative control at 3 µg/ml and panel D shows a representative image of background staining. Scale bar: 200 µm, 50 µm and 100 µm, **F:** Microscopic quantification of percentage area stained, quantified from 5 random fields of view per section in *n*=5 cases per condition. Images were acquired using Axio Scan.Z1 slide scanner (Zeiss) and quantified using ImageJ software. Data are expressed as mean +/- SEM percentage area (bars) and symbols indicate mean values per individual patient in the group. Unpaired t-test confirmed no significant difference in protein expression between groups.

The basal lamina below LSEC is modest, and this expands over time during the progression of fibrosis. To illustrate this, Figures 4.6 and 4.7 show the expression of Collagen I in healthy donor and ALD tissue specimens respectively. In healthy donor, the labelling intensity increases across the liver lobule zones 1 to 3. Collagen I was present in sinusoidal walls throughout the entire liver lobule as well as on vascular and arterial vessels in portal areas. The intensity of expression was most intense in venous walls in the central and periportal areas. In ALD specimens, expression of collagen was much more abundant and was particularly pronounced in fibrotic septa (Figure 4.7 panel B). Interestingly, there appeared to be less subendothelial Collagen I present within regenerative nodules seen in ALD liver specimens compared to the uniform expression seen in healthy donor liver tissue. Overall, Collagen I expression was significantly increased in ALD specimens.

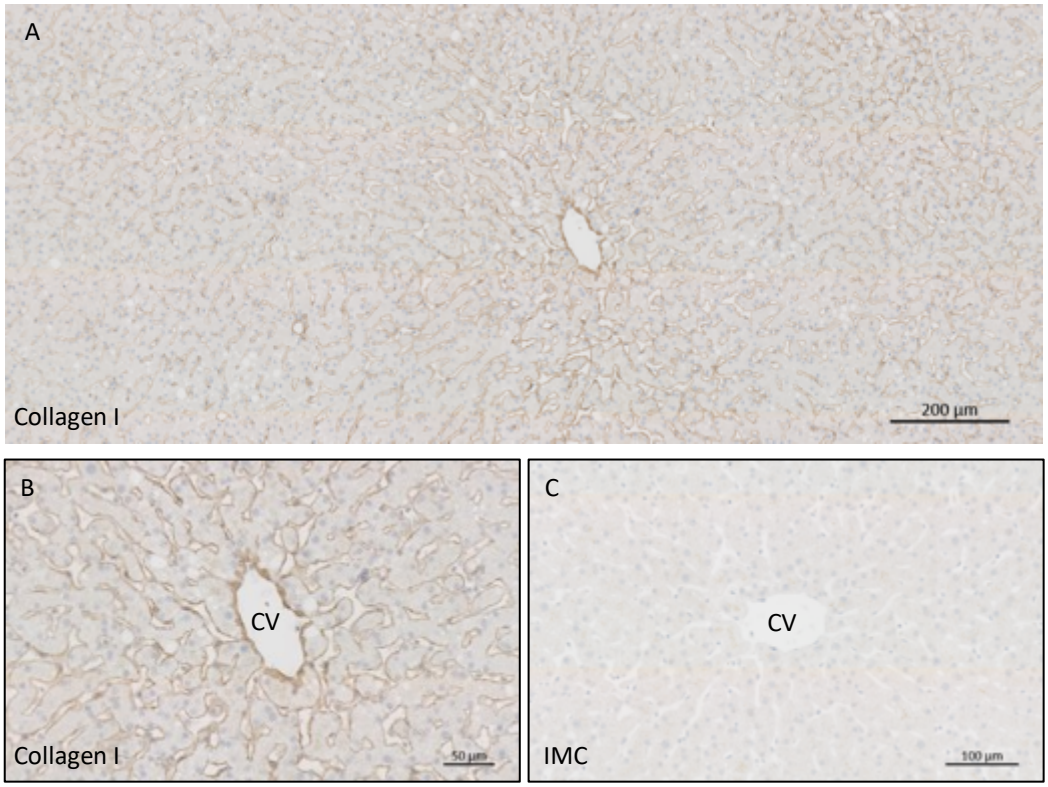

Figure 4.6: Collagen I expression in healthy donor liver tissue specimens

FFPE liver tissue was sectioned (4µm) and stained with anti-Collagen I antibody (ab34710) at 5 ug/ml. Representative images of Collagen I stained liver sections from healthy donor are shown. Rabbit IgG (ab34417) was used as a negative control at 5 µg/ml and panel C shows a representative image of background staining. Scale bar: 200, 100 and 50 µm.

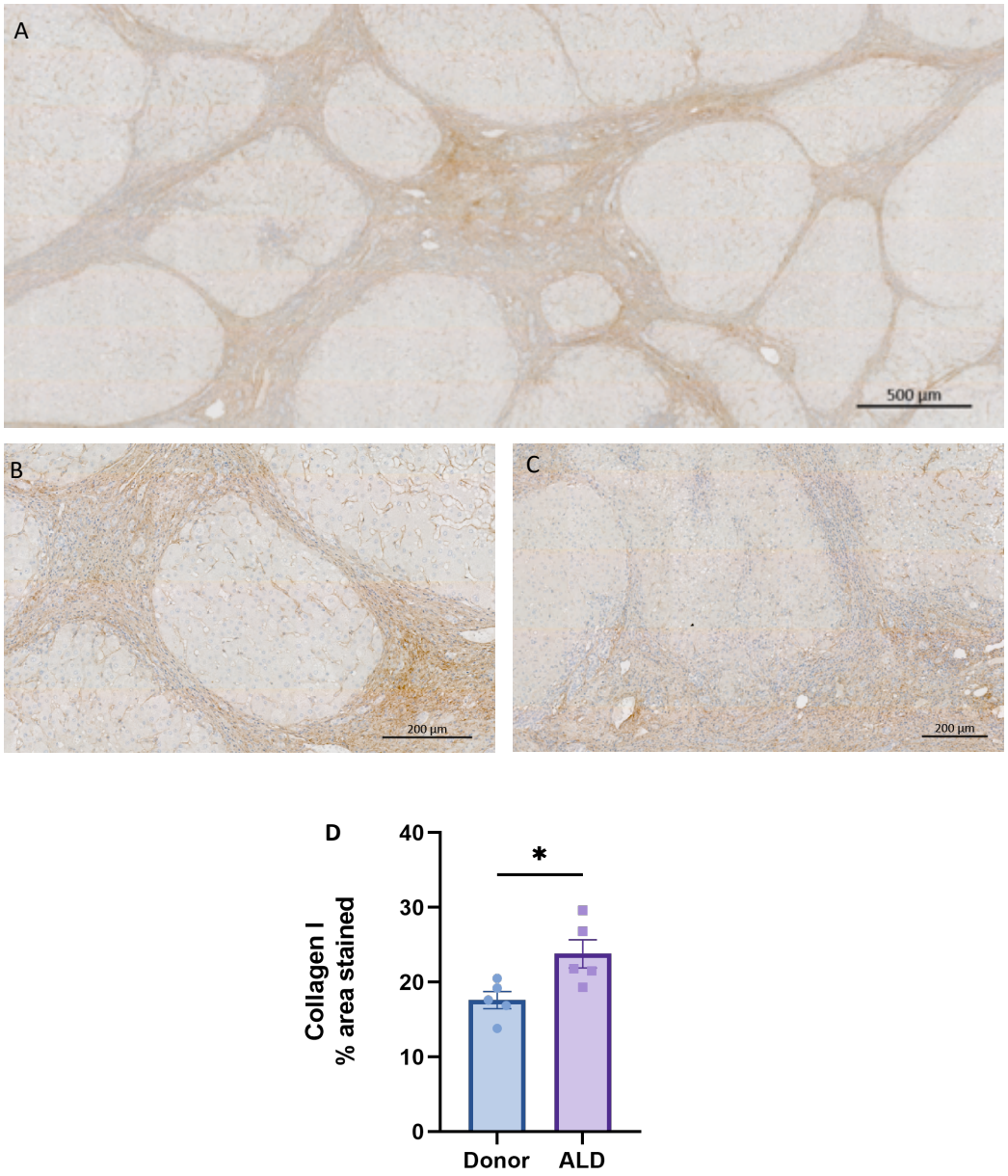

Figure 4.7: Collagen I expression in chronic liver disease tissue specimens

FFPE liver tissue was sectioned (4µm) and stained with anti-Collagen I antibody (ab34710) at 5 ug/ml. Representative images of Collagen I stained liver sections from ALD (alcoholic liver disease) are shown. Scale bar: 200 µm and 50 µm. **D:** Microscopic quantification of percentage area stained, quantified from 5 random fields of view per section in *n*=5 cases per condition. Images were acquired using Axio Scan.Z1 slide scanner (Zeiss) and quantified using ImageJ software. Data are expressed as mean +/- SEM percentage area (bars) and symbols indicate mean values per individual patient in the group. Unpaired t-test confirmed a significant difference between groups with *p-value <0.05.

4.2.2 Gene expression analysis using quantitative PCR for sinusoidal endothelial markers in human whole liver tissue.

In addition to immunohistochemical analysis, mRNA expression was analysed using quantitative PCR of whole tissue RNA extracted from healthy donor, ALD, and NASH specimens. Analysed genes were chosen based on endothelial relevance, but expression of collagen was also confirmed using this method.

Figure 4.8 illustrates relative mRNA expression of *CAV1* (Caveolin-1), *KDR (*VEGF receptor-2), *FLT1 (*VEGF receptor-1) and *NOS3* (eNOS) normalised to the housekeeping gene *SRSF4* in normal donor, ALD, and NASH cirrhotic samples. *CAV1* mRNA expression (Figure 2.8 panel A) illustrated a clear trend whereby expression increased in ALD and NASH compared to healthy donor. However, in line with staining findings (Figure 4.4 and Figure 4.5) this increase was not statistically significant. It is notable that there was slightly greater variation in expression within the NASH group of specimens. *KDR* relative expression is shown in panel B. *KDR* encodes VEGFR2, and its expression remained relatively unchanged between healthy donor, ALD, and NASH specimens. Despite this, mRNA expression of *KDR* showed inter individual variation between biological replicates in healthy donor and NASH, while mRNA levels remined comparable for biological replicates of ALD. Similarly, Panel C illustrates the relative expression of *FLT1* encoding for VEGFR1, which appears slightly elevated in diseased tissue specimens but again was variable between individuals with no significant differences in the mean for groups. mRNA expression for *NOS3* which is the gene encoding for the endothelial isoform of the nitric oxide synthase enzyme (eNOS) is shown panel D. Expression levels for this gene were quite low for all three groups of specimens compared to expression levels of other genes presented here, with no statistically significant change in expression in disease.

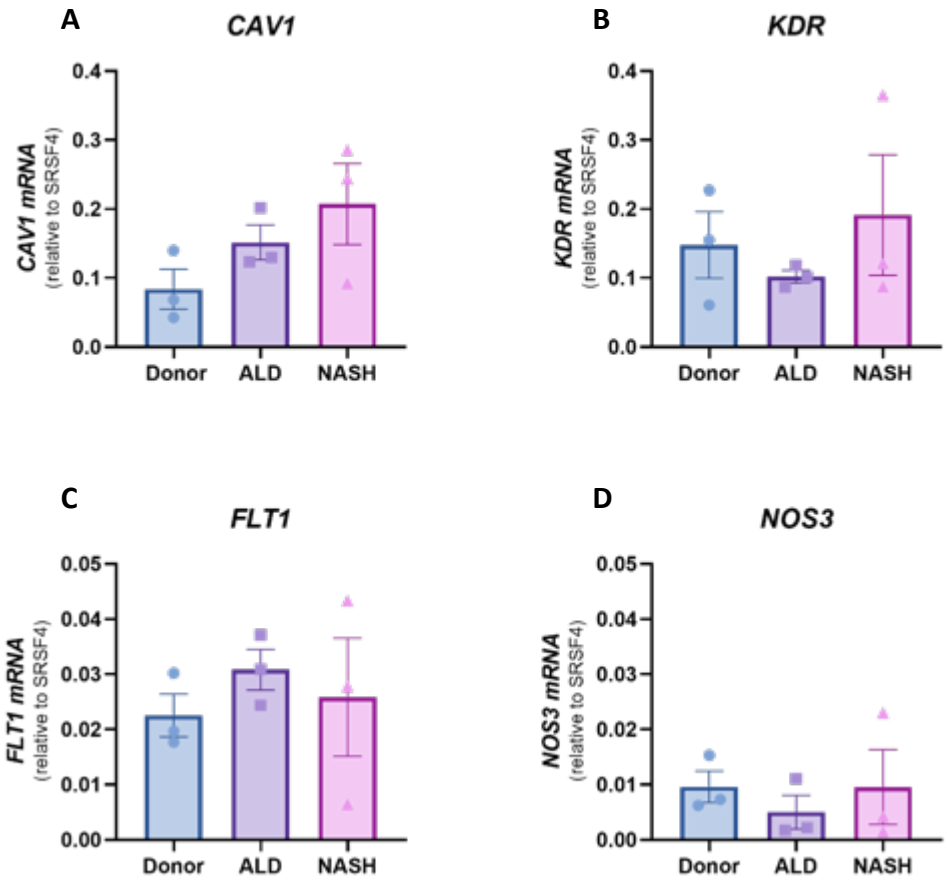

Figure 4.8: *CAV1* mRNA expression is increased in diseased livers compared to normal while *NOS3, FLT1* and *KDR* gene expression is not altered

Data represent changes in relative gene expression for *CAV1*, *KDR*, *FLT1* and *NOS3* determined by quantitative PCR. Gene expression levels are shown relative to *SRSF4* housekeeping gene and data are expressed as mean +/- SEM change in expression (bars) for *n*=3 separate cases of normal, ALD and NASH liver tissue. Symbols indicate data from individual samples. Ordinary one-way ANOVA test showed no significant difference in gene expression when normal liver was compared to either ALD or NASH tissue.

Figure 4.9 shows the relative expression of scavenger receptor genes namely *FCGR2B* (CD32B/ FcγRIIb), *MRC1* (mannose receptor), *CD36*, *CLEC4M*, *LYVE-1* and *STAB2* (stabilin-2) normalised to the housekeeping gene *SRSF4* in healthy donor, ALD, and NASH cirrhotic samples. For this set of genes some clear differences were noted in cirrhotic specimens but again interindividual variation and small sample sizes meant that values did not become statistically significant. Panel A illustrates mRNA expression of *FCGR2B*, which encodes for the FcγRIIb. Levels of expression are comparable between normal donor, ALD and NASH whole live tissue specimens which remain relatively unchanged; thus, no significant difference was detected by the ordinary one-way ANOVA test performed. This contradicts the outcome of immunohistochemical analysis presented in chapter 3 Figure 3.4 where protein expression of FcγRIIb (CD32B) was significantly reduced in ALD tissue specimens. The *MRC1* gene codes for the mannose receptor, a prominent scavenger receptor expressed by LSEC and Kupffer cells within the liver. *MRC1* mRNA expression is decreased in ALD liver tissue specimens compared to normal donor a shown in panel B. Although not statistically significant, mRNA expression of *MRC1* appeared slightly increased in NASH specimens compared to ALD. Interindividual variation within each group renders *MRC1* mRNA expression levels relatively unchanged. mRNA level of *MRC1* in healthy donor and cirrhotic specimens showed a similar trend as protein expression levels shown in Figure 4.2. *CD36* mRNA expression, illustrated in panel C is comparable across normal donor, ALD, and NASH while mRNA expression for *CLEC4M* shown in panel D follows a similar pattern with the exclusion of higher expression in one of the specimens within the healthy donor group. *LYVE1* mRNA expression appears slightly increased in NASH compared to ALD however this difference was not statistically significant. mRNA expression levels for *LYVE-1* in healthy donor tissue specimens exhibited interindividual

variation with levels comparable to cirrhotic specimens. In contrast to this, protein expression levels of LYVE-1 (Figure 3.5) analysed by immunohistochemistry revealed a significant decrease in expression in cirrhotic specimens compared to healthy donor. *STAB2* (stabilin-2) is another scavenger receptor gene shown in panel F. Its mRNA expression remained relative consistent between healthy donor, ALD, and NASH specimen groups with the exemption of one specimen within the healthy donor group. This is comparable to protein expression levels of Stabilin-2 shown in Figure 4.1. Overall, no statistical difference was detected between normal donor and the disease specimen groups in any of the genes presented in Figure 4.9.

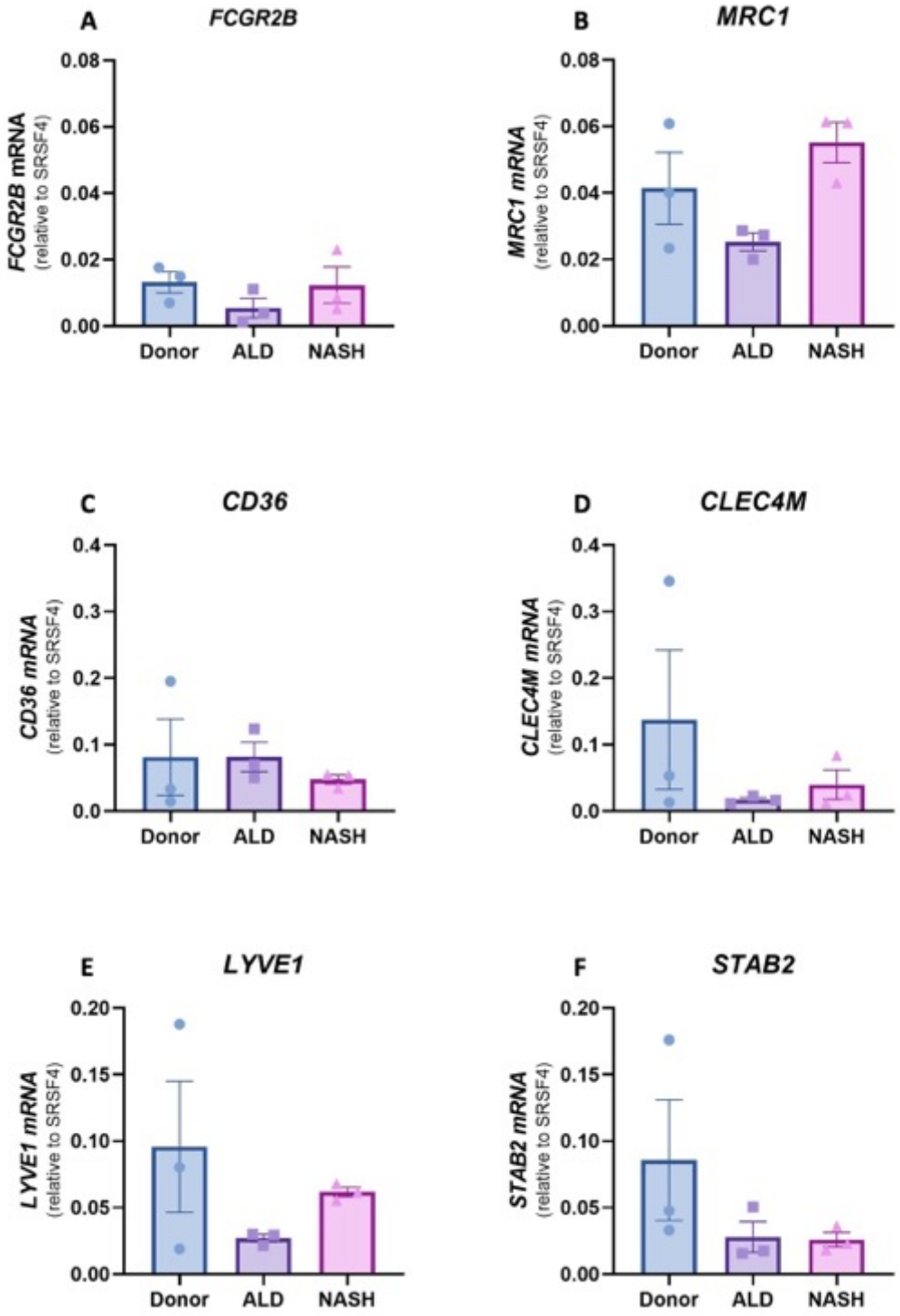

Figure 4.9: Scavenger receptor expression in healthy donor, ALD, and NASH tissue specimens

Data represent changes in relative gene expression for *FCGR2B, MRC1, CD36, CLEC4M, LYVE1* and *STAB2* determined by quantitative PCR. Gene expression levels are shown relative to *SRSF4* housekeeping gene and data are expressed as mean +/- SEM change in expression (bars) for *n*=3 separate cases of normal, ALD and NASH liver tissue. Symbols indicate data from individual samples. Ordinary one way ANOVA test showed no significant difference in gene expression when normal liver was compared to either ALD or NASH tissue.

The mRNA expression for *GATA4*, a transcription factor described to play a role in the acquisition of LSEC-specific phenotype, was also quantified (32). Figure 4.10 panel A shows that relative expression of *GATA4* is at relatively similar levels between healthy donor, ALD and NASH whole liver specimens. In comparison, panel B illustrates the relative expression of *PECAM1* (CD31) which is significantly increased in ALD and NASH specimen groups compared to normal donor. Finally, to confirm the presence of fibrogenesis in cirrhotic sample, the relative expression for *COL1A1* was screened, which is shown in panel C. The *COL1A1* gene encodes for collagen I which is one of the main types of collagens expressed within the liver. Reassuringly, *COL1A1* was overexpressed in ALD and NASH specimens compared to healthy donor.

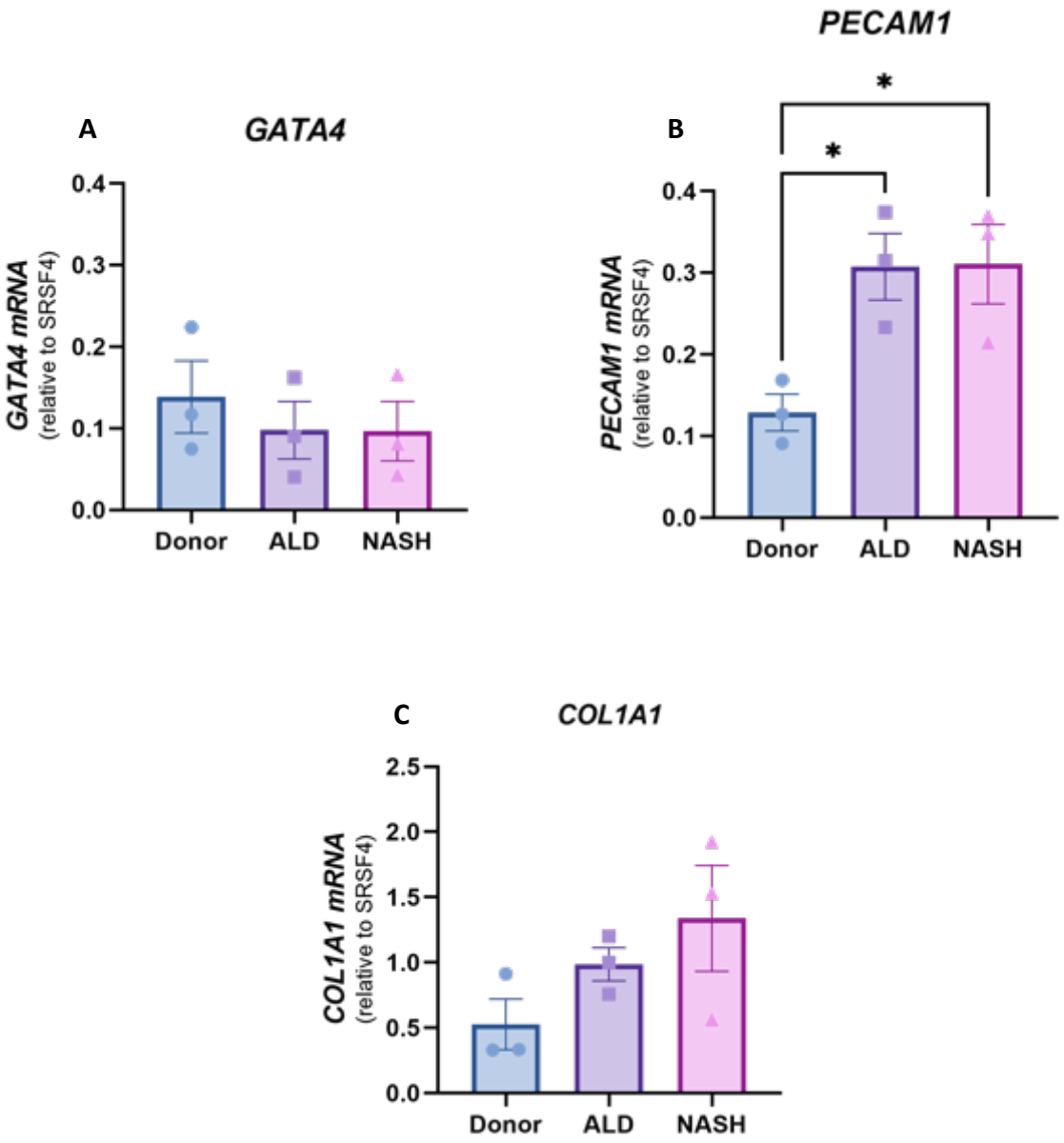

Figure 4.10: *PECAM1* and *COL1A1* mRNA expression is increased in diseased livers compared to normal while *GATA4* gene expression is altered

Data represent changes in relative gene expression for *GATA4, PECAM1* and *COL1A1* determined by quantitative PCR. Gene expression levels are shown relative to *SRSF4* housekeeping gene and data are expressed as mean +/- SEM change in expression (bars) for *n*=3 separate cases of normal, ALD and NASH liver tissue. Symbols indicate data from individual samples. Ordinary one-way ANOVA test showed significant difference in gene expression when normal liver was compared to either ALD or NASH tissue where indicated by * p-value < 0.05.

4.3 Gene expression analysis using quantitative PCR of sinusoidal endothelium markers in passaged LSEC.

Following the analysis of conventional and LSEC specific markers by quantitative PCR in whole liver specimens it was crucial to also obtain the levels of expression of these markers in the specific cell type in question. Thus, primary LSECs were utilised to obtain levels of mRNA expression. Low passage LSEC were used at passage 2 and 3 while high passage LSEC were propagated in culture to passage 4 and 5 for the purpose of tracking gene expression across lifespan of donor and cirrhotic LSEC in culture.

Figure 4.11 illustrates mRNA expression of *CAV1, KDR, FLT1* and *NOS3* in passaged LSEC. Gene expression was normalised to the housekeeping gene, *SRSF4*. The first thing of note was that relative expression was much higher in purified LSEC cultures than seen in whole tissue mRNA for all genes. Panel A illustrates mRNA expression of *CAV1* in early and late passage LSEC isolated from healthy donor and cirrhotic samples. Again, this was found to be one of the highest expressed genes in this set although quite variable amongst individual samples in each group. Notably, both normal and cirrhotic cells at low and high passage had similar expression of this gene. *KDR* mRNA expression also was relatively consistent, and more abundant in LSEC than whole tissue albeit at lower levels compared to CAV1 expression (panel B). This was also similar for *FLT1* shown in Figure 4.11C. The most interesting outlier in this group of genes, *NOS3* is presented in panel D. For this gene, mRNA expression was shown to significantly increase with passage of both healthy donor and diseased liver derived LSEC. Interestingly though, starting levels were similar in both cirrhotic and healthy donor LSEC.

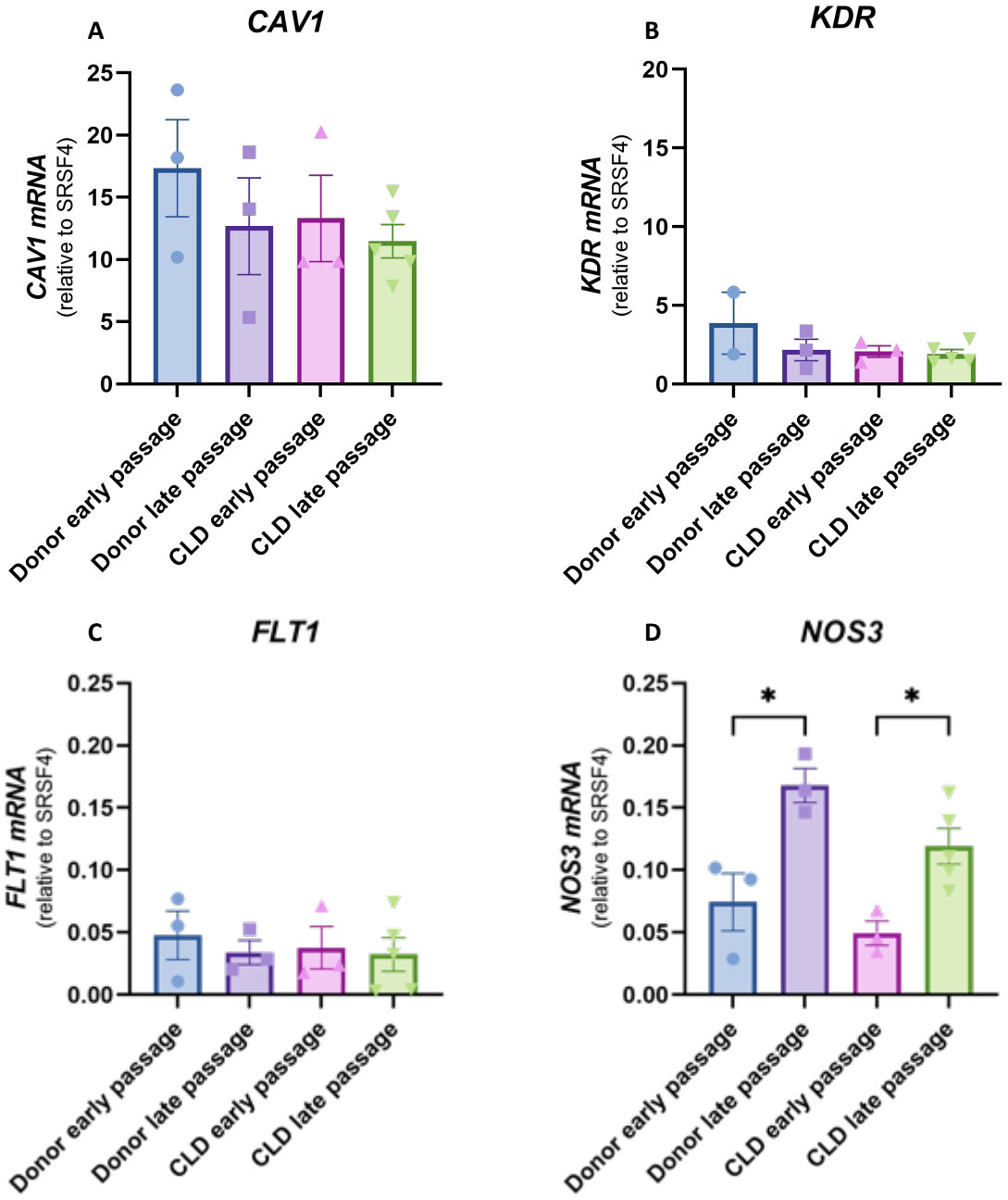

Figure 4.11: *NOS3* mRNA expression is increased in high passage LSEC compared to low passage *while CAV1, KDR* and *FLT1* gene expression is altered

Data represent changes in relative gene expression for *CAV1, KDR, FLT1* and *NOS3* determined by quantitative PCR. Gene expression levels are shown relative to *SRSF4* housekeeping gene and data are expressed as mean +/- SEM change in expression (bars) for $n \geq 3$ separate cases of donor and CLD LSEC samples. Symbols indicate data from individual samples. Early passage groups include LSEC at passage 2 and 3 while late passage include LSEC at passage 4 and 5. Ordinary one way ANOVA test showed significant difference in gene expression when Donor early passage was compared to either donor late passage or CLD early passage groups where indicated by * p-value < 0.05.

In Figure 4.12, the mRNA expression of scavenger receptor genes in cultured LSEC is shown in panels A-E. mRNA expression for *STAB2* was similar in both donor and cirrhotic early and late passage LSEC (Figure 4.12A). In contrast, *CLEC4M* mRNA expression (panel B), appeared more abundant in healthy donor LSEC compared to *STAB2.* Expression was reduced in cirrhotic LSEC and there appeared to be no impact of passage in either group. *CD36* was expressed to a high level in isolated LSEC from normal and disease tissue, with highest expression seen in passaged cells from cirrhotic donors (panel C). *LYVE1* mRNA expression is illustrated in panel D and was again more abundant in isolated LSEC than in whole tissue. Expression was comparable between healthy donor and cirrhotic early and late passage groups, with the apparent reduction in cirrhotic cells not statistically significant. Again, mRNA expression for *MRC1* was the most different in this gene set as observed in whole tissue. In LSEC, relative gene expression was increased further when cirrhotic cells were passaged with significantly increased expression in high passage cirrhotic LSEC compared to low passage cells and high passage donor LSEC.

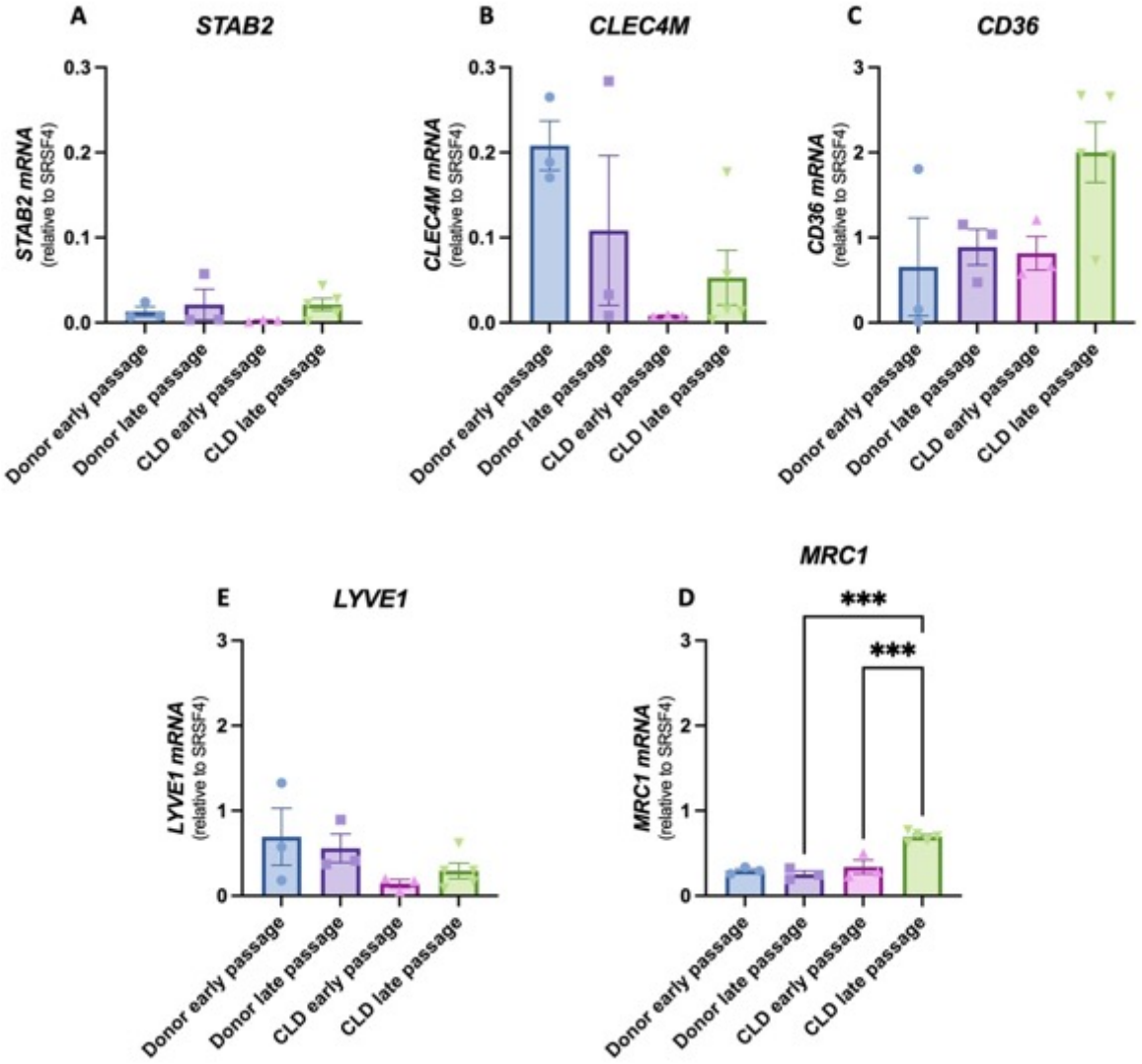

Figure 4.12: *MRC1* mRNA expression is increased in high passage LSEC compared to low passage, while *STAB2, CLEC4M CD36* and *LYVE1* gene expression is altered

Data represent changes in relative gene expression for *STAB2, CLEC4M, CD36, LYVE1* and *MRC1* determined by quantitative PCR. Gene expression levels are shown relative to *SRSF4* housekeeping gene and data are expressed as mean +/- SEM change in expression (bars) for $n \geq 3$ separate cases of donor and CLD LSEC samples. Symbols indicate data from individual samples. Early passage groups include LSEC at passage 2 and 3 while late passage include LSEC at passage 4 and 5. Ordinary one way ANOVA test showed no significant difference in gene expression between groups unless otherwise indicated by *** p-value < 0.001.

Figure 4.13 shows the mRNA expression for the characteristic LSEC and endothelial cell markers *GATA4* and *PECAM1*. *GATA4* mRNA expression (panel A) was present at a relatively low level in LSEC compared to other genes such as *PECAM1*. There was a decrease in expression in healthy donor late passage cells buts levels were comparable between CLD early and late passage groups. Unexpectedly for the sets of samples utilised herein, expression of *PECAM1* mRNA (panel B) appeared to be downregulated in late passage donor LSEC compared to early passage cells. The cirrhotic cells appeared to have the lowest relative expression regardless of passage. Again, there was considerable variation between donors however so none of the changes between groups were significant.

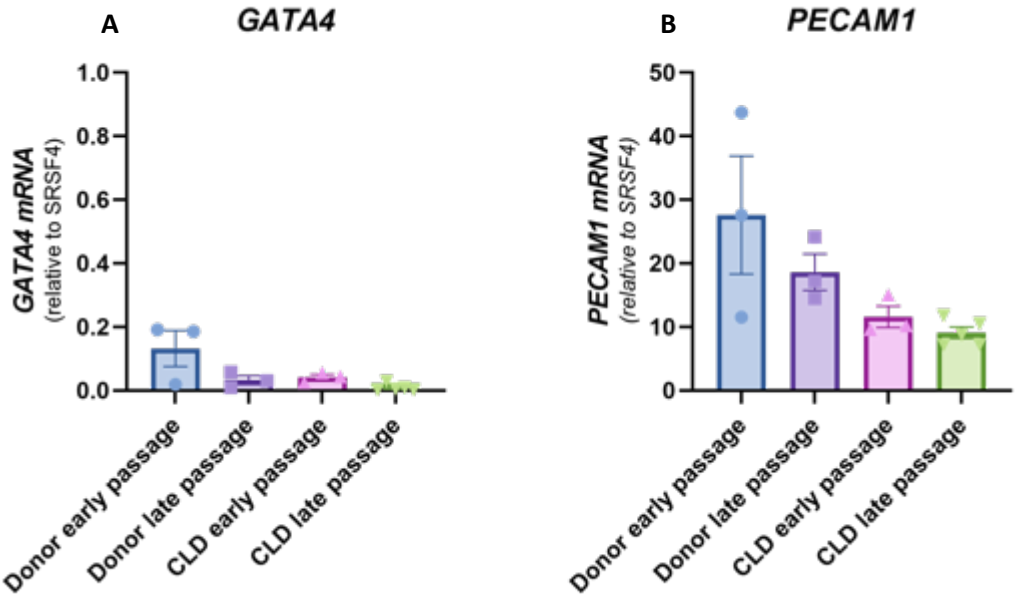

Figure 4.13: *GATA4* and *PECAM1* mRNA expression is decreased in high passage LSEC compared to low passage

Data represent changes in relative gene expression for *GATA4 and PECAM1* determined by quantitative PCR. Gene expression levels are shown relative to *SRSF4* housekeeping gene and data are expressed as mean +/- SEM change in expression (bars) for $n \geq 3$ separate cases of donor and CLD LSEC samples. Symbols indicate data from individual samples. Early passage groups include LSEC at passage 2 and 3 while late passage include LSEC at passage 4 and 5. Ordinary one way ANOVA test showed no significant difference in gene expression in comparisons between all groups.

4.4 Discussion

The process of LSEC capilarisation as well as dysregulation of function is complex and therefore assessing the expression levels of key LSEC markers can point to molecular interactions and mechanisms involved in the progression of liver disease. As LSEC are involved in multiple processes and play a key role in maintaining hepatic homeostasis, the first step was to assess the expression of key molecules enabling LSEC to perform critical functions such as scavenging and pathogen recognition.

Expression of the scavenger receptor Stabilin-2 at protein level was the lowest amongst the markers analysed by immunohistochemistry in terms of the area of positively stained cells in tissue specimens, however Stabilin-2 positive, flat cells lining the sinusoids were identified. A similar expression pattern for Stabilin-2 was reported in rat and human liver tissue sections (265,359). In contrast, a different report of Stabilin-2 expression in rat liver sections assessed by immunofluorescence, suggested uniform expression of this receptor across the liver lobule (132). While staining quantification appeared to be slightly increased in cirrhotic specimens, mRNA expression of *STAB2* quantified using quantitative PCR was unchanged between healthy donor and cirrhotic whole tissue specimens. In cultured healthy donor and cirrhotic, early, and late passage LSEC however, mRNA expression for *STAB2* was the lowest amongst the receptors analysed which are characteristic of the LSEC-specific phenotype. A factor contributing to differences in mRNA expression levels between whole tissue RNA and isolated LSEC is the fact that although the same amount of liver tissue was used as starting material (determined by weight), the proportion of each hepatic cell type present within each sample is unknown and cannot be controlled for. It is also possible to decipher cell-specific

expression from bulk mRNA. Stabilin-2 was proposed to play a role in lymphocyte adhesion to LSEC under physiological shear stress through its interaction with $\alpha M\beta 2$ integrin. This suggests mechanistic involvement of Stabilin-2 in the context of lymphocyte trafficking during liver injury as the downregulation of Stabilin-2 was shown to result in defective lymphocyte binding (265). This also indicates that stabilin-2 expression could be modulated by the hepatic immune microenvironment as well as shear stress. As LSEC culture was carried out in static conditions, this could be a potential explanation for the low mRNA levels of *STAB2* in healthy donor and cirrhotic LSEC at both early and late passage. On the other hand, maintenance of low levels of expression of Stabilin-2 could be a strategic move to protect the liver in disease as in the context of hepatocellular carcinoma, loss of this receptor in peri-tumorous live tissue correlated with increased survival (222). Hyaluronan and collagen pro-peptides are ligands cleared by the Stabilin-2 receptor, and collagen deposition is a major contributor to the process of fibrosis in chronic liver disease. Additionally, hyaluronan serum levels are elevated in liver cirrhosis (360) and in relation to this, high expression of Stabilin-2 has been reported in lymph nodes which account for a minimum of 80% of the elimination of hyaluronan from circulation(361). Despite this fact, accumulation of extracellular matrix components such as hyaluronan and collagen persists in liver fibrosis, which highlights impaired clearance. It can therefore be proposed that an increase in expression of Stabilin-2 would be useful in cirrhotic liver specimens in order for LSEC to keep up with the increasing demand for clearance of hyaluronan and other matrix proteins.

Another major contributor to LSEC's high scavenging activity is the mannose receptor which is responsible for the clearance of denatured collagen(343) as well as bacterial and yeast pathogens(362–364). Protein expression of the mannose receptor assessed by

immunohistochemical analysis in healthy donor and cirrhotic liver tissue specimens showed the expression of this receptor in both conditions as well as the presence of the mannose receptor within fibrotic areas which highlights its important clearance function. Quantitation of *MRC1* mRNA expression in whole tissue specimens showed similar results. Whole tissue specimens included Kupffer cells which also express the mannose receptor (365) and this they will contribute to the signal from while tissue. However, the transcriptome as well as proteome of this receptor was found to be more enriched in LSEC compared to Kupffer cells (132). In cultured LSEC, passaging of cirrhotic LSEC lead to significantly increased *MRC1* expression, while it was also higher in cirrhotic late passage LSEC compared to donor late passage LSEC. The expression of the mannose receptor has also been reported by immunocytochemistry in cultured rat LSEC (132). Interestingly, a soluble form of the mannose receptor in humans has been reported whereby the median plasma level of this receptor was significantly increased in patients with ALD compared to healthy controls (366). This demonstrates altered processing of mannose receptor protein in disease and is in keeping with our description of elevated expression in cirrhotic cells. A future experiment to elucidate this in cultured healthy donor and diseased LSEC is the quantification of soluble mannose receptor by ELISA.

Immunohistochemical analysis of LYVE-1 in healthy donor and cirrhotic tissue sections showed a significant reduction in LYVE-1 expression in cirrhotic specimens (Figure 3.5). These findings agree with previous reports of LYVE1 protein expression by immunohistochemistry stating the reduced expression of LYVE1 in chronically inflamed liver tissue specimens (242). LYVE-1 exhibits 43% homology with CD44 which can bind collagen (367). As LYVE-1 is significantly downregulated in ALD liver specimens, it could be postulated that the downregulation of

LYVE-1 plays a role in the progression of collagen deposition within the sinusoids due to lack of sufficient clearance. Even if scavenger receptors are not significantly downregulated, LSEC dysfunction would affect the rate at which LSEC can clear collagen and glucosaminoglycans which would be produced in excess by activated HSCs. The mRNA expression of *LYVE1* in whole tissue specimens however, showed no difference between healthy donor and cirrhotic specimens. Despite this, close comparison of mRNA levels of *LYVE1* in diseased specimens showed an increasing trend in relative expression of *LYVE1* in NASH specimens compared to ALD. In cultured LSEC again, mRNA expression of *LYVE1* remained relatively unchanged in early and late passage healthy donor and cirrhotic LSEC. In rat LSEC however, *LYVE1* was rapidly downregulated following a culture period of 42-72 hours (368). LYVE-1 has been linked to regeneration of LSEC in the process of restoring sinusoidal capillary integrity after monocrotaline-induced liver injury in mice whereby LYVE-1 expressing LSEC were reported to expand and replace injured LSEC in the peri-central area of injured livers. LYVE-1 expressing LSEC were absent from the peri-central area of uninjured livers. Expression of *LYVE1* mRNA was increased in monocrotaline treated mice at 72 hrs and 96 hrs after injury (369). This illustrates that there are many factors contributing to the regulation of gene expression such as the state the liver is in. In an isolated cell culture model, which lacks paracrine signalling and important crosstalk with neighbouring cell types such as in the case of LSEC, it is difficult to interpret mRNA levels in relation to their phenotype in the context of liver disease.

CLEC4M, a receptor involved in the clearance of bacterial and viral pathogens and VWF by LSEC (244,247) was significantly decreased in cirrhotic liver specimens (Figure 4.3F) analysed by immunohistochemistry. These findings are consistent with previous reports using immunohistochemistry as well as single cell sequencing(370). In our whole liver tissue

specimens, *CLEC4M* mRNA levels remained relatively consistent between healthy donor and cirrhotic specimens. In cultured LSEC, there is interindividual variability of *CLEC4M* mRNA expression in healthy donor and cirrhotic early and late passage cells. Therefore, specific changes in *CLEC4M* expression in LSEC in culture are difficult to deduce as each LSEC isolate originated from an entirely different hepatic micro-environment.

The scavenger receptor repertoire of LSEC also includes CD36 which plays a role in lipoprotein metabolism(371). In whole tissue specimens of healthy donor and cirrhotic livers, *CD36* mRNA expression remained relatively consistent between conditions. In cultured LSEC however, the majority of cirrhotic LSEC isolates at late passage exhibited increased relative mRNA expression for *CD36* compared to cirrhotic LSEC at early passage (even though not statistically significant). In relation to this, a study of CD36 expression in human liver samples from young and aged individuals, showed that there was a significant increase in CD36 protein expression in the liver tissue biopsy samples from young individuals compared to aged individuals and the documented increase in CD36 expression was directly correlated with age. In addition to this, CD36 gene expression was significantly increased in aged mice fed a high-fat diet compared the young mice counterparts, accompanied by pronounced hepatic steatosis in aged mice(372). Therefore, the expression and function of CD36 needs to be elucidated further in terms of lipid metabolic changes within the liver related to steatohepatitis as well as aging.

The expression of Collagen I, as expected, was significantly increased in cirrhotic specimens analysed by immunohistochemistry (Figure 4.7) as also shown by immunofluorescence(370) and this is characteristic of liver fibrosis and cirrhosis seen in chronic liver diseases(373). While

no significant change was detected in whole tissue mRNA expression of *COL1A1* between healthy donor and cirrhotic specimens, there was a tendency for increased expression in cirrhotic specimens as would be expected. Collagen I is a key ECM component in the progression of fibrosis(374) but the net concentration present within a liver is a result of the balance between new synthesis, stable deposition within the matrix and enzyme-mediated turnover and clearance. Importantly, there is a significant variation across the lobule and in the context of cirrhotic nodule formation so two samples from even the same liver would give different values for net expression. The amount of liver tissue used for the extraction of RNA and downstream quantitative PCR analysis thereafter is only a small fraction of the entire liver. In a proteomics study of fibrotic liver samples, it was interestingly shown that abundance of ECM proteins varies between different stages of fibrosis. Abundancy of fibrillar collagens I and III was increased between fibrotic stages F1 and F2, and F2 and F3 but was decreased in cirrhotic samples at F4(375). This illustrates the extent of ECM remodelling through the different stages of fibrosis which vary from patient to patient and across liver disease aetiologies. As our livers were from patients receiving a transplant, they were all at least stage F3 but it would be interesting to correlate results from my analysis with specific disease scores if I had been able to study a greater number of samples.

Adhesion molecules play an important part in the leukocyte trafficking function of LSEC as well as in cell-cell contact(376). In this regard, expression of CD31 in healthy donor and cirrhotic liver specimens was shown in Figure 3.3. Consistent expression between healthy donor and cirrhotic specimens was noted as shown previously in human and mouse liver tissue (322,377). In whole tissue specimens however, *PECAM1* mRNA expression was significantly increased in cirrhotic specimens compared to donor. This finding is line with previous reports of *PECAM1*

upregulation in liver disease, whereby *in situ* hybridisation was carried out for the detection of *PECAM1* mRNA in normal and cirrhotic human liver. Although *PECAM1* was not detectable in normal liver tissues, its detection was increased in cirrhotic specimens. The co-expression of PECAM1, laminin and α6 integrin, suggested a role for CD31 in the capilarisation of sinusoids(378). Cytoplasmic localisation of CD31 in rat LSEC was shown using confocal imaging on day 1 of culture along with 0-1% expression of CD31 on cell-cell junctions. The expression of CD31 after 3 days of culture in rat LSEC, was localised to cell-cell junctions in 20% of cells. Colloidal gold labelling of CD31 in rat LSEC cultures for 1 day showed lack of its expression, in contrast to the cell surface expression of CD31 in rat LSEC after being in culture for 3 days (visualised using immunogold-SEM in both instances) and this was linked to capilarisation of LSEC *in vitro* (355). In line with this, Figure 3.13 demonstrated the cytoplasmic localisation of CD31 in early passage cirrhotic LSEC visualised by confocal microscopy.

In a study where paired-cell sequencing of hepatocytes and attached LSECs was conducted, fluorescence-activated cell sorting based on CD31 expression was carried out in order to enrich for hepatocyte-LSEC pairs (25). Choosing a marker such as CD32B or LYVE-1 to isolate LSEC from human liver tissue would inevitably introduce selection bias (379) in the isolated LSEC population due to very different expression levels and distribution of these markers seen in healthy donor and cirrhotic liver specimens. The consistent expression of CD31 between healthy donor and cirrhotic live tissue further illustrates its suitability as selection marker for LSEC from both healthy donor and cirrhotic liver specimens. Flow cytometry analysis of rat liver non-parenchymal cells revealed that 97.4% of CD32B positive cells were also positive for CD31 (132).

In terms of what may regulate the expression of such scavenger and adhesion receptors on LSEC, transcription factors such as GATA4 are of relevance. GATA4 has been demonstrated to play a key role in the acquisition of the LSEC specific phenotype (32). Quantitative PCR analysis of *GATA4* mRNA levels in whole tissue specimens showed consistent expression across healthy donor and cirrhotic specimens. A similar pattern was observed in cultured donor and cirrhotic early and late passage LSEC. The fact that *GATA4* mRNA expression was detectable in cultured LSEC illustrates that the culture and media conditions contribute to the maintenance of expression of this transcription factor. In *GATA4* deficient mice, perisinusoidal liver fibrosis was documented, accompanied by increased deposition of collagen I confirmed by immunohistochemical staining. Additionally, downregulation of LYVE-1 and Stabilin-2 was noted as well as collagen deposition in the space of Disse, visualised by TEM (380). This highlights the importance of GATA4 as a regulator of the healthy phenotype of LSEC. This has been demonstrated further by data showing that lack of GATA4 contributed to HSC activation in adult mice (381). In the context of lipid accumulation as part of steatohepatitis observed in cases of ALD and NASH(382), GATA4 was also shown to play a role in the transcriptional regulation of hepatic lipid homeostasis (383), and therefore maintenance of its expression in diseased specimens is crucial.

Caveolin-1 is a structural membrane protein involved in hepatic lipid accumulation, glucose metabolism as well as hepatocyte proliferation (384). Immunohistochemical analysis of Caveolin-1 showed its consistent expression in healthy donor and cirrhotic liver tissue. In whole liver tissue analysed by quantitative PCR, *CAV1* mRNA expression, although not statistically significant, showed an increasing trend in cirrhotic specimens compared to healthy donor. In a study of *CAV1* mRNA expression in biopsy samples from alcoholic hepatitis

patients, expression levels were elevated(385) as well as in patients with liver cirrhosis(386). A leading regulator of lipogenesis, peroxisome proliferator-activated receptor γ1, was shown to increase Caveolin-1 expression in mice, and this was in direct correlation with steatosis (387). The absence of a detectable significant difference in the whole tissue samples analysed here, could have been impacted by the degree of steatosis in each specimen which is donor specific. In cultured LSEC isolated from healthy donor and cirrhotic livers, mRNA expression of *CAV1* in early and late passage LSEC was fairly consistent (Figure 4.11 A) in accordance with the presence of caveolin-1 positivity throughout the liver lobule of healthy donor (Figure 4.4) and LSEC within regenerative nodules in cirrhotic specimens (Figure 4.5).

The enzyme eNOS, plays a crucial regulatory role in the maintenance of hepatic homeostasis by modulating LSEC phenotype and porosity (354). In whole tissue specimens, *NOS3* mRNA expression was relatively consistent between healthy donor and cirrhotic specimens (Figure 4.8D), similar to a previous report comparing the mRNA expression of *CAV1* in liver tissue biopsies from normal livers and cirrhotic livers without inflammation. In the same study however, a significant increase was reported in liver specimens of inflammatory alcoholic hepatitis with cirrhosis (385). In addition, significantly elevated *NOS3* mRNA expression was reported in patients with liver cirrhosis (386). These findings indicate that the inflammatory state as well as stage of cirrhosis could play a role in *NOS3* mRNA expression. In cultured LSEC, there was a significant increase in *NOS3* mRNA expression in both healthy donor and cirrhotic LSEC with increasing passage (Figure 4.11D), which recapitulates the increased mRNA expression levels of this enzyme reported in cirrhotic livers, specifically in LSEC. Further elucidation of eNOS's enzymatic activity is healthy and diseased liver samples is required as this enzyme is regulated by post-translational modifications such as *S*-nitrosylation which is

closely related to the subcellular localisation of the enzyme(388). In addition, eNOS is associated indirectly with the actin cytoskeleton, through its interactions with proteins such as caveolin which has been reported to anchor to actin cytoskeletal proteins (389). LSEC fenestrations are associated with the cytoskeleton through fenestration associated cytoskeletal rings (390). Data in relation to the association of the cytoskeleton with fenestrations in human LSEC is shown in Chapter 6.

The VEGF receptors VEGFR1 (*FLT1*) and VEGFR2 (*KDR*) mediate signal transduction in response to VEGF signalling within the liver. In whole tissue specimens, the mRNA expression of *KDR* (Figure 4.8B) and *FLT1* (Figure 4.8C) were relatively consistent between healthy donor and cirrhotic specimens, although *KDR* mRNA expression was more abundant compared to *FLT1*. A similar trend was evident in cultured LSEC but again mRNA expression of *KDR* (Figure 4.11B) and *FLT1* (Figure 4.11C) were relatively consistent between healthy donor and cirrhotic LSEC at early and late passage. In contrast to this, in a study where the mRNA expression of both VEGF receptors was quantitated using real time PCR in isolated rat LSEC, *FLT1* mRNA expression was about 1.6-fold higher compared to KDR however this difference was not statistically significant(391). Increased expression of both VEGF receptors was observed following hepatectomy and therefore while the liver is actively regenerating(392). It must be taken into consideration that, LSEC culture conditions prior to downstream quantitative PCR analysis were static and VEGF was provided in regular media changes, however this does not fully recapitulate VEGF paracrine signalling as it would be derived from adjacent hepatocytes within the liver physiological environment. Despite this, VEGF signalling was maintained as illustrated by the expression of both VEGF receptors in LSEC *in vitro*.

Overall, the mRNA expression of scavenger receptors as well as key molecules involved in LSEC phenotype and function was detectable by quantitative PCR of whole tissue and isolated cells. This confirms that our chosen EC population isolated using a generic EC marker CD31, does recreate features expected of LSEC. However, CD32B, a key receptor mediating the clearance of immune complexes was not detectable in cultured LSEC but only in whole tissue specimens. This suggests that there is a phenotypic de-differentiation as cells are placed in monoculture. The impact of such culture on fenestrations will be explored in subsequent chapters.

5 Can the LSEC differentiated phenotype be restored in vitro?

5.1 Introduction

Liver sinusoidal endothelial cell dysfunction precedes fibrosis and is a major driver of dysregulation of hepatic homeostasis (76). LSEC have an emerging role in contributing to the progression of fibrosis and there is evidence supporting their role in NASH pathophysiology (393,394). Pharmacological agents such as sildenafil citrate have been shown to have the capacity to re-fenestrate the LSEC plasma membrane (202) which is a key functional characteristic gradually lost as a consequence of chronic liver disease or pseudo-capillarisation occurring in vascular aging, thereby contributing to LSEC dysfunction (331,395).

Therapeutic interventions targeting improvement of LSEC dysfunction in liver disease are currently lacking. Sildenafil citrate, originally developed to treat cardiovascular disorders, is commonly used for treatment of pulmonary hypertension and erectile dysfunction (203,396). It is a phosphodiesterase inhibitor which exerts its vasodilatory effect by preventing the breakdown of cyclic guanosine monophosphate (cGMP). It selectively inhibits phosphodiesterase-5 which is responsible for the degradation of cGMP thereby indirectly increasing the bioavailability of nitric oxide, a key modulatory molecule in LSEC porosity (397). It has been shown previously that sildenafil citrate has the potential to restore endothelial dysfunction as well as improve hypertension (398). However, its effect on human LSECs particularly in the context of liver disease remains unexplored.

VEGF is a vigorous regulator of angiogenesis and is also crucial to the maintenance of the LSEC phenotype including the presence of fenestrations *in vivo* (399). Its regulatory role in cell porosity and capacity to re-fenestrate the LSEC membrane has been well characterised in

rodent LSEC so far (180). It has also been demonstrated that VEGF prolongs the LSEC fenestrated phenotype *in vitro* (354). Both sildenafil citrate and VEGF treatments result in an increase in the bioavailability of nitric oxide (NO) which is an effective vasodilatory and anti-inflammatory molecule (400). NO is a very important signalling molecule whose downstream effects contribute to the maintenance of homeostasis such as modulating vascular tone and maintaining hepatic stellate cell quiescence(162). Thus, after establishing the baseline mRNA expression levels of scavenger receptors and key regulatory molecules of the LSEC phenotype in culture as shown in chapter 4, the next step was to assess the dosage effects of sildenafil citrate and VEGF on the LSEC genotype *in vitro*.

In this chapter, the hypothesis is that the pseudo-capillarised phenotype of LSEC acquired in culture that may also potentially resemble the LSEC phenotype under pathological conditions could be partially reversed by treatments with sildenafil citrate and VEGF. Consequently, the capacity of sildenafil citrate and VEGF to restore the differentiated LSEC phenotype at the mRNA level *in vitro* is shown in the data presented in this chapter. In order to assess the effect of sildenafil citrate and VEGF on the LSEC genotype *in vitro*, gene expression of classical endothelial and LSEC specific genes was analysed in healthy donor and cirrhotic LSEC treated with sildenafil citrate and VEGF using quantitative PCR.

5.2 Results

VEGF and sildenafil citrate were applied at the concentrations indicated on *n*=3 separate samples of healthy donor and cirrhotic LSEC. However due to a low RNA yield from some donors only n=1-2 samples were analysed by quantitative PCR for specific genes as shown in figures to follow.

5.2.1 The effect of VEGF on the LSEC gene expression *in vitro*

In order to determine the effects of VEGF on LSECs in culture, cells were serum starved in basal media only (no VEGF included) for 2 hours and then treated with VEGF at concentrations ranging from 50-400 ng/ml for 4 hours before RNA extraction. Cells treated with vehicle alone were used as baseline data. Figure 5.1 illustrates the mRNA expression of *STAB2* and *MRC1* in healthy donor and in cirrhotic LSECs. *STAB2* was significantly downregulated with increased dosage of VEGF (Fig 5.1A-B) both in healthy donor and cirrhotic liver derived LSEC treated with VEGF for 4 hours compared to treatment control. In contrast, there was no significant impact of VEGF treatment on *MRC1* mRNA expression in either healthy donor or cirrhotic LSEC (Fig 5.1C and D). Although mRNA expression levels for *MRC1* exhibited inter-individual variation, mRNA expression levels were relatively consistent with increasing VEGF dosage.

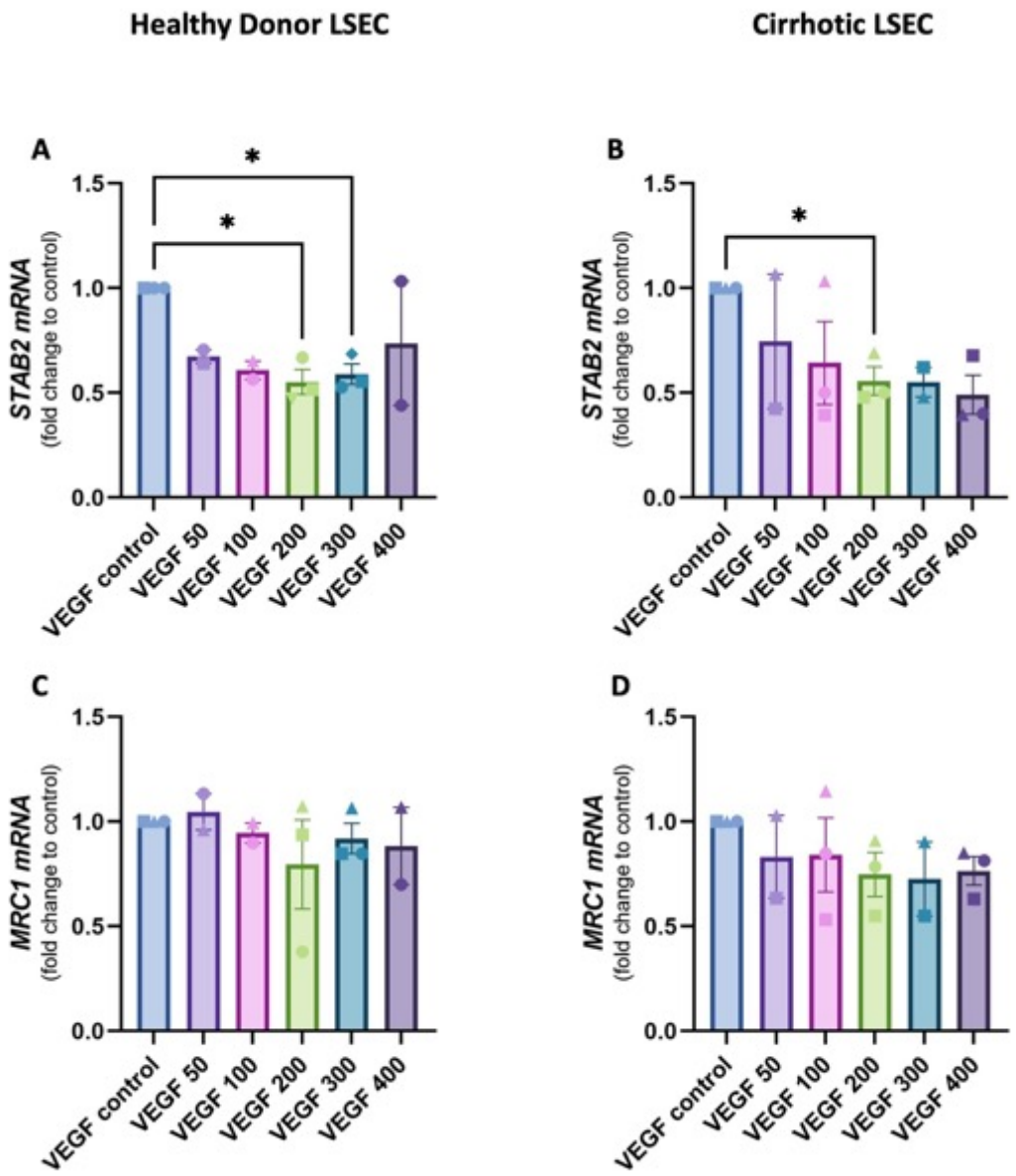

Figure 5.1: Scavenger receptor expression in healthy donor and cirrhotic LSEC treated with VEGF

Data represent changes in gene expression compared to treatment control for *STAB2* (panels A and B) and *MRC1* (panels C and D) determined by quantitative PCR. Gene expression levels were normalised to *SRSF4* housekeeping gene and are shown as fold change to vehicle control. Data are expressed as mean +/- SEM change in expression (bars) for *n*=2-3 separate cases of normal and cirrhotic LSEC. Symbols indicate data from individual samples. Ordinary one way ANOVA test showed a significant difference where indicated by *p-value < 0.05.

A similar pattern emerged in the quantitation of *CAV1* and *NOS3* mRNA expression. Figure 5.2 demonstrates the mRNA expression of *CAV1* (panels A and B) and NOS3 (panels C and D) in healthy donor and cirrhotic LSEC treated with VEGF. *CAV1* mRNA expression fluctuated around the mean of control cells with slightly different expression patterns between donors, but no significant difference was detected in LSEC treated with VEGF in either of the healthy donor or cirrhotic LSEC groups. Panels C and D illustrate the mRNA expression of *NOS3* in healthy donor and cirrhotic LSEC respectively treated with VEGF. Again, no significant differences were detected between expression in treated cells from either healthy or diseased livers. Specimen specific variation is evident within each treatment group where the highest level of variation is observed in healthy donor LSEC treated with 400 ng/ml of VEGF.

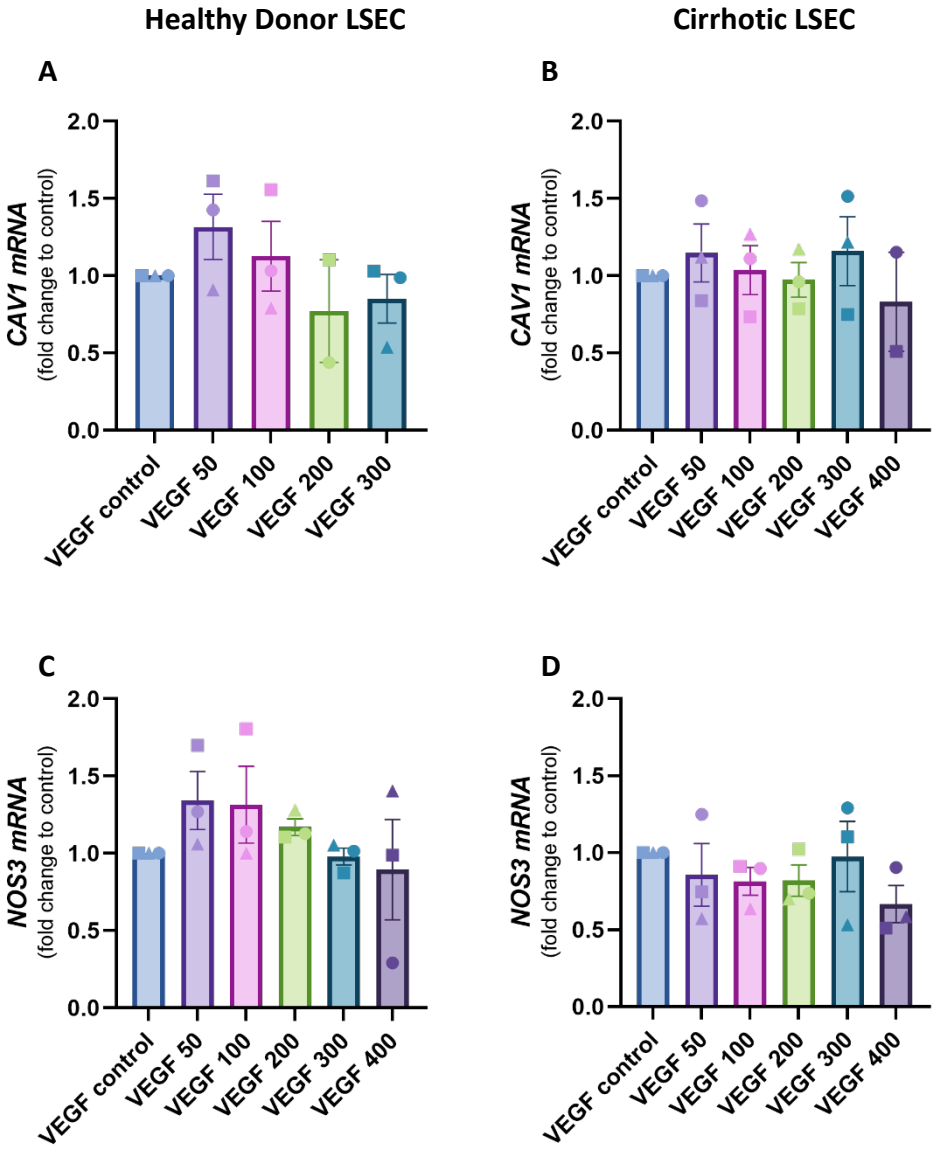

Figure 5.2: CAV1 and NOS3 expression fluctuates in healthy donor and cirrhotic LSEC treated with VEGF

Healthy donor and cirrhotic LSEC were treated with VEGF at a range of 50-400 ng/ml or vehicle control (0.1% BSA in PBS) for 4 hours. Data represent changes in gene expression compared to treatment control for *CAV1* (panels A and B) and *NOS3* (panels C and D) determined by quantitative PCR. Gene expression levels were normalised to *SRSF4* housekeeping gene and are shown as fold change to vehicle control. Data are expressed as mean +/- SEM change in expression (bars) for *n*=2-3 separate cases of normal and cirrhotic LSEC. Symbols indicate data from individual samples. Ordinary one-way ANOVA test performed showed no significant difference in gene expression between treatment and control groups.

When considering the impact of VEGF treatment on VEGF receptor mRNA expression some interesting patterns emerged. In healthy donor LSEC *FLT1* expression was upregulated by all concentrations of VEGF compared to control (Fig 5.3 A). However, although there was a clear trend for overexpression, no significant difference could be detected statistically due to *n*=1 in biological replicates available. *FLT1* mRNA expression in cirrhotic LSEC treated with VEGF showed a slightly different pattern (Fig 5.3B) where *FLT1* was upregulated in a dose dependent manner up to the dosage of 200 ng/ml. In contrast mRNA expression for *KDR* in healthy donor and cirrhotic LSEC behaved differently after exposure to VEGF. In contrast to *FLT1*, there was an inverse effect on *KDR* mRNA expression with increasing concentrations of VEGF treatment. *KDR* (VEGFR2) was significantly downregulated by VEGF treatment of healthy donor and cirrhotic LSEC.

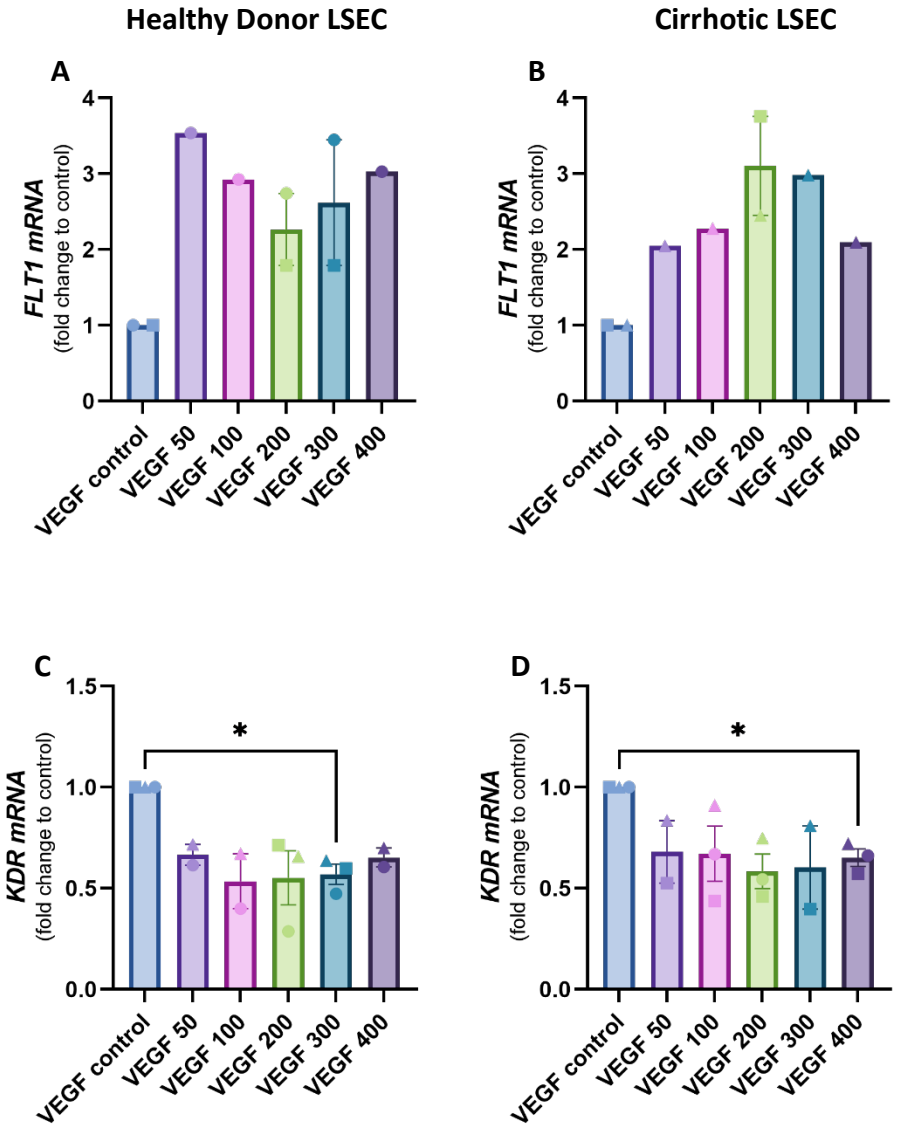

Figure 5.3: VEGF receptor expression in healthy donor and cirrhotic LSEC treated with VEGF

Healthy donor and cirrhotic LSEC were treated with VEGF at a range of 50-400 ng/ml or vehicle control (0.1% BSA in PBS) for 4 hours. Data represent changes in gene expression compared to treatment control for *FLT1* (panels A and B) and *KDR* (panels C and D) determined by quantitative PCR. Gene expression levels were normalised to *SRSF4* housekeeping gene and are shown as fold change to vehicle control. Data are expressed as mean +/- SEM change in expression (bars) for *n*=2-3 separate cases of normal and cirrhotic LSEC. Symbols indicate data from individual samples. Ordinary one way ANOVA test showed a significant difference where indicated by *p-value < 0.05.

The mRNA expression of the transcription factor *GATA4* in LSEC *in vitro*, treated with VEGF is shown in Figure 5.4. Panel A illustrates changes in *GATA4* gene expression with increasing concentrations of VEGF treatment, compared to treatment control in healthy donor LSEC. *GATA4* expression appears to be downregulated by increasing dose of VEGF. In cirrhotic LSEC on the other hand, *GATA4* mRNA expression shown in panel B appears to remain relatively stable with increasing dose of VEGF treatment. No statistical analysis could be performed in this group as only a maximum of *n*=2 samples were analysed with qPCR due to a low RNA yield.

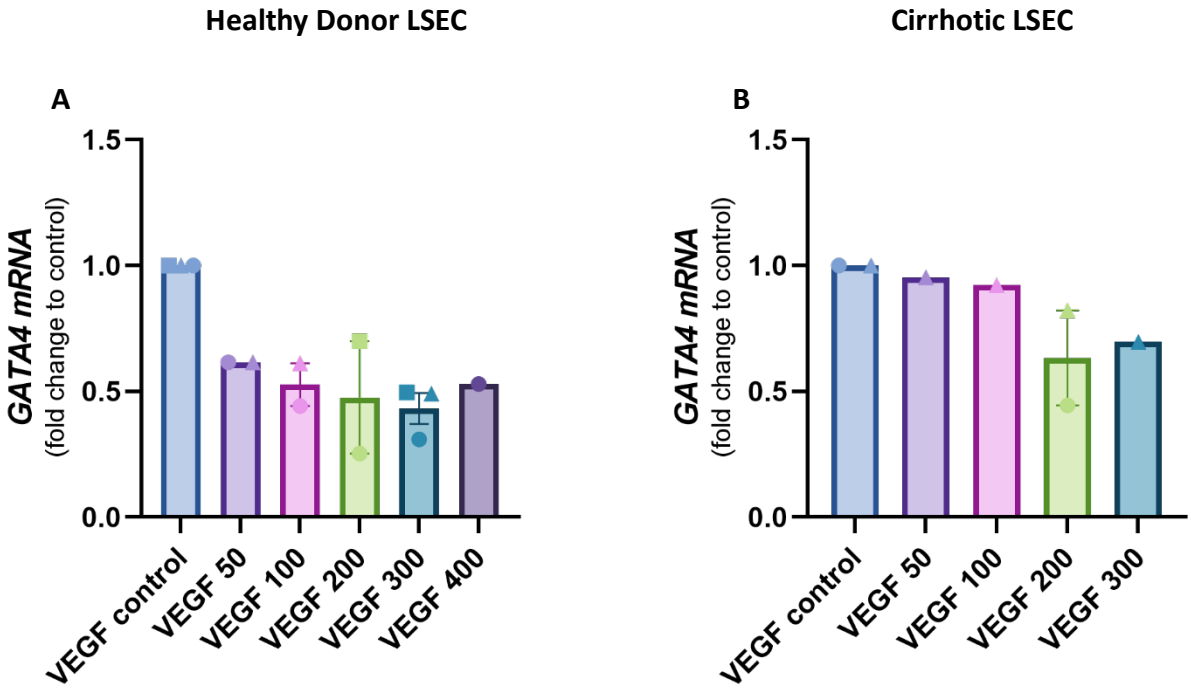

Figure 5.4: GATA4 expression is altered in healthy donor and cirrhotic LSEC

Healthy donor and cirrhotic LSEC were treated with VEGF at a range of 50-400 ng/ml or vehicle control (0.1% BSA in PBS) for 4 hours. Data represent changes in gene expression compared to treatment control for *GATA4* determined by quantitative PCR. Gene expression levels were normalised to *SRSF4* housekeeping gene and are shown as fold change to vehicle control. Data are expressed as mean +/- SEM change in expression (bars) for *n*=1-3 separate cases of normal and cirrhotic LSEC. Symbols indicate data from individual samples. Ordinary one way ANOVA test performed showed no significant difference between treatment and control groups.

5.2.2 Sildenafil citrate mediated alterations to the LSEC genotype *in vitro*

Figure 5.5 illustrates changes in gene expression for CAV1 and NOS3 in healthy and cirrhotic LSEC treated with sildenafil citrate at doses ranging from 2.5 to 25 μg/ml for 4 hours. Expression of *CAV1* in healthy donor LSEC treated with sildenafil citrate appears to remain relatively unchanged with treatment as shown in panel A. in contrast to this, *CAV1* expression was significantly downregulated in cirrhotic LSEC treated with sildenafil citrate. This effect was more apparent at higher doses of sildenafil. Panel C and D displays expression changes in *NOS3* in response to sildenafil citrate treatment in healthy donor and cirrhotic LSEC respectively. A similar trend was exhibited with fluctuations in NOS3 expression, particularly at higher doses even though there was no statistically detectable difference between treatment groups and treatment control in both healthy donor and cirrhotic LSEC.

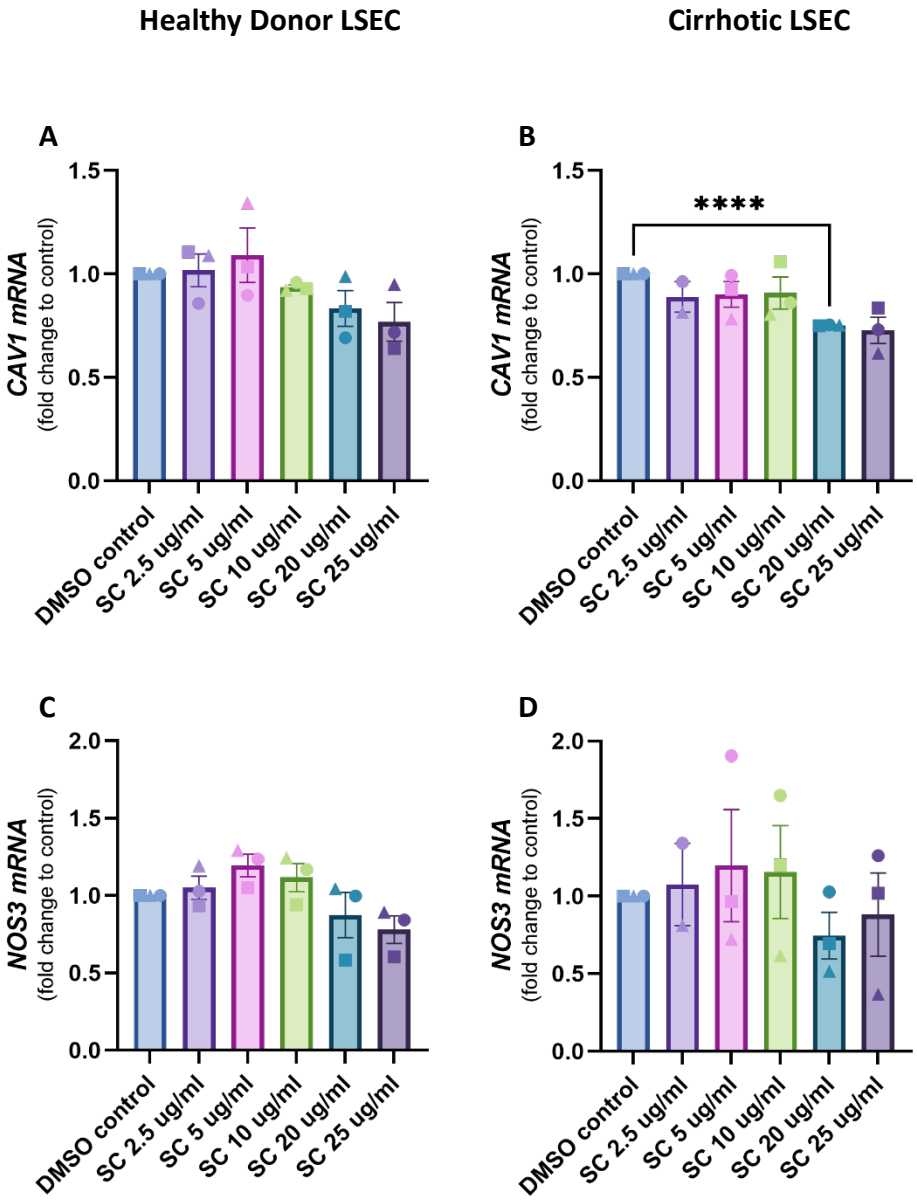

Figure 5.5: *CAV1* mRNA expression is significantly reduced in cirrhotic LSEC treated with sildenafil citrate

Data represent changes in gene expression compared to treatment control for *CAV1* (panels A and B) and *NOS3* (panels C and D) determined by quantitative PCR. Gene expression levels were normalised to *SRSF4* housekeeping gene and are shown as fold change to DMSO control. Data are expressed as mean +/- SEM change in expression (bars) for *n*=2-3 separate cases of normal and cirrhotic LSEC. Symbols indicate data from individual samples. Ordinary one way ANOVA test performed showed a significant difference where indicated. ****p-value < 0.0001.

Figure 5.6 demonstrates changes in *FLT1* and *KDR* mRNA expression in healthy donor and cirrhotic LSEC treated with sildenafil citrate. In cirrhotic LSEC, *FLT1* expression appeared to be reduced by treatment and this is significant for 20 µg/ml sildenafil citrate as shown in Fig5.6B. Healthy cells showed minimal response to treatment. Similarly, *KDR* mRNA expression appeared minimally altered in healthy donor and cirrhotic LSEC treated with sildenafil citrate as shown in panels C and D respectively. Ordinary one-way ANOVA test performed did not detect a significant difference between treatment and control groups.

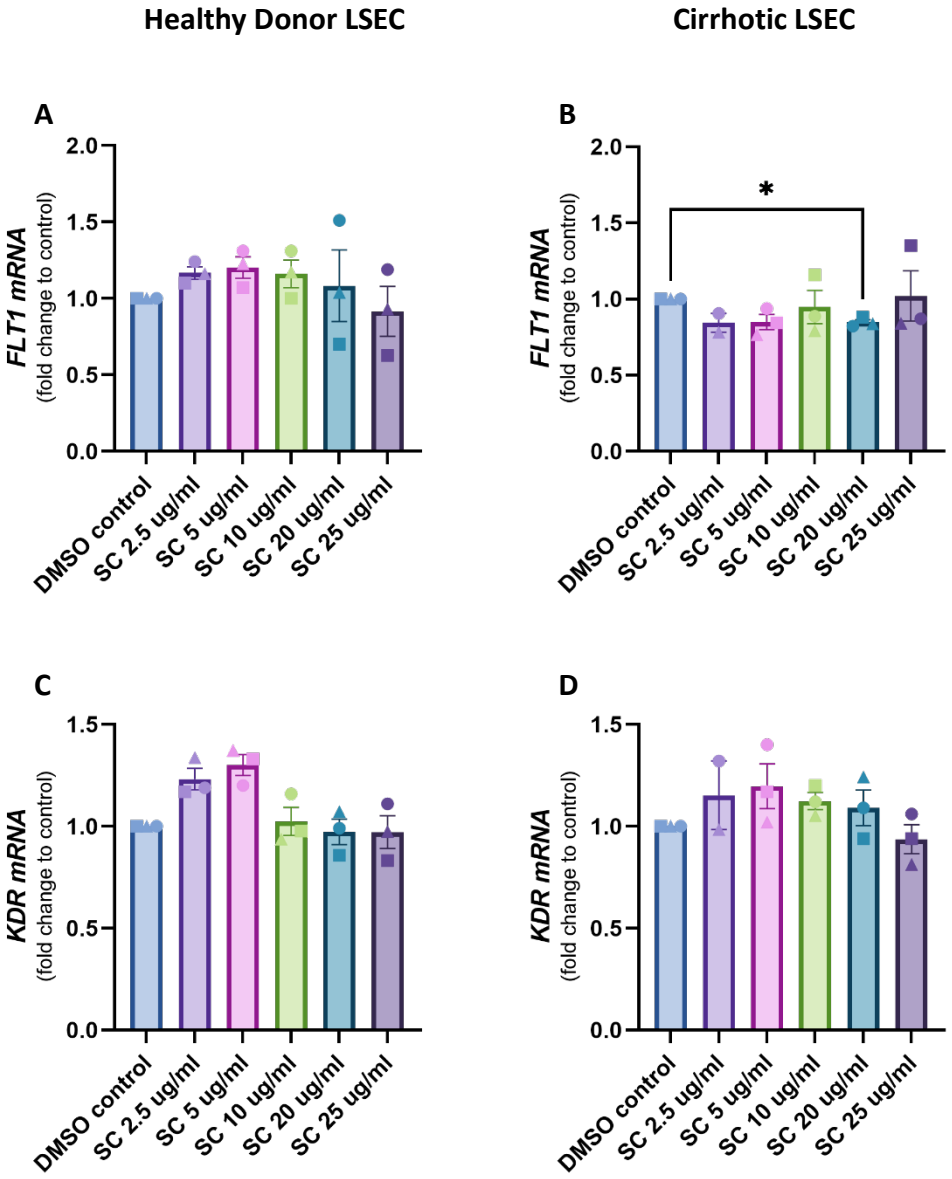

Figure 5.6: *FLT1* mRNA expression is significantly downregulated in cirrhotic LSEC treated with sildenafil citrate

Data represent changes in gene expression compared to treatment control for *FLT1* (panels A and B) and *KDR* (panels C and D) determined by quantitative PCR. Gene expression levels were normalised to *SRSF4* housekeeping gene and are shown as fold change to DMSO control. Data are expressed as mean +/- SEM change in expression (bars) for *n*=2-3 separate cases of normal and cirrhotic LSEC. Symbols indicate data from individual samples. Ordinary one-way ANOVA test performed showed a significant difference where indicated. *p value < 0.05.

Figure 5.7 demonstrates mRNA expression of *PECAM1* and *MRC1* in healthy donor and cirrhotic LSEC treated with sildenafil citrate. In healthy LSEC (panel A) *PECAM1* mRNA expression in sildenafil citrate treated groups remains comparable to treatment control however variability is exhibited whereby *PECAM1* expression in one of the biological replicates (designated by triangle symbol) appears downregulated compared to treatment control. Despite this, no statistically significant difference was detected. In cirrhotic LSEC, no statistically significant differences were detected between treatment groups and treatment control. Panel C and D represent the mRNA expression of *MRC1* in healthy and cirrhotic LSEC respectively which remains relatively stable with increasing dose of sildenafil citrate excluding an outlier which displayed upregulated expression when sildenafil citrate was applied at 10 µg/ml.

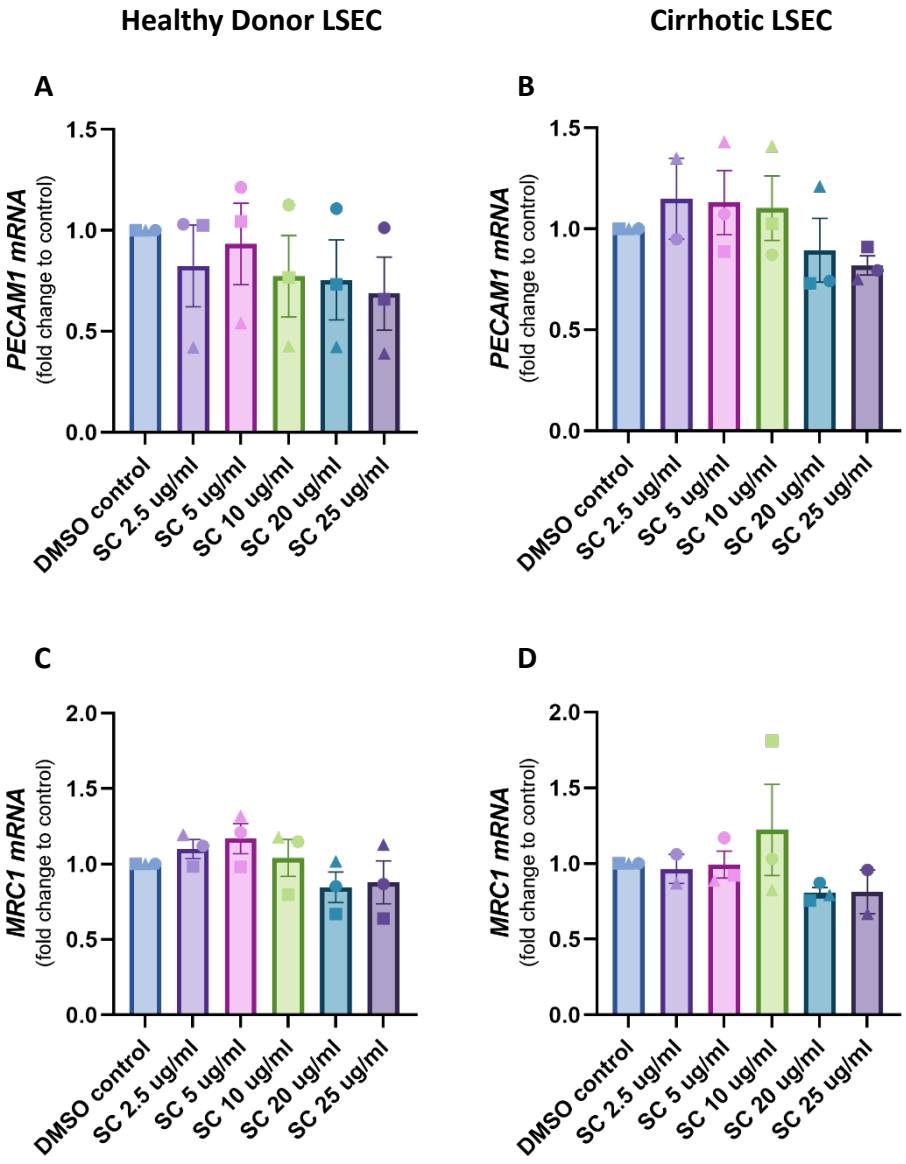

Figure 5.7: *PECAM1* and *MRC1* mRNA expression fluctuates in healthy donor and cirrhotic LSEC treated with sildenafil citrate

Data represent changes in gene expression compared to treatment control for *PECAM1* (panels A and B) and *MRC1* (panels C and D) determined by quantitative PCR. Gene expression levels were normalised to *SRSF4* housekeeping gene and are shown as fold change to DMSO control. Data are expressed as mean +/- SEM change in expression (bars) for *n*=2-3 separate cases of normal and cirrhotic LSEC. Symbols indicate data from individual samples. Ordinary one way ANOVA test performed showed no significant difference.

Figure 5.8 represents the mRNA expression of the transcription factor *GATA4* in healthy donor and cirrhotic LSEC in response to sildenafil citrate treatment. *GATA4* expression remains relatively stable in healthy door LSEC as shown in panel A, with a declining trend with treatments at 20 and 25 µg/ml although no statistically significant changes were detected. Panel B exhibits altered *GATA4* expression in cirrhotic LSEC and although there was variability within each treatment group, any fluctuations in expression were not detected as statistically significant compared to control.

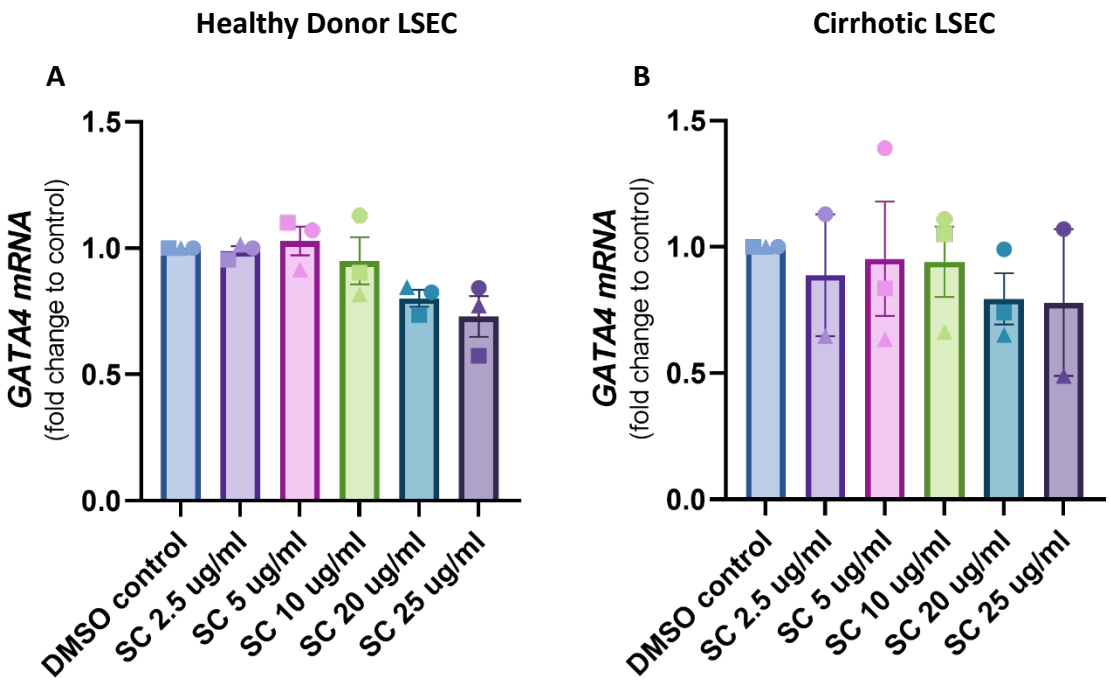

Figure 5.8: *GATA4* mRNA expression in healthy donor and cirrhotic LSEC treated with sildenafil citrate

Data represent changes in gene expression compared to treatment control for *GATA4* determined by quantitative PCR. Gene expression levels were normalised to *SRSF4* housekeeping gene and are shown as fold change to DMSO control. Data are expressed as mean +/- SEM change in expression (bars) for *n*=2-3 separate cases of normal and cirrhotic LSEC. Symbols indicate data from individual samples. Ordinary one-way ANOVA test performed showed no significant difference between treatment and control groups.

5.3 Discussion

VEGF has been reported to be a regulator of LSEC porosity as well as being a growth stimulatory factor. It is standard practise for VEGF (10 ng/ml) to be included in the LSEC complete media we use for maintenance of LSEC culture and expansion. Therefore, with every media change we are potentially inducing LSEC proliferation as well as maintaining the LSEC phenotype *in vitro*. However, this only works to a limited extent as LSEC gradually de-differentiate in culture. VEGF is known to be involved in the maintenance of the LSEC phenotype and specifically fenestrations *in vivo.* This has been demonstrated in rat liver endothelium (354) as well as in glomerular endothelial cells which also possess fenestrae to support their filtration capacity (401). To this extent, the aim of this chapter is to document its modulatory effect on gene expression of key markers such as *STAB2*, which are good indicators of differentiated cell function in liver sinusoidal endothelium. Here, VEGF treatment would be expected to activate the VEGF signalling pathway whereby nitric oxide synthase expressed by LSEC is activated and mediating the release of NO, a molecule with vasodilatory properties. NO synthesis is a crucial part of maintaining hepatic homeostasis as although it is produced in small amounts, its release is constant across the liver lobule. Release of NO is involved in maintenance of hepatic stellate cell (402,403) and Kupffer cell quiescence (404), vascular tone as well as the maintenance of the characteristic fenestrated phenotype of LSEC (161,405). This mechanism also explains the necessity to understand the impact of sildenafil citrate on LSEC. Sildenafil selectively inhibits phosphodiesterase-5 which is responsible for the degradation of cGMP thereby indirectly enhancing signalling downstream of nitric oxide, a key modulatory molecule in LSEC porosity (397). Sildenafil therefore indirectly enhances cyclic guanosine monophosphate signalling which is the second messenger in the NO signalling

cascade. NO production is a delicately regulated process as it is crucial to maintaining homeostasis. This is illustrated by the detrimental effects it has in cases it is overproduced. Sildenafil citrate essentially acts by preventing the breakdown of NO thereby increasing its bioavailability. NO activates soluble guanylate cyclase by increasing cGMP levels in the cytoplasm. A reduction in hepatic NO content and eNOS phosphorylation was observed in mice fed a high-fat diet compared with low fat-fed controls. NO signalling was then examined in an eNOS knock-out mouse model fed a high fat diet in order to induce liver inflammation and insulin resistance (406). Following sildenafil citrate administration (30 mg/kg/day), liver inflammation was shown to be improved in mice receiving a high-fat diet compared to their low-fat diet fed counterparts (404). These data illustrate the anti-inflammatory role of LSEC NO-signalling. The current clinical use of sildenafil citrate includes oral treatment of pulmonary hypertension and erectile dysfunction at 20 mg (3 times a day) and 50 mg respectively (407). Therefore, the range applied here (2.5-25 μg/ml) is well within the physiological range.

5.3.1 The impact of enhanced nitric oxide signalling on the LSEC phenotype

STAB2 encodes for the cell surface hyaluronan receptor, Stabilin-2 which has been shown to cycle between the plasma membrane and lysosomes (408). It is a scavenger receptor mediating the endocytosis of ligands such as low-density lipoprotein and advanced glycation end products (409). Stabilin-2 has been shown to mediate the adhesion of peripheral blood lymphocytes to LSEC thereby playing a role in shaping the immune cell microenvironment at the site of inflammation within the liver (410). *STAB2* mRNA expression (Figure 5.1A and B) was significantly downregulated in healthy donor and cirrhotic LSEC in response to higher doses of VEGF. Stabilin-2 activation upon hyaluronan (40-400kDa) binding, induces the NF-κB pathway (411), which has been linked to the progression of liver disease by regulating critical aspects such as hepatocyte survival, inflammation and activation in HSCs. The NF-κB pathway has a dual effect, the propagation of anti-apoptotic and proinflammatory responses which promote hepatocyte protection as well as a negative impact of increased inflammation or insufficient protection from cell apoptosis (412). This indicates that fine tuning of the NF-κB pathway is required for hepatic homeostasis and Stabilin-2 could participate in this process. To this regard, the downregulation of STAB2 could be linked to LSEC's role in regulating hepatic inflammation. As initially it was hypothesised that LSEC capillarise in culture thereby mimicking liver disease phenotypic changes, downregulation of *STAB2* in relation to NF-κB pathway following the enhancement of NO signalling potentially indicates restoration of LSEC differentiated phenotype.

Although LSEC still maintain expression of scavenger receptors such as stabilin-2 and mannose *in vitro*, static monoculture conditions are far from physiological. Therefore, the fact that

expression of scavenger receptors is maintained at all illustrates the importance of these receptors in LSEC functionality. It is plausible that the downregulation of *STAB2* shown here could be linked to altered LSEC homeostasis *in vitro* as the LSEC used in VEGF treatment experiments here were at passage 3-5.

MRC1 mRNA expression remains relatively consistent *in vitro* and was resistant to regulation by VEGF and sildenafil treatment overall, in both healthy donor and cirrhotic LSEC (Figure 5.2 A and B, Figure 5.7 C and D respectively). *MRC1*, encodes for the mannose receptor which is involved in pathogen recognition and waste clearance. Its multi- ligand binding properties mean it is constantly recycled and present on the LSEC plasma membrane and this indicates an important housekeeping role and maintenance of homeostasis. Experiments in mannose deficient mice have illustrated that the recruitment of lysosomal enzymes to maintain normal degradation capacity in LSEC is mannose receptor dependent (413). Hence widespread expression by LSEC throughout the liver lobule has been confirmed by IHC on healthy donor and cirrhotic liver tissue specimens (Figure 4.2) and this is in line with previous reports where uniform expression of the mannose receptor has been shown in both human and mouse tissue (55,56,205). In addition, in a study where a 30 gene fingerprint was established in mouse LSEC using genes corresponding to human orthologs, *MRC1* was identified in the top three LSEC specific markers(211) with expression in human liver validated at the protein level. This agrees with evidence presented for constitutive expression on human LSEC *in vitro* (Figure 4.12E). The importance of the mannose receptor in maintaining hepatic homeostasis is also highlighted by its involvement in resolving an inflammatory response by clearance of lysosomal enzymes and myeloperoxidases released under inflammatory conditions (414). Mannose receptor has the capacity to recognise and bind viral, bacterial, and fungal molecules

through its C-type lectin domains. The aforementioned functions make the mannose receptor an important pattern recognition receptor (PRR) participating in host defence (415). Consequently, scavenger receptors such as the mannose receptor contribute significantly to the function of the liver as an immune surveillance organ. Expression levels of the mannose receptor have been shown to be differentially regulated by LPS, and cytokines such as IL-10 (416,417). Therefore, the activation status of the LSEC would play a role in modulating *MRC1* expression levels.

The mRNA expression levels of the adhesion molecule CD31, encoded by *PECAM1* remain relatively consistent with increasing dosage of sildenafil citrate treatment in healthy donor and cirrhotic LSEC although exhibiting inter-individual variation in each condition (Figure 5.7 A and B). It has been proposed that CD31 in involved in the activation of eNOS by participating in signal transduction downstream of mechanical stimulation of endothelial cells by shear stress. Increased association of CD31 with eNOS was reported at 5 to 60 minutes following the application of shear stress, determined by co-immunoprecipitation experiments (418). Although in the experiments conducted here, the mRNA expression of *PECAM1* is not impacted by sildenafil citrate, NO signalling enhancement as a result of treatment could contribute to the maintenance of mRNA expression of *PECAM1* thereby allowing for downstream protein-protein interactions such as with eNOS, to take place. This is further supported by a cavernous nerve crush injury rat model whereby sildenafil administration improved erectile dysfunction in a time and dose dependent manner. This was accompanied by preservation of eNOS and CD31 expression demonstrated by immunohistochemistry, in addition to eNOS phosphorylation (419). In this case, sildenafil-induced vasodilation would

also lead to changes in shear stress which in the above report (418) has been shown to increase association of eNOS and CD31.

CAV1 mRNA expression fluctuates in healthy donor and cirrhotic LSEC treated with increasing dose of VEGF (Figure 5.2 A and B) and a similar trend was observed in healthy donor LSEC treated with sildenafil citrate (Figure 5.5A). It can be deduced that *CAV1* is resistant to regulation by VEGF at the mRNA level although a longer treatment (in these experiments LSEC were treated for 4hrs) could be necessary for VEGF to exert an effect. In contrast, *CAV1* mRNA expression is significantly downregulated in cirrhotic LSEC treated with sildenafil at increased dosage (Figure 5.5B). Caveolin-1 is marker shown to increase in cirrhosis (385,386) and despite the absence of statistical significance, there was an increasing trend in *CAV1* mRNA expression in whole tissue of cirrhotic specimens compared to healthy donor (Figure 4.8A). Caveolin-1 was increased in a dose dependent manner in the serum of ethanol-fed mice while expression of caveolin-1 in the liver was increased at 12 hours after ethanol feeding and this increase was mainly observed in hepatocytes (420). This could therefore account for differences in expression of *CAV1* between whole liver tissue specimens and isolated LSEC. In addition, the ethanol-mediated caveolin-1 increase was shown to have a protective effect on hepatocytes through the inhibition of iNOS activity. iNOS activity results in excessive amounts of NO production leading to the accumulation of reactive nitrogen species which drive inflammation (420). Consequently, the upregulation of caveolin-1 has a protective role in the pathogenesis of ALD. In addition, in a rat alcohol model, reduction in eNOS activity was associated with elevated caveolin-1 expression in the liver (421). To this extent, the downregulation of *CAV1* in sildenafil treated cirrhotic LSEC could indicate the restoration of eNOS activity and improvement of LSEC function.

Endothelial nitric oxide synthase is a vital enzyme involved in the maintenance of the differentiated LSEC phenotype. *NOS3* mRNA expression remains relatively stable and comparable to treatment control despite minimal fluctuations in expression both in healthy donor as well as cirrhotic LSEC treated with VEGF (Figure 5.2 C and D) and sildenafil citrate (Figure 5.5 C and D). *NOS3* mRNA stability plays a role in regulating eNOS levels. Cell confluency affects *NOS3* mRNA levels whereby levels can be four-six fold higher in proliferating cells compared to quiescent cells (422). All VEGF and sildenafil treatment experiments were performed on confluent/ growth arrested cells in order to ensure a good RNA yield would be obtained for downstream analysis experiments and therefore cell confluency may have contributed to the *NOS3* mRNA levels obtained. In addition, eNOS is regulated post-translationally and in response to stimuli such as VEGF leading to eNOS phosphorylation at S1177 on the C-terminal reductase domain by protein kinase Akt and this has been demonstrated to play a role in eNOS activation following stimulation by VEGF as well as shear stress (423). Further to this, actin has been shown to bind to eNOS 3' UTR during varying stages of cell growth illustrating the interaction between eNOS and cytoskeletal proteins (424). It has also been proposed that post-translational regulation of eNOS drives its subcellular localisation which can also affect NO production in response to stimuli such as VEGF (425). Hence the observation that *NOS3* mRNA remains relatively stable after treatment does not necessarily mean that a functional change in cellular response by virtue of post-translational signals is not being induced.

NO binds to the heme compartment of eNOS thereby forming a stable complex and inhibiting eNOS activity (426,427). Consequently, endogenous NO may act as a negative feedback system of eNOS activity in homeostatic conditions. Under pathological conditions such as ALD and

NAFLD, the inducible isoform of NOS (iNOS) has been shown to be upregulated as its expression can be induced in Kupffer cells, hepatocytes, and HSCs as well as LSEC. iNOS is known to produce great amounts of NO which may also contribute to the negative feedback system promoting eNOS inhibition, as well as being an important source of reactive nitrogen species (428,429). The generation of reactive nitrogen species can be detrimental to key biological processes as peroxynitrite can damage protein nitration which would thereafter alter the structure and function of downstream target proteins. This is in contrast to the vaso-protective effect achieved by eNOS derived NO leading to endothelial survival and maintenance of vascular tone (430).

FLT1 mRNA expression appears to be more abundant compared to *KDR* in response to VEGF treatment even though only an *n*=1 biological replicate was analysed for *FLT1* due to low RNA yield obtained from the remaining biological replicates. VEGFR1 (*FLT1*) has been shown to bind VEGF-A (same type of VEGF secreted by hepatocytes and also used in these experiments) at a higher affinity compared to VEGFR2 (*KDR*), thereby acting as a VEGF-A trap. In addition, VEGFR1 is considered to negatively regulate VEGFR2, leading to suppression of its pro-angiogenetic effects (431). This would explain potential upregulation of *FLT1* in the presence of increased VEGF, alongside *KDR* downregulation. In relation to this, *KDR* mRNA expression was significantly downregulated at high doses of VEGF in healthy donor LSEC (Figure 5.3C) and cirrhotic LSEC (Figure 5.3D) *KDR* encodes for VEGFR2, a tyrosine-kinase receptor protein acting downstream of VEGF, involved in mediating endothelial proliferation and survival. Its downregulation could be associated with the fact that the LSEC were treated with VEGF at a confluent density and therefore were in cell cycle arrest. Although VEGFR1 binds VEGF-A at a higher affinity, most downstream effects of VEGF-A are mediated through VEGFR2 which then

activates downstream signalling events. Firstly, following ligand binding, dimerization of VEGFR2 takes place along with cross-phosphorylation of tyrosine residues on its intracellular domain (432). Tyrosine residue phosphorylation triggers intracellular signalling pathways that are crucial for endothelial cell biology such as activation of the PI3K/AKT/mTOR pathway through the phosphorylation of tyrosine 1175. Induction of this pathway is crucial for endothelial responses such as survival, proliferation, and migration (433). Although VEGFR1 has a higher affinity for VEGFA, phosphorylation of this receptor is weakly induced (434). It has been shown in mouse embryos that *FLT1* knockdown is lethal at embryonic day 8.5-9 due to excess proliferation of endothelial cells and disorganisation of vasculature. This was due to increased VEGFR2 signalling as a result increased availability of VEGFA and binding to VEGFR2 (435). This demonstrates a regulatory role for VEGFR1 in VEGFR2 signalling for the control of angiogenesis. Although mRNA expression of *KDR* remained fairly consistent in healthy donor and cirrhotic LSEC treated with sildenafil (Figure 5.6 C and D), *FLT1* mRNA expression was significantly downregulated in cirrhotic LSEC at increased dosage of sildenafil (Figure 5.6B). This can be attributed to the fact that in the absence of VEGF, *FLT1* expression was induced less.

GATA4 encodes for the transcription factor involved in LSEC specification and function and has been identified as a master regulator driving differentiation within the liver micro-environment as well regulating LSEC fate throughout embryonic development (32,436). This is highlighted by the fact that GATA4 as well as GATA6 are integral during embryonic development of the liver by regulating the expansion of the liver bud (32,437). It has been proposed that *GATA4* modulated LSEC differentiation in synergy with other transcription factors such as MEIS2 and C-MAF in order to maintain expression of essential markers

expressed by LSEC such as mannose (211). The regulatory role of GATA4 in the maintenance of LSEC specific phenotype was demonstrated in *Gata4*$^{LSEC\text{-}KO}$ mice whereby LSEC specific markers such as Stabilin-2 and LYVE-1 were downregulated (380). In this regard, the expression of *GATA4* in both healthy and cirrhotic LSEC confirm that the cells isolated are indeed LSEC. Despite the fact that no significant changes in expression were detected in *GATA4* expression in normal and cirrhotic LSEC treated with increasing concentrations of VEGF (Figure 5.4), there is a trend towards downregulation of *GATA4* which is more evident in healthy donor LSEC treated with VEGF compared to cirrhotic LSEC however levels remain relatively unchanged. Similar trends in GATA4 expression were shown in healthy donor and cirrhotic LSEC treated with sildenafil (Figure 5.8). Despite this, it has been shown that NO which is expected to be produced following VEGF treatment, leads to downregulation of *GATA4* expression (438). Negative regulation of GATA4 by nitric oxide has been reported in the heart, which is dependent on protein kinase G (439). As nitric oxide is the signalling molecule produced downstream of eNOS activation, this accounts for potential downregulation of GATA4 in LSEC treated with VEGF. Expression of *GATA4* mRNA was also relatively unchanged in sildenafil treated healthy donor and cirrhotic LSEC (Figure 5.8).

Overall, the preliminary data presented in this chapter indicate a potential regulatory role of the enhancement of NO signalling in LSEC phenotype in liver disease and this is illustrated further in the next chapter, specifically with regards to LSEC porosity. However, regarding the effect of VEGF and sildenafil on the expression of genes presented in this chapter, duration of treatment could play a role as further enhancement of the downstream effects of NO signalling could be taking place with longer exposure of LSEC to VEGF or sildenafil citrate. As LSEC were kept in the absence of VEGF in basal media for only two hours prior to treatment

with increased dosage of VEGF or sildenafil, the effects of NO while LSEC were in normal culture conditions could be impacting gene expression levels. In addition, lack of significant gene expression changes does not reflect on protein activity which is the case of eNOS is largely dependent on post-translational modifications and protein-protein interactions. Additional biological repeats would be required in order to have greater statistical power and be able to detect clear effects on expression changes. Future work to further elucidate the role of nitric oxide synthases and NO signalling on modulating the LSEC phenotype would entail quantitation of the basal expression of iNOS in LSEC at low and high passage as homeostasis of LSEC could be altered *in vitro* which would be compatible with their de-differentiation in culture. Mechanisms of eNOS activation include phosphorylation at serine 1177 via the PI3K/Akt pathway. As phosphorylation is a post-translational modification, detection of eNOS protein levels by western blotting would be required as well as the co-immunoprecipitation of eNOS with proteins regulating its activity such as caveolin-1 and CD31 (405,440). NO quantitation in healthy donor and diseased tissues as well as in LSEC under normal culture conditions and following VEGF and sildenafil treatment can also be carried out, using electron spin resonance spectroscopy (441,442).

6 Super-resolving the hepatic molecular sieve

6.1 Introduction

The presence of fenestrations is considered the gold standard for confirming the identity of LSEC *in vitro* and is recognised as characteristic of a healthy LSEC phenotype (443). As defenestration is a progressive consequence of chronic liver disease irrespective of aetiology, it is important to be able to visualise and quantify the differences in fenestrae frequency and diameter between healthy and diseased specimens, as the reduction of fenestrae contributes to the dysregulation function of liver function. For example, loss of fenestrations has also been associated with alcohol-induced hyperlipoproteinemia (85).

Precise mechanisms regulating the formation, size and dynamic organisation of fenestrations have been proposed as summarised in chapter 1 (section 1.5.5), with the involvement of the actin cytoskeleton in modulating an increase in fenestration diameter and frequency as well as calcium/calmodulin regulation of the contraction and relaxation of the actomyosin cytoskeleton. FACR have been visualised by SEM and TEM in preparations of LSEC in which the membrane was removed by detergent extraction. This exposed a network of filaments closely associated with sieve plates of fenestrations which were surrounded by thicker filaments (444). FACR were demonstrated further by AFM and *d*STORM while the formation of open fenestrations within FACR was shown to require a complete actin ring (192,445). Together these data demonstrate the close association of fenestrations and the actin cytoskeleton.

Electron microscopy has contributed immensely to visualising fenestrations and their organisation on the LSEC membrane in both tissue and cultured LSEC samples originating from

human as well as animal specimens. Despite this, most of EM data originate from LSEC isolated from animal models, such as baboons, which recapitulate the effects of alcoholism on fenestrations (84) as well as in rat models recapitulating cirrhosis (446) and endotoxin-induced defenestration (447). Human specimens have provided information about the nature of fenestrations within a healthy hepatic environment (448–450). However, EM data on fenestrations from human cirrhotic specimens is less frequent. Reports have illustrated loss of fenestrae in cases of patients with chronic hepatitis C (451) as well as alcohol induced defenestration whereby a significant loss in fenestrations was observed in zone 2 of the liver lobule (452). As well as a lack of robust EM data from diseased human livers, the process of preparation of EM presents challenges. While EM techniques enable visualisation of nanosized structures such as fenestrations, samples must undergo a series of dehydration steps throughout the preparation process for EM (452). When dealing with a sample as delicate as the LSEC membrane, heavy chemical processing and dehydration can impact the output measurements deduced from acquired images (453).

The development of super-resolution techniques has revolutionised far-field light microscopy due to their capability to overcome the limitation posed by the diffraction of light. This limitation is defined as the inability of optical microscope lenses to discern details that are closer together than half of the wavelength of light (454–456). This signifies the fact that biological samples can be imaged with a light source using wet fixation instead of dry fixation approaches applied for EM sample preparation. dSTORM falls under the category of single molecule localisation microscopy techniques which collect the sub-diffraction positions of individual fluorophore molecules for the nanoscale reconstruction of the overall structure in question (457).

Super-resolution approaches such as STED (458), SIM (184,459), atomic force microscopy (445,453,460,461) and dSTORM (296) have already been utilised for imaging fenestrations in rodent LSEC. Atomic force microscopy has been utilised for tracking fenestrae-forming centres in live murine LSEC (460) while dSTORM has been implemented in order to capture the effect of sildenafil citrate on the actin cytoskeleton in LSEC from young mice and revealed that changes in the actin cytoskeleton were associated with increased fenestration frequency and porosity (202). Furthermore, two-colour dSTORM has been applied to deduce the relationship of fenestrae with the actin cytoskeleton in mouse LSEC (192). In terms of super-resolution imaging of human LSEC on the other hand, data is less abundant. Only SIM has been applied so far, in specimens originating from patients undergoing hepatectomy for liver metastasis from colorectal cancer (298).

While there are many super-resolution techniques to choose from, the choice of super-resolution technique is influenced largely by the combination of the imaging target and the limitations of each approach. Phototoxicity and bleaching for example, are two drawbacks of STED imaging. We therefore chose dSTORM as our imaging approach for visualising human liver fenestrae as it offers superior resolution by pin-pointing the position of single fluorophores (with a precision of approximately 10-20 nm). There are several microscope systems available that can be used for dSTORM such as the N-STORM by Nikon as well as the ONI Nanoimager has been utilised for dSTORM image acquisition in this project.

Sample thickness is a factor to be considered for successful dSTORM imaging. The LSEC membrane is an ideal candidate for dSTORM as the cells lack lack a basement membrane and are therefore considerably thin (462). Fenestrations have been visualised using dSTORM in rat

LSEC using Cell Mask Deep Red Plasma membrane dye (CMDR) as no fenestration-specific marker has been identified so far (296). The approach employed by using CMDR for imaging fenestrations involves relying on the absence of signal within fenestrations which can be identified as dark regions on the plasma membrane.

Although there is a plethora of super-resolution imaging data available from rodent LSEC, human LSEC data is lacking. The purpose of this chapter was to capture fenestrations in human LSEC *in vitro* in an effort to enrich the knowledge gap in differences between donor and cirrhotic LSEC using dSTORM. Consequently, dSTORM images of fenestrations in human LSEC *in vitro*, isolated from normal donor, ALD, PBC and NASH specimens are presented. Alterations in LSEC porosity following treatment with sildenafil have also been captured using dSTORM, in normal and cirrhotic LSEC. Lastly, two-colour dSTORM was implemented in order to identify the relationship between the actin cytoskeleton and fenestrations in human LSEC.

6.2 Results

6.2.1 Optimisation and development of *d*STORM imaging parameters

The key aims of this chapter were to develop an optimized protocol to enable us to visualise fenestrae in healthy and cirrhotic human LSEC *in vitro*. We wanted to assess both the number and physical features of the sieve in healthy and diseased states, as well as determine the effect of sildenafil citrate treatment on fenestrae frequency and diameter. In order to do this, I tested a series of different parameters to allow optimisation of a protocol and set of imaging conditions allowing the visualisation of fenestrations using CMDR using dSTORM microscopy. As the seeding density is key for super-resolution microscopy, it was important to have a confluency of about 40-50% in order to be able to have single cells in a field of view. A final seeding density of 30 000 LSEC per ibidi channel was therefore used. This was challenging as human LSEC grow best in a monolayer with very close proximity to each other and low confluency can lead to morphological changes. Moreover, challenges of cell attachment to the hydrophobic glass coverslip bottom (1.5H) were met by washing the glass bottom ibidi µ-channels with potassium hydroxide (1 M), followed by overnight coating of the glass bottom with 10x more concentrated RTC compared RTC used to coat tissue culture treated flasks where LSEC were routinely grown and expanded. As sample preparation began with fixation, a key factor was fixative quality and for this reason the 4% PFA used for each experiment was prepared fresh, 1-2 hours prior to use.

In order to perform *d*STORM, the imaging parameters summarised in Figure 6.1, needed to be implemented. To begin with, all fluorophores need to be reduced back to their dark state so that stochastic photo-switching of individual fluorophores can follow. In this case, this was

achieved by the addition of mercaptoethylamine (MEA) to the imaging buffer at an initial concentration of 100 mM. However, to due to the high density of staining of CMDR, the concentration of MEA in the final imaging buffer was increased to 150 mM in order to facilitate more efficient reduction of CMDR fluorophores to the dark state. Another important criterion for successful *d*STORM imaging is the exclusion of oxygen from the sample during acquisition so as to avoid photobleaching as much as possible. The imaging parameters included the acquisition of 20 000 frames which resulted in image acquisition time of 10 minutes per cell imaged. An oxygen scavenger system was included in the imaging buffer which consisted of the enzymes glucose oxidase, catalase, and glucose. In order to improve the efficiency of the oxygen scavenging system, the MEA stock solution used for buffer preparation was increased to double the initial concentration in order to allow for more glucose in the final buffer.

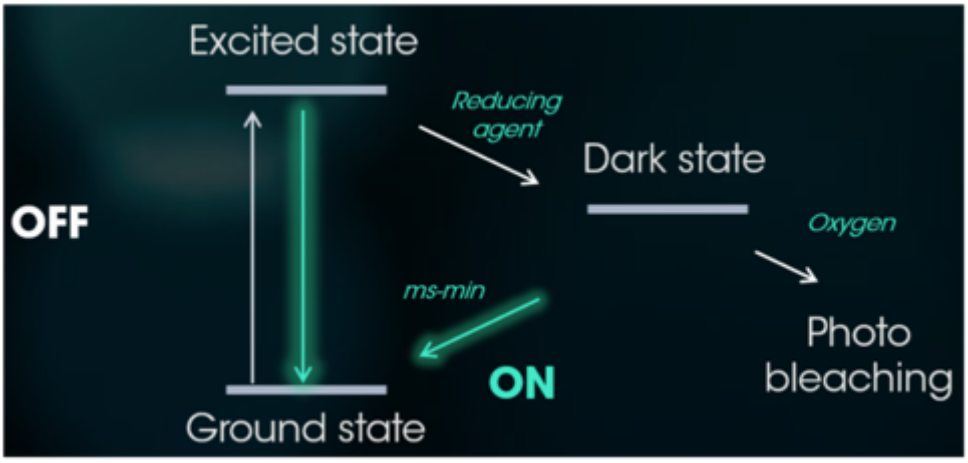

Figure 6.1: Stochastic fluorophore photo-switching during dSTORM imaging
The combination of optimal chemical and excitation parameters achieves the transition of fluorophores to the dark state in a stochastic manner. This is followed by random blinking of fluorophores over a series of frames. The system works best when oxygen is excluded from the sample in order to avoid photobleaching.

6.2.2 *d*STORM imaging of healthy and cirrhotic LSEC *in vitro*

Following the optimisation of imaging parameters, I next wanted to measure and quantify fenestrations in normal and cirrhotic LSEC. Consequently, LSEC cultured O/N in complete media on glass bottom ibidi chambers to attach and spread, were fixed in freshly made 4% PFA and stored under PBS until imaged using dSTORM on the ONI Nanoimager. Figure 6.2 presents a representative image of an untreated donor LSEC acquired using dSTORM. The membrane region illustrated in panel A, shows fenestrations organised in a sieve plate on the edge of the plasma membrane and fenestrations are designated by dark regions in the plasma membrane. This region is expanded further at a higher magnification in panel B which clearly shows the variation is fenestration diameter as well as shape. The smallest fenestration diameter within the sieve plate is 112.9 nm while the largest measures 524.6 nm. There was also variation in circularity of fenestrations ranging from a circle-like shape to an elliptical one. Additionally, there was variation in the membrane boundary of fenestrae, with fenestrations surrounded by a uniform membranous boundary with occasional membrane accumulation indicated by brighter areas depicted by red arrows in panel B, contradictory to fenestrae with poorly formed membrane boundary. Importantly this culture of donor LSEC was imaged at passage 5 and the presence of the sieve plate indicates that even passaged LSEC still have the capacity to maintain fenestrations *in vitro*.

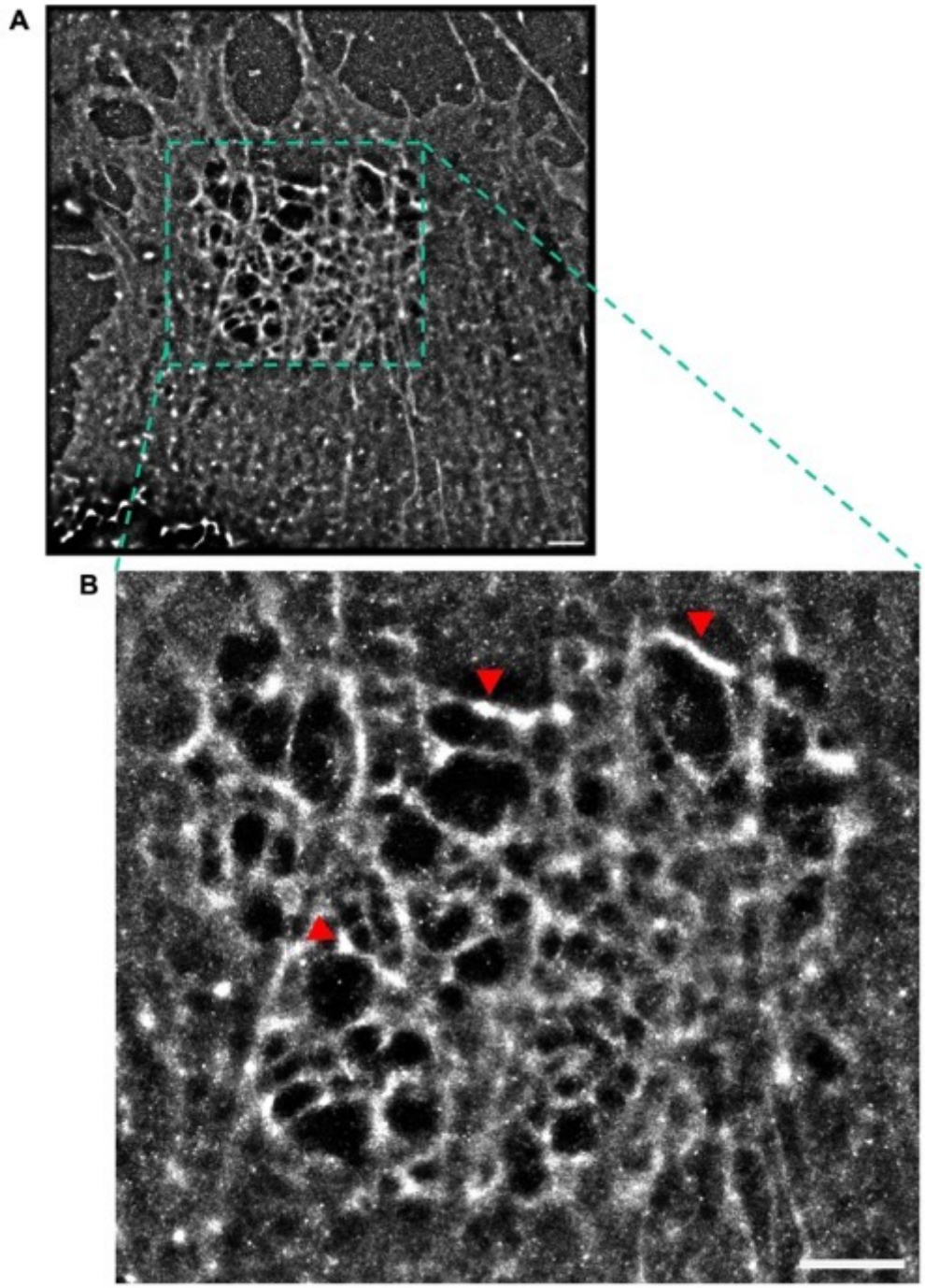

Figure 6.2: Use of dSTORM to visualise fenestrations in human LSEC isolated from healthy donor liver tissue

(A) Representative image of an LSEC derived from healthy donor liver tissue acquired using dSTORM. LSEC were stained with Cell Mask Deep Red plasma membrane dye at 5 µg/ml and this image was reconstructed using the ThunderSTORM plugin in Fiji software using 20 000 frames. Drift correction was applied using cross-correlation. The Normalised Gaussian method was applied for image rendering with lateral uncertainty of 20 nm. The highlighted area indicating fenestrations organised in a sieve plate is shown in (B) at a higher magnification. Fenestrations can be seen as dark regions within the plasma membrane and bright membrane areas on the periphery of fenestrations are illustrated by red arrows. Pixel size: 10 nm. Scale bar: 2 µm.

This was true even in cirrhotic LSEC although there were marked differences between healthy and diseased cells. Figure 6.3 (A) shows a representative dSTORM image of fenestrations in part of the membrane of an untreated cirrhotic LSEC isolated from PBC liver tissue. Fenestrations can be seen scattered throughout the plasma membrane region (captured in the expanded field of view magnified in panel B). These fenestrations are more dispersed than those in the normal LSEC and the fenestration diameter range is between 112.9 nm and 518.4 nm in this image. However, we did note occasional clusters of fenestrations (see example in Fig 6.6). Although less pronounced in comparison with the donor LSEC in figure 6.2, there are still regions of brighter membranous staining accumulation surrounding individual fenestrae in the PBC LSEC (Fig 6.3 (B) red arrows). Importantly not only was this cell isolated from a diseased liver, but the cells were also imaged at passage 4. Thus, fenestrations are still present in cirrhotic LSEC even after some time in culture in our media conditions.

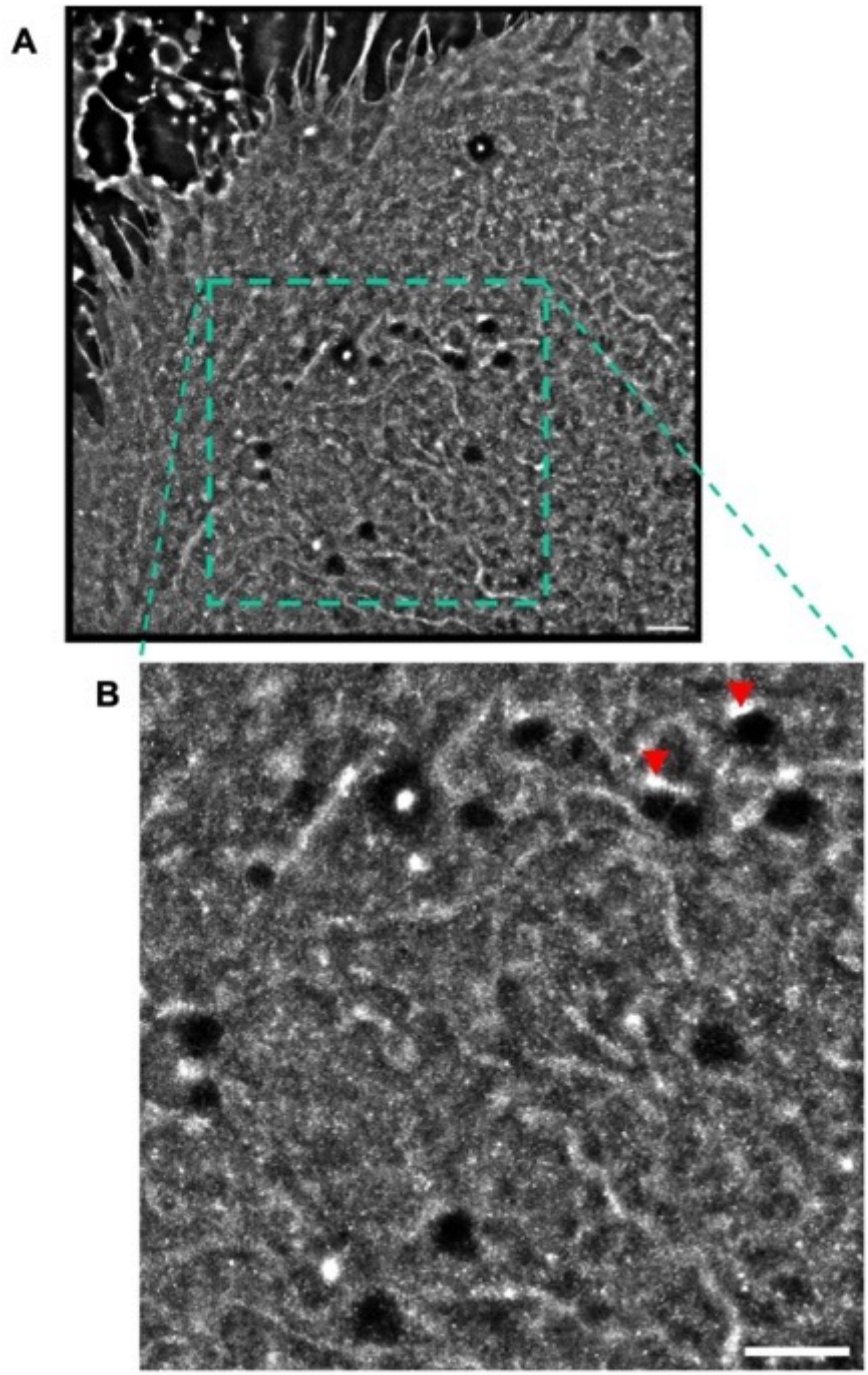

Figure 6.3: Use of dSTORM to visualise fenestrations in LSEC isolated from cirrhotic (PBC) liver tissue

(A) Representative image of an LSEC derived from a PBC liver acquired using dSTORM is shown in panel A. LSEC were stained with Cell Mask Deep Red plasma membrane dye at 5 µg/ml and this image was reconstructed using the ThunderSTORM plugin in Fiji software using 20 000 frames and were drift corrected using cross correlation. The Normalised Gaussian method was applied for image rendering with lateral uncertainty of 20 nm. The highlighted area indicating fenestrations scattered within the plasma membrane is shown in (B) at a higher magnification and fenestrations can be seen as dark regions within the plasma membrane. Bright membrane areas on the periphery of fenestrations are illustrated by red arrows. Pixel size:10 nm. Scale bar: 2 µm.

An important detail evident within the sieve plate from our healthy liver (Figure 6.2) and cirrhotic specimen fenestrations (Figure 6.3) is that there are differences in the density of the cytoskeleton and membrane boundary surrounding each fenestration with denser areas indicated by red arrows. It has been suggested that fenestration boundaries may contain a network of actin filaments which are linked to control of fenestration diameter. Therefore, we confirmed whether the bright regions of the membrane observed using CMDR were associated with actin by implementing two-colour *d*STORM where CMDR and phalloidin staining were imaged sequentially in the same field of view in order to determine their colocalization at fenestrations. Two-colour *d*STORM was carried out on LSEC derived from a NASH liver and a representative image of CMDR and phalloidin *d*STORM image is shown in figures 6.4 and 6.5. Figure 6.4 (A) and (B) represent the same field of view of two adjacent LSEC, stained with CMDR and phalloidin respectively while panel C illustrates the images in panels A and B which have been aligned and merged in Fiji software. Panel B, illustrating the distribution of actin within the part of the cell visualised with actin filaments clearly seen as bright curved lines across the cell. A cluster of fenestrations labelled with phalloidin is shown in a magnified view in Figure 6.5. Emphasising the presence of actin within the periphery of fenestrations, actin-containing membrane regions can be seen as dense and brightly labelled areas are indicated by white arrows in Figure 6.5 (B). Although, the phalloidin staining is less evident in the merged image shown in Figure 6.4 (C), Figure 6.6 (B) shows a magnified view of a cluster of fenestrations where there are regions of colocalization between CMDR and phalloidin, seen as less pronounced yellow regions in the periphery of fenestrations (white arrows).

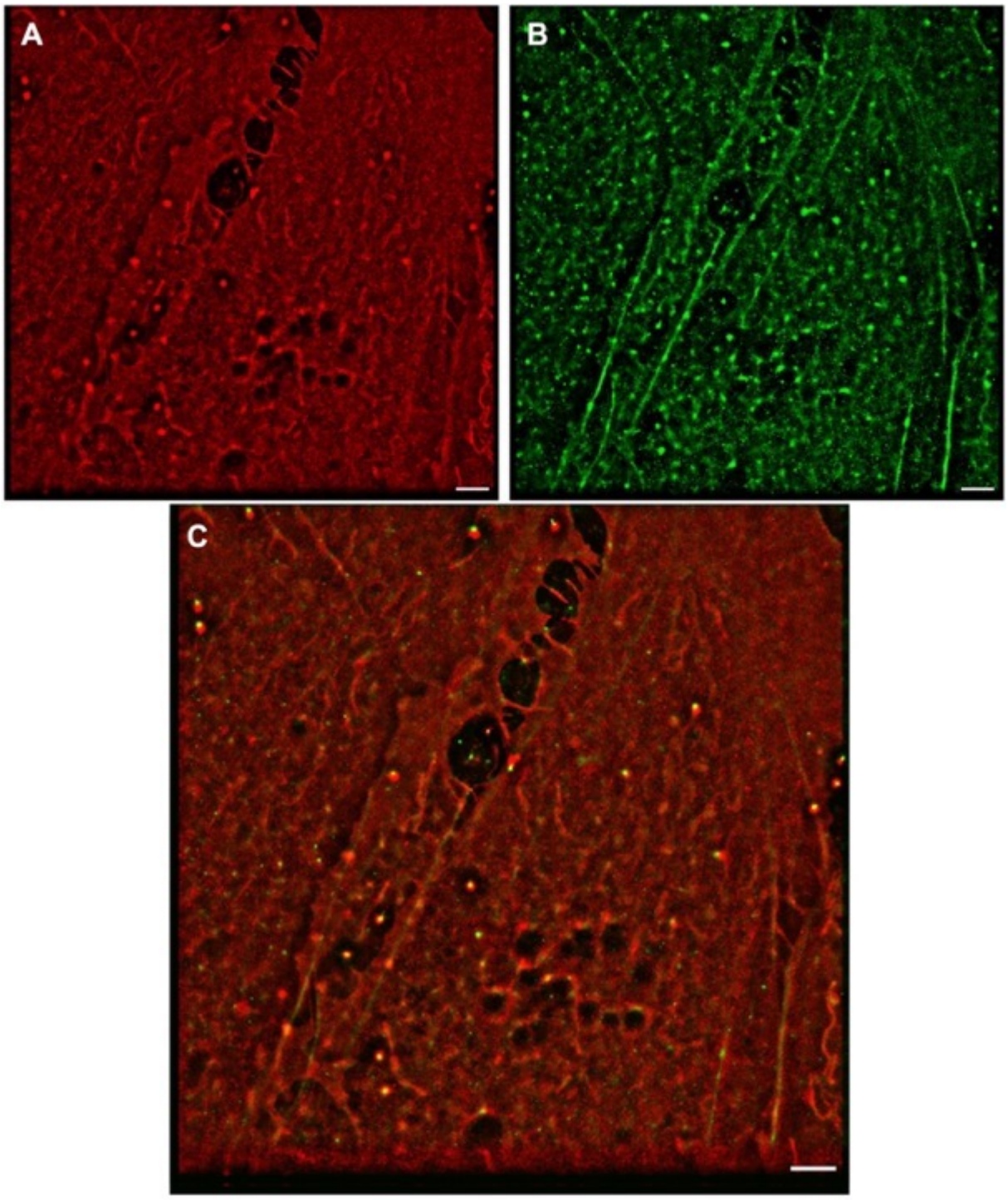

Figure 6.4: Localisation of fenestrae-associated actin using dSTORM in NASH LSEC

LSEC were stained with Cell Mask Deep red plasma membrane dye (5 µg/ml) and ATTO 488 Phalloidin. Tetraspeck microspheres (0.1 µm diameter) were also applied to the sample to allow for drift correction. CMDR and phalloidin images were acquired sequentially and 20 000 frames were collected for each channel. Images were reconstructed using the ThunderSTORM plugin in Fiji software and were drift corrected using the cross-correlation approach. The Normalised Gaussian method was applied for image rendering with lateral uncertainty of 20 nm. Pixel size: 10 nm. Scale bar: 2µm.

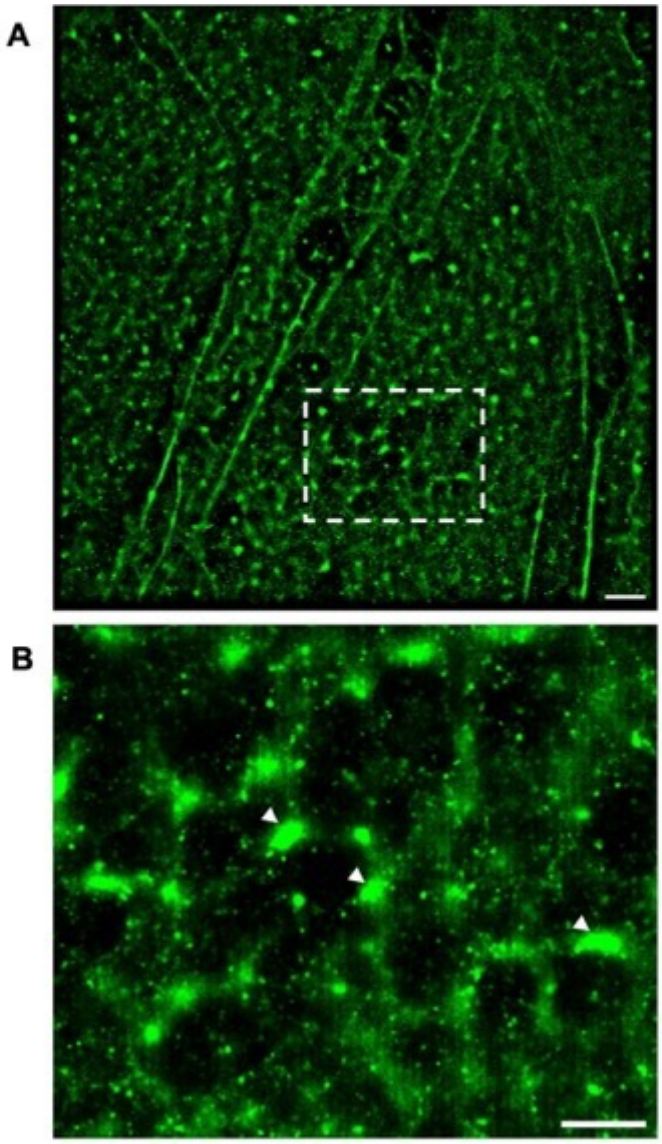

Figure 6.5: Localisation of fenestrae-associated actin using dSTORM in NASH LSEC

(A) Representative dSTORM image of LSEC isolated from a NASH liver. LSEC were stained with ATTO 488 Phalloidin and tetraspeck microspheres (0.1 µm diameter) were applied to the sample to allow for drift correction. Images were reconstructed using the ThunderSTORM plugin in Fiji software using 20 000 frames and were drift corrected using the cross-correlation approach. The Normalised Gaussian method was applied for image rendering with lateral uncertainty of 20 nm. A cluster of fenestrations is shown in panel B with white arrows indicate areas of aggregated actin in the periphery of fenestrations. Pixel size: 10 nm. Scale bar: 1 µm.

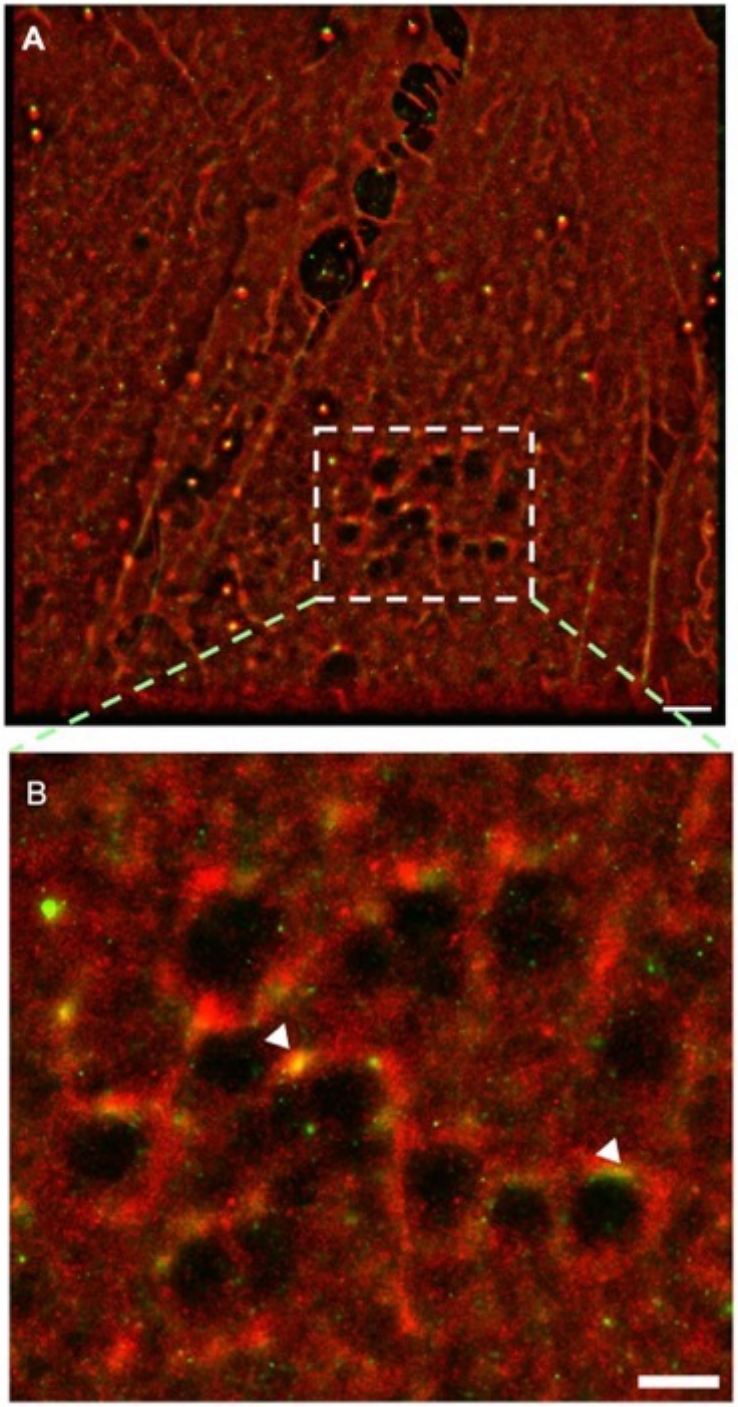

Figure 6.6: Co-localisation of actin and CMDR within fenestrae periphery using dSTORM in NASH LSEC

(A) Representative image of LSEC isolated from a NASH liver. LSEC were stained with Cell Mask Deep red plasma membrane dye (5 µg/ml) and ATTO 488 Phalloidin. Tetraspeck microspheres (0.1 µm diameter) were applied to the sample in order to allow for drift correction. CMDR and phalloidin images were acquired sequentially and 20 000 frames were collected for each channel. Images were reconstructed using the ThunderSTORM plugin in Fiji software and were drift corrected using the cross-correlation approach. The Normalised Gaussian method was applied for image rendering with a lateral uncertainty of 20 nm. Pixel size: 10 nm. Scale bar: 2µm. (B) A magnified view of a cluster of fenestrations marked in panel A. Areas of colocalization between CMDR and phalloidin are indicated by the white arrows. Pixel size: 10 nm. Scale bar: 1 µm

Next it was important to assess the size and shape of the fenestrations evident in our cells. The sieve plate captured in a normal donor LSEC as illustrated in Figure 6.2 (B) is shown in Figure 6.7, with a focus on a single fenestration in a magnified view shown in Figure 6.7 (B). Fenestration diameter is approximately 300 nm as indicated by the blue line on the intensity profile plot in panel C. The panel shows labelling intensity (y-axis) across the region indicated by the white line on panel B which spans the borders of the fenestral pore and the pore itself. There is a gray value of 2.35 on the boundary of the fenestration starting at the bottom left of the white line while gradually decreasing as the intensity profile shifts towards the inner region of the nanopore. Pixel intensity is reduced dramatically within the fenestration due to the absence of signal with the exception of single pixels which give rise to the intensity peaks pointed out by the green arrows. Intensity gradually increases again as the line profile reaches the opposite side of the fenestration. This allows assessment of the intensity in the membrane boundary of the fenestration as this can influence the shape as well as segmentation of the image for further analysis. The intensity profile demonstrates the absence of signal as a result of lack of labelling within the fenestration, expected as there is no membrane that can be stained within it. Also, it provides the approximate diameter of the fenestration is by obtaining the intensity of pixels along the length of distance where the absence of signal indicates that membrane gap identified as a fenestration.

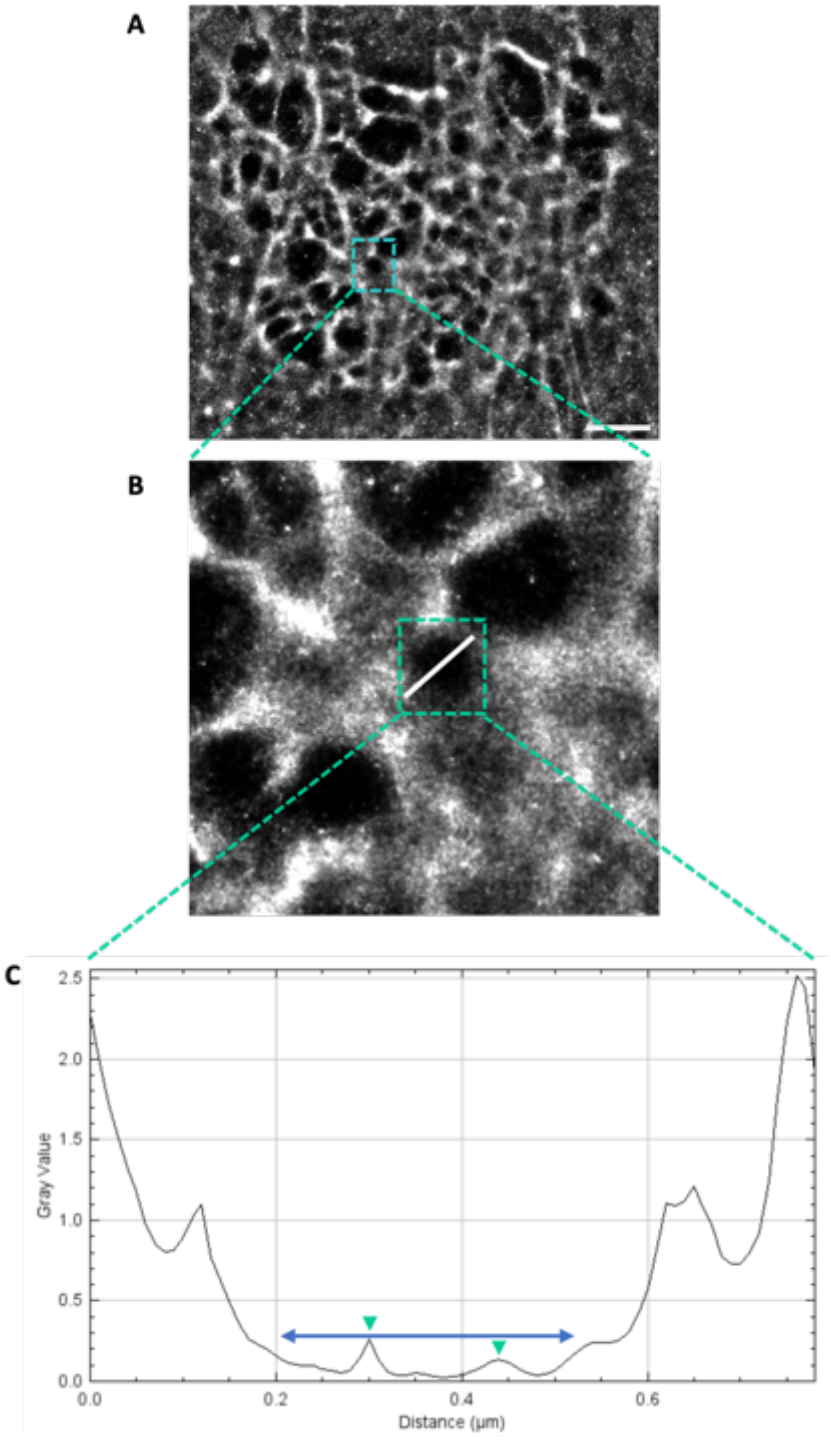

Figure 6.7: dSTORM image of an LSEC isolated from healthy donor liver tissue

(A) A representative image of a sieve plate in an LSEC derived from healthy donor liver tissue acquired using dSTORM. LSEC were stained with Cell Mask Deep Red plasma membrane dye at 5 µg/ml and this image was reconstructed using the ThunderSTORM plugin in Fiji software using 20 000 frames. The highlighted area shown in (B) indicates a single fenestration within a sieve plate. The intensity profile plot shown in panel C was generated in Fiji software and includes the fenestration (depicted in panel B) and immediate membrane boundary as shown by the white line in panel B. The blue line represents the diameter of the fenestration. Scale bar: 2 µm

Figure 6.8 shows a representative region of fenestrations from cirrhotic LSEC shown in Figure 6.3. A magnified view of the region shown in Figure 6.3 (B) is presented in Figure 6.8 (A) where on the left had side there are two adjoining fenestrae. An important structural feature in this specific region is the poorly formed membrane compartment separating them seen on the image as sparsely labelled. The intensity line profile shown in panel B is representative of the fenestration marked with a white line in panel A and shows the intensity of localisations across the region depicted by the white line from top to bottom. This fenestration is approximately 200 nm in diameter which is indicated by the length of distance on the x-axis where the pixel intensity has decreased to near 0.

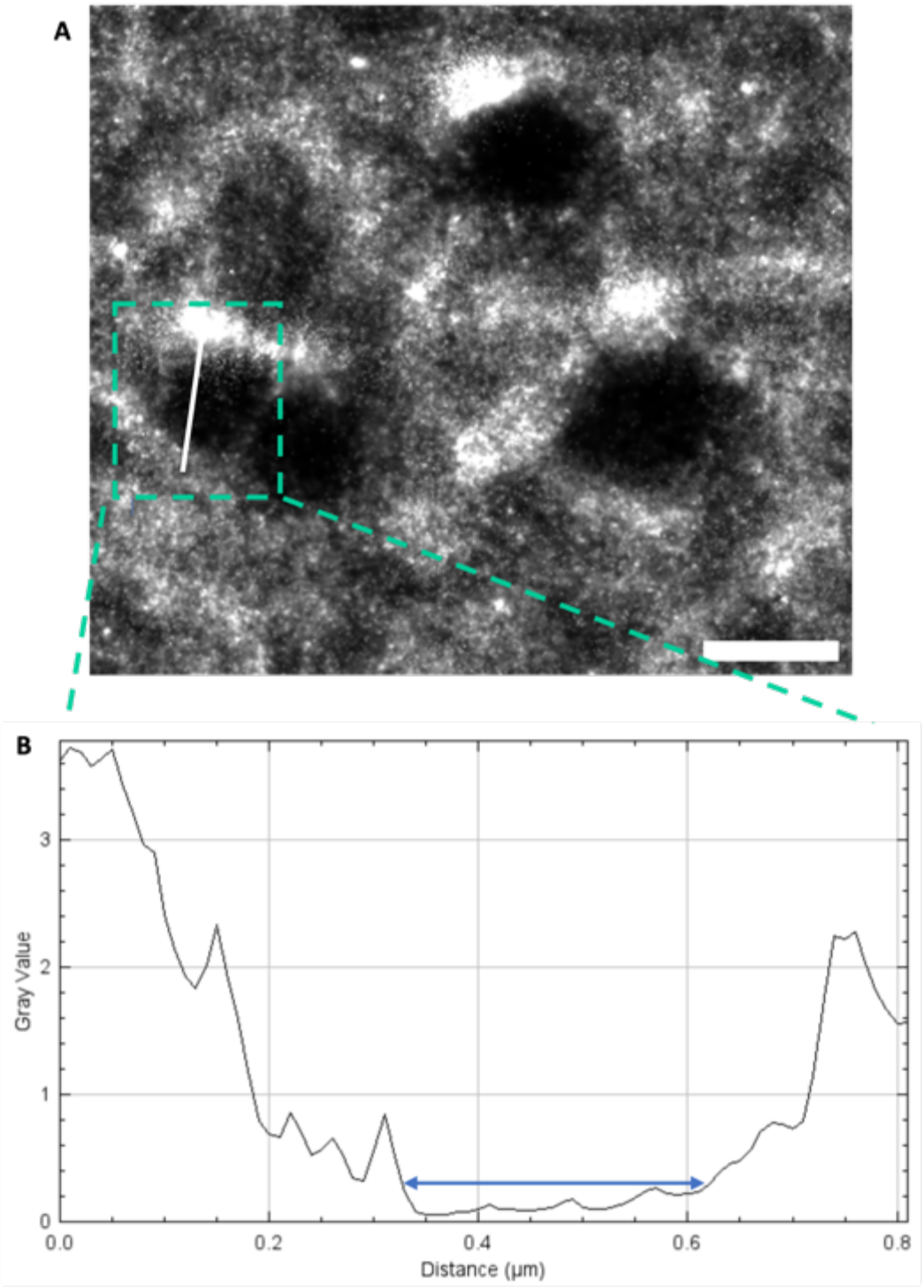

Figure 6.8: Measurement of fenestration diameter in dSTORM images of cirrhotic LSEC

(A) Representative cluster of fenestrations in an LSEC derived from cirrhotic liver tissue acquired using dSTORM. LSEC were stained with Cell Mask Deep Red plasma membrane dye at 5 µg/ml and this image was reconstructed using the ThunderSTORM plugin in Fiji software using 20 000 frames. (B) The intensity profile plot was generated in Fiji software includes the fenestration (depicted in panel A) and immediate membrane boundary as shown by the white line in panel A. The blue line represents the diameter of the fenestration. Scale bar: 1 µm.

By using the macro detailed in chapter 2 (section 2.5.4) for the automatic batch measurement of fenestrations in all images, I was able to determine the diameter of fenestrae in healthy and diseased LSEC. A total number of 1979 and 2370 fenestrations were quantified in normal and cirrhotic LSEC, respectively, and their diameters are indicated by the symbols in Figure 6.9. There is a 17% difference in the mean fenestration diameter between healthy and cirrhotic LSEC, whereby the mean diameter in healthy LSEC is 243.4 nm, and for cirrhotic LSEC it is 205 nm. Statistical analysis by a Mann-Whitney test revealed a significant difference in fenestration frequency between donor and cirrhotic LSEC.

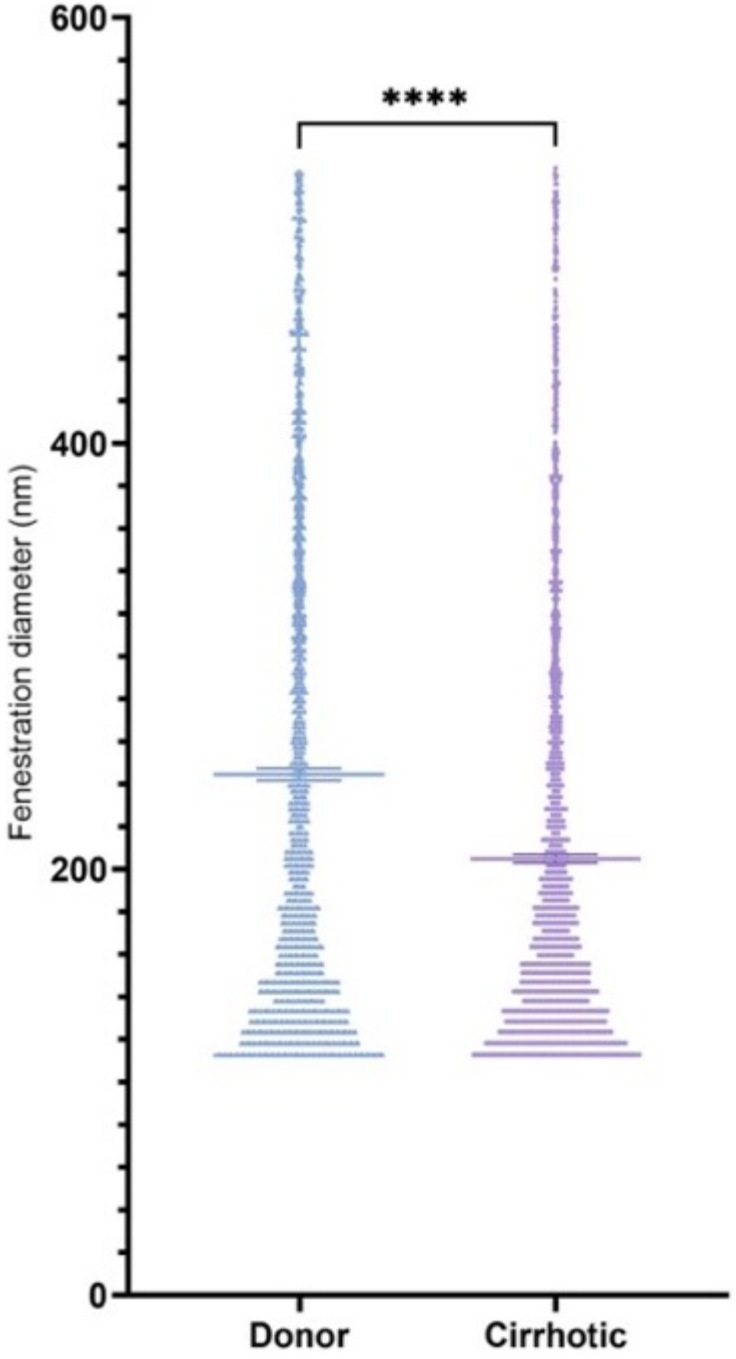

Figure 6.9: Quantification of fenestration diameter in normal donor and cirrhotic LSEC

The data presented in each scatter (with bars indicating the mean +/- SEM) are representative of fenestration diameter in all fenestrations quantified from *n* = 3 *d*STORM images acquired from each of *n* = 3 biological replicates of LSEC isolated from normal donor and cirrhotic liver tissue. **** p-value < 0.0001. Mann-Whitney test.

Next, I calculated the frequency distribution of the fenestration diameter in both normal and cirrhotic LSEC as shown in Figure 6.10. Here, frequency is expressed as a percentage of the total number of fenestrations detected. The frequency is representative of fenestrations detected in n = 3 LSEC imaged from each of n = 3 biological replicates of normal donor and cirrhotic LSEC. In donor LSEC, 22.8% of fenestrations are within a size range of 112.5 nm and 137.5 nm in diameter with a median value of 205 nm whereas 28.5% of fenestrations in cirrhotic LSEC are within the same diameter size range with a median value of 167 nm. Even though there is a higher total number of fenestrations in cirrhotic LSEC, the frequency of larger fenestrations decreases with increasing bin width. In contrast to this, there is a higher proportion of fenestrations in the 287.5 nm and 312.5 nm diameter range (4.3%) in donor LSEC compared to 3.7% in cirrhotic LSEC. In conclusion, a higher number of fenestrations was detected in cirrhotic LSEC with approximately 70% of them having a diameter below 250 nm while more fenestrations in healthy LSEC had diameters above 250 nm (≈37%).

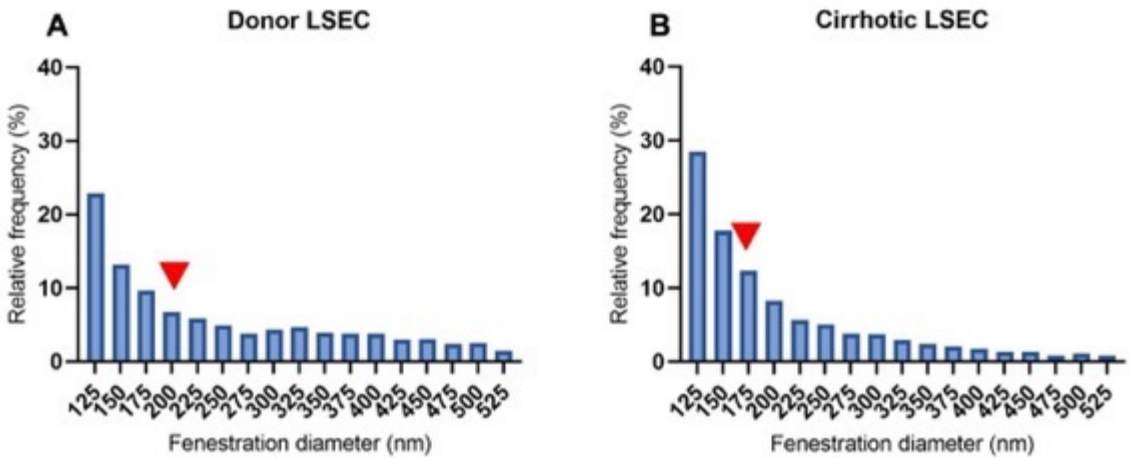

Figure 6.10: Frequency distribution of fenestration diameter in untreated normal donor and cirrhotic LSEC

The data presented in the frequency distribution histograms are representative of the following: fenestration diameter was calculated from *n* = 3 dSTORM images which were acquired for each of *n* = 3 biological replicates of LSEC isolated from normal donor (A) and cirrhotic liver tissue (B). Bin width was set at 25 nm and relative frequency of fenestrations in each bin is shown as a percentage of the total number of fenestrations detected within the range of 100nm and 525 nm. Red arrows indicate the median fenestration diameter for donor and cirrhotic LSEC.

6.2.3 Does sildenafil alter fenestration frequency and distribution in human LSEC?

Since I had successfully demonstrated the presence of fenestrations in human LSEC using *d*STORM, I next applied this approach to determine whether the porosity of human LSEC can be manipulated *in vitro* using sildenafil citrate. Again, I was interested in the comparison of sildenafil citrate treatment impact on both healthy and diseased cells. Figure 6.11 presents representative images of normal donor and cirrhotic (ALD) LSEC treated with vehicle control (DMSO) (A and C) or sildenafil citrate at 10 μg/ml (B and D) respectively. In these isolates of LSEC, I again noted the presence of fenestrations in both healthy and diseased cells which were more abundant in healthy cells and tended to localise to specific regions of the membrane surface. Fenestrations were widely and abundantly distributed across the surface of the membrane of the normal donor LSEC treated with sildenafil citrate shown in panel B, from the perinuclear area of the cell towards the outer region of the cytoplasm. In contrast to this, fenestration localisation on the cirrhotic LSEC shown in panel D is mainly on the outer edge of the plasma membrane. In the representative healthy and cirrhotic LSEC shown in panels B and D respectively, a total of 196 fenestrations were measured in healthy cells while only 140 fenestrations were measured in cirrhotic samples.

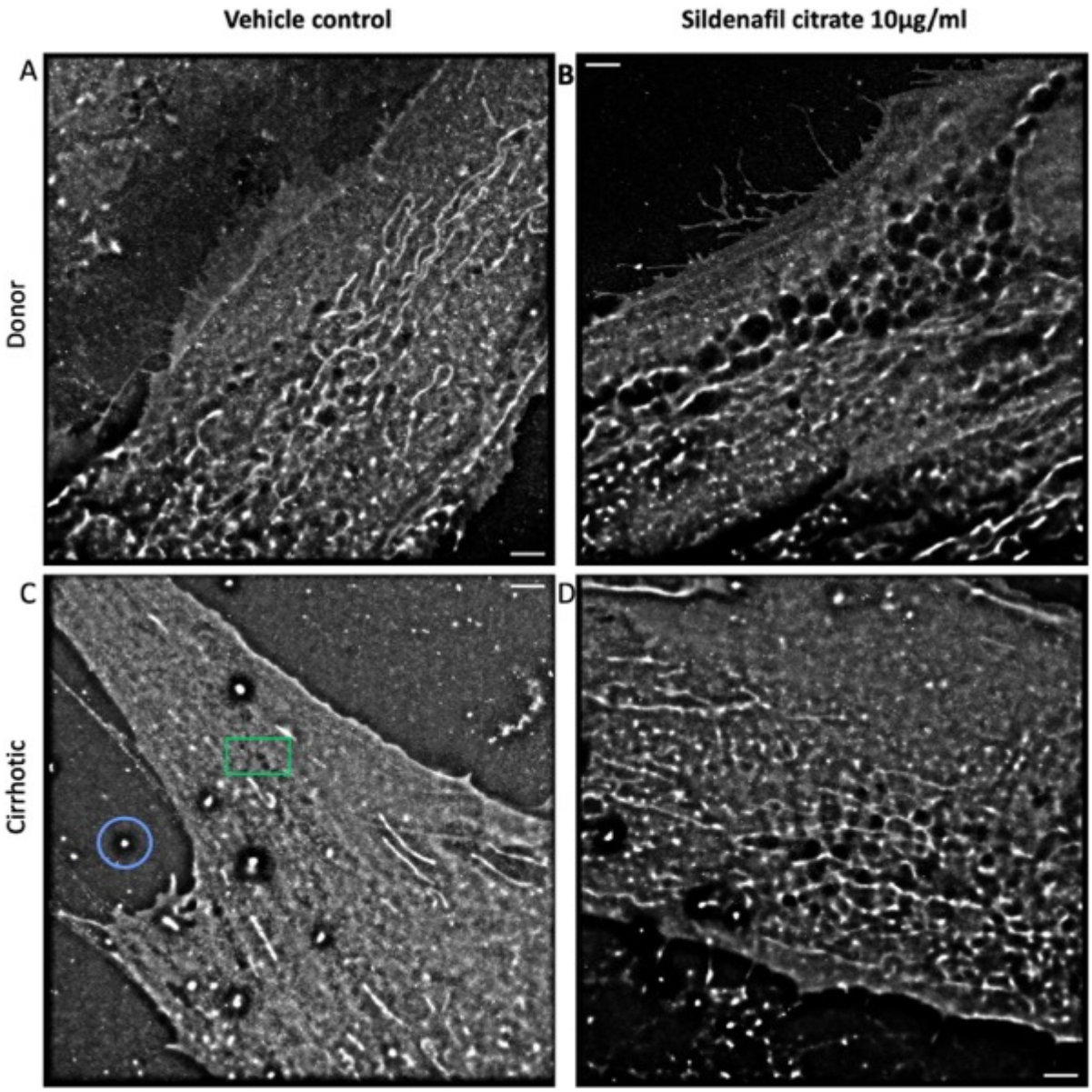

Figure 6.11: dSTORM imaging of normal and cirrhotic LSEC treated with sildenafil citrate

Representative images of normal donor (A and B) and cirrhotic (C and D) LSEC were treated with vehicle control and sildenafil citrate at 10µg/ml respectively. The green box in panel C illustrates fenestrations in the vehicle control of cirrhotic LSEC. The images were reconstructed using the ThunderSTORM plugin in Fiji software using 20 000 frames and were drift corrected using cross correlation. The Normalised Gaussian method was applied for image rendering with a lateral uncertainty of 20 nm. Feature within the blue circle indicates a fiducial. Pixel size: 10 nm. Scale bar: 2 µm.

Quantification of fenestrae and their respective diameters in healthy LSEC treated with vehicle control and sildenafil citrate is shown in Figure 6.12. The total number of fenestrations quantified in the control and sildenafil citrate treated LSEC isolated from normal liver tissue (panel A) was 2287 and 2755 respectively as shown by the symbols. The mean values for fenestration diameter were 195.5 nm in control LSEC and 218 nm in sildenafil citrate treated indicating that sildenafil citrate treatment resulted in an increase in fenestration diameter compared to control LSEC. The quantification of fenestrae in cirrhotic LSEC treated with sildenafil citrate is shown in Figure 6.12 (B), whereby a total of 1900 fenestrations were measured in LSEC treated with vehicle control and a total of 2489 fenestrations in sildenafil citrate treated cirrhotic LSEC. Again, there is an increasing shift in fenestration diameter following sildenafil citrate treatment as the mean diameter of control LSEC is 200 nm and 235 nm in sildenafil citrate treated LSEC. Statistical analysis by a Mann-Whitney test revealed a significant increase in fenestration frequency between control and sildenafil citrate treated LSEC for both donor and cirrhotic liver specimens.

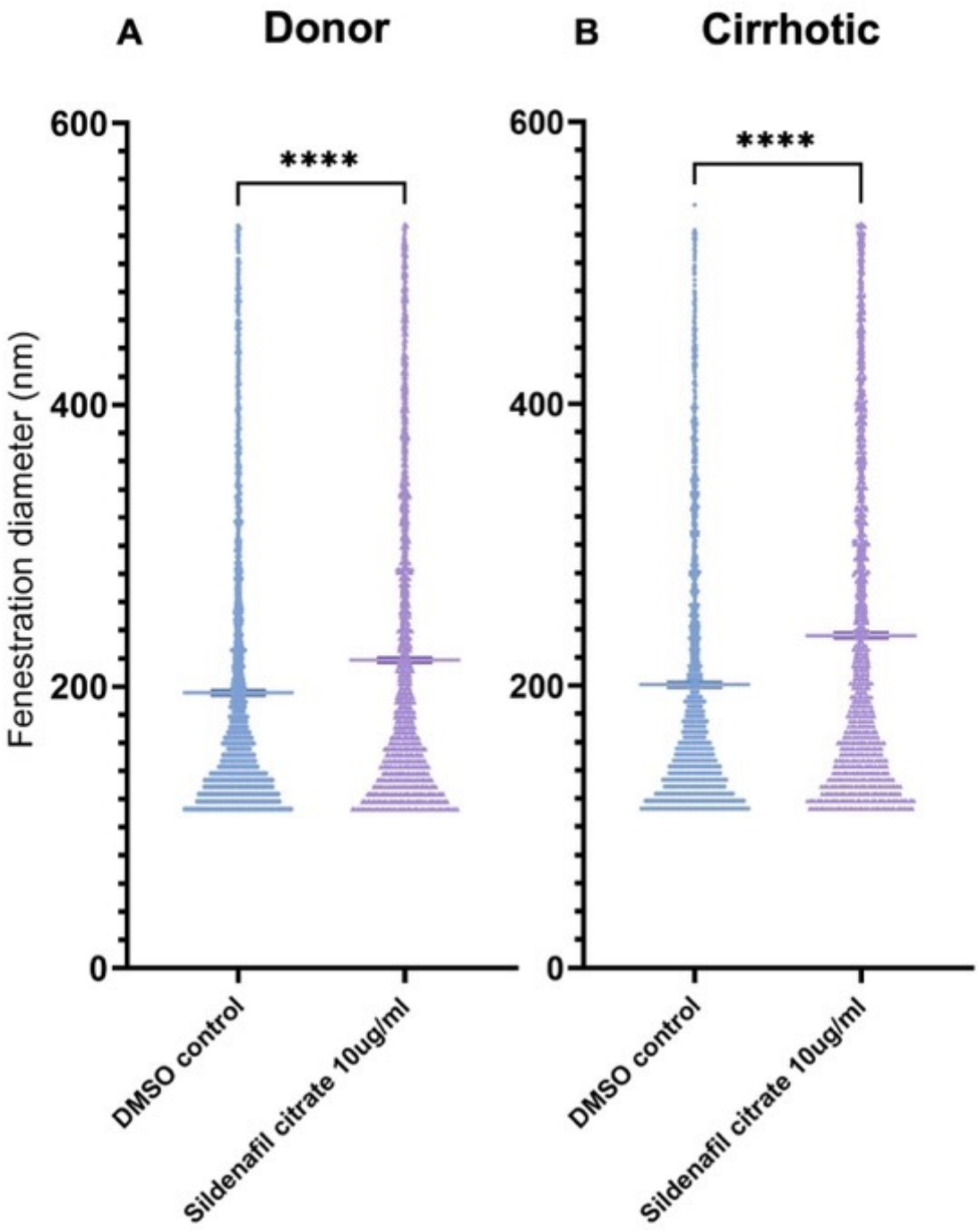

Figure 6.12: Quantification of fenestration diameter in normal donor and cirrhotic LSEC treated with sildenafil citrate

The scatter plots represent the total number of fenestrations measured in healthy (A) and cirrhotic (B) LSEC treated with vehicle control and sildenafil citrate. The data presented in each scatter dot plot (with bars indicating the mean +/- SEM) are representative of fenestration diameter in all fenestrations quantified from *n* = 3 *d*STORM images acquired from each of *n* = 3 biological replicates of LSEC isolated from normal donor and cirrhotic liver tissue. **** p-value < 0.0001. Mann-Whitney test.

The frequency distribution of the diameter of all fenestrations detected in donor and cirrhotic LSEC treated with vehicle control (A and C) and sildenafil citrate (B and D) respectively is shown in Figure 6.13. In donor LSEC treated with vehicle control shown in panel A, a total of 2287 fenestrations were detected, with a median fenestration diameter of 155.6 nm and 34.6% of fenestrations within a size range of 112.5 nm and 137.5 nm in diameter. The frequency distribution of the diameter of normal donor LSEC treated with sildenafil citrate at 10 µg/ml is displayed in panel B. In sildenafil citrate treated donor LSEC, a total of 2755 fenestrations were detected, with a median fenestration diameter of 178.5 nm. The majority of fenestrations detected, comprising 26.5% of the total count were in the diameter size range of 112.5 nm and 137.5 nm and fenestration frequency decreases with increasing bin width.

Figure 6.13 (C) displays the frequency distribution of fenestration diameter in cirrhotic LSEC treated with vehicle control. In the total of 1900 fenestrations detected, the median fenestration diameter is 160 nm in LSEC treated with vehicle control. A shift in the distribution towards larger fenestration diameter is observed in sildenafil treated cirrhotic LSEC as in control LSEC 31% of fenestrations are in the diameter size range of 112.5 nm and 137.5 nm whereas in sildenafil treated cirrhotic LSEC 23% of the total fenestration count are in this diameter range (panel D). In contrast to this, 3% of control LSEC are within the diameter range of 287.5 nm and 312.5 nm while 4.7% of sildenafil treated cirrhotic LSEC are within this diameter range. Additionally, a total of 2489 fenestrations were detected in cirrhotic LSEC treated with sildenafil which is a significantly higher frequency compared with vehicle control, with the median fenestration diameter increased to 192.2 nm. Overall, the median

fenestration diameter of cirrhotic LSEC treated with sildenafil citrate was increased by 14% compared to the median diameter of untreated cirrhotic LSEC.

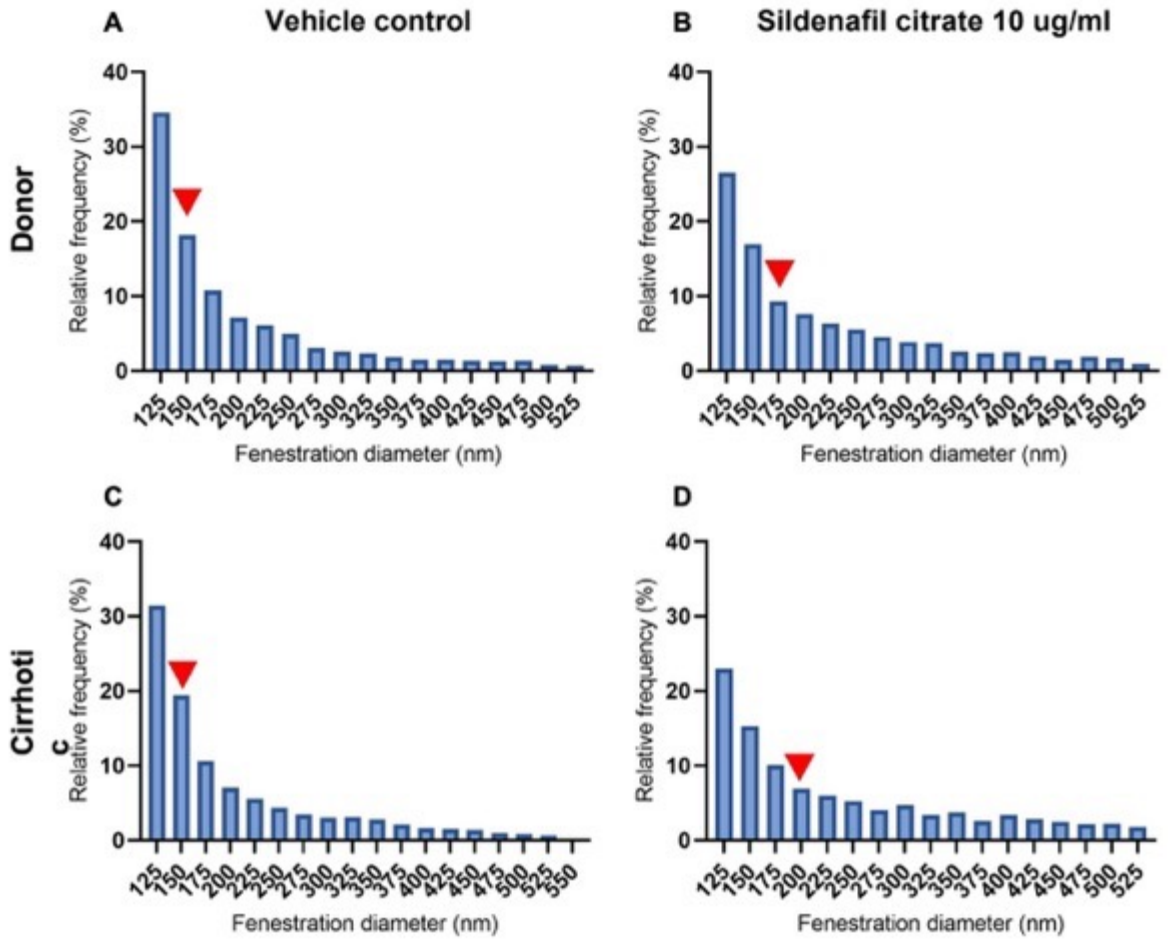

Figure 6.13: The porosity of human LSEC *in vitro* is altered with sildenafil citrate treatment

The data presented in the frequency distribution histograms are representative of the following: fenestration diameter was calculated from *n* = 3 dSTORM images which were acquired for each of *n* = 3 biological replicates of LSEC isolated from normal donor (A and B) and cirrhotic liver tissue (C and D), treated with vehicle control and sildenafil citrate respectively. Bin width was set at 25 nm and relative frequency of fenestrations in each bin is shown as a percentage of the total number of fenestrations detected within the range of 100nm and 525 nm. Red arrows indicate the median fenestration diameter for vehicle control and sildenafil citrate treatment groups for donor and cirrhotic LSEC.

6.3 Discussion

Fenestrations, constitute a morphological feature used to describe a healthy LSEC phenotype and are often used as the key evidence of the sinusoidal identity of liver sinusoidal endothelial cells. Their visualisation is a challenging task however the development of super-resolution microscopy techniques has revolutionised the visualisation of biological features beyond the limits of light diffraction. Several super-resolution techniques have been utilised so far to visualise fenestrae; however, most of these data come from animal models.

It is therefore necessary to bridge the existing knowledge gap concerning human LSEC data and fenestrations and in diseased samples, as a detrimental effect of chronic liver disease is a capillarised LSEC phenotype which, is accompanied by a reduction in fenestration frequency and diameter. Overall reduced LSEC porosity contributes to LSEC dysfunction which impacts liver function leading to metabolic dysfunction such as hyperlipidaemia (59).

This chapter presents the visualisation of fenestrations in human LSEC using the SMLM technique *d*STORM. The data is representative of distinct biological replicates as in total, the LSEC samples imaged by *d*STORM were isolated from 12 different liver tissue specimens (including healthy and diseased cells). Fenestrations were visualised in LSEC isolated from healthy donor, ALD, PBC and NASH liver specimens. The optimised protocol of imaging parameters has allowed the confirmation of the presence of fenestrations on the LSEC membrane which is the gold standard for confirming the LSEC phenotype *in vitro*. This confirms that our media and growth conditions for LSEC isolated from healthy and cirrhotic liver tissue enables the maintenance of fenestrations, and more importantly confirms that the initial cell isolation procedure does indeed select for LSEC from both healthy and diseased

tissue. Organised sieve plates were observed in a healthy LSEC (Figure 6.2) and fenestrations were maintained even in cirrhotic LSEC *in vitro*. The mean fenestration diameter of cirrhotic LSEC was smaller than the mean diameter of normal donor LSEC which is consistent with the effect of cirrhosis on the LSEC phenotype.

Changes in LSEC porosity in chronic liver disease have been linked to situations such as alcoholism where altered lipid traffic and hyperlipidaemia is a consequence (85). Similarly, reductions in transit of drugs such as paracetamol can alter clearance and metabolism (463,464). Thus, strategies to redress the changes in LSEC associated with capillarisation are of interest. Sildenafil citrate has been implemented previously for the manipulation of mouse LSEC *in vitro* and its application resulted in an overall increase in LSEC porosity (202,465). It acts by inhibiting PDE5 which mediates the breakdown of cGMP. In the NO/cGMP pathway cGMP is the second messenger in the NO signal transduction cascade leading to smooth muscle relaxation and vasodilation (466). Mechanisms implicated in regulating the state of cell contraction include the reduction of contractile tone by the decrease in intracellular calcium and a downstream effect of cGMP is the efflux of intracellular calcium into endoplasmic reticulum. Elevated intracellular calcium levels and formation of calcium/calmodulin complex lead to activation of myosin light-chain kinase (MLCK) via binding to calcium/calmodulin (467). The presence of lower calcium levels, results in smooth muscle relaxation as MLCK and myosin-light-chain (MLC) are less active(468).The state of contraction of smooth muscle is influenced by the phosphorylation status and activity of MLC which is involved in the regulation of cytoskeletal tension. An additional mode of action of cGMP that has been proposed for microvascular endothelium, is through PKG which modulates myosin light chain phosphatase (MLCP). In a phosphorylated state, MLC mediates contraction via its interaction

with actin and this can be reversed by the dephosphorylation action of MLCP leading to reduced actomyosin contractility and relaxation of the actin cytoskeleton (469). Although the precise mode of action of NO in regulation LSEC fenestrae has not been fully elucidated yet, supporting evidence has been presented suggesting a role for the cGMP and calcium pathway for VEGF mediated NO signal transduction (354,470). It has also been proposed that actin relaxation could lead to an increase in fenestration diameter and/or frequency (471).

In our human LSEC we demonstrate an increase in fenestration diameter in both healthy and diseased LSEC treated with sildenafil citrate. Median fenestration diameters were 178 nm and 192 nm in treated healthy and cirrhotic LSEC respectively as shown in Figure 6.13, which correspond to a 13.7% and 18.5% increase in diameter of fenestrations in treated donor and cirrhotic LSEC respectively, compared to treatment controls. Thus as has been observed in rodent cells, this signifies an overall increase in LSEC porosity, with a larger increase observed in cirrhotic LSEC indicating that diseased LSEC exhibited a higher response to sildenafil citrate treatment. This is particularly important in the context of the implications of reduced LSEC porosity in chronic liver disease where some of the changes associated with capillarisation would maybe corrected after treatment. The increased LSEC porosity provides supporting evidence for the usefulness of sildenafil citrate as an approach to improve LSEC defenestration, leading to restoration of the LSEC phenotype and improved filtration function. The impact of sildenafil citrate on endothelial cell dysfunction has been demonstrated in patients as well as models of cardiovascular disease and atherosclerosis. In an apolipoprotein E knock-out mouse model with spontaneous hypercholesterolemia, chronic sildenafil treatment had a beneficial effect on endothelial dysfunction and morphological analysis revealed 40% reduction in the deposition of plaque in the aorta. Data indicated that

sildenafil citrate was acting by fortifying the NO signalling pathway and also resulted in decreased oxidative stress (472). The effects oral administrated sildenafil to patients with coronary artery disease have also been tested, whereby vasodilatory effects and improvement of endothelial dysfunction were observed (473). Additionally, the long-term effects of sildenafil in hypertensive rats were investigated. Here, endothelial dysfunction was reversed, accompanied by a reduction in renal macrophage accumulation and oxidative stress leading to amelioration of severe hypertension (398). Thus, the data presented in this chapter, suggest that sildenafil treatment may benefit in correcting endothelial function in chronic liver disease and maybe particularly relevant in NAFLD where dyslipidaemia is also a risk factor.

Fluorescent labelling of the plasma membrane is a well-known approach, which has proved particularly useful here as it allowed for the identification of fenestrations based on the lack of signal within the nanopores. CMDR is a plasma membrane dye that can be used in either live or fixed cells. For our experimental conditions, CMDR was applied on fixed cells followed by a quick wash step with PBS 0.1% Tween-20 which was suggested to reduce background staining (296). There is a degree of internalisation of CMDR as fixation and Tween-20 partially permeabilises the cell membrane. A future variation of the staining procedure followed here, could be to apply CMDR staining to live LSEC immediately after treatment followed by fixation. This could be achievable as CMDR survives fixation and comparison of staining before and after fixation could be very informative in terms distribution of the dye within the plasma membrane and how this impacts the visualisation and ultimately the measurement of fenestrae. The application of live cell *d*STORM has been reported (474) and would be an interesting option to retrieve real-time dynamic data on the formation of fenestrations, i.e, fenestrae forming centres as well as changes to the actin cytoskeleton throughout this

process. However, the components within the chemical buffer used for fluorophore photoswitching in *d*STORM could compromise cell integrity (475).

A prerequisite for enhanced photo-switching of fluorophores during *d*STORM image acquisition is the use of high laser power for the adjustment of the fluorophore blinking rate per frame(476). In the case of imaging CMDR in our samples, fluorophore blinking was gradually reduced as individual fluorophores were also bleached towards the end of acquisition of 20 000 frames. However, the labelling and imaging parameters resulted in satisfactory dense labelling of the membrane which was necessary as the approach relied on absence of signal for imaging of fenestrations with a well reconstructed plasma membrane required in order to be able to discern such delicate structures like fenestrae. There was, however, variation in labelling density which resulted in adjustments in thresholding and segmentation of the images prior to fenestration measurements.

Good consistency was noted between fenestration parameters in our groups of cirrhotic and healthy donor LSEC which reassures that the approach implemented was suitable. It is important to note that the distribution of fenestration diameter and frequency exhibited variation between cells from the same biological donor. An example of this is shown in Figure 6.14 which shows the quantification of fenestrations captured in individual LSEC isolated from the same donor or cirrhotic liver. It is clear that the total fenestration count in cell 2 in considerably lower compared to the other two cells imaged using *d*STORM. This could be attributed to varying degrees of capillarisation in culture or biological variation in accordance with previous studies illustrating the heterogeneity of fenestration frequency and overall porosity in LSEC across the liver lobule(448). It is also important to acknowledge that

fenestrations were imaged in only a small part of the cell membrane of each cell and there may be variation across the whole plasma membrane.

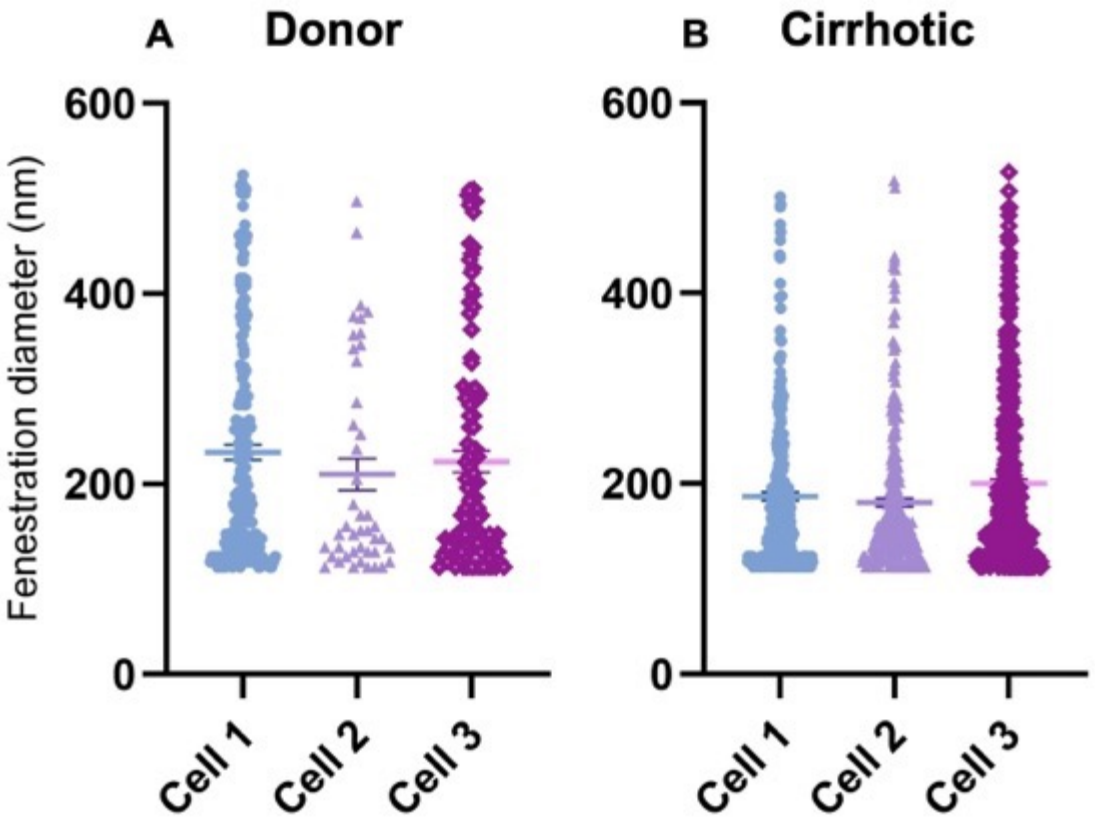

Figure 6.14: Quantification of fenestrations in healthy and cirrhotic LSEC

Dot plot of fenestrations measured for each of *n*=3 healthy donor LSEC images acquired with dSTORM from a single biological isolate (A). Dot plot of fenestrations measured for each of *n*=3 cirrhotic LSEC images acquired with dSTORM from a single biological isolate ((B); PBC liver specimen). Symbols indicate individual fenestrae.

Our fenestration parameters are in keeping with those reported in other studies. However, fenestration measurements vary between data acquired using different imaging modalities. Correlative imaging approaches have revealed a 38% increase in fenestration diameter due to dehydrating fixation and cell body shrinkage in samples prepared and imaged using SEM compared to wet-fixed samples (either glutaraldehyde or formaldehyde was used) for AFM, SIM, and STED imaging approaches (453). Glyoxal is an alternative fixative to PFA which has been tested by several labs on different types of cells such as primary hippocampal neurons and has been found to better preserve cellular morphology (477). PFA is a slow-acting fixative and 4% PFA in particular has very high osmolarity and dramatic osmotic changes could lead alterations in cell morphology again by causing shrinkage of the cell body (478). Glyoxal therefore constitutes in additional fixative option, especially concerning fenestration areas with incomplete membrane boundaries.

Despite the differences in fenestration measurements due to dry fixation employed in SEM, fusion of fenestrae has been observed in SEM preparations of LSEC and it is thought to be a result of fixation leading to arrest in fenestrae fusion. This resulted in the formation of large gaps as a result of perfusion fixation which could be a result of the fusion two individual fenestrations or multiple fenestrae within a sieve plate. Thinner cytoplasmic bridges between fenestrae were also observed (172) which relates to the poorly formed membrane boundaries observed in between adjoining fenestrae shown in Figure 6.15 (B). The lack of complete membrane boundaries could also indicate fusion of fenestrae. Differences in the three-dimensional arrangement of fenestrae visualised *in vitro* must also be considered. Labyrinth-like fenestrae in a multi-folded configuration were detected in the perinuclear area of LSEC and have been visualised using TEM and AFM (461). Additionally, the fact that there are no

clear-cut membrane boundaries surrounding some fenestrae as shown in Figure 6.15 (B) could indicate the presence of additional cytoskeletal components that were not sufficiently labelled by CMDR.

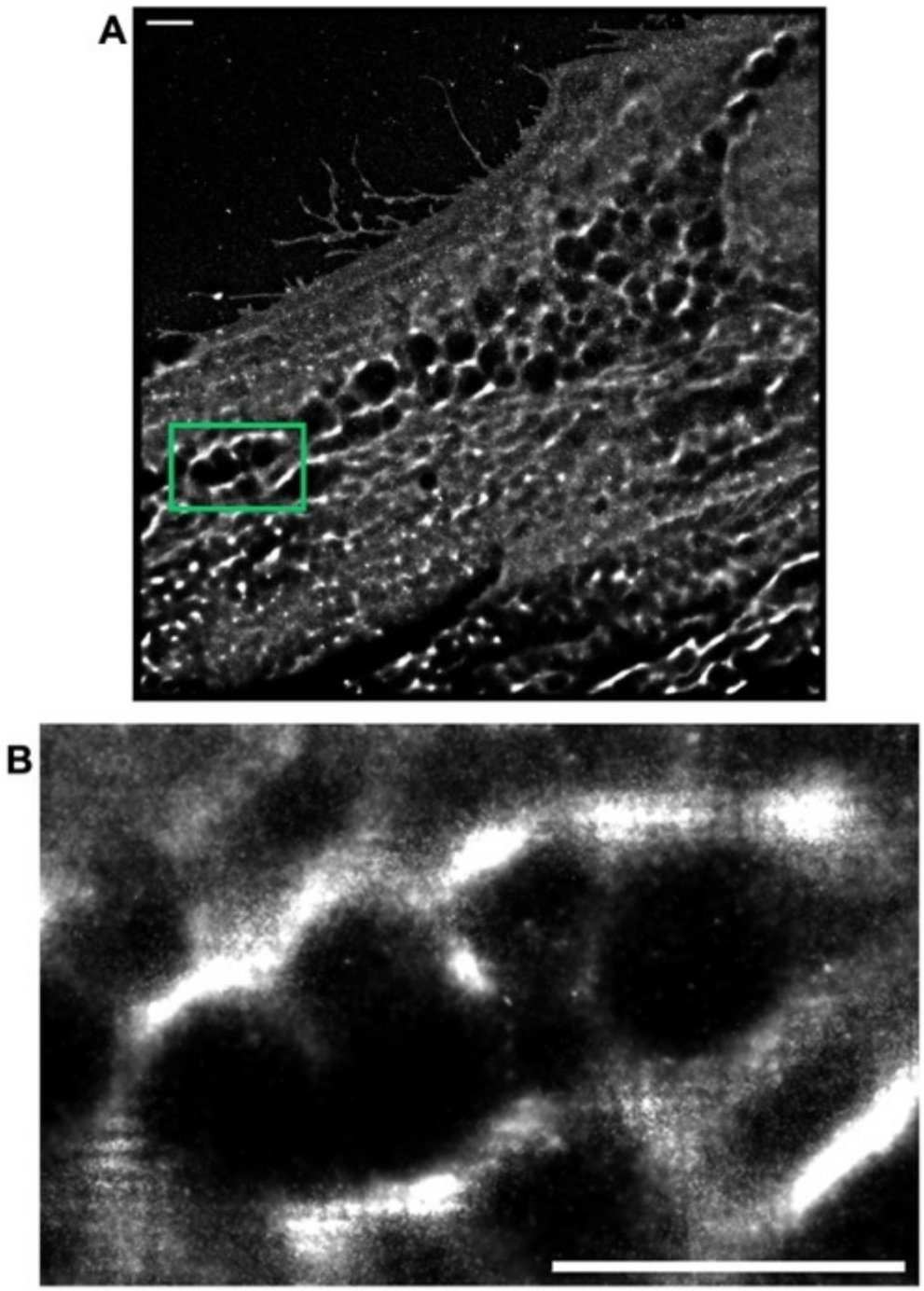

Figure 6.15: dSTORM imaging of healthy LSEC treated with sildenafil citrate

(A) Representative *d*STORM image of healthy LSEC treated with sildenafil citrate at 10µg/ml. The green box illustrates a cluster of fenestrations in a magnified view (B). The images were reconstructed using the ThunderSTORM plugin in Fiji software using 20 000 frames and were drift corrected using cross correlation. The Normalised Gaussian method was applied for image rendering with a lateral uncertainty of 20 nm. Pixel size: 10 nm. Scale bar: 2 µm.

The presence of cytoskeletal proteins within fenestration boundaries such as spectrin has been demonstrated (192). We have identified the presence of aggregated actin regions within the immediate fenestration boundary as illustrated in Figure 6.5. Actin forms a major part of the membranous boundary enclosing fenestrations, thereby contributing to the formation of fenestrae associated cytoskeleton rings. In addition, the actin labelling appears as an intermittent ring enclosing fenestrae which points to the fact that additional cytoskeletal proteins take part in forming the cytoskeleton mesh holding fenestrae in place.

In general, the diameter of fenestrations quantified in our human LSEC ranges between 112.9 nm and approximately 530 nm. This range is larger than the typical fenestration diameter reported for rodent LSEC which is typically between 50 nm and 300 nm (479). This may be attributed to biological scaling and species-specific differences (78), emphasised by the fact that the human liver and therefore LSEC are significantly larger than rodent LSEC. In addition, fenestrae have been reported to expand their diameter up to 300% of the starting diameter in murine LSEC, also influenced by rearrangements in the cell's actin cytoskeleton (390). Further to this, live atomic force microscopy imaging of the response of fenestrae in murine LSEC to treatment with antimycin-A, illustrated their dynamic size range. Fenestrations appear in a dilated state at time 0, exhibiting diameters close to 500 nm as shown in Figure 6.16 thus not too dissimilar to the human findings presented in this chapter. Antimycin-A treatment over 60 minutes resulted in contraction and reduction of fenestrae frequency in that specific cell surface area (445). Tracking the lifespan of fenestrae over a 12h window, revealed that 75% of fenestrations remained dilated (or in an open state) for less than 20 minutes while only 5% remained open for longer than 1 h. Atomic force microscopy

also demonstrated the migratory properties of fenestrations whereby their position can be altered independent of sieve plates (192).

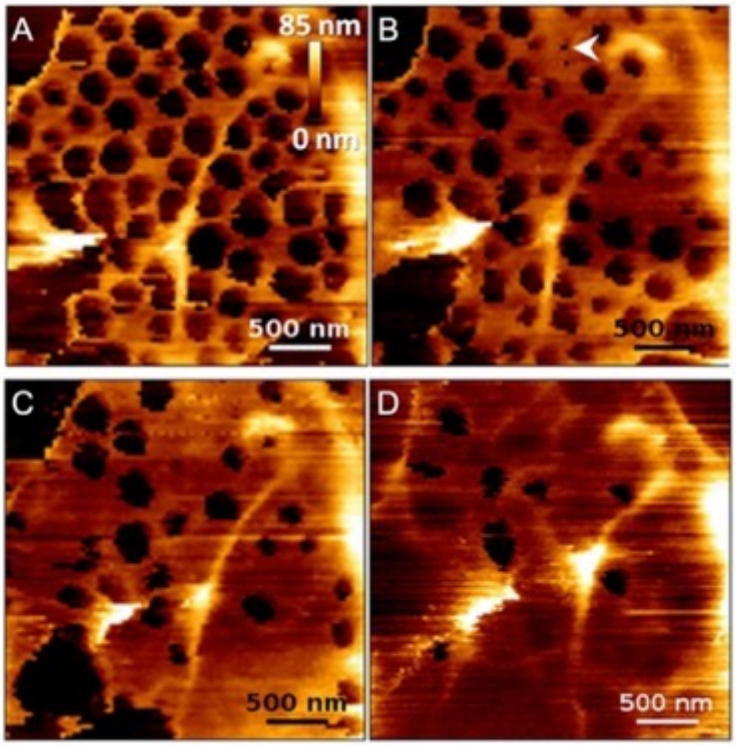

Figure 6.16: Imaging of fenestrae in live LSEC using AFM
Imaging topography of live LSEC treated with 1 µg/ml antimycin-A. Images were acquired at time points 0 (A), 8 (B), 22 (C) and 60 (D) minutes after administration of antimycin-A. White arrowhead points to a fenestration with a diameter smaller than 80 nm, prior to membrane fusion. Figure adapted from Zapotoczny et al. (445).

Despite the fact that our quantified fenestration frequency is representative of only a fraction of the cells' surface, the measurement approach enabled the identification of differences in fenestration frequency between normally cultured LSEC and LSEC treated with sildenafil citrate. Measurements of fenestrations vary considerably between tissue and cultured LSEC. It has been demonstrated that sample fixation for SEM and TEM led to shrinking of fenestrae diameters (480,481). Additionally, there is variation of up to 30% between the mean diameters of fixed and live LSEC with a decreasing trend in measurements from live, wet-fixed and fixed-dried LSEC whereby the reported fenestrae diameters are 180±41 nm, 143^{+48}_{-27} nm and 130±41 nm respectively (176,200,444,460). Consequently, an absolute range for fenestrae diameter is a debatable concept.

Quantification of fenestrae frequency and diameter is a heavily computational process. While standardisation of thresholding was carried out for subsequent segmentation of fenestrations, differences in labelling densities on different LSEC could introduce inaccuracies in the measurements. Moreover, the combination of variability between super-resolution imaging platforms and the image analysis approach including pixel size, can introduce a potential 10-20 nm margin of error (479). A particular challenge in image analysis is thresholding and the detection of the fenestration edges in fluorescent label dependent approaches such as *d*STORM. In our data, fenestrations with a diameter below 100 nm have been excluded from measurements due to the pixel size and the localisation precision. In combination the aforementioned factors could lead to under sampling (453).

In conclusion, the optimisation of a *d*STORM imaging protocol has enabled the visualisation of fenestrations in LSEC isolated from both healthy donor and cirrhotic liver specimens in our

culture conditions. Imaging of donor and cirrhotic LSEC following treatment with NO-signalling modulator sildenafil citrate has revealed significant increases in fenestration frequency and diameter in favour of sildenafil treatment.

7 Conclusions and future work

7.1 Summary of key findings

The rising global incidence of liver disease emphasises the need for methods to study the structural, phenotypic, and functional changes taking place throughout the course of liver disease. In order to achieve this, resolving cell specific changes can assist in predicting altered cell cross talk within the liver as well the impact on regulatory signalling pathways in relation to disease progression. As LSEC play a leading role in liver disease pathophysiology it is crucial to identify key changes in disease which could be therapeutically targeted, in order to improve the effects of capillarisation on the LSEC phenotype (319,482).

The differences in LSEC receptor expression identified between healthy donor and cirrhotic liver tissue specimens have important implications in the course of liver disease. The downregulation of receptors such as LYVE-1, CD32B and CLEC4M in cirrhotic liver tissue specimens indicate LSEC dysfunction. The downregulation of CD32B has been reported to have clinical implications in NAFLD patients where one of the receptors ligands, fibrinogen-like protein 2, was present in increased levels (483). This further illustrates how key receptor downregulation can compromise homeostatic functions of the liver. The co-expression of CD32B and LYVE-1 in zones 2 and 3 of the liver lobule, illustrated in Figure 3.7, highlight that liver lobule zonation influences LSEC scavenger receptor expression, in line with previous reports (23,100).

The isolation of LSEC from healthy donor and cirrhotic liver tissue permitted the study of the LSEC phenotype *in vitro*. This culture model exhibited maintenance of LSEC-specific scavenger receptors such as LYVE-1 both at protein and mRNA expression. Additionally, mRNA

expression of receptors such as stabilin-2, the mannose receptor and CLEC4M were all maintained *in vitro* as well as the expression of the transcription factor GATA4 which is critical for the maintenance of the LSEC phenotype (32,211). These findings indicate that the culture model for LSEC maintains key phenotypic and functional characteristics such as the endocytic capacity of LSEC which was demonstrated by the uptake of FITC-BSA. An interesting observation was the significant upregulation of *NOS3* with increasing passage in both healthy donor and cirrhotic LSEC. This could be the result of the LSEC routinely being provided with VEGF *in vitro* throughout regular media changes. This agrees with the fact that VEGF maintains the LSEC phenotype (354) which is also reflected in the visualisation of fenestrations in normally cultured (untreated) LSEC, even at passage 5 (Figure 6.2).

Based on the hypothesis that capillarisation of LSEC in culture recapitulates phenotypic changes observed in liver disease, this model was used for further studies such as the application of pharmaceutical agents to test the restoration of a differentiated phenotype in LSEC. Although no significant upregulation was detected in the mRNA expression of most scavenger receptors analysed following VEGF and sildenafil treatment, LSEC still maintained the expression of key receptors in culture as well as GATA4 transcription factor. *STAB2* mRNA expression levels on the other hand, were significantly downregulated with increasing dosage of VEGF. Stabilin-2 receptor activation has been linked to the progression of liver disease and activation in HSCs (411) and its downregulation in response to VEGF could indicate improvement in the LSEC capillarised phenotype.

The *in vitro* environment lacks key features that maintain the LSEC phenotype *in vivo* such as shear stress and crosstalk with other hepatic cell populations such as hepatocytes and HSCs.

This would also have had an impact on mRNA expression levels detected in LSEC in culture as well as impact the effect of VEGF and sildenafil citrate treatment.

The development of robust imaging protocols enabling the visualisation of fenestrations on the LSEC membrane is crucial. The development of an optimised dSTORM protocol enabled the visualisation of fenestrations in human LSEC isolated from both normal donor and cirrhotic liver specimens. Their successful visualisation confirmed the LSEC identity *in vitro* as well as confirming the suitability of the CLGR's LSEC isolation protocol. There have been reports that rat LSEC isolated using CD31 which is also used a selection marker in LSEC isolation here, lack fenestrations (334). The data presented in chapter 6 illustrate the contrary.

Consequently, this was followed by visualising and quantitating the impact of sildenafil citrate on fenestrations in healthy and cirrhotic LSEC. This revealed an increase in fenestration diameter which was more pronounced in cirrhotic LSEC whereby an 18.5% increase in cirrhotic LSEC diameter treated with sildenafil compared to treatment control. Additionally, there was a marked increase in fenestration number in both healthy donor and cirrhotic LSEC after sildenafil treatment. The acquired data illustrates the potential of sildenafil in modulating the fenestrated phenotype of human LSEC which has also demonstrated in rodent LSEC (202,465). Although there are currently several proposed hypotheses regarding the regulation of fenestrations as summarised in section 1.5.5, the exact mechanism of action remains to be elucidated by future research. The dSTORM imaging protocol developed can be applied on LSEC to further elucidate the association of fenestrations with the actin cytoskeleton after sildenafil treatment as well as other agents such as VEGF. Moreover, additional experimental

conditions could be explored such as comparing LSEC in static culture with LSEC cultured under varying shear stress conditions.

Sildenafil citrate constitutes a promising candidate for the improvement of NO signalling thereby enabling the re-fenestration of the LSEC membrane as well as potentially improving additional complications of liver cirrhosis. Portal hypertension is a life-threatening consequence of liver cirrhosis whereby its occurrence contributes to the transition of cirrhosis from a pre-clinical to a clinical phase (484). The hallmark of portal hypertension is increased intrahepatic vascular resistance (IHVR) which develops as a consequence of tissue remodelling in liver cirrhosis which accounts for approximately 70% of the increase in IHVR (485). Functional dysregulation of LSEC leads the initiation of the tissue remodelling process by compromising NO signalling. As NO is crucial for maintaining fenestrations as well as HSC quiescence, its deficiency leads to HSC activation which are responsible for excess ECM production (129) and gradual decrease in fenestrations. The contraction of activated HSC, modulated by vasoconstrictor peptides such as endothelin-1, also contributes approximately 30% of the increase in IHVR (486). To this extent, pharmaceutical agents such as sildenafil citrate, which is a potent vasodilator, could potentially counteract the vasoconstrictive effects if peptides such as endothelin-1 and angiotensin II which are upregulated in liver cirrhosis. Although different research groups have presented conflicting results, in a study where sildenafil (50 mg, oral) was tested in cirrhotic patients, NO production was significantly increased along with a significant decrease in hepatic sinusoidal resistance (487).

7.2 Future work

Future work concerning the implementation of imaging protocols for the imaging of fenestrations could encompass correlative imaging techniques (488) which are already being explored. There are also approaches such as MINFLUX or MINSTED which could be tested for their suitability to image fenestrae (489). Dual colour *d*STORM of actin and myosin could prove very informative with regards to the cytoskeletal protein content within fenestration boundaries. Additionally, 3D *d*STORM to reconstruct fenestrae across the LSEC membrane in the Z dimension would provide further detail in terms of the spatial arrangement of fenestrae across the LSEC plasma membrane. The ultimate goal is to be able to quantify fenestrations as differences detected between healthy and diseased cells could guide the targeting of specific mechanisms for therapeutic intervention. This could be fortified even more, by imaging greater numbers of cells as well as by comparing fenestration number and structural organisation between specific disease types. Furthermore, pharmaceutical agents such as sildenafil could be tested in live human liver tissue from healthy and disease specific specimens in perfusion systems (490). The tissue can be biopsied at different time points of perfusion to check for morphological changes and changes in expression of relevant markers at the protein and mRNA level. Microfluidic approaches (liver-on-a-chip) can also be implemented, in order to create a more physiological environment as well as recreate pathological changes to capture the effect on the LSEC phenotype *in vitro* (491).

8 Bibliography

1. Rumgay H, Arnold M, Ferlay J, Lesi O, Cabasag CJ, Vignat J, et al. Global burden of primary liver cancer in 2020 and predictions to 2040. J Hepatol [Internet]. 2022 Dec 1 [cited 2022 Dec 5];77(6):1598–606. Available from: http://www.journal-of-hepatology.eu/article/S0168827822030227/fulltext

2. Global health estimates: Leading causes of death [Internet]. [cited 2023 Apr 1]. Available from: https://www.who.int/data/gho/data/themes/mortality-and-global-health-estimates/ghe-leading-causes-of-death

3. Asrani SK, Mellinger J, Arab JP, Shah VH. Reducing the Global Burden of Alcohol-Associated Liver Disease: A Blueprint for Action. Hepatology [Internet]. 2021 May 1 [cited 2023 Apr 18];73(5):2039. Available from: /pmc/articles/PMC9361217/

4. Younossi Z, Anstee QM, Marietti M, Hardy T, Henry L, Eslam M, et al. Global burden of NAFLD and NASH: Trends, predictions, risk factors and prevention [Internet]. Vol. 15, Nature Reviews Gastroenterology and Hepatology. Nature Publishing Group; 2018 [cited 2021 Feb 18]. p. 11–20. Available from: https://pubmed.ncbi.nlm.nih.gov/28930295/

5. Jadlowiec CC, Taner T. Liver transplantation: Current status and challenges. World J Gastroenterol [Internet]. 2016 May 5 [cited 2023 Mar 23];22(18):4438. Available from: /pmc/articles/PMC4858627/

6. Rajaram RB, Jayaraman T, Yoong BK, Koh PS, Loh PS, Koong JK, et al. Non-alcoholic fatty liver disease and obesity among adult donors are major challenges to living donor liver transplantation: a single-centre experience. Asian J Surg. 2021;

7. Ceresa CDL, Nasralla D, Pollok JM, Friend PJ. Machine perfusion of the liver: applications in transplantation and beyond. Nat Rev Gastroenterol Hepatol. 2022;

8. Khan AA, Vishwakarma SK, Bardia A, Habeeb MA, Dhayal M. Repopulation of Cirrhotic Liver by Hepatic Stem/Progenitor Cells: A Promising Strategy Alternative to Liver Transplantation. A Promising Strategy Alternative to Liver Transplantation. Liver Pathophysiology: Therapies and Antioxidants. 2017 Mar 23;817–36.

9. Mazza G, Rombouts K, Rennie Hall A, Urbani L, Vinh Luong T, Al-Akkad W, et al. Decellularized human liver as a natural 3D-scaffold for liver bioengineering and transplantation. Sci Rep [Internet]. 2015 Aug 7 [cited 2019 Jun 11];5:13079. Available from: http://www.ncbi.nlm.nih.gov/pubmed/26248878

10. Abdel-Misih SRZ, Bloomston M, Bismuth H. Liver Anatomy. 2010;

11. Vernon H, Wehrle CJ, Alia VSK, Kasi A. Anatomy, Abdomen and Pelvis: Liver. StatPearls [Internet]. 2022 Nov 26 [cited 2023 Mar 24]; Available from: https://www.ncbi.nlm.nih.gov/books/NBK500014/

12. Hayashi S, Murakami G, Ohtsuka A, Itoh M, Nakano T, Fukuzawa Y. Connective tissue configuration in the human liver hilar region with special reference to the liver capsule and vascular sheath. J Hepatobiliary Pancreat Surg [Internet]. 2008 Nov 7 [cited 2023 Apr

28];15(6):640–7. Available from: https://link.springer.com/article/10.1007/s00534-008-1336-8

13. Hayashi S, Murakami G, Ohtsuka A, Itoh M, Nakano T, Fukuzawa Y. Connective tissue configuration in the human liver hilar region with special reference to the liver capsule and vascular sheath. J Hepatobiliary Pancreat Surg [Internet]. 2008 [cited 2023 Mar 19];15(6):640–7. Available from: https://pubmed.ncbi.nlm.nih.gov/18987936/

14. Abdel-Misih SRZ, Bloomston M. Liver Anatomy. Surg Clin North Am [Internet]. 2010 [cited 2023 Apr 2];90(4):643. Available from: /pmc/articles/PMC4038911/

15. XXIX. The anatomy and physiology of the liver. Philos Trans R Soc Lond. 1833 Dec 31;123:711–70.

16. Mitra V, Metcalf J. Functional anatomy and blood supply of the liver. Anaesthesia and Intensive Care Medicine. 2009;10(7):332–3.

17. Kiernan F. XXIX. The anatomy and physiology of the liver. Philos Trans R Soc Lond. 1833 Dec 31;123:711–70.

18. Rappaport AM, Wilson WD. The stuctural and functional unit in the human liver (liver acinus). Anat Rec. 1958;130(4):673–89.

19. Rappaport AM, Borowy ZJ, Lougheed WM, Lotto WN. Subdivision of hexagonal liver lobules into a structural and functional unit. Role in hepatic physiology and pathology. Anat Rec. 1954;119(1):11–33.

20. Rappaport AM. The microcirculatory hepatic unit. Microvasc Res. 1973 Sep 1;6(2):212–28.

21. Arias IM, Alter HJ, Boyer JL, Cohen DE, Fausto N, Shafritz DA, et al. The liver: Biology and pathobiology, fifth edition. The Liver: Biology and Pathobiology [Internet]. 2009 Jan 1 [cited 2023 Apr 28];1–1191. Available from: https://einstein.pure.elsevier.com/en/publications/the-liver-biology-and-pathobiology-fifth-edition-2

22. Große-Segerath L, Lammert E. Role of vasodilation in liver regeneration and health. Biol Chem [Internet]. 2021 Aug 1 [cited 2023 Apr 7];402(9):1009–19. Available from: https://www.degruyter.com/document/doi/10.1515/hsz-2021-0155/html?lang=en

23. Ben-Moshe S, Shapira Y, Moor AE, Manco R, Veg T, Bahar Halpern K, et al. Spatial sorting enables comprehensive characterization of liver zonation. Nature Metabolism 2019 1:9 [Internet]. 2019 Sep 16 [cited 2023 Apr 6];1(9):899–911. Available from: https://www.nature.com/articles/s42255-019-0109-9

24. Halpern KB, Shenhav R, Matcovitch-Natan O, Tóth B, Lemze D, Golan M, et al. Single-cell spatial reconstruction reveals global division of labour in the mammalian liver. Nature 2017 542:7641 [Internet]. 2017 Feb 6 [cited 2022 Jan 25];542(7641):352–6. Available from: https://www.nature.com/articles/nature21065

25. Halpern KB, Shenhav R, Massalha H, Toth B, Egozi A, Massasa EE, et al. Paired-cell sequencing enables spatial gene expression mapping of liver endothelial cells. Nature Biotechnology 2018 36:10 [Internet]. 2018 Sep 17 [cited 2022 Jul 31];36(10):962–70. Available from: https://www.nature.com/articles/nbt.4231

26. Shutter JR, Scully S, Fan W, Richards WG, Kitajewski J, Deblandre GA, et al. Dll4, a novel Notch ligand expressed in arterial endothelium. Genes Dev [Internet]. 2000 Jun 6 [cited 2023 Apr 7];14(11):1313. Available from: /pmc/articles/PMC316657/

27. Gualdi R, Bossard P, Zheng M, Hamada Y, Coleman JR, Zaret KS. Hepatic specification of the gut endoderm in vitro: cell signaling and transcriptional control. Genes Dev [Internet]. 1996 [cited 2023 Apr 3];10(13):1670–82. Available from: https://pubmed.ncbi.nlm.nih.gov/8682297/

28. Jung J, Zheng M, Goldfarb M, Zaret KS. Initiation of mammalian liver development from endoderm by fibroblast growth factors. Science [Internet]. 1999 Jun 18 [cited 2023 Apr 3];284(5422):1998–2003. Available from: https://pubmed.ncbi.nlm.nih.gov/10373120/

29. Bort R, Signore M, Tremblay K, Barbera JPM, Zaret KS. Hex homeobox gene controls the transition of the endoderm to a pseudostratified, cell emergent epithelium for liver bud development. Dev Biol [Internet]. 2006 Feb 1 [cited 2023 Apr 3];290(1):44–56. Available from: https://pubmed.ncbi.nlm.nih.gov/16364283/

30. Zaret KS. Genetic programming of liver and pancreas progenitors: lessons for stem-cell differentiation. Nat Rev Genet [Internet]. 2008 May [cited 2023 Apr 3];9(5):329–40. Available from: https://pubmed.ncbi.nlm.nih.gov/18398419/

31. Rossi JM, Dunn NR, Hogan BLM, Zaret KS. Distinct mesodermal signals, including BMPs from the septum transversum mesenchyme, are required in combination for hepatogenesis from the endoderm. Genes Dev [Internet]. 2001 Aug 1 [cited 2023 Apr 3];15(15):1998–2009. Available from: https://pubmed.ncbi.nlm.nih.gov/11485993/

32. Géraud C, Koch P sebastian, Zierow J, Klapproth K, Busch K, Olsavszky V, et al. GATA4-dependent organ-specific endothelial differentiation controls liver development and embryonic hematopoiesis. J Clin Invest [Internet]. 2017;1(13):1–16. Available from: http://www.ncbi.nlm.nih.gov/pubmed/28218627

33. Gouysse G, Couvelard A, Frachon S, Bouvier R, Nejjari M, Dauge MC, et al. Relationship between vascular development and vascular differentiation during liver organogenesis in humans. J Hepatol [Internet]. 2002 Dec 1 [cited 2023 Apr 3];37(6):730–40. Available from: http://www.journal-of-hepatology.eu/article/S0168827802002829/fulltext

34. Röder P V., Wu B, Liu Y, Han W. Pancreatic regulation of glucose homeostasis. Exp Mol Med [Internet]. 2016 Mar 11 [cited 2023 Apr 4];48(3):e219. Available from: /pmc/articles/PMC4892884/

35. Titchenell PM, Quinn WJ, Lu M, Chu Q, Lu W, Li C, et al. Direct Hepatocyte Insulin Signaling Is Required for Lipogenesis but Is Dispensable for the Suppression of Glucose Production. Cell Metab [Internet]. 2016 Jun 14 [cited 2023 Apr 4];23(6):1154–66. Available from: https://pubmed.ncbi.nlm.nih.gov/27238637/

36. Karim S, Adams DH, Lalor PF. Hepatic expression and cellular distribution of the glucose transporter family. World Journal of Gastroenterology : WJG [Internet]. 2012 Dec 12 [cited 2023 Apr 4];18(46):6771. Available from: /pmc/articles/PMC3520166/

37. Agius L. Glucokinase and molecular aspects of liver glycogen metabolism. Biochem J [Internet]. 2008 Aug 15 [cited 2023 Apr 4];414(1):1–18. Available from: https://pubmed.ncbi.nlm.nih.gov/18651836/

38. Raddatz D, Ramadori G. Carbohydrate metabolism and the liver: actual aspects from physiology and disease. Z Gastroenterol [Internet]. 2007 Jan [cited 2023 Apr 4];45(1):51–62. Available from: https://pubmed.ncbi.nlm.nih.gov/17236121/

39. Wu G. Principles of Animal Nutrition. Principles of Animal Nutrition. 2017 Jan 1;1–772.

40. Jungas RL, Halperin ML, Brosnan JT. Quantitative analysis of amino acid oxidation and related gluconeogenesis in humans. https://doi.org/101152/physrev1992722419 [Internet]. 1992 [cited 2023 Apr 5];72(2):419–48. Available from: https://journals.physiology.org/doi/10.1152/physrev.1992.72.2.419

41. Hou Y, Yin Y, Wu G. Dietary essentiality of "nutritionally non-essential amino acids" for animals and humans. Exp Biol Med [Internet]. 2015 Aug 19 [cited 2023 Apr 5];240(8):997. Available from: /pmc/articles/PMC4935284/

42. Maxwell JL, Terracio L, Borg TK, Baynes JW, Thorpe SR. A fluorescent residualizing label for studies on protein uptake and catabolism in vivo and in vitro. Biochemical Journal [Internet]. 1990 Apr 4 [cited 2023 Apr 5];267(1):155. Available from: /pmc/articles/PMC1131258/?report=abstract

43. Gyamfi D, Danquah KO. Nutrients and Liver Metabolism. Molecular Aspects of Alcohol and Nutrition: A Volume in the Molecular Nutrition Series. 2016 Jan 1;3–15.

44. Felig P. Amino Acid Metabolism in Man. https://doi.org/101146/annurev.bi44070175004441 [Internet]. 2003 Nov 28 [cited 2023 Apr 5];44:933–55. Available from: https://www.annualreviews.org/doi/abs/10.1146/annurev.bi.44.070175.004441

45. Khatra BS, Chawla RK, Sewell CW, Rudman D. Distribution of branched-chain alpha-keto acid dehydrogenases in primate tissues. J Clin Invest [Internet]. 1977 [cited 2023 Apr 5];59(3):558–64. Available from: https://pubmed.ncbi.nlm.nih.gov/402386/

46. Shimomura Y, Obayashi M, Murakami T, Harris RA. Regulation of branched-chain amino acid catabolism: nutritional and hormonal regulation of activity and expression of the branched-chain alpha-keto acid dehydrogenase kinase. Curr Opin Clin Nutr Metab Care [Internet]. 2001 [cited 2023 Apr 5];4(5):419–23. Available from: https://pubmed.ncbi.nlm.nih.gov/11568504/

47. Frayn KN, Arner P, Yki-Järvinen H. Fatty acid metabolism in adipose tissue, muscle and liver in health and disease. Essays Biochem [Internet]. 2006 [cited 2023 Apr 6];42:89–103. Available from: https://pubmed.ncbi.nlm.nih.gov/17144882/

48. Nutrition, Diet Therapy, and the Liver - Google Books [Internet]. [cited 2023 Apr 6]. Available from: https://books.google.co.uk/books?hl=en&lr=&id=ahWoeI4-Y34C&oi=fnd&pg=PA3&dq=liver+metabolism:+biochemical+regulations&ots=G5jMy6YF9A&sig=igk2qnW1tLvHR659TItXHIARm8o#v=onepage&q=liver%20metabolism%3A%20biochemical%20regulations&f=false

49. Sampath H, Ntambi JM. Polyunsaturated fatty acid regulation of genes of lipid metabolism. Annu Rev Nutr [Internet]. 2005 [cited 2023 Apr 6];25:317–40. Available from: https://pubmed.ncbi.nlm.nih.gov/16011470/

50. Canbay A, Bechmann L, Gerken G. Lipid metabolism in the liver. Z Gastroenterol [Internet]. 2007 Jan [cited 2023 Apr 6];45(1):35–41. Available from: https://pubmed.ncbi.nlm.nih.gov/17236119/

51. Bechmann LP, Hannivoort RA, Gerken G, Hotamisligil GS, Trauner M, Canbay A. The interaction of hepatic lipid and glucose metabolism in liver diseases. J Hepatol [Internet]. 2012 Apr [cited 2023 Apr 6];56(4):952–64. Available from: https://pubmed.ncbi.nlm.nih.gov/22173168/

52. Achour B, Barber J, Rostami-Hodjegan A. Expression of Hepatic Drug-Metabolizing Cytochrome P450 Enzymes and Their Intercorrelations: A Meta-Analysis. Drug Metabolism and Disposition [Internet]. 2014 Aug 1 [cited 2023 Apr 7];42(8):1349–56. Available from: https://dmd.aspetjournals.org/content/42/8/1349

53. Almazroo OA, Miah MK, Venkataramanan R. Drug Metabolism in the Liver. Clin Liver Dis [Internet]. 2017 Feb 1 [cited 2023 Apr 7];21(1):1–20. Available from: https://pubmed.ncbi.nlm.nih.gov/27842765/

54. Yang Y, Sangwung P, Kondo R, Jung Y, McConnell MJ, Jeong J, et al. Alcohol-induced Hsp90 acetylation is a novel driver of liver sinusoidal endothelial dysfunction and alcohol-related liver disease. J Hepatol [Internet]. 2021 Aug 1 [cited 2023 Apr 7];75(2):377. Available from: /pmc/articles/PMC8292196/

55. Simon-Santamaria J, Rinaldo CH, Kardas P, Li R, Malovic I, Elvevold K, et al. Efficient Uptake of Blood-Borne BK and JC Polyomavirus-Like Particles in Endothelial Cells of Liver Sinusoids and Renal Vasa Recta. PLoS One [Internet]. 2014 Nov 6 [cited 2022 Nov 4];9(11):e111762. Available from: https://journals.plos.org/plosone/article?id=10.1371/journal.pone.0111762

56. Ganesan LP, Mohanty S, Kim J, Clark KR, Robinson JM, Anderson CL. Rapid and Efficient Clearance of Blood-borne Virus by Liver Sinusoidal Endothelium. PLoS Pathog [Internet]. 2011 Sep [cited 2022 Jul 7];7(9):e1002281. Available from: https://journals.plos.org/plospathogens/article?id=10.1371/journal.ppat.1002281

57. Mates JM, Yao Z, Cheplowitz AM, Suer O, Phillips GS, Kwiek JJ, et al. Mouse liver sinusoidal endothelium eliminates HIV-like particles from blood at a rate of 100 million per minute by a second-order kinetic process. Front Immunol [Internet]. 2017 Jan 24 [cited 2023 Apr 9];8(JAN):35. Available from: /pmc/articles/PMC5256111/

58. Romero EL, Morilla MJ, Regts J, Koning GA, Scherphof GL. On the mechanism of hepatic transendothelial passage of large liposomes. FEBS Lett. 1999 Apr 2;448(1):193–6.

59. Fraser R, Cogger VC, Dobbs B, Jamieson H, Warren A, Hilmer SN, et al. The liver sieve and atherosclerosis. Pathology [Internet]. 2012 [cited 2023 Apr 8];44(3):181–6. Available from: https://pubmed.ncbi.nlm.nih.gov/22406487/

60. Yu KC, Cooper AD. Postprandial lipoproteins and atherosclerosis. Front Biosci [Internet]. 2001 [cited 2023 Apr 8];6. Available from: https://pubmed.ncbi.nlm.nih.gov/11229885/

61. Fraser R, Bosanquet AG, Day WA. Filtration of chylomicrons by the liver may influence cholesterol metabolism and atherosclerosis. Atherosclerosis [Internet]. 1978 Feb 1 [cited 2023 Apr 8];29(2):113–23. Available from: http://www.atherosclerosis-journal.com/article/0021915078900011/fulltext

62. Fraser R, Dobbs BR, Rogers GW. Lipoproteins and the liver sieve: the role of the fenestrated sinusoidal endothelium in lipoprotein metabolism, atherosclerosis, and cirrhosis. Hepatology. 1995 Mar;21(3):863–74.

63. Li R, Oteiza A, Sørensen KK, McCourt P, Olsen R, Smedsrød B, et al. Role of liver sinusoidal endothelial cells and stabilins in elimination of oxidized low-density lipoproteins. Am J Physiol Gastrointest Liver Physiol [Internet]. 2011 Jan [cited 2023 Apr 9];300(1):G71. Available from: /pmc/articles/PMC3025507/

64. Shetty S, Lalor PF, Adams DH. Liver sinusoidal endothelial cells — gatekeepers of hepatic immunity. Vol. 15, Nature Reviews Gastroenterology and Hepatology. Nature Publishing Group; 2018. p. 555–67.

65. Gao B, Jeong W Il, Tian Z. Liver: An organ with predominant innate immunity. Hepatology. 2008 Feb;47(2):729–36.

66. Bode JG, Albrecht U, Häussinger D, Heinrich PC, Schaper F. Hepatic acute phase proteins--regulation by IL-6- and IL-1-type cytokines involving STAT3 and its crosstalk with NF-κB-dependent signaling. Eur J Cell Biol. 2012 Jun;91(6–7):496–505.

67. Jenne CN, Kubes P. Immune surveillance by the liver. Nat Immunol. 2013;14(10):996–1006.

68. Ganesan LP, Kim J, Wu Y, Mohanty S, Phillips GS, Birmingham DJ, et al. FcγRIIb on liver sinusoidal endothelium clears small immune complexes. J Immunol [Internet]. 2012 Nov 15 [cited 2022 Jan 25];189(10):4981. Available from: /pmc/articles/PMC4381350/

69. Oda M, Yokomori H, Han JY. Regulatory mechanisms of hepatic microcirculatory hemodynamics: Hepatic arterial system. Clin Hemorheol Microcirc. 2006;34(1–2):11–26.

70. Ebe Y, Hasegawa G, Takatsuka H, Umezu H, Mitsuyama M, Arakawa M, et al. The role of Kupffer cells and regulation of neutrophil migration into the liver by macrophage inflammatory protein-2 in primary listeriosis in mice. Pathol Int. 1999;49(6):519–32.

71. Lee WY, Moriarty TJ, Wong CHY, Zhou H, Strieter RM, Van Rooijen N, et al. An intravascular immune response to Borrelia burgdorferi involves Kupffer cells and iNKT cells. Nat Immunol. 2010;11(4):295–302.

72. Wong CHY, Jenne CN, Lee WY, Léger C, Kubes P. Functional innervation of hepatic iNKT cells is immunosuppressive following stroke. Science (1979). 2011 Oct 7;334(6052):101–5.

73. Geissmann F, Cameron TO, Sidobre S, Manlongat N, Kronenberg M, Briskin MJ, et al. Intravascular immune surveillance by CXCR6+ NKT cells patrolling liver sinusoids. PLoS Biol. 2005;3(4):0650–61.

74. Babbs C, Haboubi NY, Mellor JM, Smith A, Rowan BP, Warnes TW. Endothelial cell transformation in primary biliary cirrhosis: A morphological and biochemical study.

Hepatology [Internet]. 1990 May 1 [cited 2023 Apr 12];11(5):723–9. Available from: https://onlinelibrary.wiley.com/doi/full/10.1002/hep.1840110503

75. Lalor PF, Hields PS, Grant AJ, Adams DH. Recruitment of lymphocytes to the human liver. Immunol Cell Biol [Internet]. 2002 Feb 1 [cited 2023 Mar 25];80(1):52–64. Available from: https://onlinelibrary.wiley.com/doi/full/10.1046/j.1440-1711.2002.01062.x

76. Wilkinson AL, Qurashi M, Shetty S. The Role of Sinusoidal Endothelial Cells in the Axis of Inflammation and Cancer Within the Liver [Internet]. Vol. 11, Frontiers in Physiology. Frontiers; 2020 [cited 2020 Sep 27]. p. 990. Available from: https://www.frontiersin.org/article/10.3389/fphys.2020.00990/full

77. Bataller R, Brenner DA. Liver fibrosis. Journal of Clinical Investigation [Internet]. 2005 Feb 2 [cited 2023 Apr 12];115(2):209. Available from: /pmc/articles/PMC546435/

78. Braet F, Wisse E. Structural and functional aspects of liver sinusoidal endothelial cell fenestrae: A review. Comp Hepatol. 2002;1:1–17.

79. Lepreux S, Desmoulière A. Human liver myofibroblasts during development and diseases with a focus on portal (myo)fibroblasts. Front Physiol. 2015 Jun 23;6(MAY):173.

80. Lemoinne S, Cadoret A, El Mourabit H, Thabut D, Housset C. Origins and functions of liver myofibroblasts. Biochimica et Biophysica Acta (BBA) - Molecular Basis of Disease. 2013 Jul 1;1832(7):948–54.

81. Xu B, Broome U, Uzunel M, Nava S, Ge X, Kumagai-Braesch M, et al. Capillarization of Hepatic Sinusoid by Liver Endothelial Cell-Reactive Autoantibodies in Patients with Cirrhosis and Chronic Hepatitis. Am J Pathol [Internet]. 2003 Oct 1 [cited 2023 Apr 12];163(4):1275. Available from: /pmc/articles/PMC1868294/

82. Wisse E, Braet F, Duimel H, Vreuls C, Koek G, Olde Damink SWM, et al. Fixation methods for electron microscopy of human and other liver. World Journal of Gastroenterology : WJG [Internet]. 2010 Jun 6 [cited 2022 Oct 3];16(23):2851. Available from: /pmc/articles/PMC2887580/

83. BARDADIN KA, DESMET VJ. Ultrastructural observations on sinusoidal endothelial cells in chronic active hepatitis. Histopathology [Internet]. 1985 Feb 1 [cited 2023 Apr 12];9(2):171–81. Available from: https://onlinelibrary.wiley.com/doi/full/10.1111/j.1365-2559.1985.tb02433.x

84. Mak KM, Lieber CS. Alterations in Endothelial Fenestrations in Liver Sinusoids of Baboons Fed Alcohol: A Scanning Electron Microscopic Study. Hepatology [Internet]. 1984 May 1 [cited 2023 Apr 10];4(3):386–91. Available from: https://onlinelibrary.wiley.com/doi/full/10.1002/hep.1840040306

85. Clark SA, Bramwell Cook H, Oxner RBG, Angus HB, George PM, Fraser R. DEFENESTRATION OF HEPATIC SINUSOIDS AS A CAUSE OF HYPERLIPOPROTEINAEMIA IN ALCOHOLICS. The Lancet [Internet]. 1988 Nov 26 [cited 2023 Apr 10];332(8622):1225–7. Available from: http://www.thelancet.com/article/S0140673688908136/fulltext

86. Fraser R, Bowler LM, Day WA. Damage of rat liver sinusoidal endothelium by ethanol. Pathology [Internet]. 1980 [cited 2023 Apr 12];12(3):371–6. Available from: https://pubmed.ncbi.nlm.nih.gov/7432815/

87. HORN T, JUNGE J, CHRIS-TOFFERSEN P. Early alcoholic liver injury: changes of the Disse space in acinar zone 3. Liver. 1985;5(6):301–10.

88. Horn T, Christoffersen P, Henriksen JH. Alcoholic liver injury: Defenestration in noncirrhotic livers—a scanning electron microscopic study. Hepatology [Internet]. 1987 [cited 2023 Apr 10];7(1):77–82. Available from: https://aasldpubs.onlinelibrary.wiley.com/doi/10.1002/hep.1840070117

89. Fernando H, Wiktorowicz JE, Soman K V., Kaphalia BS, Khan MF, Shakeel Ansari GA. Liver proteomics in progressive alcoholic steatosis. Toxicol Appl Pharmacol [Internet]. 2013 Feb 2 [cited 2023 Apr 5];266(3):470. Available from: /pmc/articles/PMC3565568/

90. Francque S, Laleman W, Verbeke L, Van Steenkiste C, Casteleyn C, Kwanten W, et al. Increased intrahepatic resistance in severe steatosis: endothelial dysfunction, vasoconstrictor overproduction and altered microvascular architecture. Lab Invest [Internet]. 2012 Oct [cited 2023 Apr 12];92(10):1428–39. Available from: https://pubmed.ncbi.nlm.nih.gov/22890552/

91. Rockey DC, Chung JJ. Reduced nitric oxide production by endothelial cells in cirrhotic rat liver: endothelial dysfunction in portal hypertension. Gastroenterology [Internet]. 1998 [cited 2023 Apr 12];114(2):344–51. Available from: https://pubmed.ncbi.nlm.nih.gov/9453496/

92. Xie G, Choi SS, Syn WK, Michelotti GA, Swiderska M, Karaca G, et al. Hedgehog signalling regulates liver sinusoidal endothelial cell capillarisation. Gut. 2013 Feb 1;62(2):299–309.

93. Rockey DC, Chung JJ. Regulation of inducible nitric oxide synthase in hepatic sinusoidal endothelial cells. https://doi.org/101152/ajpgi19962712G260 [Internet]. 1996 [cited 2023 Apr 12];271(2 34-2). Available from: https://journals.physiology.org/doi/10.1152/ajpgi.1996.271.2.G260

94. La Mura V, Pasarín M, Rodriguez-Vilarrupla A, García-Pagán JC, Bosch J, Abraldes JG. Liver sinusoidal endothelial dysfunction after LPS administration: A role for inducible-nitric oxide synthase. J Hepatol. 2014 Dec 1;61(6):1321–7.

95. Aschoff L. Das reticulo-endotheliale System. Ergebnisse die innere Medizinund Kinderheilkunde. 1924;(26):1–118.

96. Wisse E. An ultrastructural characterization of the endothelial cell in the rat liver sinusoid under normal and various experimental conditions, as a contribution to the distinction between endothelial and Kupffer cells. Journal of Ultrasructure Research. 1972;38(5–6):528–62.

97. Lalor PF, Lai WK, Curbishley SM, Shetty S, Adams DH. Human hepatic sinusoidal endothelial cells can be distinguished by expression of phenotypic markers related to their specialised functions in vivo. World J Gastroenterol. 2006;12(34):5429–39.

98. Aird WC. Phenotypic heterogeneity of the endothelium: I. Structure, function, and mechanisms. Circ Res [Internet]. 2007 Feb [cited 2023 Apr 2];100(2):158–73. Available from: http://circres.ahajournals.org

99. Blood Vessels and Endothelial Cells - Molecular Biology of the Cell - NCBI Bookshelf [Internet]. [cited 2023 Apr 3]. Available from: https://www.ncbi.nlm.nih.gov/books/NBK26848/

100. Strauss O, Phillips A, Ruggiero K, Bartlett A, Dunbar PR. Immunofluorescence identifies distinct subsets of endothelial cells in the human liver. Sci Rep [Internet]. 2017;7(May 2016):1–13. Available from: http://dx.doi.org/10.1038/srep44356

101. Tanaka M, Iwakiri Y. Lymphatics in the liver. Curr Opin Immunol [Internet]. 2018 Aug 1 [cited 2023 Apr 3];53:137. Available from: /pmc/articles/PMC6986420/

102. Fu J, Gerhardt H, McDaniel JM, Xia B, Liu X, Ivanciu L, et al. Endothelial cell O-glycan deficiency causes blood/lymphatic misconnections and consequent fatty liver disease in mice. J Clin Invest [Internet]. 2008 Nov 11 [cited 2023 Apr 3];118(11):3725. Available from: /pmc/articles/PMC2567837/

103. Motta PM, Fujita T, Nishi M. Scanning Electron Microscopy of the Mammalian Liver. Basic and Clinical Hepatology. 1982;31–50.

104. McEnerney L, Duncan K, Bang BR, Elmasry S, Li M, Miki T, et al. Dual modulation of human hepatic zonation via canonical and non-canonical Wnt pathways. Exp Mol Med [Internet]. 2017 [cited 2023 Mar 30];49(12). Available from: https://pubmed.ncbi.nlm.nih.gov/29244788/

105. Ben-Moshe S, Itzkovitz S. Spatial heterogeneity in the mammalian liver. Nature Reviews Gastroenterology & Hepatology 2019 16:7 [Internet]. 2019 Apr 1 [cited 2023 Apr 1];16(7):395–410. Available from: https://www.nature.com/articles/s41575-019-0134-x

106. MacParland SA, Liu JC, Ma XZ, Innes BT, Bartczak AM, Gage BK, et al. Single cell RNA sequencing of human liver reveals distinct intrahepatic macrophage populations. Nat Commun [Internet]. 2018;9(1):4383. Available from: http://www.nature.com/articles/s41467-018-06318-7

107. Dziarski R, Gupta D. Review: Mammalian peptidoglycan recognition proteins (PGRPs) in innate immunity. Innate Immun [Internet]. 2010 Jun [cited 2023 Apr 1];16(3):168–74. Available from: https://pubmed.ncbi.nlm.nih.gov/20418257/

108. Wolkoff AW, Cohen DE. Bile acid regulation of hepatic physiology I. Hepatocyte transport of bile acids. Am J Physiol Gastrointest Liver Physiol. 2003 Feb 1;284(2 47-2).

109. Crawford JM. Role of vesicle-mediated transport pathways in hepatocellular bile secretion. Semin Liver Dis. 1996;16(2):169–89.

110. Maroni L, Haibo B, Ray D, Zhou T, Wan Y, Meng F, et al. Functional and Structural Features of Cholangiocytes in Health and Disease. Cell Mol Gastroenterol Hepatol. 2015 Jul 1;1(4):368.

111. Kanno N, LeSage G, Glaser S, Alvaro D, Alpini G. Functional heterogeneity of the intrahepatic biliary epithelium. Hepatology [Internet]. 2000 [cited 2023 Mar 26];31(3):555–61. Available from: https://pubmed.ncbi.nlm.nih.gov/10706542/

112. Alpini G, McGill JM, LaRusso NF. The pathobiology of biliary epithelia. Hepatology. 2002;35(5):1256–68.

113. Fitz JG. Regulation of cholangiocyte secretion. Semin Liver Dis. 2002 Aug;22(3):241–9.

114. Guerra MT, Nathanson MH. Calcium signaling and secretion in cholangiocytes. Pancreatology. 2015 Jul 1;15(4 0):S44.

115. Alpini G, Lenzi R, Zhai WR, Slott PA, Liu MH, Sarkozi L, et al. Bile secretory function of intrahepatic biliary epithelium in the rat. https://doi.org/101152/ajpgi19892571G124. 1989;257(1).

116. Ros JE, Libbrecht L, Geuken M, Jansen PLM, Roskams TAD. High expression of MDR1, MRP1, and MRP3 in the hepatic progenitor cell compartment and hepatocytes in severe human liver disease. J Pathol. 2003 Aug 1;200(5):553–60.

117. Hofmann AF. The enterohepatic circulation of bile acids in mammals: form and functions. Front Biosci (Landmark Ed) [Internet]. 2009 Jan 1 [cited 2023 Mar 26];14(7):2584–98. Available from: https://pubmed.ncbi.nlm.nih.gov/19273221/

118. Tabibian JH, Masyuk AI, Masyuk T V., O'Hara SP, LaRusso NF. Physiology of Cholangiocytes. Compr Physiol [Internet]. 2013 [cited 2023 Mar 26];3(1):541–65. Available from: https://onlinelibrary.wiley.com/doi/full/10.1002/cphy.c120019

119. Dawson PA. Bile Formation and the Enterohepatic Circulation. Physiology of the Gastrointestinal Tract, Sixth Edition. 2018 Jan 1;2:931–56.

120. Alpini G, Glaser SS, Rodgers R, Phinizy JL, Robertson WE, Lasater J, et al. Functional expression of the apical Na+-dependent bile acid transporter in large but not small rat cholangiocytes. Gastroenterology [Internet]. 1997 [cited 2023 Mar 26];113(5):1734–40. Available from: https://pubmed.ncbi.nlm.nih.gov/9352879/

121. WILSON JW, LEDUC EH. Role of cholangioles in restoration of the liver of the mouse after dietary injury. J Pathol Bacteriol [Internet]. 1958 [cited 2023 Mar 26];76(2):441–9. Available from: https://pubmed.ncbi.nlm.nih.gov/13588479/

122. Shizonuka H, Lombardi B, Sell S, Iammarino RM. Early histological and functional alterations of ethionine liver carcinogenesis in rats fed a choline-deficient diet. Cancer Res. 1978 Apr;38(4):1092–8.

123. Duncan AW, Dorrell C, Grompe M. Stem Cells and Liver Regeneration. Gastroenterology [Internet]. 2009 [cited 2023 Mar 26];137(2):466. Available from: /pmc/articles/PMC3136245/

124. Alison MR. Regulation of hepatic growth. https://doi.org/101152/physrev1986663499 [Internet]. 1986 [cited 2023 Mar 26];66(3):499–541. Available from: https://journals.physiology.org/doi/10.1152/physrev.1986.66.3.499

125. Alison MR, Golding M, Sarraf CE, Edwards RJ, Lalani EN. Liver damage in the rat induces hepatocyte stem cells from biliary epithelial cells. Gastroenterology. 1996;110(4):1182–90.

126. KAWADA N, TRAN-THI T -A, KLEIN H, DECKER K. The contraction of hepatic stellate (Ito) cells stimulated with vasoactive substances. Eur J Biochem [Internet]. 1993 Apr 1 [cited 2023 Apr

3];213(2):815–23. Available from: https://onlinelibrary.wiley.com/doi/full/10.1111/j.1432-1033.1993.tb17824.x

127. Rockey DC, Chung JJ. Reduced nitric oxide production by endothelial cells in cirrhotic rat liver: Endothelial dysfunction in portal hypertension. Gastroenterology [Internet]. 1998 Feb 1 [cited 2023 Apr 3];114(2):344–51. Available from: http://www.gastrojournal.org/article/S0016508598704871/fulltext

128. Geerts A. History, heterogeneity, developmental biology, and functions of quiescent hepatic stellate cells. Semin Liver Dis. 2001;21(3):311–35.

129. Lepreux S, Bioulac-Sage P, Gabbiani G, Sapin V, Housset C, Rosenbaum J, et al. Cellular retinol-binding protein-1 expression in normal and fibrotic/cirrhotic human liver: Different patterns of expression in hepatic stellate cells and (myo)fibroblast subpopulations. J Hepatol [Internet]. 2004 May 1 [cited 2023 Jan 15];40(5):774–80. Available from: http://www.journal-of-hepatology.eu/article/S0168827804000200/fulltext

130. Chen Y, Choi SS, Michelotti GA, Chan IS, Swiderska-Syn M, Karaca GF, et al. Hedgehog controls hepatic stellate cell fate by regulating metabolism. Gastroenterology [Internet]. 2012 Nov 1 [cited 2023 Mar 29];143(5):1319-1329.e11. Available from: http://www.gastrojournal.org/article/S0016508512011584/fulltext

131. Dobie R, Wilson-Kanamori JR, Henderson BEP, Smith JR, Matchett KP, Portman JR, et al. Single-Cell Transcriptomics Uncovers Zonation of Function in the Mesenchyme during Liver Fibrosis. Cell Rep [Internet]. 2019 Nov 12 [cited 2023 Mar 30];29(7):1832-1847.e8. Available from: https://pubmed.ncbi.nlm.nih.gov/31722201/

132. Bhandari S, Li R, Simón-Santamaría J, McCourt P, Johansen SD, Smedsrød B, et al. Transcriptome and proteome profiling reveal complementary scavenger and immune features of rat liver sinusoidal endothelial cells and liver macrophages. BMC Mol Cell Biol [Internet]. 2020 Dec 27 [cited 2020 Dec 4];21(1):85. Available from: https://bmcmolcellbiol.biomedcentral.com/articles/10.1186/s12860-020-00331-9

133. Gale RP, Sparkes RS, Golde DW. Bone Marrow Origin of Hepatic Macrophages (Kupffer Cells) in Humans. Science (1979). 1978;201(4359):937–8.

134. Bouwens L, Baekeland M, Wisse E. Cytokinetic analysis of the expanding Kupffer-cell population in rat liver. Cell Tissue Kinet. 1986;19(2):217–26.

135. Johnson SJ, Hines JE, Burt AD. Macrophage and perisinusoidal cell kinetics in acute liver injury. J Pathol. 1992 Apr 1;166(4):351–8.

136. Gomez Perdiguero E, Klapproth K, Schulz C, Busch K, Azzoni E, Crozet L, et al. Tissue-resident macrophages originate from yolk-sac-derived erythro-myeloid progenitors. 2015;

137. van de Laar L, Saelens W, De Prijck S, Martens L, Scott CL, Van Isterdael G, et al. Yolk Sac Macrophages, Fetal Liver, and Adult Monocytes Can Colonize an Empty Niche and Develop into Functional Tissue-Resident Macrophages. Immunity. 2016 Apr 19;44(4):755–68.

138. Jung K, Kang M, Park C, Hyun Choi Y, Jeon Y, Park SH, et al. Protective role of V-set and immunoglobulin domain-containing 4 expressed on kupffer cells during immune-mediated

liver injury by inducing tolerance of liver T- and natural killer T-cells. Hepatology [Internet]. 2012 Nov [cited 2023 Apr 1];56(5):1838–48. Available from: https://pubmed.ncbi.nlm.nih.gov/22711680/

139. Kenna T, Golden-Mason L, Norris S, Hegarty JE, O'Farrelly C, Doherty DG. Distinct subpopulations of γδ T cells are present in normal and tumor-bearing human liver. Clinical Immunology [Internet]. 2004 Oct [cited 2023 Apr 2];113(1):56–63. Available from: https://pubmed.ncbi.nlm.nih.gov/15380530/

140. Jeffery HC, Van Wilgenburg B, Kurioka A, Parekh K, Stirling K, Roberts S, et al. Biliary epithelium and liver B cells exposed to bacteria activate intrahepatic MAIT cells through MR1. J Hepatol [Internet]. 2016 May 1 [cited 2023 Apr 2];64(5):1118–27. Available from: https://pubmed.ncbi.nlm.nih.gov/26743076/

141. Forkel M, Berglin L, Kekäläinen E, Carlsson A, Svedin E, Michaëlsson J, et al. Composition and functionality of the intrahepatic innate lymphoid cell-compartment in human nonfibrotic and fibrotic livers. Eur J Immunol [Internet]. 2017 Aug 1 [cited 2023 Apr 2];47(8):1280–94. Available from: https://pubmed.ncbi.nlm.nih.gov/28613415/

142. The human liver contains multiple populations of NK cells, T cells, and CD3+CD56+ natural T cells with distinct cytotoxic activities and Th1, Th2, and Th0 cytokine secretion patterns - PubMed [Internet]. [cited 2023 Apr 2]. Available from: https://pubmed.ncbi.nlm.nih.gov/10438977/

143. Dusseaux M, Martin E, Serriari N, Péguillet I, Premel V, Louis D, et al. Human MAIT cells are xenobiotic-resistant, tissue-targeted, CD161hi IL-17–secreting T cells. Blood [Internet]. 2011 Jan 27 [cited 2023 Apr 2];117(4):1250–9. Available from: https://ashpublications.org/blood/article/117/4/1250/28598/Human-MAIT-cells-are-xenobiotic-resistant-tissue

144. Verykokakis M, Kee BL. Transcriptional and epigenetic regulation of innate-like T lymphocyte development. Curr Opin Immunol [Internet]. 2018 Apr 1 [cited 2023 Apr 2];51:39–45. Available from: https://pubmed.ncbi.nlm.nih.gov/29452898/

145. Lee YJ, Starrett GJ, Lee ST, Yang R, Henzler CM, Jameson SC, et al. Lineage-Specific Effector Signatures of Invariant NKT Cells Are Shared amongst γδ T, Innate Lymphoid, and Th Cells. The Journal of Immunology [Internet]. 2016 Aug 15 [cited 2023 Apr 2];197(4):1460–70. Available from: https://journals.aai.org/jimmunol/article/197/4/1460/106004/Lineage-Specific-Effector-Signatures-of-Invariant

146. Engel I, Seumois G, Chavez L, Samaniego-Castruita D, White B, Chawla A, et al. Innate-like functions of natural killer T cell subsets result from highly divergent gene programs. Nature Immunology 2016 17:6 [Internet]. 2016 Apr 18 [cited 2023 Apr 2];17(6):728–39. Available from: https://www.nature.com/articles/ni.3437

147. Crosby CM, Kronenberg M. Tissue-specific functions of invariant natural killer T cells. Nature Reviews Immunology 2018 18:9 [Internet]. 2018 Jul 2 [cited 2023 Apr 2];18(9):559–74. Available from: https://www.nature.com/articles/s41577-018-0034-2

148. Ginhoux F, Guilliams M. Tissue-Resident Macrophage Ontogeny and Homeostasis. Immunity [Internet]. 2016 Mar 15 [cited 2023 Apr 2];44(3):439–49. Available from: https://pubmed.ncbi.nlm.nih.gov/26982352/

149. Knoll P, Schlaak J, Uhrig A, Kempf P, zum Büschenfelde KHM, Gerken G. Human Kupffer cells secrete IL-10 in response to lipopolysaccharide (LPS) challenge. J Hepatol [Internet]. 1995 Feb 1 [cited 2023 Apr 2];22(2):226–9. Available from: http://www.journal-of-hepatology.eu/article/0168827895804331/fulltext

150. Jung K, Kang M, Park C, Hyun Choi Y, Jeon Y, Park SH, et al. Protective role of V-set and immunoglobulin domain-containing 4 expressed on kupffer cells during immune-mediated liver injury by inducing tolerance of liver T- and natural killer T-cells. Hepatology [Internet]. 2012 Nov 1 [cited 2023 Apr 2];56(5):1838–48. Available from: https://onlinelibrary.wiley.com/doi/full/10.1002/hep.25906

151. Heymann F, Peusquens J, Ludwig-Portugall I, Kohlhepp M, Ergen C, Niemietz P, et al. Liver inflammation abrogates immunological tolerance induced by Kupffer cells. Hepatology [Internet]. 2015 Jul 1 [cited 2023 Apr 2];62(1):279–91. Available from: https://pubmed.ncbi.nlm.nih.gov/25810240/

152. Erhardt A, Biburger M, Papadopoulos T, Tiegs G. IL-10, regulatory T cells, and Kupffer cells mediate tolerance in concanavalin A-induced liver injury in mice. Hepatology [Internet]. 2007 Feb [cited 2023 Apr 2];45(2):475–85. Available from: https://pubmed.ncbi.nlm.nih.gov/17256743/

153. Crispe IN. Hepatic T cells and liver tolerance. Nature Reviews Immunology 2003 3:1 [Internet]. 2003 Jan [cited 2023 Apr 2];3(1):51–62. Available from: https://www.nature.com/articles/nri981

154. Steinert EM, Schenkel JM, Fraser KA, Beura LK, Manlove LS, Igyártó BZ, et al. Quantifying memory CD8 T cells reveals regionalization of immunosurveillance. Cell [Internet]. 2015 May 7 [cited 2023 Apr 2];161(4):737–49. Available from: http://www.cell.com/article/S0092867415003190/fulltext

155. Drescher HK, Bartsch LM, Weiskirchen S, Weiskirchen R. Intrahepatic TH17/TReg Cells in Homeostasis and Disease—It's All About the Balance. Front Pharmacol. 2020 Oct 2;11:1598.

156. Miyara M, Sakaguchi S. Natural regulatory T cells: mechanisms of suppression. Trends Mol Med [Internet]. 2007 Mar 1 [cited 2023 Apr 2];13(3):108–16. Available from: http://www.cell.com/article/S1471491407000044/fulltext

157. Saraiva M, O'Garra A. The regulation of IL-10 production by immune cells. Nature Reviews Immunology 2010 10:3 [Internet]. 2010 Feb 15 [cited 2023 Apr 2];10(3):170–81. Available from: https://www.nature.com/articles/nri2711

158. Breous E, Somanathan S, Vandenberghe LH, Wilson JM. Hepatic regulatory T cells and Kupffer cells are crucial mediators of systemic T cell tolerance to antigens targeting murine liver. Hepatology [Internet]. 2009 Aug 1 [cited 2023 Apr 2];50(2):612–21. Available from: https://onlinelibrary.wiley.com/doi/full/10.1002/hep.23043

159. McCuskey RS, Ekataksin W, LeBouton A V., Nishida J, McCuskey MK, McDonnell D, et al. Hepatic Microvascular Development in Relation to the Morphogenesis of Hepatocellular Plates in Neonatal Rats. Anatomical Record - Part A Discoveries in Molecular, Cellular, and Evolutionary Biology. 2003;275(1):1019–30.

160. Fraser R, Dobbs BR, Rogers GWT. Lipoproteins and the liver sieve: The role of the fenestrated sinusoidal endothelium in lipoprotein metabolism, atherosclerosis, and cirrhosis. Hepatology [Internet]. 1995 Mar 1 [cited 2022 Jul 4];21(3):863–74. Available from: https://onlinelibrary.wiley.com/doi/full/10.1002/hep.1840210337

161. Iwakiri Y, Groszmann RJ. The hyperdynamic circulation of chronic liver diseases: From the patient to the molecule. Hepatology. 2006 Feb;43(2 SUPPL. 1).

162. Deleve LD, Wang X, Guo Y. Sinusoidal Endothelial Cells Prevent Rat Stellate Cell Activation and Promote Reversion to Quiescence. 2008;

163. Hess DT, Matsumoto A, Kim SO, Marshall HE, Stamler JS. Protein S-nitrosylation: purview and parameters. Nature Reviews Molecular Cell Biology 2005 6:2. 2005 Feb;6(2):150–66.

164. Ignarro LJ. Nitric oxide: A unique endogenous signaling molecule in vascular biology (Nobel lecture). Vol. 38, Angewandte Chemie - International Edition. 1999. p. 1882–92.

165. García-Cardeña G, Martasek P, Masters BSS, Skidd PM, Couet J, Li S, et al. Dissecting the interaction between nitric oxide synthase (NOS) and caveolin. Functional significance of the nos caveolin binding domain in vivo. Journal of Biological Chemistry. 1997 Oct 10;272(41):25437–40.

166. Iwakiri Y, Satoh A, Chatterjee S, Toomre DK, Chalouni CM, Fulton D, et al. Nitric oxide synthase generates nitric oxide locally to regulate compartmentalized protein S-nitrosylation and protein trafficking. Proc Natl Acad Sci U S A. 2006 Dec 26;103(52):19777–82.

167. Iwakiri Y. S-Nitrosylation of Proteins: A New Insight into Endothelial Cell Function Regulated by eNOS-derived NO. Nitric oxide : biology and chemistry / official journal of the Nitric Oxide Society. 2011 Aug 8;25(2):95.

168. Sangwung P, Greco TM, Wang Y, Ischiropoulos H, Sessa WC, Iwakiri Y. Proteomic identification of S-nitrosylated Golgi proteins: New insights into endothelial cell regulation by eNOS-derived NO. PLoS One. 2012 Feb 21;7(2).

169. Yamagishi M. Electron Microscope Studies on the Fine Structure of the Sinusoidal Wall and Fat-Storing Cells of Rabbit Livers. Arch Histol Cytol. 1959;18(2):223–61.

170. Wisse E. An electron microscopic study of the fenestrated endothelial lining of rat liver sinusoids. Journal of Ultrasructure Research. 1970;31(1–2):125–50.

171. Satchell SC, Braet F. Glomerular endothelial cell fenestrations: an integral component of the glomerular filtration barrier. Am J Physiol Renal Physiol [Internet]. 2009 [cited 2023 Apr 8];296(5):F947. Available from: /pmc/articles/PMC2681366/

172. Wisse E, de Zanger RB, Charels K, van der Smissen P, McCuskey RS. The liver sieve: Considerations concerning the structure and function of endothelial fenestrae, the sinusoidal wall and the space of disse. Hepatology. 1985;5(4):683–92.

173. Braet F. How molecular microscopy revealed new insights into the dynamics of hepatic endothelial fenestrae in the past decade. Liver International. 2004 Dec 1;24(6):532–9.

174. Butola A, Coucheron DA, Szafranska K, Ahmad A, Mao H, Tinguely JC, et al. Multimodal on-chip nanoscopy and quantitative phase imaging reveals the nanoscale morphology of liver sinusoidal endothelial cells. Proceedings of the National Academy of Sciences. 2021 Nov 23;118(47):e2115323118.

175. Wisse E, Jacobs F, Topal B, Frederik P, De Geest B. The size of endothelial fenestrae in human liver sinusoids: implications for hepatocyte-directed gene transfer. Gene Therapy 2008 15:17. 2008 Apr 10;15(17):1193–9.

176. Zapotoczny B, Szafranska K, Kus E, Chlopicki S, Szymonski M. Quantification of fenestrations in liver sinusoidal endothelial cells by atomic force microscopy. Micron [Internet]. 2017;101(April):48–53. Available from: http://dx.doi.org/10.1016/j.micron.2017.06.005

177. Braet F, Wisse E. Structural and functional aspects of liver sinusoidal endothelial cell fenestrae: A review. Vol. 1, Comparative Hepatology. BioMed Central; 2002. p. 1.

178. Wisse E, De Zanger RB, Jacobs R, McCuskey RS. SCANNING ELECTRON MICROSCOPE OBSERVATIONS ON THE STRUCTURE OF PORTAL VEINS, SINUSOIDS AND CENTRAL VEINS IN RAT LIVER. Scan Electron Microsc. 1983 Jan 1;v(pt 3):1441–52.

179. Wisse, Eddie, De Wilde A. DZR. Perfusion fixation of human and rat liver tissue for light and electron microcopy: a review and assessment of existing methods with special emphasis on sinusoidal cells and microcirculation. In: Science of Biological Tissue Preparation. 1984.

180. Funyu J, Mochida S, Inao M, Matsui A, Fujiwara K. VEGF can act as vascular permeability factor in the hepatic sinusoids through upregulation of porosity of endothelial cells. Biochem Biophys Res Commun. 2001 Jan 19;280(2):481–5.

181. Walter TJ, Cast AE, Huppert KA, Huppert SS. Epithelial VEGF signaling is required in the mouse liver for proper sinusoid endothelial cell identity and hepatocyte zonation in vivo. Am J Physiol Gastrointest Liver Physiol [Internet]. 2014 May 15 [cited 2023 Nov 8];306(10). Available from: https://journals.physiology.org/doi/10.1152/ajpgi.00426.2013

182. Ceci C, Atzori MG, Lacal PM, Graziani G. Role of VEGFs/VEGFR-1 Signaling and Its Inhibition in Modulating Tumor Invasion: Experimental Evidence in Different Metastatic Cancer Models. Int J Mol Sci [Internet]. 2020 Feb 2 [cited 2023 Nov 13];21(4). Available from: /pmc/articles/PMC7073125/

183. BRAET F, ZANGER R DE, CRABBÉ E, WISSE E. New observations on cytoskeleton and fenestrae in isolated rat liver sinusoidal endothelial cells. J Gastroenterol Hepatol. 1995;10 Suppl 1(1 S):S3–7.

184. Mönkemöller V, Øie C, Hübner W, Huser T, McCourt P. Multimodal super-resolution optical microscopy visualizes the close connection between membrane and the cytoskeleton in liver sinusoidal endothelial cell fenestrations. Sci Rep [Internet]. 2015;5(November):1–10. Available from: http://dx.doi.org/10.1038/srep16279

185. Braet F, de Zanger R, Jans D, Spector I, Wisse E. Microfilament-disrupting agent latrunculin A induces and increased number of fenestrae in rat liver sinusoidal endothelial cells: comparison with cytochalasin B. Hepatology [Internet]. 1996 [cited 2023 Feb 17];24(3):627–35. Available from: https://pubmed.ncbi.nlm.nih.gov/8781335/

186. Yokomori H, Yoshimura K, Funakoshi S, Nagai T, Fujimaki K, Nomura M, et al. Rho modulates hepatic sinusoidal endothelial fenestrae via regulation of the actin cytoskeleton in rat endothelial cells. Laboratory Investigation [Internet]. 2004 Jul 26 [cited 2020 Sep 24];84(7):857–64. Available from: www.laboratoryinvestigation.org

187. Van Der Smissen P, Van Bossuyt H, Charels K, Wisse E. The structure and function of the cytoskeleton in sinusoidal endothelial cells in the rat liver . In: Kirn A, Knook D, Wisse E, editors. Cells of the Hepatic Sinusoid. Rijswijk: Kuppfer Cell Foundation; 1986. p. 517–22.

188. Oda M, Tsukada N, Komatsu H, Kaneko K, Nakamura M, Tsuchiya M. Electron microscopic localisations of actin, calmodulin and calcium in the hepatic sinusoidal endothelium in the rat. . In: Kirn A, Knook D, Wisse E, editors. Cells of the Hepatic Sinusoid. Rijswijk: Kuppfer Cell Foundation; 1986. p. 511–2.

189. Svistounov D, Warren A, McNerney GP, Owen DM, Zencak D, Zykova SN, et al. The Relationship between Fenestrations, Sieve Plates and Rafts in Liver Sinusoidal Endothelial Cells. PLoS One. 2012;7(9):1–9.

190. Simons K, Toomre D. Lipid rafts and signal transduction. Nature Reviews Molecular Cell Biology 2000 1:1 [Internet]. 2000 [cited 2023 Feb 17];1(1):31–9. Available from: https://www.nature.com/articles/35036052

191. Levental I, Levental KR, Heberle FA. Lipid rafts: controversies resolved, mysteries remain. Trends Cell Biol [Internet]. 2020 May 1 [cited 2023 Feb 17];30(5):341. Available from: /pmc/articles/PMC7798360/

192. Zapotoczny B, Braet F, Kus E, Ginda-Mäkelä K, Klejevskaja B, Campagna R, et al. Actin-spectrin scaffold supports open fenestrae in liver sinusoidal endothelial cells. Traffic [Internet]. 2019 Dec 1 [cited 2022 Aug 11];20(12):932–42. Available from: https://onlinelibrary.wiley.com/doi/full/10.1111/tra.12700

193. MacHnicka B, Grochowalska R, Bogusławska DM, Sikorski AF, Lecomte MC. Spectrin-based skeleton as an actor in cell signaling. Cell Mol Life Sci [Internet]. 2012 Jan [cited 2023 Feb 17];69(2):191–201. Available from: https://pubmed.ncbi.nlm.nih.gov/21877118/

194. Baek HJ, Lee YM, Kim TH, Kim JY, Park EJ, Iwabuchi K, et al. Caspase-3/7-mediated Cleavage of β2-spectrin is Required for Acetaminophen-induced Liver Damage. Int J Biol Sci [Internet]. 2016 Jan 1 [cited 2023 Feb 17];12(2):172–83. Available from: https://pubmed.ncbi.nlm.nih.gov/26884715/

195. Spector I, Braet F, Shochet NR, Bubb MR. New Anti-Actin Drugs in the Study of the Organization and Function of the Actin Cytoskeleton. Microsc Res Tech [Internet]. 1999 [cited 2023 Feb 17];47:18–37. Available from: https://analyticalsciencejournals.onlinelibrary.wiley.com/doi/10.1002/

196. di Martino J, Mascalchi P, Legros P, Lacomme S, Gontier E, Bioulac-Sage P, et al. Actin Depolymerization in Dedifferentiated Liver Sinusoidal Endothelial Cells Promotes Fenestrae Re-Formation. Hepatol Commun [Internet]. 2018 Feb 1 [cited 2023 Feb 17];3(2):213–9. Available from: https://pubmed.ncbi.nlm.nih.gov/30766959/

197. Braet F, Wisse E. AFM imaging of fenestrated liver sinusoidal endothelial cells. Micron. 2012 Dec;43(12):1252–8.

198. Zapotoczny B, Braet F, Wisse E, Lekka M, Szymonski M. Biophysical nanocharacterization of liver sinusoidal endothelial cells through atomic force microscopy [Internet]. Vol. 12, Biophysical Reviews. 2020 [cited 2020 May 22]. p. 625–36. Available from: http://link.springer.com/10.1007/s12551-020-00699-0

199. Steffan A -M, Gendrault J -L, McCuskey RS, McCuskey PA, Kirn A. Phagocytosis, an unrecognized property of murine endothelial liver cells. Hepatology [Internet]. 1986 Sep 1 [cited 2023 Mar 23];6(5):830–6. Available from: https://onlinelibrary.wiley.com/doi/full/10.1002/hep.1840060505

200. Steffan A -M, Gendrault J -L, Kirn A. Increase in the number of fenestrae in mouse endothelial liver cells by altering the cytoskeleton with cytochalasin B. Hepatology [Internet]. 1987 [cited 2023 Mar 23];7(6):1230–8. Available from: https://pubmed.ncbi.nlm.nih.gov/3679088/

201. Walker RM, Racz WJ, McElligott TF. Scanning electron microscopic examination of acetaminophen-induced hepatotoxicity and congestion in mice. American Journal of Pathology. 1983;113(3):321–30.

202. Hunt NJ, Lockwood GP, Warren A, Mao H, McCourt PAG, Le Couteur DG, et al. Manipulating fenestrations in young and old liver sinusoidal endothelial cells. Am J Physiol Gastrointest Liver Physiol [Internet]. 2019 Jan 1 [cited 2020 Sep 24];316(1):G144–54. Available from: https://pubmed.ncbi.nlm.nih.gov/30285464/

203. Boolell M, Allen MJ, Ballard SA, Gepi-Attee S, Muirhead GJ, Naylor AM, et al. Sildenafil: an orally active type 5 cyclic GMP-specific phosphodiesterase inhibitor for the treatment of penile erectile dysfunction. Int J Impot Res. 1996;8(2):47–52.

204. Sorensen KK, McCourt P, Berg T, Crossley C, Couteur DL, Wake K, et al. The scavenger endothelial cell: a new player in homeostasis and immunity. AJP: Regulatory, Integrative and Comparative Physiology. 2012;303(12):R1217–30.

205. Martens JH, Kzhyshkowska J, Falkowski-Hansen M, Schledzewski K, Gratchev A, Mansmann U, et al. Differential expression of a gene signature for scavenger/lectin receptors by endothelial cells and macrophages in human lymph node sinuses, the primary sites of regional metastasis. Journal of Pathology. 2006 Mar 1;208(4):574–89.

206. Taylor ME, Bezouska K, Drickamer K. Contribution to ligand binding by multiple carbohydrate-recognition domains in the macrophage mannose receptor. Journal of Biological Chemistry. 1992;267(3):1719–26.

207. Alan R, Ezekowitz B, Sastry K, Bailly P, Warner A. Molecular characterization of the human macrophage mannose receptor: Demonstration of multiple carbohydrate recognition-like

domains and phagocytosis of yeasts in cos-1 cells. Journal of Experimental Medicine. 1990;172(6):1785–94.

208. Smedsrod B, Einarsson M. Clearance of tissue plasminogen activator by mannose and galactose receptors in the liver. Thromb Haemost. 1990;63(1):60–6.

209. Smedsrod B, Melkko J, Risteli L, Risteli J. Circulating C-terminal propeptide of type I procollagen is cleared mainly via the mannose receptor in liver endothelial cells. Biochemical Journal. 1990 Oct 15;271(2):345–50.

210. Simpson DZ, Hitchen PG, Elmhirst EL, Taylor ME. Multiple interactions between pituitary hormones and the mannose receptor. Biochem J. 1999;343:403–11.

211. De Haan W, Øie C, Benkheil M, Dheedene W, Vinckier S, Coppiello G, et al. Unraveling the transcriptional determinants of liver sinusoidal endothelial cell specialization. Am J Physiol Gastrointest Liver Physiol [Internet]. 2020 Apr 4 [cited 2022 Oct 6];318(4):G803–15. Available from: /pmc/articles/PMC7191457/

212. Mousavi SA, Sporstøl M, Fladeby C, Kjeken R, Barois N, Berg T. Receptor-mediated endocytosis of immune complexes in rat liver sinusoidal endothelial cells is mediated by FcγRIIb2. Hepatology. 2007;46(3):871–84.

213. Muro H, Shirasawa H, Maeda M, Nakamura S. Fc receptors of liver sinusoidal endothelium in normal rats and humans. A histologic study with soluble immune complexes. Gastroenterology. 1987;93(5):1078–85.

214. Muro H, Shirasawa H, Takahashi Y, Maeda M, Nakamura S. Localization of Fc receptors on liver sinusoidal endothelium. A histological study by electron microscopy. Acta Pathol Jpn. 1988;38(3):291–301.

215. Yajima K, Nakamura A, Sugahara A, Takai T. FcgammaRIIB deficiency with Fas mutation is sufficient for the development of systemic autoimmune disease. Eur J Immunol. 2003 Apr 1;33(4):1020–9.

216. Yamazaki H, Oda M, Takahashi Y, Iguchi H, Yoshimura K, Okada N, et al. Relation between ultrastructural localization, changes in caveolin-1, and capillarization of liver sinusoidal endothelial cells in human hepatitis C-related cirrhotic liver. J Histochem Cytochem. 2013;61(2):169–76.

217. Anania JC, Chenoweth AM, Wines BD, MarkHogarth P. The human FcγRII (CD32) family of leukocyte FCR in health and disease. Front Immunol. 2019;10(MAR).

218. Miettinen HM, Rose JK, Mellman I. Fc receptor isoforms exhibit distinct abilities for coated pit localization as a result of cytoplasmic domain heterogeneity. Cell. 1989;58(2):317–27.

219. Liu H, Ã1 S, Manuel J, He W, Leung E, Crookshank J, et al. The FGL2-FccRIIB pathway: A novel mechanism leading to immunosuppression.

220. Ravanel K, Castelle C, Defrance T, Wild TF, Charron D, Lotteau V, et al. Measles Virus Nucleocapsid Protein Binds to Fc RII and Inhibits Human B Cell Antibody Production. J Exp Med. 1997;186(2):269–78.

221. Muro H, Shirasawa H, Kosugi I, Nakamura S. Defect of Fc receptors and phenotypical changes in sinusoidal endothelial cells in human liver cirrhosis. Am J Pathol [Internet]. 1993 [cited 2023 Feb 3];143(1):105. Available from: /pmc/articles/PMC1886954/?report=abstract

222. Géraud C, Mogler C, Runge A, Evdokimov K, Lu S, Schledzewski K, et al. Endothelial transdifferentiation in hepatocellular carcinoma: Loss of Stabilin-2 expression in peri-tumourous liver correlates with increased survival. Liver International [Internet]. 2013;33(9):1428–40. Available from: https://onlinelibrary.wiley.com/doi/10.1111/liv.12262

223. Martens JH, Kzhyshkowska J, Falkowski-Hansen M, Schledzewski K, Gratchev A, Mansmann U, et al. Differential expression of a gene signature for scavenger/lectin receptors by endothelial cells and macrophages in human lymph node sinuses, the primary sites of regional metastasis. J Pathol [Internet]. 2006 [cited 2023 Apr 12];208(4):574–89. Available from: https://pubmed.ncbi.nlm.nih.gov/16440291/

224. Goerdt S, Walsh LJ, Murphy GF, Pober JS. Identification of a novel high molecular weight protein preferentially expressed by sinusoidal endothelial cells in normal human tissues. J Cell Biol [Internet]. 1991 Jun 6 [cited 2023 Apr 12];113(6):1425. Available from: /pmc/articles/PMC2289031/?report=abstract

225. Prevo R, Banerji S, Ni J, Jackson DG. Rapid plasma membrane-endosomal trafficking of the lymph node sinus and high endothelial venule scavenger receptor/homing receptor stabilin-1 (FEEL-1/CLEVER-1). J Biol Chem [Internet]. 2004 Dec 10 [cited 2023 Apr 12];279(50):52580–92. Available from: https://pubmed.ncbi.nlm.nih.gov/15345716/

226. Adachi H, Tsujimoto M. FEEL-1, a novel scavenger receptor with in vitro bacteria-binding and angiogenesis-modulating activities. J Biol Chem [Internet]. 2002 Sep 13 [cited 2023 Apr 12];277(37):34264–70. Available from: https://pubmed.ncbi.nlm.nih.gov/12077138/

227. Maxfield FR, McGraw TE. Endocytic recycling. Nat Rev Mol Cell Biol [Internet]. 2004 Feb [cited 2023 Apr 12];5(2):121–32. Available from: https://pubmed.ncbi.nlm.nih.gov/15040445/

228. Kzhyshkowska J, Gratchev A, Goerdt S. Stabilin-1, a homeostatic scavenger receptor with multiple functions. J Cell Mol Med. 2006;10(3):635–49.

229. Kupprion C, Motamed K, Sage EH. SPARC (BM-40, osteonectin) inhibits the mitogenic effect of vascular endothelial growth factor on microvascular endothelial cells. J Biol Chem [Internet]. 1998 Nov 6 [cited 2023 Apr 12];273(45):29635–40. Available from: https://pubmed.ncbi.nlm.nih.gov/9792673/

230. Bradshaw AD, Sage EH. SPARC, a matricellular protein that functions in cellular differentiation and tissue response to injury. J Clin Invest [Internet]. 2001 [cited 2023 Apr 12];107(9):1049–54. Available from: https://pubmed.ncbi.nlm.nih.gov/11342565/

231. Kzhyshkowska J, Workman G, Cardó-Vila M, Arap W, Pasqualini R, Gratchev A, et al. Novel function of alternatively activated macrophages: stabilin-1-mediated clearance of SPARC. J Immunol [Internet]. 2006 May 15 [cited 2023 Apr 12];176(10):5825–32. Available from: https://pubmed.ncbi.nlm.nih.gov/16670288/

232. Mazzolini G, Atorrasagasti C, Onorato A, Peixoto E, Schlattjan M, Sowa JP, et al. SPARC expression is associated with hepatic injury in rodents and humans with non-alcoholic fatty

liver disease. Scientific Reports 2018 8:1 [Internet]. 2018 Jan 15 [cited 2023 Apr 12];8(1):1–11. Available from: https://www.nature.com/articles/s41598-017-18981-9

233. Mccourt PAG, Smedsrød BH, Melkko J, Johansson S. Characterization of a hyaluronan receptor on rat sinusoidal liver endothelial cells and its functional relationship to scavenger receptors. Hepatology [Internet]. 1999 Nov 1 [cited 2022 Oct 6];30(5):1276–86. Available from: https://onlinelibrary.wiley.com/doi/full/10.1002/hep.510300521

234. Politz O, Gratchev A, McCourt PAG, Schledzewski K, Guillot P, Johansson S, et al. Stabilin-1 and -2 constitute a novel family of fasciclin-like hyaluronan receptor homologues. Biochemical Journal [Internet]. 2002 Feb 2 [cited 2023 Apr 12];362(Pt 1):155. Available from: /pmc/articles/PMC1222372/?report=abstract

235. Falkowski M, Schledzewski K, Hansen B, Goerdt S. Expression of stabilin-2, a novel fasciclin-like hyaluronan receptor protein, in murine sinusoidal endothelia, avascular tissues, and at solid/liquid interfaces. Histochem Cell Biol [Internet]. 2003 Nov [cited 2023 Apr 12];120(5):361–9. Available from: https://pubmed.ncbi.nlm.nih.gov/14598175/

236. Weigel JA, Raymond RC, Weigel PH. The hyaluronan receptor for endocytosis (HARE) is not CD44 or CD54 (ICAM-1). Biochem Biophys Res Commun [Internet]. 2002 [cited 2023 Apr 12];294(4):918–22. Available from: https://pubmed.ncbi.nlm.nih.gov/12061795/

237. Weigel PH. Systemic Glycosaminoglycan Clearance by HARE/Stabilin-2 Activates Intracellular Signaling. Cells [Internet]. 2020 Oct 28 [cited 2023 Apr 12];9(11). Available from: https://pubmed.ncbi.nlm.nih.gov/33126404/

238. Harris EN, Weigel JA, Weigel PH. Endocytic function, glycosaminoglycan specificity, and antibody sensitivity of the recombinant human 190-kDa hyaluronan receptor for endocytosis (HARE). J Biol Chem [Internet]. 2004 Aug 27 [cited 2023 Apr 12];279(35):36201–9. Available from: https://pubmed.ncbi.nlm.nih.gov/15208308/

239. Kayashima Y, Clanton CA, Lewis AM, Sun X, Hiller S, Huynh P, et al. Reduction of Stabilin-2 Contributes to a Protection Against Atherosclerosis. Front Cardiovasc Med. 2022 Mar 11;9:491.

240. Yong J, Huang L, Chen G, Luo X, Chen H, Wang L. High expression of Stabilin-2 predicts poor prognosis in non-small-cell lung cancer. Bioengineered. 2021;12(1):3426–33.

241. Carreira CM, Nasser SM, di Tomaso E, Padera TP, Boucher Y, Tomarev SI, et al. LYVE-1 Is Not Restricted to the Lymph Vessels: Expression in Normal Liver Blood Sinusoids and Down-Regulation in Human Liver Cancer and Cirrhosis. Cancer Res. 2001 Nov 15;61:8079–84.

242. Arimoto J, Ikura Y, Suekane T, Nakagawa M, Kitabayashi C, Iwasa Y, et al. Expression of LYVE-1 in sinusoidal endothelium is reduced in chronically inflamed human livers. J Gastroenterol. 2010 Mar;45(3):317–25.

243. Jauch AS, Wohlfeil SA, Weller C, Dietsch B, Häfele V, Stojanovic A, et al. Lyve-1 deficiency enhances the hepatic immune microenvironment entailing altered susceptibility to melanoma liver metastasis. Cancer Cell Int [Internet]. 2022 Dec 1 [cited 2023 Apr 12];22(1):1–17. Available from: https://cancerci.biomedcentral.com/articles/10.1186/s12935-022-02800-x

244. Leyte A, Verbeet MP, Brodniewicz-Proba T, Van Mourik JA, Mertens K. The interaction between human blood-coagulation factor VIII and von Willebrand factor. Characterization of a high-affinity binding site on factor VIII. Biochemical Journal [Internet]. 1989 Feb 2 [cited 2023 Apr 12];257(3):679. Available from: /pmc/articles/PMC1135641/?report=abstract

245. Rydz N, Swystun LL, Notley C, Paterson AD, Riches JJ, Sponagle K, et al. The C-type lectin receptor CLEC4M binds, internalizes, and clears von Willebrand factor and contributes to the variation in plasma von Willebrand factor levels. Blood [Internet]. 2013 Jun 27 [cited 2023 Apr 12];121(26):5228–37. Available from: https://pubmed.ncbi.nlm.nih.gov/23529928/

246. Swystun LL, Notley C, Georgescu I, Lai JD, Nesbitt K, James PD, et al. The endothelial lectin clearance receptor CLEC4M binds and internalizes factor VIII in a VWF-dependent and independent manner. Journal of Thrombosis and Haemostasis. 2019;17(4):681–94.

247. Lai WK, Sun PJ, Zhang J, Jennings A, Lalor PF, Hubscher S, et al. Expression of DC-SIGN and DC-SIGNR on Human Sinusoidal Endothelium : A Role for Capturing Hepatitis C Virus Particles. Am J Pathol [Internet]. 2006 [cited 2022 Jul 19];169(1):200. Available from: /pmc/articles/PMC1698775/

248. Ley K, Laudanna C, Cybulsky MI, Nourshargh S. Getting to the site of inflammation: the leukocyte adhesion cascade updated. Nature Reviews Immunology 2007 7:9. 2007 Sep;7(9):678–89.

249. Vestweber D. How leukocytes cross the vascular endothelium. Nature Reviews Immunology 2015 15:11. 2015 Oct 16;15(11):692–704.

250. Muller WA. Transendothelial migration: unifying principles from the endothelial perspective. Immunol Rev. 2016 Sep 1;273(1):61–75.

251. Edwards S, Lalor PF, Nash GB, Rainger GE, Adams DH. Lymphocyte traffic through sinusoidal endothelial cells is regulated by hepatocytes. Hepatology. 2005 Mar;41(3):451–9.

252. Wong J, Johnston B, Lee SS, Bullard DC, Smith CW, Beaudet AL, et al. A Minimal Role for Selectins in the Recruitment of Leukocytes into the Inflamed Liver Microvasculature. J Clin Invest. 1997;99(11):2782–90.

253. Campbell JJ, Hedrick J, Zlotnik A, Siani MA, Thompson DA, Butcher EC. Chemokines and the Arrest of Lymphocytes Rolling Under Flow Conditions. Science (1979) [Internet]. 1998 Jan 16 [cited 2023 Mar 25];279(5349):381–4. Available from: https://www.science.org/doi/10.1126/science.279.5349.381

254. Campbell JJ, Qin S, Bacon KB, Mackay CR, Butcher EC. Biology of chemokine and classical chemoattractant receptors: differential requirements for adhesion-triggering versus chemotactic responses in lymphoid cells. J Cell Biol [Internet]. 1996 Jul [cited 2023 Mar 25];134(1):255–66. Available from: https://pubmed.ncbi.nlm.nih.gov/8698820/

255. Lalor PF, Clements JM, Pigott R, Humphries MJ, Spragg JH, Nash GB. Association between receptor density, cellular activation, and transformation of adhesive behavior of flowing lymphocytes binding to VCAM-1. Eur J Immunol [Internet]. 1997 Jun 1 [cited 2023 Mar 25];27(6):1422–6. Available from: https://onlinelibrary.wiley.com/doi/full/10.1002/eji.1830270619

256. Grant AJ, Lalor PF, Salmi M, Jalkanen S, Adams DH. Homing of mucosal lymphocytes to the liver in the pathogenesis of hepatic complications of inflammatory bowel disease. Lancet [Internet]. 2002 Jan 12 [cited 2023 Mar 25];359(9301):150–7. Available from: http://www.thelancet.com/article/S0140673602073749/fulltext

257. Grant AJ, Lalor PF, Hübscher SG, Briskin M, Adams DH. MAdCAM-1 expressed in chronic inflammatory liver disease supports mucosal lymphocyte adhesion to hepatic endothelium (MAdCAM-1 in chronic inflammatory liver disease). Hepatology [Internet]. 2001 [cited 2023 Mar 25];33(5):1065–72. Available from: https://pubmed.ncbi.nlm.nih.gov/11343233/

258. Salmi M, Tohka S, Berg EL, Butcher EC, Jalkanen S. Vascular Adhesion Protein 1 (VAP-1) Mediates Lymphocyte Subtype-specific, Selectin-independent Recognition of Vascular Endothelium in Human Lymph Nodes. J Exp Med [Internet]. 1997 Aug 8 [cited 2023 Mar 25];186(4):589. Available from: /pmc/articles/PMC2199032/

259. Lalor PF, Edwards S, McNab G, Salmi M, Jalkanen S, Adams DH. Vascular adhesion protein-1 mediates adhesion and transmigration of lymphocytes on human hepatic endothelial cells. J Immunol [Internet]. 2002 Jul 15 [cited 2023 Mar 25];169(2):983–92. Available from: https://pubmed.ncbi.nlm.nih.gov/12097405/

260. Bonder CS, Norman MU, Swain MG, Zbytnuik LD, Yamanouchi J, Santamaria P, et al. Rules of recruitment for Th1 and Th2 lymphocytes in inflamed liver: a role for alpha-4 integrin and vascular adhesion protein-1. Immunity [Internet]. 2005 Aug [cited 2023 Mar 25];23(2):153–63. Available from: https://pubmed.ncbi.nlm.nih.gov/16111634/

261. Liaskou E, Karikoski M, Reynolds GM, Lalor PF, Weston CJ, Pullen N, et al. Regulation of mucosal addressin cell adhesion molecule 1 expression in human and mice by vascular adhesion protein 1 amine oxidase activity. Hepatology [Internet]. 2011 Feb [cited 2023 Mar 25];53(2):661–72. Available from: https://pubmed.ncbi.nlm.nih.gov/21225644/

262. Weston CJ, Shepherd EL, Claridge LC, Rantakari P, Curbishley SM, Tomlinson JW, et al. Vascular adhesion protein-1 promotes liver inflammation and drives hepatic fibrosis. J Clin Invest [Internet]. 2015 Feb 2 [cited 2023 Mar 25];125(2):501. Available from: /pmc/articles/PMC4319424/

263. Lalor PF, Sun PJ, Weston CJ, Martin-Santos A, Wakelam MJO, Adams DH. Activation of vascular adhesion protein-1 on liver endothelium results in an NF-κB-dependent increase in lymphocyte adhesion. Hepatology. 2007 Feb;45(2):465–74.

264. Shetty S, Weston CJ, Oo YH, Westerlund N, Stamataki Z, Youster J, et al. Common lymphatic endothelial and vascular endothelial receptor-1 mediates the transmigration of regulatory T cells across human hepatic sinusoidal endothelium. J Immunol [Internet]. 2011 Apr 1 [cited 2023 Mar 26];186(7):4147–55. Available from: https://pubmed.ncbi.nlm.nih.gov/21368224/

265. Jung MY, Park SY, Kim IS. Stabilin-2 is involved in lymphocyte adhesion to the hepatic sinusoidal endothelium via the interaction with alphaMbeta2 integrin. J Leukoc Biol [Internet]. 2007 Nov 1 [cited 2023 Mar 26];82(5):1156–65. Available from: https://pubmed.ncbi.nlm.nih.gov/17675564/

266. Vestweber D. How leukocytes cross the vascular endothelium. Nature Reviews Immunology 2015 15:11 [Internet]. 2015 Oct 16 [cited 2023 Mar 26];15(11):692–704. Available from: https://www.nature.com/articles/nri3908

267. Phillipson M, Heit B, Colarusso P, Liu L, Ballantyne CM, Kubes P. Intraluminal crawling of neutrophils to emigration sites: a molecularly distinct process from adhesion in the recruitment cascade. J Exp Med [Internet]. 2006 Nov [cited 2023 Mar 26];203(12):2569–75. Available from: https://pubmed.ncbi.nlm.nih.gov/17116736/

268. Carman C V., Sage PT, Sciuto TE, de la Fuente MA, Geha RS, Ochs HDD, et al. Transcellular Diapedesis Is Initiated by Invasive Podosomes. Immunity [Internet]. 2007 Jun 22 [cited 2023 Mar 26];26(6):784. Available from: /pmc/articles/PMC2094044/

269. Patten DA, Wilson GK, Bailey D, Shaw RK, Jalkanen S, Salmi M, et al. Human liver sinusoidal endothelial cells promote intracellular crawling of lymphocytes during recruitment: A new step in migration. Hepatology [Internet]. 2017 Jan 1 [cited 2023 Mar 26];65(1):294–309. Available from: https://pubmed.ncbi.nlm.nih.gov/27770554/

270. Burgdorf S, Kautz A, Böhnert V, Knolle PA, Kurts C. Distinct pathways of antigen uptake and intracellular routing in CD4 and CD8 T cell activation. Science (1979) [Internet]. 2007 Apr 27 [cited 2023 Mar 26];316(5824):612–6. Available from: https://www.science.org/doi/10.1126/science.1137971

271. Limmer A, Ohl J, Kurts C, Ljunggren HG, Reiss Y, Groettrup M, et al. Efficient presentation of exogenous antigen by liver endothelial cells to CD8+ T cells results in antigen-specific T-cell tolerance. Nat Med [Internet]. 2000 [cited 2023 Mar 26];6(12):1348–54. Available from: https://pubmed.ncbi.nlm.nih.gov/11100119/

272. Höchst B, Schildberg FA, Böttcher J, Metzger C, Huss S, Türler A, et al. Liver sinusoidal endothelial cells contribute to CD8 T cell tolerance toward circulating carcinoembryonic antigen in mice. Hepatology [Internet]. 2012 Nov [cited 2023 Mar 26];56(5):1924–33. Available from: https://pubmed.ncbi.nlm.nih.gov/22610745/

273. Schurich A, Böttcher JP, Burgdorf S, Penzler P, Hegenbarth S, Kern M, et al. Distinct kinetics and dynamics of cross-presentation in liver sinusoidal endothelial cells compared to dendritic cells. Hepatology [Internet]. 2009 [cited 2023 Mar 26];50(3):909–19. Available from: https://pubmed.ncbi.nlm.nih.gov/19610048/

274. Diehl L, Schurich A, Grochtmann R, Hegenbarth S, Chen L, Knolle PA. Tolerogenic maturation of liver sinusoidal endothelial cells promotes B7-homolog 1-dependent CD8+ T cell tolerance. Hepatology [Internet]. 2008 Jan [cited 2023 Apr 5];47(1):296–305. Available from: https://pubmed.ncbi.nlm.nih.gov/17975811/

275. Limmer A, Ohl J, Wingender G, Berg M, Jüngerkes F, Schumak B, et al. Cross-presentation of oral antigens by liver sinusoidal endothelial cells leads to CD8 T cell tolerance. Eur J Immunol [Internet]. 2005 Oct [cited 2023 Apr 5];35(10):2970–81. Available from: https://pubmed.ncbi.nlm.nih.gov/16163670/

276. Limmer A, Ohl J, Kurts C, Ljunggren HG, Reiss Y, Groettrup M, et al. Efficient presentation of exogenous antigen by liver endothelial cells to CD8+ T cells results in antigen-specific T-cell

tolerance. Nat Med [Internet]. 2000 [cited 2023 Apr 5];6(12):1348–54. Available from: https://pubmed.ncbi.nlm.nih.gov/11100119/

277. Schurich A, Berg M, Stabenow D, Böttcher J, Kern M, Schild HJ, et al. Dynamic regulation of CD8 T cell tolerance induction by liver sinusoidal endothelial cells. J Immunol [Internet]. 2010 Apr 15 [cited 2023 Apr 5];184(8):4107–14. Available from: https://pubmed.ncbi.nlm.nih.gov/20212092/

278. Lohse AW, Knolle PA, Bilo K, Uhrig A, Waldmann C, Ibe M, et al. Antigen-presenting function and B7 expression of murine sinusoidal endothelial cells and Kupffer cells. Gastroenterology [Internet]. 1996 [cited 2023 Apr 5];110(4):1175–81. Available from: https://pubmed.ncbi.nlm.nih.gov/8613007/

279. Carambia A, Freund B, Schwinge D, Heine M, Laschtowitz A, Huber S, et al. TGF-β-dependent induction of $CD4^+CD25^+Foxp3^+$ Tregs by liver sinusoidal endothelial cells. J Hepatol [Internet]. 2014 [cited 2023 Apr 5];61(3):594–9. Available from: https://pubmed.ncbi.nlm.nih.gov/24798620/

280. Knolle PA, Schmitt E, Jin S, Germann T, Duchmann R, Hegenbarth S, et al. Induction of cytokine production in naive CD4(+) T cells by antigen-presenting murine liver sinusoidal endothelial cells but failure to induce differentiation toward Th1 cells. Gastroenterology [Internet]. 1999 [cited 2023 Apr 5];116(6):1428–40. Available from: https://pubmed.ncbi.nlm.nih.gov/10348827/

281. Carambia A, Frenzel C, Bruns OT, Schwinge D, Reimer R, Hohenberg H, et al. Inhibition of inflammatory CD4 T cell activity by murine liver sinusoidal endothelial cells. J Hepatol [Internet]. 2013 Jan [cited 2023 Apr 5];58(1):112–8. Available from: https://pubmed.ncbi.nlm.nih.gov/22989568/

282. Egerton RF. Physical Principles of Electron Microscopy . Second. Vol. 56. New York: Springer; 2005.

283. Sanderson MJ, Smith I, Parker I, Bootman MD. Fluorescence Microscopy. Cold Spring Harb Protoc [Internet]. 2014 Oct 1 [cited 2023 Mar 18];2014(10):pdb.top071795. Available from: /pmc/articles/PMC4711767/

284. Paddock SW. Confocal Laser Scanning Microscopy. https://doi.org/102144/99275ov01 [Internet]. 2018 Aug 22 [cited 2023 Mar 20];27(5):992–1004. Available from: https://www.future-science.com/doi/10.2144/99275ov01

285. Paddock SW. Principles and practices of laser scanning confocal microscopy. Applied Biochemistry and Biotechnology - Part B Molecular Biotechnology [Internet]. 2000 [cited 2023 Mar 19];16(2):127–49. Available from: https://link.springer.com/article/10.1385/MB:16:2:127

286. Gray N. Knowing the limit. Nature Cell Biology 2009 11:1 [Internet]. 2009 Oct 1 [cited 2023 Mar 20];11(1):S8–S8. Available from: https://www.nature.com/articles/milelight03

287. Gustafsson MGL. Surpassing the lateral resolution limit by a factor of two using structured illumination microscopy. J Microsc [Internet]. 2000 [cited 2023 Mar 20];198(Pt 2):82–7. Available from: https://pubmed.ncbi.nlm.nih.gov/10810003/

288. Hell SW, Wichmann J. Breaking the diffraction resolution limit by stimulated emission: stimulated-emission-depletion fluorescence microscopy. Opt Lett. 1994 Jun 1;19(11):780–2.

289. Betzig E, Patterson GH, Sougrat R, Lindwasser OW, Olenych S, Bonifacino JS, et al. Imaging intracellular fluorescent proteins at nanometer resolution. Science (1979) [Internet]. 2006 Sep 15 [cited 2023 Mar 20];313(5793):1642–5. Available from: www.sciencemag.org/cgi/content/full/313/5793/1638/DC1

290. Hess ST, Girirajan TPK, Mason MD. Ultra-High Resolution Imaging by Fluorescence Photoactivation Localization Microscopy. Biophys J [Internet]. 2006 Dec 12 [cited 2023 Mar 20];91(11):4258. Available from: /pmc/articles/PMC1635685/

291. Point Spread Function (PSF) | Scientific Volume Imaging [Internet]. [cited 2023 Mar 21]. Available from: https://svi.nl/Point-Spread-Function-(PSF)

292. Rust MJ, Bates M, Zhuang X. Sub-diffraction-limit imaging by stochastic optical reconstruction microscopy (STORM). Nature Methods 2006 3:10 [Internet]. 2006 Aug 9 [cited 2022 Oct 6];3(10):793–6. Available from: https://www.nature.com/articles/nmeth929

293. Van De Linde S, Löschberger A, Klein T, Heidbreder M, Wolter S, Heilemann M, et al. Direct stochastic optical reconstruction microscopy with standard fluorescent probes. Nat Protoc. 2011;6(7):991–1009.

294. Heilemann M, Van De Linde S, Schüttpelz M, Kasper R, Seefeldt B, Mukherjee A, et al. Subdiffraction-resolution fluorescence imaging with conventional fluorescent probes. Angewandte Chemie - International Edition. 2008 Aug 4;47(33):6172–6.

295. Bates M, Jones SA, Zhuang X. Stochastic optical reconstruction microscopy (STORM): a method for superresolution fluorescence imaging. Cold Spring Harb Protoc [Internet]. 2013 Jun [cited 2023 Mar 22];2013(6):498–520. Available from: https://pubmed.ncbi.nlm.nih.gov/23734025/

296. Mönkemöller V, Schüttpelz M, McCourt P, Sørensen K, Smedsrød B, Huser T. Imaging fenestrations in liver sinusoidal endothelial cells by optical localization microscopy. Physical Chemistry Chemical Physics. 2014;16(24):12576–81.

297. Lambert TJ, Waters JC. Navigating challenges in the application of superresolution microscopy. Journal of Cell Biology. 2017;216(1):53–63.

298. Kong C, Bobe S, Pilger C, Lachetta M, Øie CI, Kirschnick N, et al. Multiscale and Multimodal Optical Imaging of the Ultrastructure of Human Liver Biopsies. Front Physiol. 2021 Feb 17;12:149.

299. Sørensen KK, Simon-Santamaria J, McCuskey RS, Smedsrød B. Liver Sinusoidal Endothelial Cells. Compr Physiol [Internet]. 2015 Oct 1 [cited 2021 Jul 14];5(4):1751–74. Available from: https://onlinelibrary.wiley.com/doi/full/10.1002/cphy.c140078

300. Takahashi Y, Fukusato T. Animal Models of Liver Diseases. Animal Models for the Study of Human Disease: Second Edition. 2017 Jan 1;313–39.

301. Kaur S, Kidambi S, Ortega-Ribera M, Thuy LTT, Nieto N, Cogger VC, et al. In Vitro Models for the Study of Liver Biology and Diseases: Advances and Limitations. Cell Mol Gastroenterol

Hepatol [Internet]. 2022 Jan 1 [cited 2023 Jan 19];15(3):559–71. Available from: http://www.cmghjournal.org/article/S2352345X22002454/fulltext

302. Schneider CA, Rasband WS, Eliceiri KW. NIH Image to ImageJ: 25 years of image analysis. Nature Methods 2012 9:7. 2012 Jun 28;9(7):671–5.

303. Shields PL, Morland CM, Salmon M, Qin S, Hubscher SG, Adams DH. Chemokine and chemokine receptor interactions provide a mechanism for selective T cell recruitment to specific liver compartments within hepatitis C-infected liver. J Immunol. 1999 Dec 1;163(11):6236–43.

304. Schmittgen TD, Livak KJ. Analyzing real-time PCR data by the comparative CT method. Nature Protocols 2008 3:6. 2008 Jun 5;3(6):1101–8.

305. Jainarayanan AK, Capera J, Céspedes PF, Conceição M, Elanchezhian M, Thomas T, et al. Comparison of different methods for isolating CD8+ T lymphocyte-derived extracellular vesicles and supramolecular attack particles. Journal of Extracellular Biology [Internet]. 2023 Mar 1 [cited 2023 Apr 29];2(3):e74. Available from: https://onlinelibrary.wiley.com/doi/full/10.1002/jex2.74

306. Ovesný M, Křížek P, Borkovec J, Švindrych Z, Hagen GM. ThunderSTORM: A comprehensive ImageJ plug-in for PALM and STORM data analysis and super-resolution imaging. Bioinformatics. 2014 Aug 15;30(16):2389–90.

307. Ito Y, Sørensen KK, Bethea NW, Svistounov D, McCuskey MK, Smedsrød BH, et al. Age-related Changes in the Hepatic Microcirculation in Mice. Exp Gerontol. 2007 Aug;42(8):789.

308. Lalor PF, Edwards S, McNab G, Salmi M, Jalkanen S, Adams DH. Vascular adhesion protein-1 mediates adhesion and transmigration of lymphocytes on human hepatic endothelial cells. J Immunol [Internet]. 2002 Jul 15 [cited 2023 Apr 21];169(2):983–92. Available from: https://pubmed.ncbi.nlm.nih.gov/12097405/

309. Lisman T, Bongers TN, Adelmeijer J, Janssen HLA, De Maat MPM, De Groot PG, et al. Elevated levels of von Willebrand Factor in cirrhosis support platelet adhesion despite reduced functional capacity. Hepatology. 2006 Jul 1;44(1):53–61.

310. Carreira CM, Nasser SM, Tomaso D, Padera TP, Boucher Y, Tomarev SI, et al. LYVE-1 Is Not Restricted to the Lymph Vessels: Expression in Normal Liver Blood Sinusoids and Down-Regulation in Human Liver Cancer and Cirrhosis 1. 2001;

311. Scoazec J -Y, Feldmann G. In situ immunophenotyping study of endothelial cells of the human hepatic sinusoid: results and functional implications. Hepatology [Internet]. 1991 [cited 2023 Apr 21];14(5):789–97. Available from: https://pubmed.ncbi.nlm.nih.gov/1937383/

312. Dey P. Staining Principle and General Procedure of Staining of the Tissue. Basic and Advanced Laboratory Techniques in Histopathology and Cytology. 2018;57–67.

313. Fischer AH, Jacobson KA, Rose J, Zeller R. Hematoxylin and eosin staining of tissue and cell sections. CSH Protoc. 2008 May;2008(5).

314. Renshaw S. Immunohistochemistry and Immunocytochemistry. The Immunoassay Handbook. 2013 Jan 1;357–77.

315. Chan JKC. The wonderful colors of the hematoxylin-eosin stain in diagnostic surgical pathology. Int J Surg Pathol. 2014 Feb;22(1):12–32.

316. Kalof AN, Evans MF, Dantey K, Cooper K. Special Diagnostic Techniques in Surgical Pathology. Gattuso's Differential Diagnosis in Surgical Pathology. 2022 Jan 1;1–40.

317. Elvevold K, Smedsrod B, Martinez I. The liver sinusoidal endothelial cell: a cell type of controversial and confusing identity. AJP: Gastrointestinal and Liver Physiology. 2007;294(2):G391–400.

318. Bataller R, Brenner DA. Liver fibrosis. Journal of Clinical Investigation. 2005;115(2):209.

319. Schaffner F, Popper H. Capillarization of Hepatic Sinusoids in Man. Gastroenterology [Internet]. 1963 Mar 1 [cited 2022 Jan 24];44(3):239–42. Available from: http://www.gastrojournal.org/article/S0016508563801304/fulltext

320. Muro H, Shirasawa H, Kosugi I, Nakamura S. Defect of Fc receptors and phenotypical changes in sinusoidal endothelial cells in human liver cirrhosis. Am J Pathol [Internet]. 1993 [cited 2023 Apr 22];143(1):105. Available from: /pmc/articles/PMC1886954/?report=abstract

321. Pan J, Dinh TT, Rajaraman A, Lee M, Scholz A, Czupalla CJ, et al. Patterns of expression of factor VIII and von Willebrand factor by endothelial cell subsets in vivo. Blood. 2016 Jul 7;128(1):104–9.

322. Neubauer K, Wilfling T, Ritzel A, Ramadori G. Platelet-endothelial cell adhesion molecule-1 gene expression in liver sinusoidal endothelial cells during fiver injury and repair. J Hepatol [Internet]. 2000 Jun 1 [cited 2023 Apr 22];32(6):921–32. Available from: http://www.journal-of-hepatology.eu/article/S0168827800800963/fulltext

323. Poisson J, Lemoinne S, Boulanger C, Durand F, Moreau R, Valla D, et al. Liver sinusoidal endothelial cells: Physiology and role in liver diseases. J Hepatol. 2017;66(1):212–27.

324. Pusztaszeri MP, Seelentag W, Bosman FT. Immunohistochemical expression of endothelial markers CD31, CD34, von Willebrand factor, and Fli-1 in normal human tissues. J Histochem Cytochem [Internet]. 2006 Apr [cited 2023 Apr 22];54(4):385–95. Available from: https://pubmed.ncbi.nlm.nih.gov/16234507/

325. March S, Hui EE, Underhill GH, Khetani S, Bhatia SN. Microenvironmental Regulation of the Sinusoidal Endothelial Cell Phenotype In Vitro. Hepatology. 2009;50(3):920.

326. Su T, Yang Y, Lai S, Jeong J, Jung Y, McConnell M, et al. Single-Cell Transcriptomics Reveals Zone-Specific Alterations of Liver Sinusoidal Endothelial Cells in Cirrhosis. Cell Mol Gastroenterol Hepatol. 2021 Jan 1;11(4):1139–61.

327. Ishikawa T, Yokoyama H, Matsuura T, Fujiwara Y. Fc gamma RIIb expression levels in human liver sinusoidal endothelial cells during progression of non-alcoholic fatty liver disease. Wang Y, editor. PLoS One [Internet]. 2019 Jan 29 [cited 2020 Dec 30];14(1):e0211543. Available from: https://dx.plos.org/10.1371/journal.pone.0211543

328. LENZI R, ALPINI G, LIU MH, RAND JH, TAVOLONI N. Von Willebrand factor antigen is not an accurate marker of rat and guinea pig liver endothelial cells. Liver. 1990 Dec 1;10(6):372–9.

329. GW D, SA L, SW C, RA S, AH F, CA S, et al. Culture and characterization of sinusoidal endothelial cells isolated from human liver. In Vitro Cell Dev Biol Anim. 1998;34(5):370–7.

330. Fukuda Y, Nagura H, Imoto M, Koyama Y. Immunohistochemical Studies on Structural Changes of the Hepatic Lobules in Chronic Liver Diseases. Am J Gastroenterol. 1986;81(12):1149–56.

331. McLean AJ, Cogger VC, Chong GC, Warren A, Markus AMA, Dahlstrom JE, et al. Age-related pseudocapillarization of the human liver. J Pathol [Internet]. 2003 May 1 [cited 2023 Jan 14];200(1):112–7. Available from: https://onlinelibrary.wiley.com/doi/full/10.1002/path.1328

332. Maeso-Díaz R, Ortega-Ribera M, Fernández-Iglesias A, Hide D, Muñoz L, Hessheimer AJ, et al. Effects of aging on liver microcirculatory function and sinusoidal phenotype. Aging Cell [Internet]. 2018 Dec 1 [cited 2023 Apr 23];17(6). Available from: https://pubmed.ncbi.nlm.nih.gov/30260562/

333. Tokairin T, Nishikawa Y, Doi Y, Watanabe H, Yoshioka T, Su M, et al. A highly specific isolation of rat sinusoidal endothelial cells by the immunomagnetic bead method using SE-1 monoclonal antibody. J Hepatol. 2002 Jun 1;36(6):725–33.

334. DeLeve LD, Wang X, McCuskey MK, McCuskey RS. Rat liver endothelial cells isolated by anti-CD31 immunomagnetic separation lack fenestrae and sieve plates. Am J Physiol Gastrointest Liver Physiol [Internet]. 2006 Dec [cited 2022 Jan 25];291(6):1187–9. Available from: https://journals.physiology.org/doi/abs/10.1152/ajpgi.00229.2006

335. Onoe T, Ohdan H, Tokita D, Shishida M, Tanaka Y, Hara H, et al. Liver Sinusoidal Endothelial Cells Tolerize T Cells across MHC Barriers in Mice. The Journal of Immunology. 2005 Jul 1;175(1):139–46.

336. Lalor PF, Edwards S, McNab G, Salmi M, Jalkanen S, Adams DH. Vascular Adhesion Protein-1 Mediates Adhesion and Transmigration of Lymphocytes on Human Hepatic Endothelial Cells. The Journal of Immunology. 2002;169(2):983–92.

337. Bhandari S, Larsen AK, McCourt P, Smedsrød B, Sørensen KK. The Scavenger Function of Liver Sinusoidal Endothelial Cells in Health and Disease. Vol. 12, Frontiers in Physiology. Frontiers Media SA; 2021. p. 1711.

338. Blomhoff R, Eskild W, Berg T. Endocytosis of formaldehyde-treated serum albumin via scavenger pathway in liver endothelial cells. Biochemical Journal. 1984;218(1):81–6.

339. van der Zande HJP, Nitsche D, Schlautmann L, Guigas B, Burgdorf S. The Mannose Receptor: From Endocytic Receptor and Biomarker to Regulator of (Meta)Inflammation. Front Immunol. 2021 Oct 14;12:4274.

340. Weigel JA, Raymond RC, McGary C, Singh A, Weigel PH. A Blocking Antibody to the Hyaluronan Receptor for Endocytosis (HARE) Inhibits Hyaluronan Clearance by Perfused Liver *. Journal of Biological Chemistry. 2003 Mar 14;278(11):9808–12.

341. McGary CT, Raja RH, Weigel PH. Endocytosis of hyaluronic acid by rat liver endothelial cells. Evidence for receptor recycling. Biochemical Journal. 1989 Feb 2;257(3):875.

342. Laurent TC, Fraser JRE, Pertoft H, Smedsrod B. Binding of hyaluronate and chondroitin sulphate to liver endothelial cells. Biochemical Journal. 1986 Mar 3;234(3):653.

343. Malovic I, Sørensen KK, Elvevold KH, Nedredal GI, Paulsen S, Erofeev A V., et al. The mannose receptor on murine liver sinusoidal endothelial cells is the main denatured collagen clearance receptor. Hepatology [Internet]. 2007 Jun 1 [cited 2019 Jun 9];45(6):1454–61. Available from: http://doi.wiley.com/10.1002/hep.21639

344. Pöhlmann S, Soilleux EJ, Baribaud F, Leslie GJ, Morris LS, Trowsdale J, et al. DC-SIGNR, a DC-SIGN homologue expressed in endothelial cells, binds to human and simian immunodeficiency viruses and activates infection in trans. Proc Natl Acad Sci U S A. 2001 Feb 27;98(5):2670–5.

345. Le Couteur DG, Warren A, Cogger VC, Smedsrød B, Sørensen KK, De Cabo R, et al. Old age and the hepatic sinusoid. Anatomical Record. 2008 Jun 1;291(6):672–83.

346. Fraser R, Rogers GWT, Bowler LM, Day WA, Dobbs BR. Defenestration and vitamin A status in a rat model of cirrhosis. Cells of the hepatic sinusoid. 1991;3(January 1991):195–8.

347. Horn T, Christoffersen P, Henriksen JH. Alcoholic liver injury: Defenestration in noncirrhotic livers—a scanning electron microscopic study. Hepatology. 1987;7(1):77–82.

348. Clark SA, Bramwell Cook H, Oxner RBG, Angus HB, George PM, Fraser R. DEFENESTRATION OF HEPATIC SINUSOIDS AS A CAUSE OF HYPERLIPOPROTEINAEMIA IN ALCOHOLICS. The Lancet. 1988 Nov 26;332(8622):1225–7.

349. Pandey E, Nour AS, Harris EN. Prominent Receptors of Liver Sinusoidal Endothelial Cells in Liver Homeostasis and Disease [Internet]. Vol. 11, Frontiers in Physiology. Frontiers; 2020 [cited 2020 Jul 29]. p. 873. Available from: https://www.frontiersin.org/article/10.3389/fphys.2020.00873/full

350. Hernndezgea V, Ghiassinejad Z, Rozenfeld R, Gordon R, Fiel MI, Yue Z, et al. Autophagy Releases Lipid That Promotes Fibrogenesis by Activated Hepatic Stellate Cells in Mice and in Human Tissues. Gastroenterology [Internet]. 2012 [cited 2022 Oct 10];142(4):938. Available from: /pmc/articles/PMC3439519/

351. Thomas CM, Smart EJ. Caveolae structure and function. J Cell Mol Med. 2008 Jun;12(3):796.

352. Feron O, Belhassen L, Kobzik L, Smith TW, Kelly RA, Michel T. Endothelial Nitric Oxide Synthase Targeting to Caveolae. Journal of Biological Chemistry. 1996 Sep 13;271(37):22810–4.

353. García-Cardeña G, Oh P, Liu J, Schnitzer JE, Sessa WC. Targeting of nitric oxide synthase to endothelial cell caveolae via palmitoylation: Implications for nitric oxide signaling. Proc Natl Acad Sci U S A. 1996 Jun 25;93(13):6448–53.

354. Xie G, Wang X, Wang L, Wang L, Atkinson RD, Kanel GC, et al. Role of differentiation of liver sinusoidal endothelial cells in progression and regression of hepatic fibrosis in rats. Gastroenterology [Internet]. 2012;142(4):918-927.e6. Available from: http://dx.doi.org/10.1053/j.gastro.2011.12.017

355. DeLeve LD, Wang X, Hu L, McCuskey MK, McCuskey RS. Rat liver sinusoidal endothelial cell phenotype is maintained by paracrine and autocrine regulation. Am J Physiol Gastrointest Liver Physiol. 2004 Oct;287(4 50-4).

356. Elvevold K, Nedredal GI, Revhaug A, Bertheussen K, Smesrøø B. Long-term preservation of high endocytic activity in primary cultures of pig liver sinusoidal endothelial cells. Eur J Cell Biol. 2005 Sep 21;84(9):749–64.

357. Géraud C, Schledzewski K, Demory A, Klein D, Kaus M, Peyre F, et al. Liver sinusoidal endothelium: A microenvironment-dependent differentiation program in rat including the novel junctional protein liver endothelial differentiation-associated protein-1. Hepatology. 2010 Jul 1;52(1):313–26.

358. Bale SS, Golberg I, Jindal R, McCarty WJ, Luitje M, Hegde M, et al. Long-term coculture strategies for primary hepatocytes and liver sinusoidal endothelial cells. Tissue Eng Part C Methods. 2015 Apr 1;21(4):413–22.

359. Weigel JA, Raymond RC, McGary C, Singh A, Weigel PH. A blocking antibody to the hyaluronan receptor for endocytosis (HARE) inhibits hyaluronan clearance by perfused liver. J Biol Chem [Internet]. 2003 Mar 14 [cited 2023 Apr 24];278(11):9808–12. Available from: https://pubmed.ncbi.nlm.nih.gov/12645574/

360. Gudowska M, Gruszewska E, Panasiuk A, Cylwik B, Flisiak R, Świderska M, et al. Hyaluronic acid concentration in liver diseases. Clin Exp Med [Internet]. 2016 Nov 1 [cited 2023 Apr 24];16(4):523. Available from: /pmc/articles/PMC5063891/

361. Weigel PH, Yik JHN. Glycans as endocytosis signals: The cases of the asialoglycoprotein and hyaluronan/chondroitin sulfate receptors. Biochim Biophys Acta Gen Subj [Internet]. 2002 Sep 19 [cited 2023 Apr 24];1572(2–3):341–63. Available from: https://pubmed.ncbi.nlm.nih.gov/12223279/

362. Stahl PD, Ezekowitz RAB. The mannose receptor is a pattern recognition receptor involved in host defense. Curr Opin Immunol. 1998 Feb 1;10(1):50–5.

363. Gordon S. Pattern recognition receptors: Doubling up for the innate immune response. Cell [Internet]. 2002 Dec 27 [cited 2023 Apr 24];111(7):927–30. Available from: https://pubmed.ncbi.nlm.nih.gov/12507420/

364. Allavena P, Chieppa M, Monti P, Piemonti L. From pattern recognition receptor to regulator of homeostasis: the double-faced macrophage mannose receptor. Crit Rev Immunol [Internet]. 2004 [cited 2023 Apr 24];24(3):179–92. Available from: https://pubmed.ncbi.nlm.nih.gov/15482253/

365. Linehan SA, Martínez-Pomares L, Stahl PD, Gordon S. Mannose Receptor and Its Putative Ligands in Normal Murine Lymphoid and Nonlymphoid Organs: In Situ Expression of Mannose Receptor by Selected Macrophages, Endothelial Cells, Perivascular Microglia, and Mesangial Cells, but not Dendritic Cells. J Exp Med [Internet]. 1999 Jun 6 [cited 2023 Apr 24];189(12):1961. Available from: /pmc/articles/PMC2192961/

366. Sandahl TD, Støy SH, Laursen TL, Rødgaard-Hansen S, Møller HJ, Møller S, et al. The soluble mannose receptor (sMR) is elevated in alcoholic liver disease and associated with disease severity, portal hypertension, and mortality in cirrhosis patients. PLoS One [Internet]. 2017 Dec 1 [cited 2023 Apr 24];12(12):e0189345. Available from: https://journals.plos.org/plosone/article?id=10.1371/journal.pone.0189345

367. Kitadai Y, Kodama M, Cho S, Kuroda T, Ochiumi T, Kimura S, et al. Quantitative analysis of lymphangiogenic markers for predicting metastasis of human gastric carcinoma to lymph nodes. Int J Cancer [Internet]. 2005 Jun 20 [cited 2023 Apr 23];115(3):388–92. Available from: https://pubmed.ncbi.nlm.nih.gov/15688374/

368. Géraud C, Schledzewski K, Demory A, Klein D, Kaus M, Peyre F, et al. Liver sinusoidal endothelium: A microenvironment-dependent differentiation program in rat including the novel junctional protein liver endothelial differentiation-associated protein-1. Hepatology [Internet]. 2010 Jul 1 [cited 2022 Jul 31];52(1):313–26. Available from: https://onlinelibrary.wiley.com/doi/full/10.1002/hep.23618

369. OTAKA F, ITO Y, GOTO T, KOJO K, TANABE M, HOSONO K, et al. Recovery of Liver Sinusoidal Endothelial Cells Following Monocrotaline-induced Liver Injury. In Vivo (Brooklyn) [Internet]. 2021 Aug 17 [cited 2023 Apr 24];35(5):2577. Available from: /pmc/articles/PMC8408714/

370. Ramachandran P, Dobie R, Wilson-Kanamori JR, Dora EF, Henderson BEP, Luu NT, et al. Resolving the fibrotic niche of human liver cirrhosis at single-cell level. Nature [Internet]. 2019 Nov 9 [cited 2020 Jan 10];575(7783):512–8. Available from: http://www.nature.com/articles/s41586-019-1631-3

371. Febbraio M, Hajjar DP, Silverstein RL. CD36: a class B scavenger receptor involved in angiogenesis, atherosclerosis, inflammation, and lipid metabolism. Journal of Clinical Investigation [Internet]. 2001 Sep 9 [cited 2023 Apr 24];108(6):785. Available from: /pmc/articles/PMC200943/

372. Sheedfar F, Sung MMY, Aparicio-Vergara M, Kloosterhuis NJ, Miquilena-Colina ME, Vargas-Castrillón J, et al. Increased hepatic CD36 expression with age is associated with enhanced susceptibility to nonalcoholic fatty liver disease. Aging [Internet]. 2014 Apr 9 [cited 2023 Apr 24];6(4):281–95. Available from: https://www.aging-us.com/article/100652

373. Karsdal MA, Daniels SJ, Holm Nielsen S, Bager C, Rasmussen DGK, Loomba R, et al. Collagen biology and non-invasive biomarkers of liver fibrosis. Liver International. 2020 Apr 1;40(4):736–50.

374. Karsdal MA, Daniels SJ, Holm Nielsen S, Bager C, Rasmussen DGK, Loomba R, et al. Collagen biology and non-invasive biomarkers of liver fibrosis. Liver International [Internet]. 2020 Apr 1 [cited 2023 Apr 25];40(4):736–50. Available from: https://onlinelibrary.wiley.com/doi/full/10.1111/liv.14390

375. Baiocchini A, Montaldo C, Conigliaro A, Grimaldi A, Correani V, Mura F, et al. Extracellular Matrix Molecular Remodeling in Human Liver Fibrosis Evolution. PLoS One [Internet]. 2016 Mar 1 [cited 2023 Apr 25];11(3):e0151736. Available from: https://journals.plos.org/plosone/article?id=10.1371/journal.pone.0151736

376. Privratsky JR, Newman DK, Newman PJ. PECAM-1: conflicts of interest in inflammation. Life Sci [Internet]. 2010 Jul [cited 2023 Apr 25];87(3–4):69–82. Available from: https://pubmed.ncbi.nlm.nih.gov/20541560/

377. Liu L, Tsai JC, Aird WC. Egr-1 gene is induced by the systemic administration of the vascular endothelial growth factor and the epidermal growth factor. Blood. 2000 Sep 1;96(5):1772–81.

378. Couvelard A, Scoazec JY, Feldmann G. Expression of cell-cell and cell-matrix adhesion proteins by sinusoidal endothelial cells in the normal and cirrhotic human liver. Am J Pathol [Internet]. 1993 [cited 2023 Apr 25];143(3):738. Available from: /pmc/articles/PMC1887198/?report=abstract

379. DeLeve LD, Maretti-Mira AC. Liver Sinusoidal Endothelial Cell: An Update. Semin Liver Dis [Internet]. 2017 Nov 1 [cited 2023 Apr 8];37(4):377. Available from: /pmc/articles/PMC6005648/

380. Winkler M, Staniczek T, Kürschner SW, Schmid CD, Schönhaber H, Cordero J, et al. Endothelial GATA4 controls liver fibrosis and regeneration by preventing a pathogenic switch in angiocrine signaling. J Hepatol [Internet]. 2021 Feb 1 [cited 2023 Apr 25];74(2):380–93. Available from: https://pubmed.ncbi.nlm.nih.gov/32916216/

381. Arroyo N, Villamayor L, Díaz I, Carmona R, Ramos-Rodríguez M, Muñoz-Chápuli R, et al. GATA4 induces liver fibrosis regression by deactivating hepatic stellate cells. JCI Insight [Internet]. 2021 Dec 12 [cited 2023 Apr 25];6(23). Available from: /pmc/articles/PMC8675192/

382. Sakhuja P. Pathology of alcoholic liver disease, can it be differentiated from nonalcoholic steatohepatitis? World Journal of Gastroenterology : WJG [Internet]. 2014 Nov 11 [cited 2023 Apr 25];20(44):16474. Available from: /pmc/articles/PMC4248190/

383. Bideyan L, Rodríguez ML, Priest C, Kennelly JP, Gao Y, Ferrari A, et al. Hepatic GATA4 regulates cholesterol and triglyceride homeostasis in collaboration with LXRs. Genes Dev [Internet]. 2022 Nov 1 [cited 2023 Apr 25];36(21–24):1129–44. Available from: http://genesdev.cshlp.org/content/36/21-24/1129.full

384. Fernandez-Rojo MA, Ramm GA. Caveolin-1 Function in Liver Physiology and Disease. Trends Mol Med. 2016 Oct 1;22(10):889–904.

385. Mookerjee RP, Wiesenthal A, Icking A, Hodges SJ, Davies NA, Schilling K, et al. Increased Gene and Protein Expression of the Novel eNOS Regulatory Protein NOSTRIN and a Variant in Alcoholic Hepatitis. Gastroenterology. 2007 Jun 1;132(7):2533–41.

386. Goh BJ, Tan BT, Hon WM, Lee KH, Khoo HE. Nitric oxide synthase and heme oxygenase expressions in human liver cirrhosis. World J Gastroenterol [Internet]. 2006 Jan 28 [cited 2023 Apr 25];12(4):588–94. Available from: https://www.wjgnet.com/1007-9327/full/v12/i4/588.htm

387. Yu S, Matsusue K, Kashireddy P, Cao WQ, Yeldandi V, Yeldandi A V., et al. Adipocyte-specific Gene Expression and Adipogenic Steatosis in the Mouse Liver Due to Peroxisome Proliferator-activated Receptor γ1 (PPARγ1) Overexpression. Journal of Biological Chemistry. 2003 Jan 3;278(1):498–505.

388. Heiss EH, Dirsch VM. Regulation of eNOS Enzyme Activity by Posttranslational Modification. Curr Pharm Des [Internet]. 2014 Jun 13 [cited 2023 Apr 25];20(22):3503. Available from: /pmc/articles/PMC4401012/

389. Su Y. Regulation of Endothelial Nitric oxide Synthase Activity by Protein-Protein Interaction. Curr Pharm Des [Internet]. 2014 Jun 13 [cited 2023 Apr 25];20(22):3514. Available from: /pmc/articles/PMC7039309/

390. Zapotoczny B, Szafranska K, Kus E, Braet F, Wisse E, Chlopicki S, et al. Tracking Fenestrae Dynamics in Live Murine Liver Sinusoidal Endothelial Cells. Hepatology. 2019;69(2):876–88.

391. Mousavi SA, Skjeldal F, Fønhus MS, Haugen LH, Eskild W, Berg T, et al. Receptor-Mediated Endocytosis of VEGF-A in Rat Liver Sinusoidal Endothelial Cells. Biomed Res Int. 2019;2019.

392. Mochida S, Ishikawa K, Inao M, Shibuya M, Fujiwara K. Increased Expressions of Vascular Endothelial Growth Factor and Its Receptors,flt-1 andKDR/flk-1, in Regenerating Rat Liver. Biochem Biophys Res Commun. 1996 Sep 4;226(1):176–9.

393. Bravo M, Raurell I, Hide D, Fernández-Iglesias A, Gil M, Barberá A, et al. Restoration of liver sinusoidal cell phenotypes by statins improves portal hypertension and histology in rats with NASH. Sci Rep. 2019 Dec 1;9(1).

394. Miyao M, Kotani H, Ishida T, Kawai C, Manabe S, Abiru H, et al. Pivotal role of liver sinusoidal endothelial cells in NAFLD/NASH progression. Laboratory Investigation 2015 95:10. 2015 Jul 27;95(10):1130–44.

395. Le Couteur DG, Fraser R, Cogger VC, McLean AJ. Hepatic pseudocapillarisation and atherosclerosis in ageing. Lancet. 2002 May 4;359(9317):1612–5.

396. Herrmann HC, Chang G, Klugherz BD, Mahoney PD. Hemodynamic Effects of Sildenafil in Men with Severe Coronary Artery Disease. New England Journal of Medicine. 2000;342(22):1622–6.

397. Schalcher C, Schad K, Brunner-La Rocca HP, Schindler R, Oechslin E, Scharf C, et al. Interaction of sildenafil with cAMP-mediated vasodilation in vivo. Hypertension [Internet]. 2002 Nov 1 [cited 2022 Apr 7];40(5):763–7. Available from: https://www.ahajournals.org/doi/abs/10.1161/01.HYP.0000036027.71527.3E

398. Yaguas K, Bautista R, Quiroz Y, Ferrebuz A, Pons H, Franco M, et al. Chronic sildenafil treatment corrects endothelial dysfunction and improves hypertension. Am J Nephrol [Internet]. 2010 Apr [cited 2023 Apr 14];31(4):283–91. Available from: https://www.karger.com/Article/FullText/279307

399. Carpenter B, Lin Y, Stoll S, Raffai RL, McCuskey R, Wang R. VEGF is crucial for the hepatic vascular development required for lipoprotein uptake. Development. 2005 Jul 15;132(14):3293–303.

400. Cyr AR, Huckaby L V., Shiva SS, Zuckerbraun BS. Nitric Oxide and Endothelial Dysfunction. Vol. 36, Critical Care Clinics. W.B. Saunders; 2020. p. 307–21.

401. Chen J, Braet F, Brodsky S, Weinstein T, Romanov V, Noiri E, et al. VEGF-induced mobilization of caveolae and increase in permeability of endothelial cells. Am J Physiol Cell Physiol. 2002;282(5 51-5).

402. Akaike T, Okamoto S, Sawa T, Yoshitake J, Tamura F, Ichimori K, et al. 8-Nitroguanosine formation in viral pneumonia and its implication for pathogenesis. Proc Natl Acad Sci U S A. 2003 Jan 1;100(2):685.

403. Terasaki Y, Akuta T, Terasaki M, Sawa T, Mori T, Okamoto T, et al. Guanine nitration in idiopathic pulmonary fibrosis and its implication for carcinogenesis. Am J Respir Crit Care Med. 2006;174(6):665–73.

404. Tateya S, Rizzo NO, Handa P, Cheng AM, Morgan-Stevenson V, Daum G, et al. Endothelial NO/cGMP/VASP Signaling Attenuates Kupffer Cell Activation and Hepatic Insulin Resistance Induced by High-Fat Feeding. Diabetes [Internet]. 2011 Nov 1 [cited 2022 Jun 21];60(11):2792–801. Available from: https://diabetesjournals.org/diabetes/article/60/11/2792/33448/Endothelial-NO-cGMP-VASP-Signaling-Attenuates

405. Iwakiri Y. Endothelial dysfunction in the regulation of cirrhosis and portal hypertension [Internet]. Vol. 32, Liver International. NIH Public Access; 2012 [cited 2022 Jul 28]. p. 199–213. Available from: /pmc/articles/PMC3676636/

406. Kim F, Pham M, Luttrell I, Bannerman DD, Tupper J, Thaler J, et al. Toll-like receptor-4 mediates vascular inflammation and insulin resistance in diet-induced obesity. Circ Res [Internet]. 2007 Jun [cited 2023 Apr 26];100(11):1589–96. Available from: https://pubmed.ncbi.nlm.nih.gov/17478729/

407. How and when to take sildenafil - NHS [Internet]. [cited 2023 Apr 26]. Available from: https://www.nhs.uk/medicines/sildenafil-viagra/how-and-when-to-take-sildenafil/

408. Harris EN, Cabral F. Ligand binding and signaling of HARE/Stabilin-2. Biomolecules. 2019 Jul 1;9(7).

409. Fraser JRE, Laurent TC, Pertoft H, Baxter E. Plasma clearance, tissue distribution and metabolism of hyaluronic acid injected intravenously in the rabbit. Biochemical Journal. 1981 Nov 15;200(2):415–24.

410. Jung MY, Park SY, Kim IS. Stabilin-2 is involved in lymphocyte adhesion to the hepatic sinusoidal endothelium via the interaction with αMβ2 integrin. J Leukoc Biol. 2007 Nov;82(5):1156–65.

411. Pandey MS, Baggenstoss BA, Washburn J, Harris EN, Weigel PH. The hyaluronan receptor for endocytosis (HARE) activates NF-κB-mediated gene expression in response to 40-400-kDa, but not smaller or larger, hyaluronans. J Biol Chem [Internet]. 2013 May 17 [cited 2023 Apr 26];288(20):14068–79. Available from: https://pubmed.ncbi.nlm.nih.gov/23530033/

412. Luedde T, Schwabe RF. NF-κB in the liver—linking injury, fibrosis and hepatocellular carcinoma. Nat Rev Gastroenterol Hepatol [Internet]. 2011 Feb [cited 2023 Apr 26];8(2):108. Available from: /pmc/articles/PMC3295539/

413. Elvevold K, Simon-Santamaria J, Hasvold H, McCourt P, Smedsrød B, Sørensen KK. Liver sinusoidal endothelial cells depend on mannose receptor-mediated recruitment of lysosomal enzymes for normal degradation capacity. Hepatology. 2008;48(6):2007–15.

414. Gazi U, Martinez-Pomares L. Influence of the mannose receptor in host immune responses. Immunobiology. 2009 Jul 1;214(7):554–61.

415. Stahl PD, Ezekowitz RAB. The mannose receptor is a pattern recognition receptor involved in host defense. Curr Opin Immunol. 1998;10(1):50–5.

416. Longoni D, Piemonti L, Bernasconi S, Mantovani A, Allavena P. Interleukin-10 increases mannose receptor expression and endocytic activity in monocyte-derived dendritic cells. Int J Clin Lab Res [Internet]. 1998 Sep [cited 2023 Apr 26];28(3):162–9. Available from: https://link.springer.com/article/10.1007/s005990050037

417. Shepherd VL, Abdolrasulnia R, Garrett M, Cowan HB. Down-regulation of mannose receptor activity in macrophages after treatment with lipopolysaccharide and phorbol esters. The Journal of Immunology [Internet]. 1990 Sep 1 [cited 2023 Apr 26];145(5):1530–6. Available from: https://journals.aai.org/jimmunol/article/145/5/1530/23068/Down-regulation-of-mannose-receptor-activity-in

418. Fleming I, Fisslthaler B, Dixit M, Busse R. Role of PECAM-1 in the shear-stress-induced activation of Akt and the endothelial nitric oxide synthase (eNOS) in endothelial cells. J Cell Sci. 2005;118:4103–11.

419. Mulhall JP, Müller A, Donohue JF, Mullerad M, Kobylarz K, Paduch DA, et al. The Functional and Structural Consequences of Cavernous Nerve Injury are Ameliorated by Sildenafil Citrate. J Sex Med [Internet]. 2008 May 1 [cited 2023 Apr 27];5(5):1126–36. Available from: https://academic.oup.com/jsm/article/5/5/1126/6862186

420. Gao L, Zhou Y, Zhong W, Zhao X, Chen C, Chen X, et al. Caveolin-1 is essential for protecting against binge drinking-induced liver damage through inhibiting reactive nitrogen species. Hepatology. 2014;60(2):687–99.

421. Wang X, Abdel-Rahman AA. Effect of chronic ethanol administration on hepatic eNOS activity and its association with caveolin-1 and calmodulin in female rats. Am J Physiol Gastrointest Liver Physiol [Internet]. 2005 Sep [cited 2023 Apr 27];289(3). Available from: https://pubmed.ncbi.nlm.nih.gov/15845868/

422. Arnal JF, Yamin J, Dockery S, Harrison DG. Regulation of endothelial nitric oxide synthase mRNA, protein, and activity during cell growth. https://doi.org/101152/ajpcell19942675C1381. 1994;267(5 36-5).

423. Dimmeler S, Fleming I, Fisslthaler B, Hermann C, Busse R, Zeiher AM. Activation of nitric oxide synthase in endothelial cells by Akt-dependent phosphorylation. Nature 1999 399:6736. 1999 Jun 10;399(6736):601–5.

424. Searles CD, Ide L, Davis ME, Cai H, Weber M. Actin cytoskeleton organization and posttranscriptional regulation of endothelial nitric oxide synthase during cell growth. Circ Res. 2004 Sep 3;95(5):488–95.

425. Förstermann U, Sessa WC. Nitric oxide synthases: regulation and function. Eur Heart J. 2012 Apr;33(7).

426. Hurshman AR, Marletta MA. Nitric Oxide Complexes of Inducible Nitric Oxide Synthase: Spectral Characterization and Effect on Catalytic Activity. Biochemistry. 1995;34(16):5627–34.

427. Henry Y, Lepoivre M, Drapier JC, Boucher JL, Guissani' A. EPR characterization of molecular targets for NO in mammalian cells and organelles; EPR characterization of molecular targets for NO in mammalian cells and organelles.

428. Carnovale CE, Ronco MT. Role of nitric oxide in liver regeneration. Ann Hepatol. 2012 Sep 1;11(5):636–47.

429. Abu-Amara M, Yang SY, Seifalian A, Davidson B, Fuller B. The nitric oxide pathway – evidence and mechanisms for protection against liver ischaemia reperfusion injury. Liver International. 2012 Apr 1;32(4):531–43.

430. Abdelmegeed MA, Song BJ. Functional Roles of Protein Nitration in Acute and Chronic Liver Diseases. Oxid Med Cell Longev. 2014;2014.

431. Ambati BK, Nozaki M, Singh N, Takeda A, Jani PD, Suthar T, et al. Corneal avascularity is due to soluble VEGF receptor-1. Nature [Internet]. 2006 Oct 10 [cited 2023 Apr 26];443(7114):993. Available from: /pmc/articles/PMC2656128/

432. Yang Y, Xie P, Opatowsky Y, Schlessinger J. Direct contacts between extracellular membrane-proximal domains are required for VEGF receptor activation and cell signaling. Proc Natl Acad Sci U S A [Internet]. 2010 Feb 2 [cited 2023 Apr 26];107(5):1906. Available from: /pmc/articles/PMC2836632/

433. Takahashi T, Yamaguchi S, Chida K, Shibuya M. A single autophosphorylation site on KDR/Flk-1 is essential for VEGF-A-dependent activation of PLC-γ and DNA synthesis in vascular endothelial cells. EMBO J [Internet]. 2001 Jun 6 [cited 2023 Apr 26];20(11):2768. Available from: /pmc/articles/PMC125481/

434. Ito N, Wernstedt C, Engström U, Claesson-Welsh L. Identification of vascular endothelial growth factor receptor-1 tyrosine phosphorylation sites and binding of SH2 domain-containing molecules. J Biol Chem [Internet]. 1998 Sep 4 [cited 2023 Apr 26];273(36):23410–8. Available from: https://pubmed.ncbi.nlm.nih.gov/9722576/

435. Fong GH, Rossant J, Gertsenstein M, Breitman ML. Role of the Flt-1 receptor tyrosine kinase in regulating the assembly of vascular endothelium. Nature [Internet]. 1995 Jul 6 [cited 2023 Apr 26];376(6535):66–70. Available from: https://pubmed.ncbi.nlm.nih.gov/7596436/

436. Watt AJ, Zhao R, Li J, Duncan SA. Development of the mammalian liver and ventral pancreas is dependent on GATA4. BMC Dev Biol [Internet]. 2007 [cited 2023 Apr 26];7. Available from: https://pubmed.ncbi.nlm.nih.gov/17451603/

437. Zhao R, Watt AJ, Li J, Luebke-Wheeler J, Morrisey EE, Duncan SA. GATA6 is essential for embryonic development of the liver but dispensable for early heart formation. Mol Cell Biol. 2005 Apr;25(7):2622–31.

438. Suzuki YJ. Cell signaling pathways for the regulation of GATA4 transcription factor: Implications for cell growth and apoptosis. Vol. 23, Cellular Signalling. 2011. p. 1094–9.

439. Suzuki YJ, Nagase H, Day RM, Das DK. GATA-4 regulation of myocardial survival in the preconditioned heart. J Mol Cell Cardiol [Internet]. 2004 [cited 2023 Apr 26];37(6):1195–203. Available from: https://pubmed.ncbi.nlm.nih.gov/15572049/

440. Iwakiri Y, Shah V, Rockey DC. Vascular pathobiology in chronic liver disease and cirrhosis – Current status and future directions. J Hepatol. 2014 Oct 1;61(4):912–24.

441. Khoo JP, Alp NJ, Bendall JK, Kawashima S, Yokoyama M, Zhang YH, et al. EPR quantification of vascular nitric oxide production in genetically modified mouse models. Nitric Oxide [Internet]. 2004 May [cited 2023 Apr 26];10(3):156–61. Available from: https://pubmed.ncbi.nlm.nih.gov/15158695/

442. Kim F, Pham M, Maloney E, Rizzo NO, Morton GJ, Wisse BE, et al. Vascular inflammation, insulin resistance, and reduced nitric oxide production precede the onset of peripheral insulin resistance. Arterioscler Thromb Vasc Biol [Internet]. 2008 Nov [cited 2023 Apr 26];28(11):1982–8. Available from: https://pubmed.ncbi.nlm.nih.gov/18772497/

443. Cogger VC, Hunt NJ, Couteur DG Le. Fenestrations in the Liver Sinusoidal Endothelial Cell. The Liver. 2020 Feb 12;435–43.

444. Braet F, Kalle WHJ, De Zanger RB, De Grooth BG, Raap AK, Tanke HJ, et al. Comparative atomic force and scanning electron microscopy: an investigation on fenestrated endothelial cells in vitro. J Microsc [Internet]. 1996 Jan 1 [cited 2023 Apr 14];181(1):10–7. Available from: https://onlinelibrary.wiley.com/doi/full/10.1046/j.1365-2818.1996.72348.x

445. Zapotoczny B, Szafranska K, Owczarczyk K, Kus E, Chlopicki S, Szymonski M. Atomic Force Microscopy Reveals the Dynamic Morphology of Fenestrations in Live Liver Sinusoidal Endothelial Cells. Sci Rep [Internet]. 2017;7(1):1–6. Available from: http://dx.doi.org/10.1038/s41598-017-08555-0

446. Mori T, Okanoue T, Sawa Y, Hori N, Ohta M, Kagawa K. Defenestration of the sinusoidal endothelial cell in a rat model of cirrhosis. Hepatology [Internet]. 1993 May 1 [cited 2023 Apr 10];17(5):891–7. Available from: https://onlinelibrary.wiley.com/doi/full/10.1002/hep.1840170520

447. Braet F, Muller M, Vekemans K, Wisse E, Le Couteur DG. Antimycin A–induced defenestration in rat hepatic sinusoidal endothelial cells. Hepatology [Internet]. 2003 Aug 1 [cited 2023 Apr 10];38(2):394–402. Available from: https://onlinelibrary.wiley.com/doi/full/10.1053/jhep.2003.50347

448. HORN T, HENRIKSEN JH, CHRISTOFFERSEN P. The sinusoidal lining cells in “normal” human liver. A scanning electron microscopic investigation. Liver [Internet]. 1986 [cited 2022 Feb 24];6(2):98–110. Available from: https://pubmed.ncbi.nlm.nih.gov/3736357/

449. Braet F, Bomans PHH, Wisse E, Frederik PM. The observation of intact hepatic endothelial cells by cryo-electron microscopy. J Microsc. 2003;212(2):175–85.

450. Ito T, Shibasaki S. Electron Microscopic Study on the Hepatic Sinusoidal Wall and the Fat-Storing Cells in the Normal Human Liver. Archivum histologicum japonicum. 1968;29(2):137–92.

451. Baiocchini A, Nonno F Del, Taibi C, Visco-Comandini U, D’Offizi G, Piacentini M, et al. Liver sinusoidal endothelial cells (LSECs) modifications in patients with chronic hepatitis C. Scientific Reports 2019 9:1 [Internet]. 2019 Jun 19 [cited 2023 Apr 10];9(1):1–10. Available from: https://www.nature.com/articles/s41598-019-45114-1

452. Horn T, Christoffersen P, Henriksen JH. Alcoholic liver injury: Defenestration in noncirrhotic livers—a scanning electron microscopic study. Hepatology. 1987;7(1):77–82.

453. Szafranska K, Neuman T, Baster Z, Rajfur Z, Szelest O, Holte C, et al. From fixed-dried to wet-fixed to live - Comparative super-resolution microscopy of liver sinusoidal endothelial cell fenestrations. Nanophotonics [Internet]. 2022 Apr 20 [cited 2022 May 3];11(10):2253–70. Available from: https://www.degruyter.com/document/doi/10.1515/nanoph-2021-0818/html

454. Stefan W. Hell. Far-Field Optical Nanoscopy. Science (1979). 2007;316(5828):1153–8.

455. Wichmann J, Hell SW. Breaking the diffraction resolution limit by stimulated emission: stimulated-emission-depletion fluorescence microscopy. Optics Letters, Vol 19, Issue 11, pp 780-782. 1994 Jun 1;19(11):780–2.

456. Betzig E, Patterson GH, Sougrat R, Lindwasser OW, Olenych S, Bonifacino JS, et al. Imaging intracellular fluorescent proteins at nanometer resolution. Science (1979). 2006 Sep 15;313(5793):1642–5.

457. Valli J, Garcia-Burgos A, Rooney LM, de Melo e Oliveira BV, Duncan RR, Rickman C. Seeing beyond the limit: A guide to choosing the right super-resolution microscopy technique. Journal of Biological Chemistry. 2021 Jul 1;297(1):100791.

458. Martino J Di, Mascalchi P, Legros P, Lacomme S, Gontier E, Bioulac-Sage P, et al. STED microscopy: A simplified method for liver sinusoidal endothelial fenestrae analysis. Biol Cell. 2018 Jul 1;110(7):159–68.

459. Øie CI, Mönkemöller V, Hübner W, Schüttpelz M, Mao H, Ahluwalia BS, et al. New ways of looking at very small holes - Using optical nanoscopy to visualize liver sinusoidal endothelial cell fenestrations. Nanophotonics. 2018;7(3):575–96.

460. Zapotoczny B, Szafranska K, Kus E, Braet F, Wisse E, Chlopicki S, et al. Tracking Fenestrae Dynamics in Live Murine Liver Sinusoidal Endothelial Cells. Hepatology. 2019 Feb 1;69(2):876–88.

461. Braet F, Riches J, Geerts W, Jahn KA, Wisse E, Frederik P. Three-dimensional organization of fenestrae labyrinths in liver sinusoidal endothelial cells. Liver International [Internet]. 2009 [cited 2023 Feb 17];29(4):603–13. Available from: https://pubmed.ncbi.nlm.nih.gov/18662275/

462. Wisse E, Braet F, Luo D, De Zanger R, Jans D, Crabbé E, et al. Structure and function of sinusoidal lining cells in the liver. Toxicol Pathol. 1996;24(1):100–11.

463. Le Couteur DG, Fraser R, Hilmer S, Rivory LP, McLean AJ. The hepatic sinusoid in aging and cirrhosis: effects on hepatic substrate disposition and drug clearance. Clin Pharmacokinet [Internet]. 2005 [cited 2023 Apr 29];44(2):187–200. Available from: https://pubmed.ncbi.nlm.nih.gov/15656697/

464. Mitchell SJ, Huizer-Pajkos A, Cogger VC, McLachlan AJ, Le Couteur DG, Jones B, et al. Age-Related Pseudocapillarization of the Liver Sinusoidal Endothelium Impairs the Hepatic Clearance of Acetaminophen in Rats. J Gerontol A Biol Sci Med Sci [Internet]. 2011 Apr [cited 2023 Apr 29];66A(4):400. Available from: /pmc/articles/PMC3055277/

465. Mao H, Diekmann R, Liang HPH, Cogger VC, Le Couteur DG, Lockwood GP, et al. Cost-efficient nanoscopy reveals nanoscale architecture of liver cells and platelets. Nanophotonics [Internet]. 2019 Jul 1 [cited 2023 Apr 11];8(7):1299–313. Available from: https://www.degruyter.com/document/doi/10.1515/nanoph-2019-0066/html

466. Webb DJ, Freestone S, Allen MJ, Muirhead GJ. Sildenafil citrate and blood-pressure-lowering drugs: Results of drug interaction studies with an organic nitrate and a calcium antagonist. American Journal of Cardiology [Internet]. 1999 Mar 4 [cited 2023 Apr 15];83(5 A):21–8. Available from: http://www.ajconline.org/article/S0002914999000442/fulltext

467. Stull JT, Tansey MG, Tang DC, Word RA, Kamm KE. Phosphorylation of myosin light chain kinase: a cellular mechanism for Ca2+ desensitization. Mol Cell Biochem [Internet]. 1993 Nov [cited 2023 Apr 15];127–128(1):229–37. Available from: https://pubmed.ncbi.nlm.nih.gov/7935354/

468. Francis SH, Busch JL, Corbin JD. cGMP-dependent protein kinases and cGMP phosphodiesterases in nitric oxide and cGMP action. Vol. 62, Pharmacological Reviews. American Society for Pharmacology and Experimental Therapeutics; 2010. p. 525–63.

469. Rigor RR, Shen Q, Pivetti CD, Wu MH, Yuan SY. Myosin light chain kinase signaling in endothelial barrier dysfunction. Med Res Rev. 2013 Sep;33(5):911–33.

470. Deleve LD. Liver Sinusoidal Endothelial Cells in Hepatic Fibrosis. Hepatology. 2015 May 1;61(5):1740.

471. Szafranska K, Kruse LD, Holte CF, McCourt P, Zapotoczny B. The wHole Story About Fenestrations in LSEC. Vol. 12, Frontiers in Physiology. Frontiers; 2021. p. 1468.

472. Balarini CM, Leal MA, Gomes IBS, Pereira TMC, Gava AL, Meyrelles SS, et al. Sildenafil restores endothelial function in the apolipoprotein E knockout mouse. J Transl Med. 2013 Jan 5;11(1):3.

473. Halcox JPJ, Nour KRA, Zalos G, Mincemoyer R, Waclawiw MA, Rivera CE, et al. The effect of sildenafil on human vascular function, platelet activation, and myocardial ischemia. J Am Coll Cardiol [Internet]. 2002 Oct 2 [cited 2023 Apr 16];40(7):1232–40. Available from: https://pubmed.ncbi.nlm.nih.gov/12383570/

474. Klein T, Löschberger A, Proppert S, Wolter S, Van De Linde S, Sauer M. Live-cell dSTORM with SNAP-tag fusion proteins. Nature Methods 2011 8:1. 2010 Dec 29;8(1):7–9.

475. Jones SA, Shim SH, He J, Zhuang X. Fast three-dimensional super-resolution imaging of live cells. Nat Methods. 2011 Jun;8(6):499.

476. van de Linde S, Sauer M, Heilemann M. Subdiffraction-resolution fluorescence imaging of proteins in the mitochondrial inner membrane with photoswitchable fluorophores. J Struct Biol. 2008 Dec;164(3):250–4.

477. Richter KN, Revelo NH, Seitz KJ, Helm MS, Sarkar D, Saleeb RS, et al. Glyoxal as an alternative fixative to formaldehyde in immunostaining and super-resolution microscopy. EMBO J. 2018 Jan 4;37(1):139–59.

478. Loqman MY, Bush PG, Farquharson C, Hall AC. A cell shrinkage artefact in growth plate chondrocytes with common fixative solutions: importance of fixative osmolarity for maintaining morphology. Eur Cell Mater. 2010;19:214–27.

479. Szafranska K, Holte CF, Kruse LD, Mao H, Øie CI, Szymonski M, et al. Quantitative analysis methods for studying fenestrations in liver sinusoidal endothelial cells. A comparative study. Micron. 2021 Jul 28;103121.

480. Braet F, De Zanger R, Sasaoki T, Baekeland M, Janssens P, Smedsrod B, et al. Assessment of a method of isolation, purification, and cultivation of rat liver sinusoidal endothelial cells. Lab Invest [Internet]. 1994 Jun 1 [cited 2023 Apr 14];70(6):944–52. Available from: https://europepmc.org/article/med/8015298

481. Gatmaitan Z, Varticovski L, Ling L, Mikkelsen R, Steffan AM, Arias IM. Studies on fenestral contraction in rat liver endothelial cells in culture. Am J Pathol. 1996 Jun;148(6):2027.

482. Xu B, Broome U, Uzunel M, Nava S, Ge X, Kumagai-Braesch M, et al. Capillarization of Hepatic Sinusoid by Liver Endothelial Cell-Reactive Autoantibodies in Patients with Cirrhosis and Chronic Hepatitis. Am J Pathol [Internet]. 2003 Oct 1 [cited 2023 Apr 25];163(4):1275. Available from: /pmc/articles/PMC1868294/

483. Colak Y, Senates E, Ozturk O, Yilmaz Y, Coskunpinar E, Kahraman OT, et al. Plasma fibrinogen-like protein 2 levels in patients with non-alcoholic fatty liver disease. Hepatogastroenterology [Internet]. 2011 Nov [cited 2023 Oct 21];58(112):2087–90. Available from: https://pubmed.ncbi.nlm.nih.gov/22024080/

484. De Franchis R, Primignani M. NATURAL HISTORY OF PORTAL HYPERTENSION IN PATIENTS WITH CIRRHOSIS. Clin Liver Dis. 2001 Aug 1;5(3):645–63.

485. Bosch J, Groszmann RJ, Shah VH. Evolution in the understanding of the pathophysiological basis of portal hypertension: How changes in paradigm are leading to successful new treatments. J Hepatol [Internet]. 2015 [cited 2023 Oct 20];62(1 Suppl):S121–30. Available from: https://pubmed.ncbi.nlm.nih.gov/25920081/

486. Gunarathne LS, Rajapaksha H, Shackel N, Angus PW, Herath CB. Cirrhotic portal hypertension: From pathophysiology to novel therapeutics. http://www.wjgnet.com/ [Internet]. 2020 Oct 28 [cited 2023 Oct 20];26(40):6111–40. Available from: https://www.wjgnet.com/1007-9327/full/v26/i40/6111.htm

487. Lee KC, Yang YY, Wang YW, Hou MC, Lee FY, Lin HC, et al. Acute administration of sildenafil enhances hepatic cyclic guanosine monophosphate production and reduces hepatic sinusoid resistance in cirrhotic patients. Hepatology Research [Internet]. 2008 Dec 1 [cited 2023 Oct 20];38(12):1186–93. Available from: https://onlinelibrary.wiley.com/doi/full/10.1111/j.1872-034X.2008.00388.x

488. Braet F, Wisse E, Bomans P, Frederik P, Geerts W, Koster A, et al. Contribution of high-resolution correlative imaging techniques in the study of the liver sieve in three-dimensions. Microsc Res Tech. 2007 Mar;70(3):230–42.

489. Weber M, Leutenegger M, Stoldt S, Jakobs S, Mihaila TS, Butkevich AN, et al. MINSTED fluorescence localization and nanoscopy. Nat Photonics. 2021 Mar 15;15(5):361–6.

490. Abbott RD, Raja WK, Wang RY, Stinson JA, Glettig DL, Burke KA, et al. Long term perfusion system supporting adipogenesis. Methods [Internet]. 2015 Aug 1 [cited 2023 Apr 29];84:84. Available from: /pmc/articles/PMC4526405/

491. Ortega-Ribera M, Gibert-Ramos A, Abad-Jordà L, Magaz M, Tellez L, Paule L, et al. Increased sinusoidal pressure impairs liver endothelial mechanosensing, uncovering novel biomarkers of portal hypertension. JHEP Reports [Internet]. 2023 Mar [cited 2023 Apr 1];0(0):100722. Available from: http://www.jhep-reports.eu/article/S2589555923000538/fulltext

492. Qin L, Crawford JM. Anatomy and Cellular Functions of the Liver. In: Zakim and Boyer's Hepatology. Elsevier; 2018. p. 2-19.e4.

493. Washabau RJ, Meyer HP, Rothuizen J, Lidbury JA, Steiner JM, Richter K, et al. Liver. Canine and Feline Gastroenterology [Internet]. 2013 [cited 2023 Apr 28];849. Available from: /pmc/articles/PMC7161409/